UNIVERSITÀ DI PARMA

UNIVERSITA' DEGLI STUDI DI PARMA

DOTTORATO DI RICERCA IN

"Biologia Evoluzionistica ed Ecologia"

CICLO XXXV

Applications of chlorophyll *a* fluorometry: from photosynthetic regulation to crop phenotyping

Coordinatore:

Chiar.mo Prof. Pier Luigi Viaroli

Tutore:

Chiar.mo Prof. Lorenzo Ferroni

Dottorando: Andrea Colpo

Anni Accademici 2019/2020 – 2021/2022

Il dottorato in Biologia Evoluzionistica ed Ecologia – XXXV ciclo è in convenzione tra le Università di Ferrara, Firenze e Parma (sede amministrativa Università di Parma)

Contents

Introduction

The photosynthetic process

Photosynthesis is the basic process that modelled the biosphere, creating and sustaining the food chain. Solar energy trapping is the trigger to convert water and CO_2 into complex organic molecules, which are the basis to ensure life on Earth. Moreover, oxygenic photosynthesis produces molecular oxygen (O_2) as a side-product, which is responsible for the formation of the ozone layer, the evolution of the aerobic respiration, and consequently the proliferation of multicellular organisms. Plants, algae, and cyanobacteria are the photosynthetizers which provide the biosphere with both the organic compounds (such as glucose, sucrose, and starch) and the O_2.

The overall process is conventionally divided into two phases. In the first set of reactions, called the "light reactions", solar energy is trapped and used to oxidize water to produce oxygen, protons, and electrons, leading to the reduction of $NADP^+$ to NADPH and the production of ATP. In the second phase, namely the "dark reactions", NADPH and ATP are used to fix the atmospheric CO_2 to produce glucose. The two phases and the overall process can be summarized as follows to yield one glucose molecule:

Light reactions: $12H_2O + \text{light energy} \rightarrow 6O_2 + 24H^+ + 24e^-$

Dark reactions: $6CO_2 + 24H^+ + 24e^- \rightarrow C_6H_{12}O_6 + 6H_2O$

Overall: $6CO_2 + 12H_2O + \text{light energy} \rightarrow C_6H_{12}O_6 + 6O_2 + 6H_2O$.

Photosynthetic process annually converts approximately 200 billion tons of CO_2 into organic compounds while releasing around 140 billion tons of O_2 in the atmosphere (Johnson, 2016). Nearly half of photosynthesis on Earth is operated by cyanobacteria, while the rest is provided by algae and plants.

In vascular land plants, photosynthesis takes place in leaves. Both light and dark reactions take place inside the chloroplast, an organelle that, with very few exceptions, is lens-shaped and 2-3 μm in length: in every photosynthetic cell, around 100 chloroplasts are present. Each chloroplast is enveloped by two outer membranes delimiting the stroma, an aqueous space containing the thylakoids (Fig. 1). The thylakoids can be seen as a single, continuous, and closed membrane layer, whose shape and organization is modulated in response to external stimuli. The thylakoid contains an aqueous space, the thylakoid lumen, and is the site where the light reactions occur (Fig. 2).

The trigger of photosynthesis, *i.e.*, the oxidation of water, is operated by a large chlorophyll-protein complex embedded in the thylakoid membrane, the Photosystem II (PSII). The oxidation of water produces O_2 as a by-product and reduces the first mobile electron acceptor of the electron transport chain, the plastoquinone (PQ). The reduced PQ (plastoquinol, PQH_2) serves as a carrier for the reduction of the subsequent enzymatic member of the electron transport chain, the Cytochrome b_{6f} (Cyt b_{6f}). After the oxidation of the PQH_2 to PQ, the Cyt b_{6f} continues the electron transport chain by reducing the plastocyanin, a small water-soluble copper-protein that needs a second light-driven reaction to return to its oxidized form. The second light-driven reaction involves

another large protein-chlorophyll complex, the Photosystem I (PSI). PSI complex harvests light and catalyzes the oxidation of plastocyanin and the reduction of the stroma-soluble mobile electron carrier ferredoxin. The final step of the electron transport is operated by the ferredoxin-$NADP^+$ oxido-reductase, the enzyme that uses the reducing power provided by ferredoxin to reduce $NADP^+$ to NADPH. This sequence of oxidoreductions constitutes the linear electron transport and is summarized by the Z-scheme (Fig. 3).

The Z-scheme provides important insights about the energetic balance of the light reactions. Most of the electron transfer steps happen between redox couples with low potential to redox couples with higher potential (Fig. 3). Since all these steps are exergonic, the products of every reaction have a lower energy content compared to the reagent. However, light-driven reactions include two endergonic processes in which PSII and PSI harvest energy in form of photons and funnel the excitation to a special chlorophyll inside each reaction center (P680 in PSII, P700 in PSI), causing the transition of one electron of the chlorophyll molecule to a higher energetic level. The excited chlorophyll reduces the subsequent acceptors in the chain, and once oxidized to a chlorophyll radical cation, it is brought back to its basal energetic level with an electron extracted from water (PSII) or plastocyanin (PSI).

Oxidation of water is not only the trigger of photosynthesis and the responsible for O_2 production, but it also releases protons that are pumped into the thylakoid lumen (Fig. 3). The creation of a proton gradient across the thylakoid membrane is also sustained by the PQH_2 oxidation operated by the Cyt b_6f and serves as a store of free energy. The only proton way back across the thylakoid membrane to restore the electrochemical balance between stroma and lumen is the ATP synthase. This enzyme works as a molecular motor, allowing protons to pass from the high proton-concentrated lumen to the low proton-concentrated stroma. The energy made available by the process is used for the endergonic synthesis of ATP from ADP and inorganic phosphate, a process known as photophosphorylation.

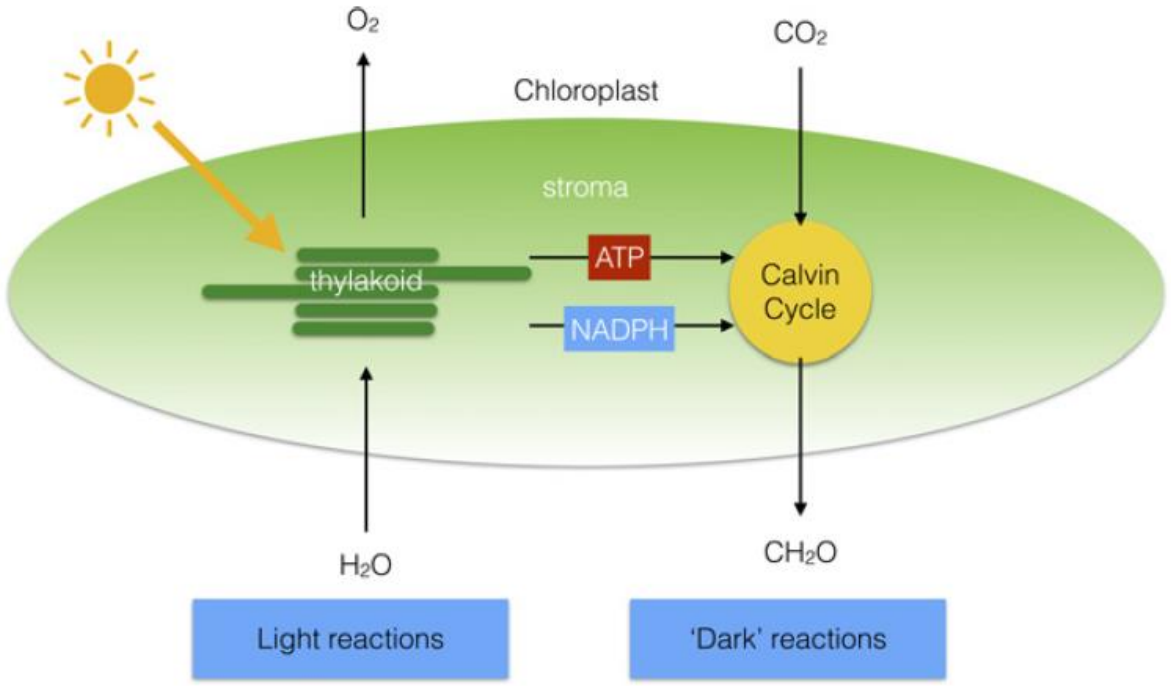

Figure 1. Chloroplast schematic structure and inner organization with the special division between dark and light reactions (from Johnson 2016).

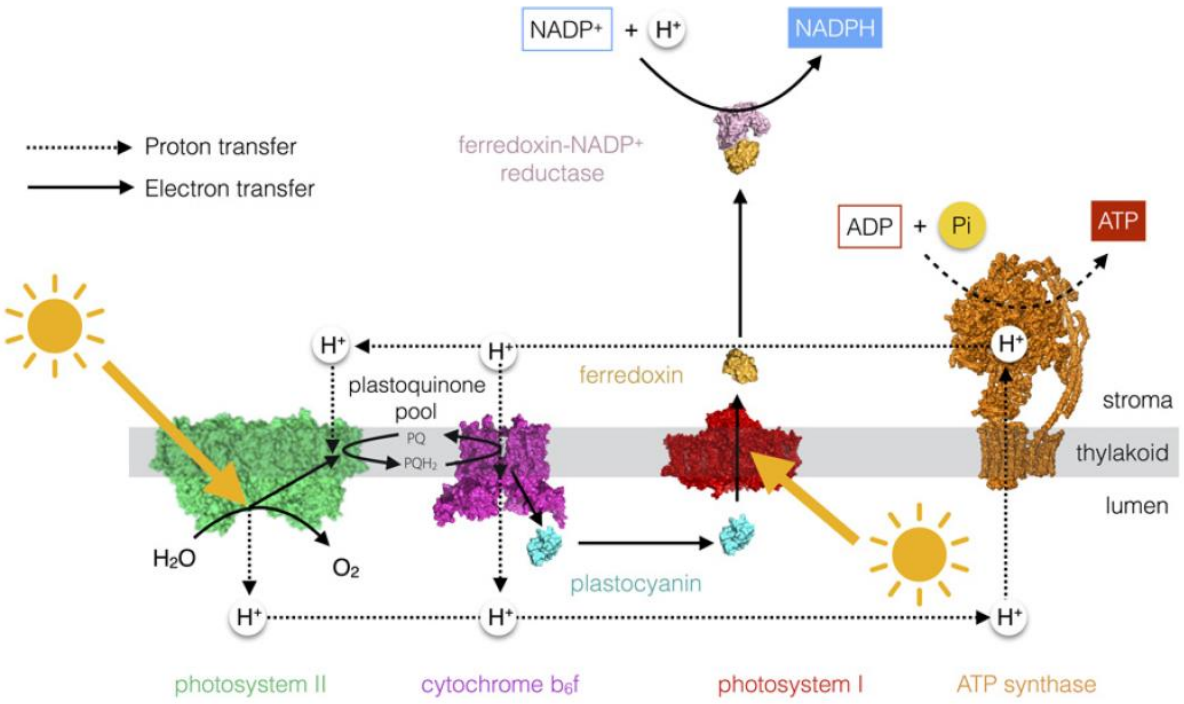

Figure 2. Organization of the thylakoid membrane complexes involved in the linear electron transport chain (from Johnson 2016).

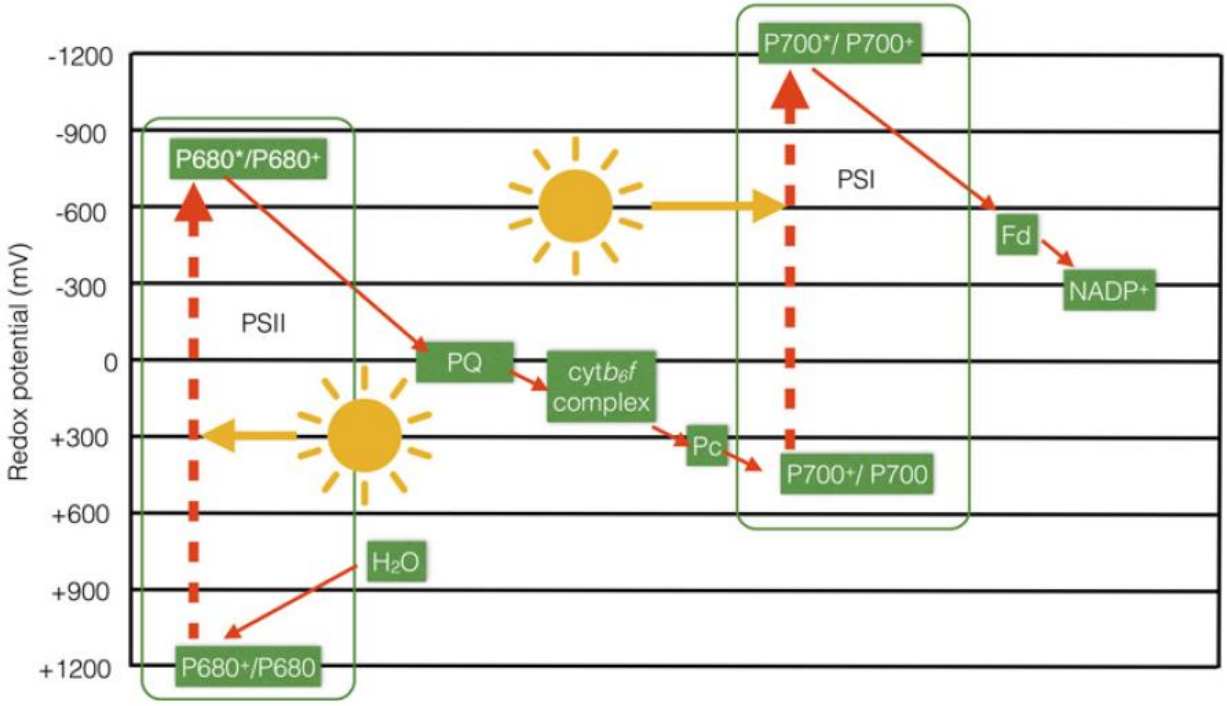

Figure 3. Z-scheme and redox potential relative to each step of the linear electron transfer (from Johnson 2016).

Structure and organization of the photosynthetic membrane in land plants

In the chloroplasts of land plants, the thylakoid system organizes into stacks of appressed thylakoids, called grana, and thylakoids entirely exposed to the stroma, namley the stroma or intergrana thylakoids connected to the grana (Fig. 4). A granum has a cylindrical shape and is composed of several layers (5 to 20) of appressed thylakoids (Rantala et al. 2020). The diameter of the cylinders is almost invariably in a range between 300 and 600 nm depending on the plant species and the light conditions. Light also has an influence on the granum thylakoid lumen width (from 4.5 nm in darkness to 9 nm in the light) and the proportion of grana membranes on the total amount of thylakoid membranes.

Stroma thylakoids have a lamellar shape and interconnect the grana. Such structures tend to be less abundant than the grana domains, but their proportion also varies largely depending on the illumination conditions.

The grana-intergrana differentiation depends on the ability of the thylakoids to adhere at their stromal side, generating appressed and non-appressed domains of the photosynthetic membrane. The appressed domains are exclusive of the granum core; the non-appressed domains characterize the stroma thylakoids, but also the upper and lower granum end membranes, as well as the grana margins. In fact, a third fraction of the thylakoid membranes exists and is constituted by the grana margins located at the border of each granum. Two theories have been proposed about the exact location and composition of such structures: in the first, grana margins are deemed to be highly curved regions of the grana membranes, not containing proteins (Armbruster et al. 2013); a second hypothesis proposed that grana margins are large annular rings at the periphery of the grana stacks, enriched in protein complexes (Danielsson et al. 2004).

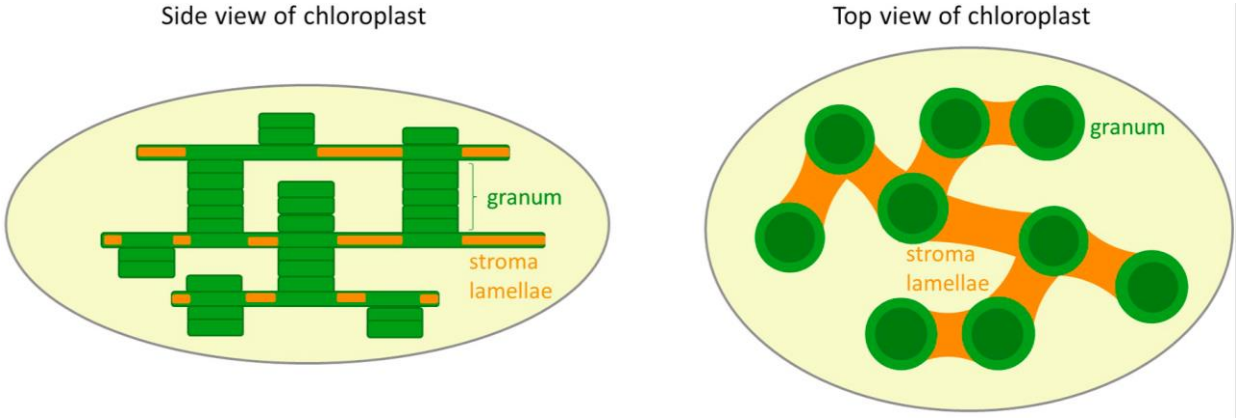

Figure 4. Schematic side and top views of the thylakoid membranes structure and organization inside the chloroplast. Green portions of the thylakoid membranes represent the grana, which are characterized by a cylindrical tridimensional structure. Orange portions are the stroma regions/lamellae, which interconnect the separated grana domains. Image from Johnson and Wientjes (2020)

The tridimensional organization of the thylakoid system in land plants has been a hotly debated topic for many decades (reviewed by Kirchhoff 2019, Staehelin and Paolillo 2020). At present, reliable tridimensional reconstructions of the granum are available based on cryo-electron tomography and illustrate the very complex relation between the granum and the surrounding stroma thylakoids, as well as the plastoglobuli associated with the membranes (Fig. 5). The tridimensional models of the grana may help solve disputes about the organization of the grana margins, which include two types of membranes: the margins proper, that is flat

regions of continuity between the appressed grana regions and the stroma thylakoids, and the curvature areas, that is the highly bended regions of the granum thylakoid (Rantala et al. 2020).

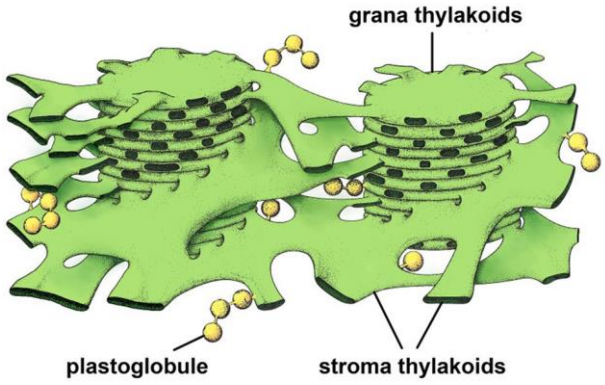

Figure 5. Model of thylakoid membranes based on electron tomographic images. The stroma thylakoids are arranged spirally at the border of each granum, forming right-handed helices. The tridimensional connection of stroma thylakoids involves bifurcations that create left-handed helices. The plastoglobuli are in continuity with each other and with the membranes (from Staehelin and Paolillo 2020).

Photosynthetic complexes are distributed unequally in the two fundamental domains of the thylakoid membrane, *i.e.*, appressed and non-appressed. PSII and its light harvesting complex (LHCII) are present in the grana and become particularly dense in their inner part, the grana core. PSI, its light harvesting complex (LHCI), and the ATP synthase are found only in the stroma lamellae since their respective size hinders the possibility for them to enter the grana core. Particularly, their stromal protrusions are too large to be accommodated in the narrow space between the stacked membranes, the so-called stromal gap or grana partition. The third complex, Cyt b_6f, is ubiquitous, and can be differently distributed between the two domains according to the light condition (Johnson et al. 2014). This uneven distribution of the complexes along the thylakoid membrane is called the "lateral heterogeneity" (Andersson and Anderson 1980).

Supramolecular organization of the photosystems in land plants

The event of light absorption is operated by the LHCII and LHCI antennae energetically connected to PSII and PSI, respectively.

The PSII monomer is formed by 20 to 23 protein subunits and includes several pigments, including chlorophyll *a*, pheophytin and carotenoids, together with co-factors like the quinones (Rantala et al. 2020). The reaction center is located in the inner region of the core and it is constituted by PsbA (D1), PsbD (D2) and PsbI subunits together with the α (PsbE) and β (PsbF) subunits of the Cyt_{b559}, and it is connected to two large chlorophyll *a*-binding harvesting complexes, the CP43 and CP47 inner antennae (Rantala et al. 2020). Associated to the PSII core are six types of Lhcb proteins subunits, which form the light harvesting complex of the PSII (LHCII). Three of these subunits (Lhcb4, Lhcb5, Lhcb6) are directly bound to the PSII core and serve as an energetic bridge to connect the PSII core with the major antenna trimers formed by combinations of Lhcb1, Lhcb2 and Lhcb3 subunits. The LHCII subunits host chlorophyll *a*, chlorophyll *b* and xanthophylls, the most abundant of which is lutein.

The complete functional unit of the charge separation is the PSII-LHCII supercomplex. A single supercomplex is composed of a dimeric PSII core complex (C_2) connected with a variable amount of peripheral antenna complexes (Fig. 6). The different degrees of association between the core dimers and the antennae are dictated by the strength of their binding. One PSII dimeric core strongly connected with two LHCII trimers, each constituted by Lhcb1 and Lhcb2, along with the bridging antenna monomer Lhcb5, forms the minimal PSII-LHCII supercomplex, namely the C_2S_2. Other two LHCII trimers formed by Lhcb1and Lhcb3, together with the bridging antenna monomers Lhcb4 and Lhcb6, can be moderately bound to the C_2 core to build the $C_2S_2M_2$ supercomplex (Fig. 6). The dimeric core of PSII can be involved in a further connection with one or more antenna trimers composed of Lhcb1 and Lhcb2, which are considered as loosely bound antennae, to form putative $C_2S_2M_2L_n$ supercomplexes. L-trimers constitute the largest pool of trimeric antennae and are also known as "free trimers" or also "extra-LHCII" (Kouril et al. 2013), since they form the lake of antennae in which the PSII-LHCII supercomplexes are immersed in the grana core membranes and, moreover, can establish transient labile associations with both PSII and PSI in the grana margin regions, *i.e.*, the thylakoid regions in which the two photosystems are closer to each other (Suorsa et al. 2015, Grieco et al. 2015, Rantala et al. 2017). Such flexibility of the L-trimers is extremely important because it allows to balance the excitation between the two photosystems depending on the light conditions (Wientjes et al. 2013, Goldschmidt-Clermont and Bassi 2015). Moreover, some studies converged on the idea that L-trimers can mediate the formation of a megacomplex involving PSII and PSI, with bridging LHCI and LHCII, in the grana margins (Suorsa et al. 2015, Grieco et al. 2015, Rantala et al. 2017). Different from the PSII-LHCII supercomplexes, the PSI-LHCI-PSII-LHCII megacomplexes have not been revealed by electron microscopy yet. While the energetic connection between PSI and PSII in putative megacomplexes has been documented (Yokono et al. 2015, 2019), an open question still exists whether the megacomplexes are individual supramolecular entities or, alternatively, the result of artifactual aggregations due to the use of detergents to solubilize the membrane (Galka et al. 2012).

The second complex of the thylakoid membrane is the PSI complex. PSI core is formed by a PsaA/PsaB heterodimer and also contains the cofactors that enable the electron transfer: 6 chlorophyll *a* molecules, 2 phylloquinones and a Fe_4S_4 cluster (Caffarri et al. 2014). PSI core includes a set of other subunits (PsaC-L, PsaN, PsaO) among which PsaC binds the redox active Fe_4S_4 cluster and, together with PsaD and PsaE, serves as the docking site for ferredoxin on the stromal side of the PSI (Fig. 7, Rantala et al. 2020). The formation of the PSI-LHCI supercomplex is mediated by the PsaF subunit of the PSI complex (Boekema et al, 2001). Differently from the LHCII, LHCI is composed of two types of heterodimeric subunits: Lhca1/Lhca4 and Lhca2/Lhca3, both located at one side of the PSI core like a belt (Fig. 7). On the other side, the PSI core is available to the transient association with one LHCII trimer, originating a PSI-LHCI-LHCII supercomplex known as the "state transition complex" (Pesaresi et al. 2009). At the PSI side opposite to the LHCI belt, the docking site for LHCII to PSI is constituted by PsaL, PsaH, and PsaO subunits of PSI core, with a stabilizing role proposed for the PsaI subunit (Pan et al. 2018, Plöchinger et al. 2016). Because LHCI significantly affects

the energy transfer from LHCII to PSI, another route exists for LHCII to serve PSI through the mediation of the LHCI belt (Benson et al. 2016).

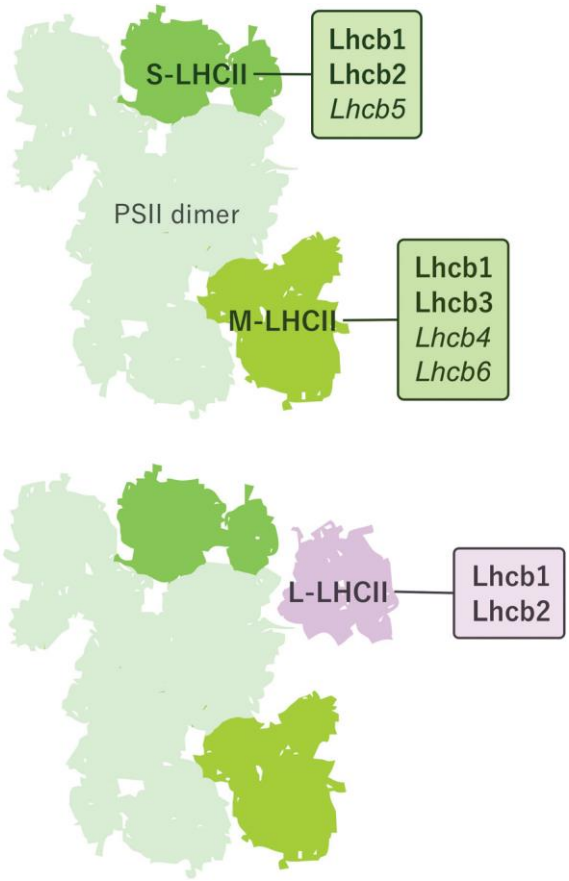

Figure 6. Structure and components of the PSII-LHCII supercomplexes. In the upper part are depicted the interaction between the S- and M-trimers with the PSII dimer to form the $C_2S_2M_2$ supercomplex. In the lower part is represented the $C_2S_2M_2L_2$ formation due to the binding of the L-trimers (from Rantala et al. 2020).

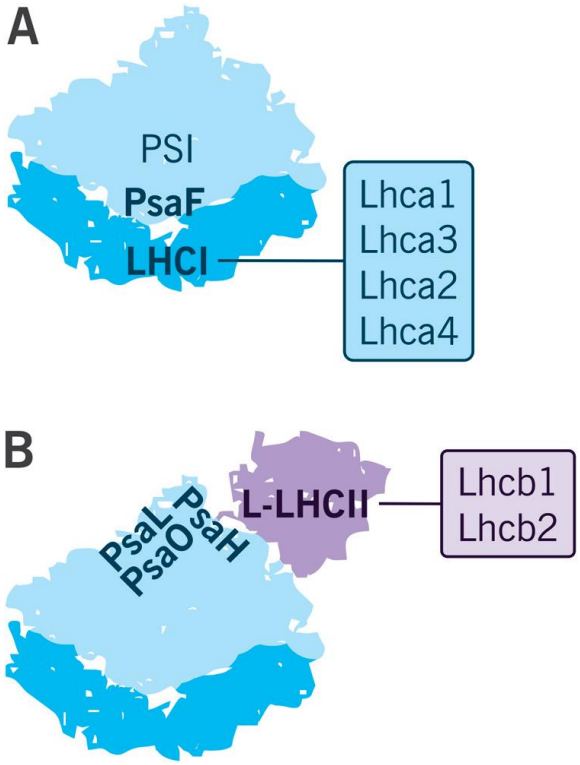

Figure 7. Structure and components of the PSI-LHCI supercomplex. In the upper part is represented the formation of the PSI-LHCI supercomplex mediated by PsaF. In the lower part is reported the binding of L-LHCII trimers to PsaH mediated by PsaL and PsaO when LHCII is performing the harvesting function for the PSI (from Rantala et al. 2020).

Regulation of the light energy management in land plants

The high level of organization of the thylakoid membrane is a key factor that allows plants to dynamically acclimate to light fluctuations, from short (seconds, minutes) to long (hours, days, season) timescales. At the photosynthetic membrane level, the principal mechanisms that are adopted by plants in response to the everchanging light conditions involve adjustments of the light harvesting process, dissipation of the excess of absorbed energy, and photosynthetic regulation of electron transport between the two photosystems.

The light harvesting complexes rearrangement on the short timescale ensures the correct repartition of the excitation energy between PSII and PSI in response to their unbalanced excitation. This unbalance is mainly due the quantity and quality of the light available to the plant. Light can be scarce and therefore limiting for the photosynthetic carbon fixation at sunrise, sunset and on cloudy days (Johnson and Wientjes 2020). In these conditions, PSII tends to be overexcited in comparison to PSI (Wientjes et al. 2013). The sensor of the unbalance between PSII and PSI is the redox state of the PQ pool: the accumulation of PQH_2 on the binding site of the Cyt b_6f leads to the activation of the kinase STN7 and the phosphorylation of the LHCII antenna associated to the PSII (Horton and Black 1980). Phosphorylated LHCII trimers are charge-repulsed by the grana domains and migrate to the stroma lamellae domains, where they become an antenna for PSI (Sheng et al. 2021). According to a wider context interpretation, the LHCII-L trimers form a lake embedding both PSII and PSI, and they mediate an extensive energetic connectivity of the photosystems even in the absence of phosphorylation. Therefore, the LHCII trimer movement from PSII to PSI should be considered as a particular aspect of a more extensive mobility of phosphorylated LHCII under the low-light-acclimated state to enhance

the PSI-LHCII interaction and relieve the potential over-excitation of PSII (Grieco et al. 2015). In contrast, shadowing due to the presence of upper leaves (from the same plant or from other plants) modifies the quality of the light. In fact, since the photosynthetic pigments absorb preferentially blue and red light, the shadowed leaves are exposed to a green and far red-enriched light, the latter being preferentially absorbed by PSI. The overexcitation of PSI is also sensed by the PQ cool, which in this case is mostly found in its oxidized form and less interacting with the Cyt b_6f. As a response, the STN7 kinase is inactivated, allowing the dephosphorylation of LHCII by the constitutively active TAP38 phosphatase and the migration of the LHCII back to the grana regions, where they enlarge the antenna size of PSII to maximize its light harvesting capacity (Pribil et al. 2010). The two opposite processes, modulated by the dual activity of STN7 and TAP38, are called state transition 1 and state transition 2, respectively.

In presence of high light, the harvesting process is no more limiting, whereas the limit to photosynthesis is imposed by the saturation of the electron sink represented by the Calvin-Benson-Bassham Cycle enzymes (Farquhar et al. 1980, Horton 2012). Consequently, a bottleneck for the electron transport is formed beyond PSI, saturating the electron transport chain, and increasing the persistency of excited chlorophyll states. When chlorophyll remains excited for a longer-than usual time, the probability of the chlorophyll triplet state formation increases, thus leading to the generation of singlet oxygen in PSII and to the reduction of O_2 to superoxide in PSI. When reactive species of oxygen are formed, they can easily react with the surrounding environment, leading to the photoinhibition and photodamage of the two photosystems (Li et al. 2009). The photosynthetic membrane employs three main mechanisms to avoid the photodamage of PSII and PSI: the "high-energy" dependent non-photochemical quenching of chlorophyll fluorescence (qE, Ruban 2016), the photosynthetic control of the linear electron transport operated at the Cyt b_6f (Takagi et al. 2017), and the O_2 photoreduction by the pseudocyclic electron flow (Chaux et al. 2015).

qE is usually the major component of the measurable non-photochemical quenching of chlorophyll fluorescence (NPQ) and sometimes the scientific literature has used the two terms as quasi-synonyms. However, NPQ is a complex phenomenon, hiding a multiplicity of processes together with qE (Gilmore et al. 1998), such as the occurrence of state transitions that reduce the antenna cross section of PSII (qT, Demmig et al. 1987, Quick and Stitt 1989), long-lasting zeaxanthin dependent quenching (qZ, Nilkens et al. 2010), PSII photoinhibition (qI, Aro et al. 1993, Nawrocki et al. 2021), chloroplast avoidance movements (qM, Cazzaniga et al. 2013), sustained quenching processes (qH and others; Demmig-Adams et al. 2015, Malnoe et al. 2017) and energy spillover from PSII to PSI (Tiwari et al. 2016; extra-qT Ferroni et al. 2018). qE and photosynthetic control are activated by the progressive acidification of the thylakoid lumen due to the proton-pumping activity of PSII oxygen evolving complex and the PQH_2 oxidation at the Cyt b_6f; importantly, the extent of the proton concentration difference between stroma and lumen also depends on the proton conductance through the ATP synthase (Kramer et al. 2004). The activation of qE is promoted by the protonation of the PsbS lumen-exposed residues (Li et al. 2004) and the activation of the violaxanthin de-epoxidase enzyme, responsible for the conversion of violaxanthin to zeaxanthin (Jahns et al. 2009). Zeaxanthin and PsbS are modulators of the NPQ activity, which is considered the result of a conformational change involving PSII and LHCII, although the

precise mechanism and location of the quenching site continues to be a debated issue. According to a predominant idea, the switch from harvesting to dissipative/photoprotective conformation involves the major LHCII, which is considered the quenching site of qE (Horton et al. 1996). In this scenario, such switch is produced by a progressive detachment of the LHCII antennae from the PSII supercomplexes, leading to a decrease in the PSII antenna size and the aggregation of the detached LHCII, which quenches the energy of the photons that it has absorbed (Betterle et al. 2009, Ruban 2018). Actually, the minor monomeric PSII antennae can also act as quenching sites, leading to an extension of the above mentioned scenario to include two quenching sites, *i.e.,* the LHCII trimers and the minor antennae (Holzwarth et al. 2009). Another hypothesis does not involve any disassembly of the PSII supercomplex but a change in the functionality of the LHCII: in this case, the sites of quenching are not only the minor and major antenna complexes, where qE depends on PsbS, but also the RC itself (Nicol et al. 2019, Bielczynski et al. 2022).

The ΔpH formation across the thylakoid membrane is also the trigger for the activation of the photosynthetic control of the electron flow included in the P700 oxidation system (Takagi et al. 2017, Shimakawa and Miyake, 2019). Avoiding the overreduction of PSI is extremely important in land plants, since the damage of the latter could require up to several days to be reversed (Sonoike 2011, Lima-Melo et al. 2019, Rodriguez-Heredia et al. 2022). This simple observation leads to consider that the regulation of the membrane should primarily limit the accumulation of electrons reaching PSI and not efficiently flowing out of it. A well-regulated photosynthetic membrane will therefore favor the donor-side limited, oxidized state of PSI, because a reaction center with $P700^+$ is stably photoprotected, $P700^+$ itself acting as a thermal quencher of excitation (Bukov and Carpetier 2003). The maintenance of oxidized P700 is ensured by the presence of flavodiidron proteins (Flv) in bryophytes, pteridophytes and gymnosperms, with Flv acting as oxidizers on the PSI acceptor side to prevent the reduction of the latter (Takagi et al. 2017). In angiosperms the principle is the same, however, given the absence of Flv, other mechanisms operate to ensure the P700 oxidation (Takagi et al. 2017). The P700 oxidation system includes a PSI donor-side mechanism, represented by the limitation of linear electron transport at the Cyt b_6f, and mechanisms operating at the PSI acceptor side, which increase the efficiency with which electrons are removed from PSI. The latter are the cyclic electron flow around PSI, the photorespiratory carbon oxidation, and the exploitation of electron sinks alternative to photosynthesis and respiration (reviewed by Shimakawa & Miyake 2018).

Cyt b_6f plays an important role in controlling the electron transfer between PSII and PSI, acting as donor-side regulator of the electron flow to PSI. In presence of high light and following the formation of the ΔpH across the thylakoid membrane, Cyt b_6f is subjected to a downregulation which constrains the electron transfer from PQH_2 pool and the oxidized plastocyanin; the change occurs in favor of the cyclic electron transport and reduces the electron pressure on the PSI acceptor side (Huang et al. 2018, Yamamoto and Shikanai 2019, Tan et al. 2020, Zhang et al. 2021). In the cyclic electron transfer, electrons are recycled from the acceptor side of PSI to the PQH_2 pool through ferredoxin, going backwards to PSI via Cyt b_6f and plastocyanin. Hence, cyclic electron transport does not contribute to form NADPH, whereas it supports the formation of ΔpH across the thylakoid membrane, thus enabling the synthesis of ATP. Being a modulator of ΔpH, cyclic electron transport

is an activator of both qE and photosynthetic regulation (Johnson and Wientjes 2020). Two distinct pathways are involved in cyclic electron transport: one is the chloroplast NADPH- dehydrogenase (NDH) dependent pathway, where the NDH mediates the electron transfer from ferredoxin to PQ, while pumping protons into the thylakoid lumen (Schuller et al. 2019); the second mechanism is the PGR5-PGRL1-dependent pathway, in which PGR5-PGRL1 can be itself the oxido-reductase for the ferredoxin-PQ couple or, alternatively, it can regulate the PQ reduction state at the Cyt b_6f level (Joliot and Johnson 2011). Observational evidence shows that the relative importance of the mechanisms alleviating the electron pressure on PSI at the acceptor side is variable depending on the plant material and the experiment, e.g., the environmental adaptation of the species and the stress under which the regulatory mechanisms have been probed (Zivcak et al. 2013, Sun et al. 2020, 2021, Shi et al. 2022).

The final level of short-term response in light energy management in the photosynthetic membrane is due to ultrastructural changes in the thylakoid. STN7 kinase activity is suppressed when the photosynthetic membrane is exposed to high light due to negative regulation by thioredoxin and ΔpH (Fernyhough et al. 1984, Rintamäki et al. 2000, Mekala et al. 2015). The increase in non-phosphorylated LHCII results in a general increment of grana diameter and thylakoid stacking degree because of the tendency of the LHCII trimers to stabilize the granum layers (Johnson and Wientjes 2020). A progressive compartmentalization of the PQ pool also occurs, which is hindered in reaching the Cyt b_6f population residing in the stroma lamellae and, therefore, less subjected to oxidation (Wood et al. 2020). Increase in grana size and stacking was proposed as a trigger of the cyclic electron transport (Johnson 2018, Wood et al. 2020). Larger grana are also present in dark condition and when shade is provided by upper leaves, which over-excite the PSI as previously mentioned. A most recent hypothesis invites to consider the general ultrastructural level as a site of regulation beyond the individual mechanisms involving the molecular and supramolecular level (Gu et al. 2022). It is proposed that grana stacks control photosynthesis through thylakoid swelling/shrinking induced by osmotic water fluxes: such changes could modify the diffusional pathlengths of mobile electron carriers, help the division of function of Cyt b_6f complex between linear and cyclic electron transport, modulate the luminal pH via osmotic water fluxes with impact on the qE extent and kinetics.

Long term light acclimation acts at the gene expression level to fine-tune the thylakoid structure for an optimal light harvesting capacity in coordination with the carbon fixing potential of the plant (Anderson 1986). For instance, long-term light acclimation to high light induces a reduction in the grana size and stacking due to the decrease in the LHCII population, which in turn is accompanied by an increase in the electron transport capacity (Schumann et al. 2017). The reduction in grana size is accompanied by an increase in the ATP synthase expression, which is hosted in the increasingly available stroma lamellae, thus leading to an increased ATP production in plants long-term acclimated to high light. Conversely, low light long-term acclimation promotes an increased light harvesting capacity for PSII (Johnson and Wientjes 2020). The long-term light acclimation has also an impact on the PSI/PSII stoichiometry, but the direction of the change seems to depend on the plant material. Along with these main molecular and structural modulations, the sun-shade acclimation involves a large number of additional changes, which are summarized in Table 1 (Anderson et al. 1988,

Lichtenthaler and Babani 2004, Schöttler and Toth 2013, Zivcak et al. 2014, Schumann et al. 2017, Mathur et al. 2018).

Phenotypic trait	**Sun (or high light or blue light)**	**Shade (or low light or far red light)**
Ultrastructure		
Chloroplast size	Regular	Large
Thylakoid/stroma volume (or thylakoid extension)	Small	Large
Stacking degree (thylakoids/granum)	Low	High (up to hundreds of stacked thylakoids under deep shade)
Appressed/Non-appressed membranes	1-1.5	4-5
Starch granules	Abundant	Small or absent
Photosynthetic pigments		
Chlorophyll content per chloroplast	Low	High
Chlorophyll a/b ratio	2.9-4.5	2.3-2.8
Chlorophylls/carotenoids	4.3-5.5	5.5-7.0
Xanthophyll cycle pigment pool	Large	Small
Photosynthetic complexes		
Reaction centres/Chlorophyll	High	Low
LHCII/Chlorophyll	Low	High
Electron transport chains/Chlorophyll	Many	A few
Electron transporters per chain	High	A few
LHCII/PSII	Low	High
PSI/PSII	0.6-1.0	Lower if plant grown under far red enrichment (0.4-0.5), similar or higher if not
ATP synthase activity /Chlorophyll	High	Low
Cyt b6f/Chlorophyll	High	Low
PsbS/Chlorophyll	High	Low
Photosynthetic function		
Carbon fixing capacity	High (up to 40 μmol CO_2 m^{-2} s^{-1})	Low (< 10 μmol CO_2 m^{-2} s^{-1})
Intensity required for saturation of electron transport	High	Low
Reaction centers activity	High	Low
Linear electron transport/Chlorophyll	High	Low
PSII functional antenna size	Small	Large
PSII connectivity	High	Low
PSII quantum efficiency (actual quantum yield based on the same irradiance)	High	Low
Cyclic electron flow	High	Low
Thermal dissipation (NPQ)	High	Low
Susceptibility to PSII photoinhibition	Low	High

Table 1. Contrasting photosynthetic characteristics of sun- and shade-acclimated angiosperms.

Principles of chlorophyll *a* fluorescence measurement

A complete description of the biophysical processes underlying light absorption and photosynthetic electron transport is necessary to understand the regulatory mechanisms through which the plant optimizes its photosynthetic efficiency under various environmental conditions. Measurements of chlorophyll *a* fluorescence (ChlF) are used to obtain detailed information regarding the primary events of light harvesting and conservation in the electron transport chain (Kalaji et al. 2017) and, more specifically, regarding the photochemistry of PSII. The two most widespread methods of ChlF analysis are pulse amplitude-modulated fluorimetry (PAM) and continuous excitation fluorometry (Kalaji et a. 2014). The former is popular for the quenching analysis of ChlF, the latter was mainly designed for the study of the fast polyphasic kinetics of ChlF induction. Nonetheless, both methods can be used for both types of analysis (Kalaji et al. 2014).

PAM fluorometry, quenching analysis and energy partitioning

PAM fluorimetry is widely used to study the photochemical efficiency of PSII and the function of the entire electron transport chain by means of the light re-emitted by PSII as fluorescence following excitation (Kalaji et al. 2014, Baker 2008). To understand the principles of the PAM technique, it is important to consider the concept of fluorescence intensity and fluorescence yield. Fluorescence intensity is an absolute value that depends on illumination conditions and can vary by many orders of magnitude, because the intensity of fluorescence emission is proportional to the intensity of excitation; fluorescence yield, on the other hand, is much less variable because it expresses the ratio of re-emitted photons to absorbed photons. In PAM fluorimetry, the light source used to measure fluorescence is modulated, that is, applied in the form of very short (1-3 μs) high-frequency (100 Hz) pulses, and the measurement is performed only on the part of the fluorescence generated by the modulated pulses. For this reason, the fluorescence yield of these pulses can be measured under any environmental illumination condition, including solar illumination. The light received by the sample, different from the measuring system lights and producing a biological effect (activation of photosynthesis and associated regulatory processes), in called “actinic light”. Two conditions are therefore considered for the study of PSII by the PAM method: i) dark-acclimated sample, ii) light-acclimated sample, i.e., exposed to actinic light.

Under the conditions in which a sample is incubated in the dark for a sufficient time prior to analysis, plastoquinone Q_A is in a fully oxidized form and PSII is in the so-called ‘open’ state, i.e., it is available to perform charge separation as soon as it is reached by a photon/exciton. By applying a weak measuring light (ML) of very low intensity and unable to start the electron transport chain, a fluorescence signal Fo is obtained, representing the baseline fluorescence in the dark-acclimated state. The moment the sample is subjected to a saturating light pulse (Saturation Pulse, SP), lasting less than one second and of very high intensity (as high as 10-15.000 μmol photons m^{-2} s^{-1}), Q_A is completely reduced and all PSII are in the 'closed' state, i.e., no longer available to perform further charge separation. Following the gradual closure of all PSII centers, the fluorescence increases until it reaches its maximum value, Fm (maximum fluorescence in the dark-acclimated state) (Baker 2008) (Fig. 8). This interpretation of the ChlF fluorescence increase from Fo’ to Fm’ follows the

pure "Q_A model" originally proposed by Duysens and Sweers (1963) and commonly accepted as a good approximation (Stirbet and Govindjee 2012, Tsimilli-Michael 2020). Nevertheless, alternative models exist and will be shortly mentioned in the paragraph dedicated to the continuous excitation fluorescence.

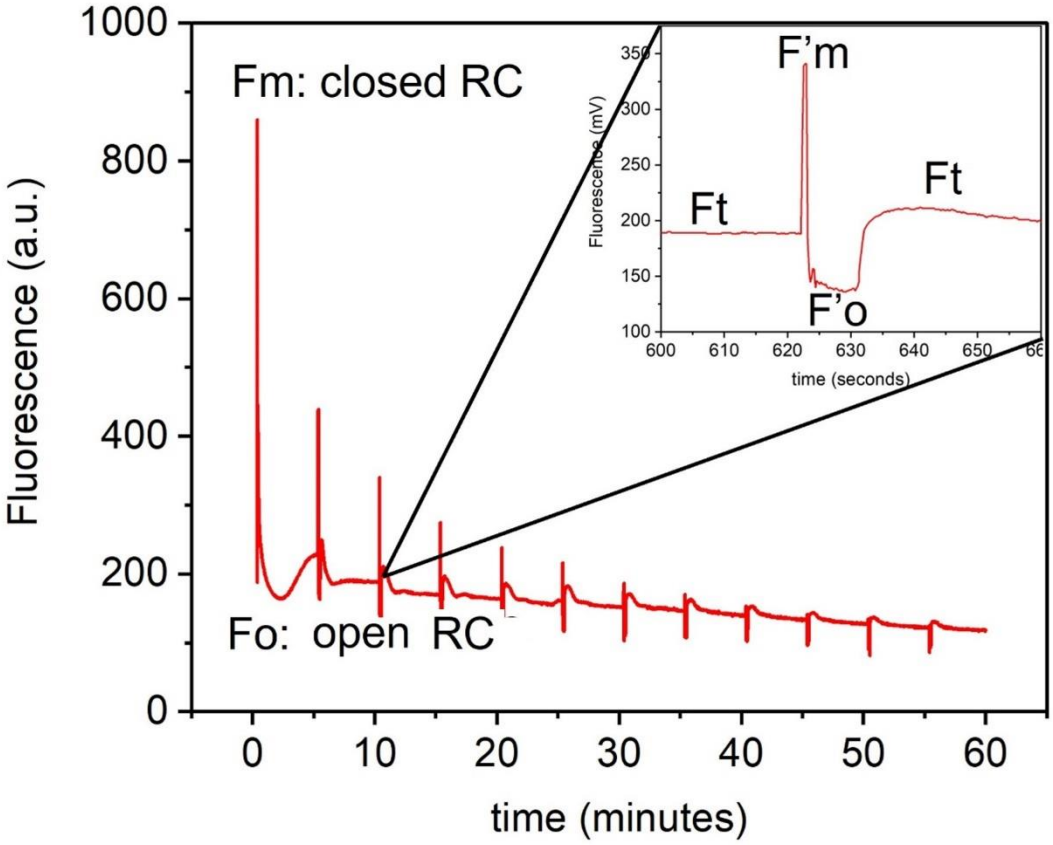

Figure 8. Example of a chlorophyll fluorescence analysis routine performed in *Selaginella martensii*. Prior to the start of the light-response curve, the leaf was acclimated to dark in order to open all the reaction centers and reach basal fluorescence level Fo. After the application of a saturating pulse, the maximum fluorescence emission in the dark-acclimated state is reached (Fm), *i.e.*, the fluorescence emitted when all the reaction centers are closed. During the light curve, the leaf is exposed to increasing actinic light intensities, and saturating pulses are applied every 5 minutes to measure the quenching of the maximum fluorescence (Fm'). After the saturating pulse, the plant is exposed to 7 seconds of far-red light to temporarily oxidize the PQ pool and obtain the minimum fluorescence level in the light-acclimated state (Fo'). The fluorescence level measured at any given moment of exposure to actinic light illumination is Ft.

The difference between Fm and Fo is called the PSII variable fluorescence, Fv, while the ratio Fv/Fm is used as an estimate of the maximum photochemical quantum yield of PSII in the dark-adapted sample. Fv/Fm is the most frequently used fluorescence ratio to assess the maximum photosynthetic efficiency of PSII, and its value could theoretically range between 0 and 1. In fact, in unstressed C3 vascular plants, its value is about 0.83, meaning that 83% of the absorbed light is used by PSII to accomplish photochemical processes, while the remaining 17% is dispersed in dissipation processes including fluorescence itself (Hendrickson et al. 2004). Actually, since fluorescence is generally probed in the near far red spectral region (>700 nm), there is a non-negligible contribution of PSI fluorescence emission to the Fo value, leading to an underestimation of Fv/Fm (Pfündel 1998). In C3 plants, a more close-to-real Fv/Fm value is estimated as 0.88 (Pfündel 1998, Wientjes

et al. 2013b); although it is possible to correct the measured Fv/Fm for the PSI contribution, this option remains seldom applied in the routine (Kalaji et al. 2017).

When a plant is subjected to stress, 'unregulated' dissipation processes occur as consequence of PSII damage and, as a result, the Fv/Fm ratio decreases. Although Fv/Fm represents a very useful parameter for obtaining information on the photosynthetic efficiency of PSII, often this cannot be considered as an absolute index since, in order to be considered as such, assumptions would have to be met that are not always valid (Baker 2008). Moreover, some little changes could be overlooked with Fv/Fm; as an alternative, a wider variation range characterizes the fluorescence ratio Fv/Fo, sometimes used as a photochemical index, though not being a quantum yield (Lichtenthaler et al. 2005). More information can be sought beyond the maximum PSII photochemical activity, examining the response of ChlF fluorescence under the light acclimation condition with the so-called "quenching analysis." Quenching analysis refers to the study of coefficients that quantify the ability that different processes have to 'quench' the fluorescence relative to the Fm value. Quenching analysis allows the two components of photochemical and nonphotochemical quenching to be evaluated (Kalaji et al. 2014).

Quenching analysis is performed in the presence of light called actinic light, which has the effect of activating the photosynthetic process, includingelectron transport, ATP synthesis and Calvin-Benson-Bassham cycle. A quenching analysis routine is exemplified in Fig. 8. The fluorescence measured moment by moment is denoted Ft. Since actinic light induces the closure of a certain portion of PSII centers, it turns out that Ft is higher than Fo. When a pulse of saturating light is then applied to the sample with the actinic light background, the maximum fluorescence F'm is measured, which allows calculation of the difference F'm- Ft, denoted F'q. The F'q/F'm ratio is the actual quantum yield of photosystem II, Y(PSII), which estimates the photochemical efficiency of PSII under any illumination condition (Genty et al. 1989, Baker 2008). The value of Fm' is lower than Fm because of the regulatory dissipative mechanisms induced to ensure the PSII photoprotection. Per extension, the nonphotochemical fluorescence quenching of Fm, termed NPQ, is taken as a measure of the thermal dissipation capacity of a plant and can be quantified in different ways, most frequently by a Stern-Volmer type equation: NPQ = (Fm-F'm)/F'm. However, as previously recalled, the technical parameter NPQ actually hides a multiplicity of processes and, moreover, it is not free from theoretical caveats (Holzwart et al. 2013).

Photochemical quenching parameters determine the position of Ft on a scale ranging from Fo' to F'm and is generally quantified by a coefficient referred to as qP or its transformation qL, which is applied when connectivity between PSII is deemed relevant (Kramer et al. 2004b, Kalaji et al. 2017). PSII connectivity is a property of energetic coupling between neighboring PSII centers that allows excitation transfer from a close to an open center (Stirbet 2013). However, qP has been suggested to be a more straightforward parameter and should be preferred to qL (Schansker 2022) qP and qL focus the analysis only the PSII population which can do a photochemical charge separation and therefore they exclude the PSII centers not reached by excitons because of concomitant non-photochemical quenching. The complement to one of these parameters (1-qP or

1-qL) is used to quantify the relative proportion of Q_A^- under any specific light intensity and is also referred to as the excitation pressure inside PSII (Björkmann and Demmig-Adams 1995).

Alternatively and to complement the quenching analysis, an 'energy partitioning' approach can also be used (Lazar 2015) (Fig. 9). In energy partitioning assessments, the distribution of energy absorbed by PSII is described by quantum yields representing competing processes. Part of the energy is used for photochemical activity, the efficiency of which, as mentioned above, is expressed in terms of Y(PSII). The fraction of energy dissipated as heat through inducible processes, that is having a regulatory role, is described by analogy in terms of the nonphotochemical quenching yield, Y(NPQ). The portion of the absorbed energy dissipated constitutively as heat or fluorescence, that is without implicating a regulatory function and due to the presence of a portion of PSII in the 'closed' state is expressed as Y(NO). The sum Y(PSII)+ Y(NO) + Y(NPQ) is equal to 1. There are formalisms that apply the concept of energy partitioning, the most widely used of which are due to Kramer et al. (2004) and to Hendrickson et al. (2004). The former takes into account the potential effect of PSII connectivity and depends on the availability of Fo' (either measured or estimated); the latter uses a simpler equation set and is independent of Fo'. However, the results obtained with the two methods are generally compatible. It can be demonstrated that in the Hendrickson's formulation, NPQ = Y(NPQ)/Y(NO); recently the ratio PQ = Y(PSII)/Y(NO) has been introduced by analogy, which is useful for quantifying the total photochemical capacity (Lazar 2015; Ferroni et al. 2014). Related to the meaning of the quantum yields, from a functional point of view the efficiency of a plant will be related to its ability to limit Y(NO) especially at higher irradiances and, at the same time, to secure maximum Y(PSII) (Klughammer and Schreiber 2008). PAM fluorescence, used either for quenching analysis or energy partitioning, is therefore believed to be informative over the entire electron transport chain from PSII to final acceptors, including the electron sink capacity of the Calvin-Benson-Bassham cycle. Indeed, the ability to control Y(NO) depends on the efficiency with which electrons are consumed downstream of PSI. In fact, an insufficient consumption capacity can lead to an increase in the reduction state of plastoquinone, which in turn increases the proportion of closed PSII. An excess of electrons in the membrane increases the probability of PSII photodamage (Kalaji et al. 2014, Lazar 2015). Particularly, a net accumulation of photodamaged PSII centers occurs when the repair cycle of PSII is saturated (for review on the PSII repair cycle, Järvi et al. 2015). In that case, a population of damaged PSII remains embedded in the appressed domains of the grana cores. According to a hypothesis originally formulated by Anderson and Aro (1994), the grana stacks could have such an additional function and be a kind of reservoir of unfunctional PSII units, acting themselves as a safe dissipative conduit to protect the functional PSII centers (see also Matsubara and Chow 2004). Extending this hypothesis, the accumulation of inactive PSII centers can limit the inflow of electrons into the transport chain, participating in the alleviation of the electron pressure to PSI (Huang et al. 2016). Therefore, the evaluation of PSII photoinhibition (i.e., any sustained loss of PSII photochemical activity), which is commonly performed using PAM fluorimetry, should be interpreted carefully based on the specific context.

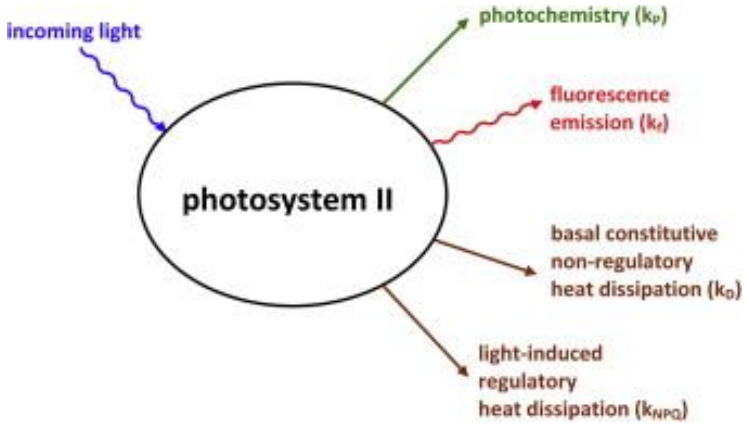

Figure 9. Schematic representation of the energy partitioning concept (from Lazar 2015).

Prompt chlorophyll a *measurement and OJIP transient analysis*

The direct fluorescence technique involves the direct measurement of the ChlF signal by application of unmodulated light; it is therefore called continuous excitation fluorometry. This technique is carried out on dark-acclimated samples and allows measurement of the so-called fast kinetics of ChlF, that is, its increase from a minimum (Fo) to a maximum value (Fm). This kinetics is called "fluorescence transient", as it is a transient response that is not stable over time. A lot of information regarding the photosynthetic membrane can be derived from the shape of the transient. This is a very rapid measurement that involves subjecting the sample to an excitation light with a wavelength less than 670 nm. When the sample is illuminated, the fluorescence intensity increases from a low value, Fo at step O to a maximum value, Fm at plateau P, in a time of about 200 to 600 ms, passing through two intermediate inflections called F_J at step J and F_I at step I (Strasser and Srivastava 1995, Tsimilli-Michael 2020) (Fig. 10). For this typical feature, the transient is commonly known as OJIP. The system being unmodulated, the intensity of the emitted light is proportional to the intensity of the excitation light.

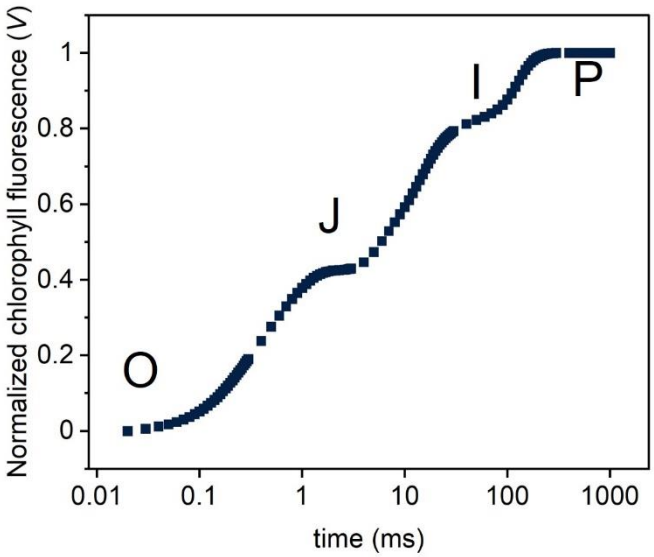

Figure 10. The typical shape of a normalized OJIP transient on logarithmic timescale from a *Triticum aestivum* sample. Fluorescence at the O value is measured depending on the sensitivity of the PEA device at 0.02 or 0.05 ms and corresponds to the minimal chlorophyll fluorescence emission of the dark-acclimated state. Fluorescence rise has a first inflection around 2 ms which corresponds to the J step. The second inflection is at 30 ms and it is known as the I step. Finally, chlorophyll fluorescence emission reaches its plateau around 200-600 ms in the P step, corresponding to Fm.

The fluorescence induction curve is represented graphically by plotting the fluorescence values on a logarithmic scale of time, expressed in ms (Fig. 10, Strasser et al. 1995, Kalaji et al. 2014, Tsimilli-Michael 2020). On the logarithmic scale representation of time, the polyphasic pattern of the transient is emphasized. In the Q_A model of fluorescence origin in PSII, the different phases of the fluorescence increase (O-J, J-I, I-P) can be related to subsequent moments of the reduction of the electron transport chain from PSII to PSI (Fig. 10).

More specifically, the first O-J phase, called the 'photochemical phase', is related to the reduction of Q_A, the primary acceptor of PSII, and is also identified as the single turnover region. At the J step, Q_A is deemed to have been reduced once. The J-I phase corresponds to the reduction of the plastoquinone pool, up to the I step indicating the complete reduction of Q_B followed by the reoxidation of PQH_2 by Cyt b_{6f} (Joliot and Joliot 2002, Schreiber et al. 1989, Tóth et al. 2007, Schansker et al. 2014, Tsimilli-Michael 2020). Finally, the I-P phase represents the reduction of electron acceptors of PSI (Schreiber et al. 1989, Schansker et al. 2005, Tsimilli-Michael 2020). The overall J-P phase is referred to as the 'thermal phase': the progressive increase in the fraction of PSII with reduced Q_A and reduced transporters is driven by the multiple turnovers of Q_A reduction up to the complete closure of all PSII (multiple turnover region) (Bussotti et al. 2012, Stirbet and Govindjee 2011, 2012, Tsimilli-Michael 2020).

For the experimental purposes of photosynthetic biology, the goal is to highlight and compare the differences between transients obtained after treatments and control transients. To achieve this, the transients are routinely double normalized between O and P (assigning consequently values of Fo= 0 and Fm= 1).At each time t

between O and P, the value of the variable fluorescence Vt is therefore the normalized corresponding Ft value: Vt = (Ft-Fo)/(Fm-Fo).

The O-J single turnover photochemical phase (0.02/0.05 ms to 2 ms) describes the first cycle of Q_A reduction,. This mainstream interpretation of the meaning of the J step is based on pure Q_A model, in its turn supported by the experimental evidence that the kinetics of the O-J phase is very similar to the relative variable fluorescence obtained in the presence of DCMU (3-(3,4-dichlorophenyl)-1,1-dimethylurea) (Stirbet and Govindjee 2011). It is known that in the presence of DCMU, electron transport from Q_A to Q_B is blocked and Q_A is can only be reduced once between Fo and Fm (single turnover). The fact that the level of fluorescence at J is lower than Fm is due to the re-oxidation of Q_A by acceptors downstream of PSII. Particularly, the O-J phase can be mathematically modelled according to the concept that the relative fluorescence at step J corresponds to a temporarily stabilized Q_A reduction state, i.e., a balanced condition between the electron donation to Q_A by photochemistry and the electron departure from Q_A to Q_B (Laisk and Oja 2018). However, interpretations other than a pure Q_A model have been proposed to explain the O-J rise. For example, the time needed for the O-J rise is also consistent with the waiting time for PSII conformational changes, suggesting that the J step may reflect the competition between electric field-related fluorescence rise in PSII reaction center and re-oxidation of Q_A (Magyar et al. 2018, Sipka et al. 2021). Even in that scenario, the J step will depend on the efficiency for electrons to move beyond PSII to Q_B and relates to the plastoquinone pool size (Strasser et al. 2004, Stirbet and Govindjee 2011). The relative fluorescence V_J is commonly used used as an estimate of the availability of oxidized plastoquinone molecules to reoxidise Q_A (Toth et al. 2007, Guo et al. 2020).Immediately after step J a depression indicated by D (Dip), given by a temporary decrease in fluorescence intensity, may be graphically visible. This is indicative of a partial re-oxidation of Q_A (Ilik et al. 2006). It was proposed that the cause for D can be the quenching action of $P680^+$ (Laisk and Oja 2013). The dip is more marked when the excitation light is excessively high (see Stirbet and Govindjee 2012).

When a *Pisum sativum* specimen was subjected to heat stress conditions, an additional band, so-called K, appeared between O and J, visible at about 200-300 µs (Srivastava et at. 1997). The appearance of the K band is considered to be the consequence of (i) a limitation of the electron donation efficiency of the OEC and (ii) changes in the architecture of PSII with altered energy distribution in the pigment-protein complexes and in the entire photosynthetic unit. A deficit at the level of the OEC causes a decrease in electron supply to the PSII reaction center. So, after a rapid increase in fluorescence due to the reduction of Q_A, the electron transfer continues to Q_B leading to the re-oxidation of Q_A but, due to the lack of electrons from the OEC, the fluorescence after 200-300 µs, instead of continuing to increase, decreases, generating the K peak. K does not appear at a specific time, but within a time interval, which is why it is usually preferred to a band and not a step in fluorescent transient (Tsimilli-Michael et al. 2020). In normalized O-J transients, the state of the PSII donor site, i.e., the OEC, can be probed by calculating the V_K/V_J ratio, which is a very robust index of plant susceptibility particularly to heat stress (Brestic et al. 2012, Kalaji et al. 2017).

The multiple turnover region, also called the thermal phase, corresponds to the part of the transient between J and P, when multiple redox reactions occur until the complete reduction of Q_A is achieved (Fig. 10). At about

30 ms, the I step is found. The J-I phase represents the (partial) progressive reduction of the PQ-pool, whose kinetics depends on the reoxidation of the plastoquinol by the Cyt b_6f complex interposed between PSII and PSI (Toth et al. 2007). The subsequent P level is reached when the entire transport chain is reduced and the electrons cannot flow beyond the PSI. Indeed, it should be remembered that FNR operating on the stromal side of PSI is inactive in the dark (Schansker et al. 2006).Therefore, there is a general consensus about the region between I and P being affected by the activity of PSI. The I-P amplitude relates with the pool size of PSI electron acceptors that are progressively reduced up to saturation (Tsimilli-Michael and Strasser 2008, Zivcak et al. 2015). Moreover, the I-P amplitude is empirically associated to the relative amount of PSI and the PSI/PSII stoichiometry (Ceppi et al. 2012), although the photoinactivation of PSI does not have any significant impact on the I-P amplitude (Zivcak et al. 2015). An alternative explanation of the I-P phase is due to Vredenberg (2011), who links it to the membrane potential generated by cyclic electron flow around in PSI. His model is however not supported by the OJIP transient recorded from mutants defective in cyclic electron flow (Joly et al. 2010). The attribution of the I-P transition to the reduction of the entire linear electron transport chain is also accepted in the most recent formulation of the alternative "PSII conformational change model" by Sipka et al. 2021.

Based on the Q_A model, the OJIP transient phases have been comprehensively described in the *Theory of Energy flux*, which led to the elaboration of one of the most popular tests in photosynthesis studies, i.e., the JIP-test (Strasser et al. 2004, Stirbet and Govindjee 2011, Tsimilli-Michael 2020). The theory includes several concept, assumptions and approximations and is aimed at evaluating the impact of environmental stresses on the photosynthetic function, while also providing some information on structural aspects, such as the antenna size of PSII. Among the characterizing features of the theory, the values sampled from the OJIP transient are used to calculate probabilities (ψ) of electron transport from Q_A to Q_B (based on J step) and then to PSI (based on I step), allowing the definition of a series of quantum yields (ϕ) that represent the energy conservation from light absorption to the reduction of the entire chain. The third set of parameters quantifies the flux of energy per PSII reaction centre. Fig. 11 illustrated schematically the parameters included in the model, according to the version published by Merope Tsimilli-Michael (2020) in her educational review on the JIP test.

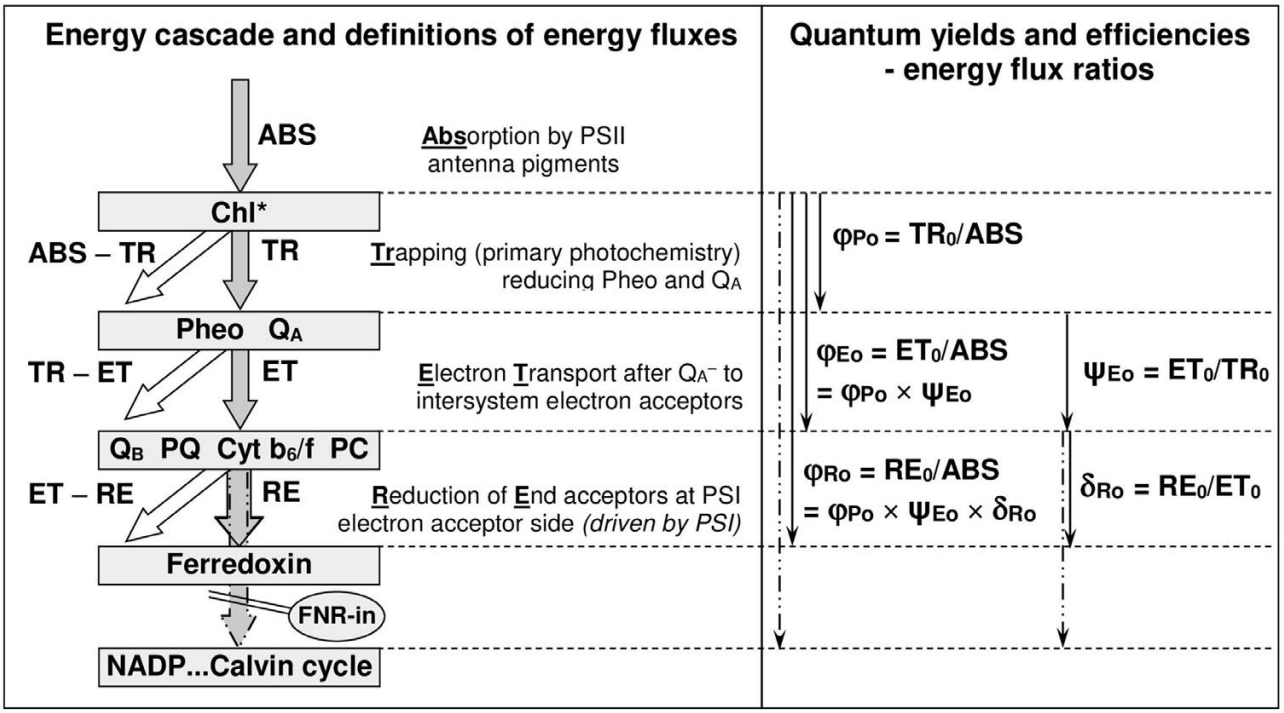

Figure 11. The energy fluxes theory describes and models the sequential transformations of energy from its absorption in the antennae to the final reduction of ferredoxin: from ABS (absorption by PSII antenna) to TR (reduction of Q_A) to ET (reduction of the intersystem electron acceptors) up to RE (reduction PSI end electron acceptors). At each step a part of the energy is lost, including the thermal dissipation in PSII reaction center and the progressive emission of light. The quantum yields (ϕ) and the efficiencies/probabilities (ψ) for energy conservation, as flux ratios, are also defined. Image from Tsimilli-Michael (2020).

Application of chlorophyll fluorescence in plant phenotyping

The study of the photosynthetic process and its regulation are essential tools for understanding how a plant adapts to its environment. Particular environmental contexts may involve the presence of different types of conditions, in which the plant faces both abiotic and biotic stresses. In addition, the characterization of the photosynthetic apparatus can provide important perspectives regarding the productivity of crops in the most diverse cultivation contexts. Phenotyping methodologies used nowadays provide fundamental support for the study of biological processes occurring in the plant. The principle of phenotyping is based on the nondestructive collection of large amounts of data in a short period of time and. Advances in modern phenotyping technologies have made it possible to make use of multiple instrumentations that are capable of performing simultaneous integrative analyses preferably with a high level of automation (phenotyping platforms, e.g., Yang et al. 2020). Being fast and noninvasive, the use of chlorophyll fluorescence measurement techniques fits well with the purpose of plant phenotyping. The application of fluorometric tools is possible both for "pocket phenotyping" applications(where, for example, the use of PEA-type instruments is widespread – PEA stands for *Photosynthesis Efficiency Analyser*) and in automated phenotyping applications carried out in phenotyping units, or in aerial phenotyping for in-field experiments (sun-induced fluorescence, Porcar-Castell et al. 2014).

PEA-type fluorimetry is particularly suitable to pocket phenotyping experiments. This type of analysis has provided valuable insights in both basic and agricultural-related research. Measurement of photochemical processes at the PSII provides precise indications regarding, for example, the impact of various stressors on the plant. Practical examples are studies conducted in the presence of various stressors, such as high or low temperature, changes in light quality and intensity, water deficit, salinity, presence of photosynthesis inhibitors (herbicides), heavy metals and other environmental pollutants, including airborne phytotoxic materials (Fracheboud and Leipner 2003, Dai et al. 2009, Metha et al. 2010, Mathur et al. 2011, Tomar and Jajoo 2014, Mathur et al. 2016, Kalaji et al. 2018). One of the main ambitions for a fluorometric phenotyping test is the detection of early responses to stress possibly before sufferance signs are manifest in an overt form.

PAM fluorometry is the technology that gave rise to the chlorophyll fluorescence imaging technique, which is nowadays the most widespread in photosynthetic plant phenotyping. The first attempt to image the chlorophyll fluorescence information has been done around 1990 (Daley et al. 1989, Osmond et al. 1990, Siebke and Weis 1995, Bro et al. 1996). The improvement of the instrumentation and the computational power that become available subsequently made the exploitation of chlorophyll fluorescence imaging more feasible and promoted a widespread use of this technique (Valcke 2021) The combination of chlorophyll fluorescence, hyperspectral and thermal imaging put a new light in the characterization of the fundamental mechanisms involved in the regulation of photosynthesis (Valcke 2021). In the recent years, several works have advanced the application of chlorophyll fluorescence imaging in the study of photosynthesis. For instance, along with adaptations of common measuring routines to shorten the time of the quenching analysis, a new set of parameters has been developed to estimate and image the non-photochemical quenching occurring in PSII and in its antenna complexes in the absence of a direct determination of dark-acclimated fluorescence values (NPQ_T, Tietz et al. 2017). Examples of application of ChlF imaging regarded the analysis of chlorosis induced by viral infections (Li et al. 2017), the detection of the PSII inhibitory activity by a herbicide (Noble et al. 2017), the screening of maize genotypes for drought stress resistance (de Sousa et al. 2017), the sensitivity of *Arabidopsis thaliana* mutants for drought stress (Sun et al. 2019) or heat stress (Gao et al. 2020), the response of basil to both drought and heat stress (Lazarevic et al. 2022), of rice to salinity (Tsai et al. 2019) and of trifoliate orange to cold stress (Wang et al. 2019). Some attempts have tried to include the OJIP induction kinetics in the imaging systems, but this is a difficult task because of the speed limitation of the available cameras for chlorophyll imaging. However, the development of a new macroscopic and microscopic system equipped with an ultrafast camera was successful in imaging some fluorescence parameters in a study about cadmium and zinc toxicity (Küpper et al. 2019).

Chapter 1:

Photosystem II photoinhibition and photoprotection in a lycophyte, *Selaginella martensii*

Premise

Ancestral tracheophytes belonging to the Lycophyte division experienced their period of maximum proliferation in the Carboniferous, about 300 million years ago (Pryer et al. 2004). During that geological period, environmental conditions were very different from those we know today. The average temperature at the beginning of the Carboniferous was about 20 ºC, while the concentration of atmospheric CO_2 was as much as eight times higher than that recorded today. However, the situation changed profoundly as time went on, bringing a drop in temperature down to 12 ºC and in CO_2 concentration to levels similar to those recorded today. The photosynthetic activity of the plants that existed at the time is certainly among the main contributors to this environmental transformation. During the Early Carboniferous, the vegetation was very different from today; it was dominated by lycophytes, *i.e.*, plants with microphylls, which are particularly suited to grow in a CO_2-rich environment. The proliferation of lycophytes, including herbaceous species belonging to the genus *Selaginella*, caused the CO_2 levels to gradually decrease in parallel with the increase in O_2 concentration. Therefore, these new environmental conditions led to the radiation of plant species belonging to the other clade of vascular plants, the euphyllophytes. Such plants were more competitive than lycophytes, as they have larger leaves (macrohphylls) with higher carbon fixation capacity, namely they could make a better use of a low CO_2 pressure in the atmosphere, while benefitting from a much higher efficiency in leaf cooling by water evapo-transpiration (Beerling et al. 2001). Nowadays, euphyllophytes constitute 99% of the vascular plant species on Earth, while lycophytes only around 1%. The latter have often found space in specific ecological niches, where the habitat has features enabling them to compete successfully with more modern vascular plants, particularly angiosperms. Likewise other *Selaginella* species (Liu et al. 2020), it is precisely in one of these contexts that *Selaginella martensii* finds its home, that is the shade environments of the lowest vegetation layers in tropical-equatorial rainforests, mainly in Central America. *S. martensii* therefore exhibits some typical morpho-functional characteristics of adaptation to the shade, but nevertheless it has a surprising ability to long-term acclimate not only to extreme shade but also to direct sunlight (Ferroni et al. 2016, 2021). Some very important differences were previously evidenced in the photosynthetic membrane organization and functioning compared to more modern vascular plants. First of all, S. *martensii* exhibits peculiar phosphorylation patterns of the antenna complexes of PSII, resulting in a greater capacity for thermal dissipation of excess energy absorbed under high light conditions (Ferroni et al. 2014, 2018). Moreover, the acclimation to different light regimes involves the modulation of the stoichiometric ratio between the two photosystems (in favor of PSI upon acclimation to higher light regimes) but does not involve the regulation of the LHCII antenna content (Ferroni et al. 2016). Rather than the amount of LHCII antenna, which is extremely abundant in comparison with the two photosystems, *S. martensii* modulates the association of the free LHCII trimers with the two photosystems. It was observed that in plants acclimated to high light intensities, the formation of megacomplexes involving PSII, PSI-LHCI and LHCII is promoted, with possible photoprotective implications for both the photosystems. Interestingly, such extensive re-organization of the thylakoid complexes, accompanied by the re-arrangement of the thylakoid architecture, is not followed by any major modulation of the thermal dissipation capacity, which remains invariably high even when the plants are grown under an

extreme shade regime. Therefore, there is a major gap in our understanding about how an ancient vascular plant inhabiting shade environments can be able to cope with extreme light regimes, such as the deep shade and the full sunlight, without seemingly change its potential for safe thermal dissipation. We do not known whether the level of PSII photoprotection under such contrasting light regimes is the same or not.

This Chapter examines this problem exploiting a chlorophyll *a* fluorescence method based on the parameter called "photochemical quenching in the dark" (qP_d), which can allow to determine the photoprotective potential of NPQ. The Chapter proposes the following paper in editorial version, including the accompanying supplementary materials:

Colpo, A., Baldisserotto, C., Pancaldi, S., Sabia, A., & Ferroni, L. (2022). Photosystem II photoinhibition and photoprotection in a lycophyte, *Selaginella martensii*. *Physiologia Plantarum*, *174*(1), e13604.

References

Beerling, D. J., Osborne, C. P., & Chaloner, W. G. (2001). Evolution of leaf-form in land plants linked to atmospheric CO2 decline in the Late Palaeozoic era. *Nature*, 410(6826), *352*-354.

Ferroni, L., Angeleri, M., Pantaleoni, L., Pagliano, C., Longoni, P., Marsano, F., Aro, E. M., Suorsa, M., Baldisserotto, C., Giovanardi, M., Cella, R., & Pancaldi, S. (2014). Light-dependent reversible phosphorylation of the minor photosystem II antenna Lhcb6 (CP 24) occurs in lycophytes. The Plant Journal, 77(6), 893-905.

Ferroni, L., Brestič, M., Živčak, M., Cantelli, R., & Pancaldi, S. (2021). Increased photosynthesis from a deep-shade to high-light regime occurs by enhanced CO2 diffusion into the leaf of *Selaginella martensii*. *Plant Physiology and Biochemistry*, 160, 143-154.

Ferroni, L., Cucuzza, S., Angeleri, M., Aro, E. M., Pagliano, C., Giovanardi, M., Baldisserotto, C., & Pancaldi, S. (2018). In the lycophyte *Selaginella martensii* is the "extra-qT" related to energy spillover? Insights into photoprotection in ancestral vascular plants. *Environmental and Experimental Botany*, *154*, 110-122.

Ferroni, L., Suorsa, M., Aro, E. M., Baldisserotto, C., & Pancaldi, S. (2016). Light acclimation in the lycophyte Selaginella martensii depends on changes in the amount of photosystems and on the flexibility of the light-harvesting complex II antenna association with both photosystems. *New Phytologist*, *211*(2), 554-568.

Liu, J. W., Li, S. F., Wu, C. T., Valdespino, I. A., Ho, J. F., Wu, Y. H., Chang, H. M., Guu, T. Y., Kao, M. F., Chesson, C., Das. S., Oppenheimer, H., Bakutis, A., Saenger, P., Allen, N. S., Yong, J. W. H., Adjie, B., Kiew, R., Nadkarni, N., Huang, C. L., Chesson, P., & Sheue, C. R. (2020). Gigantic chloroplasts, including bizonoplasts, are common in shade-adapted species of the ancient vascular plant family Selaginellaceae. *American Journal of Botany*, *107*(4), 562-576.

Pryer, K. M., Schuettpelz, E., Wolf, P. G., Schneider, H., Smith, A. R., & Cranfill, R. (2004). Phylogeny and evolution of ferns (monilophytes) with a focus on the early leptosporangiate divergences. *American Journal of Botany*, *91*(10), 1582-1598.

Received: 24 May 2021 | Revised: 9 November 2021 | Accepted: 19 November 2021

DOI: 10.1111/ppl.13604

ORIGINAL ARTICLE

Physiologia Plantarum

Photosystem II photoinhibition and photoprotection in a lycophyte, *Selaginella martensii*

Andrea Colpo | **Costanza Baldisserotto** | **Simonetta Pancaldi** | **Alessandra Sabia** | **Lorenzo Ferroni**

Department of Environmental and Prevention Sciences, University of Ferrara, Ferrara

Correspondence
Lorenzo Ferroni, Department of Environmental and Prevention Sciences, University of Ferrara, Corso Ercole I d'Este 32, 44121 Ferrara.
Email: lorenzo.ferroni@unife.it

Edited by A. Krieger-Liszkay

Abstract

The Lycophyte *Selaginella martensii* efficiently acclimates to diverse light environments, from deep shade to full sunlight. The plant does not modulate the abundance of the Light Harvesting Complex II, mostly found as a free trimer, and does not alter the maximum capacity of thermal dissipation (NPQ). Nevertheless, the photoprotection is expected to be modulatable upon long-term light acclimation to preserve the photosystems (PSII, PSI). The effects of long-term light acclimation on PSII photoprotection were investigated using the chlorophyll fluorometric method known as "photochemical quenching measured in the dark" (qP_d). Singularly high-qP_d values at relatively low irradiance suggest a heterogeneous antenna system (PSII antenna uncoupling). The extent of antenna uncoupling largely depends on the light regime, reaching the highest value in sun-acclimated plants. In parallel, the photoprotective NPQ (pNPQ) increased from deep-shade to high-light grown plants. It is proposed that the differences in the long-term modulation in the photoprotective capacity are proportional to the amount of uncoupled LHCII. In deep-shade plants, the inconsistency between invariable maximum NPQ and lower pNPQ is attributed to the thermal dissipation occurring in the PSII core.

1 | INTRODUCTION

The evolution of the photosynthetic apparatus allowed land plants to adapt to a broad range of light conditions, from extreme shade to full sunlight. However, any change in light regime during the plants' lifetime represents a major threat to their survival and requires structural and functional adjustments of their photosynthetic machinery (developmental acclimation) (Lichtenthaler et al., 2007; Pribil et al., 2014; Ruban et al., 2012).

Selaginella martensii Spring is a shade plant typical of the understory of tropical and equatorial rainforests. However, this ancient tracheophyte is sufficiently flexible to acclimate to extreme light regimes, such as deep shade or full sunlight (Ferroni et al., 2016; Ferroni, Brestič, et al., 2021). Its long-term acclimation to different light regimes produces major rearrangements in the thylakoid organization and photosystem I (PSI) and II (PSII) relative abundance, whereas, unlike most angiosperms, it does not modulate the light-harvesting antenna complex II (LHCII) content and the total thermal dissipation capacity of absorbed excess energy (Ferroni et al., 2016).

Deep-shade (L) acclimated thylakoids of *S. martensii* are characterized by a peculiar pseudo-lamellar organization, while both mid-shade (M) and full-sunlight (H) plants display a predominant granal structure. The PSI/PSII ratio increases from L to H plants because the PSI content rises in parallel to the increasing light availability, while PSII is more abundant in L and M plants than H. In contrast, the relative amount of LHCII does not change in response to light acclimation (Ferroni et al., 2016). This characteristic seems typical of seedless plants (Gerotto et al., 2011), while angiosperms generally cope with

increasing light availability by decreasing the LHCII content (Albanese et al., 2019; Ballottari et al., 2007; Flannery et al., 2021; Schumann et al., 2017). However, despite the invariable LHCII content, the long-term light acclimation in *S. martensii* strongly influences the LHCII association with PSII. PSII-LHCII supercomplexes are not high in abundance in native gels of *S. martensii* thylakoids, but the amount is clearly higher in L and M than in H plants (Ferroni et al., 2014, 2016). Higher abundance of PSII-LHCII supercomplexes in L plants responds to the need for a larger PSII antenna to enhance the harvesting process under limiting light conditions. In contrast, H plants conceivably need a smaller PSII antenna because the light availability is not limiting, and the safe management of excess light is instead the priority. In fact, in *S. martensii* the great majority of LHCII antennae do not form stable complexes with PSII but are found in the form of free trimers (Ferroni et al., 2016). Free LHCII trimers are common in *Viridiplantae*, and their function is a hot topic in photosynthesis research, being possibly involved in thermal dissipation of excess absorbed energy (Holzwarth et al., 2009; Horton et al., 2005; Johnson et al., 2011; Nicol et al., 2019; Shukla et al., 2020), PSII connectivity (Haferkamp et al., 2010; Zivcak et al., 2014), PSI-PSII interconnectivity (Grieco et al., 2015; Wientjes et al., 2013; Wood & Johnson, 2020). Moreover, the thylakoid membrane of *S. martensii* is characterized by permanent megacomplexes comprised of PSII, PSI, and LHCII, which presence increases from L to H plants (Ferroni et al., 2016). The abundance of these megacomplexes is regulated in response to a short-term high-light exposure; in particular, their increase suggests a facilitating role for the energy repartition between PSI and PSII through a mechanism of energy spillover (Ferroni et al., 2016; Yokono et al., 2015).

Non-photochemical quenching (NPQ) is an operative parameter in fluorescence analysis quantifying the decrease in maximum fluorescence of PSII (F_m) in the dark-acclimated state to a lower value F_m' in the light-acclimated state (Bilger & Björkman, 1990). NPQ is due to a series of light-induced dissipative processes in competition with PSII photochemistry, and, in general, NPQ can be divided into photoprotective and photoinhibitory quenching components. The main photoprotective component is qE, the high energy-dependent quenching caused by the onset of the transthylakoid ΔpH and upregulated by PsbS activity and zeaxanthin formation (see for review Ruban, 2016). The other minor NPQ components are related to a sustained violaxanthin de-epoxidation to zeaxanthin (qZ), state transitions linked to phosphorylated LHCII movement from PSII to PSI (qT), light avoidance chloroplast movements (qM) and plastid lipocalin-dependent antenna quenching qH (see for review Malnoë, 2018; Roach & Krieger-Liszkay, 2014). The photoinhibitory component is qI, which depends on the thermal dissipation occurring at the photoinactivated PSII (Aro et al., 1993; Demmig-Adams et al., 2012). In angiosperms, the total NPQ amplitude is mostly due to its qE component and modulated in response to the light environment, increasing from shade to sun plants (Ballottari et al., 2007; Demmig-Adams, 1998; Demmig-Adams et al., 2015; Mishra et al., 2012; Schumann et al., 2017; Stewart et al., 2015). Accordingly, angiosperms grown under high light are characterized by a higher photoprotective capacity compared to the shade-grown (Mathur et al., 2018; Wilson & Ruban, 2020a). Conversely, *S. martensii* plants display a high and invariable total NPQ amplitude, particularly qE amplitude and PsbS content are the same regardless of the light acclimation history of the plant (Ferroni et al., 2016; Ferroni, Brestič, et al., 2021). Nevertheless, there is no evidence whether the PSII photoprotective fraction of NPQ, which prevents PSII photoinactivation, could similarly be independent of long-term light acclimation in *S. martensii*.

Upon exposure to intense light, PSII photoinactivation can be quantified destructively by monitoring the degradation rate of the D1 PSII core protein (Aro et al., 1993; Kato et al., 2012; Keren et al., 1995) or by the light-saturated oxygen evolution of PSII in the presence of an artificial electron acceptor (Delieu & Walker, 1983; Mattila et al., 2020; Öquist et al., 1992; Schansker & van Rensen, 1999); however, it is more easily and precisely analyzed in vivo as the decline of PSII photochemical quantum yield (Campbell & Tyystjärvi, 2012; Chow et al., 1991; Mattila et al., 2020; Schansker & van Rensen, 1999) and/or the persistence of a sustained NPQ fraction in darkness (Demmig-Adams et al., 2012; Nilkens et al., 2010). Ruban and Murchie (2012) proposed an alternative, fast and non-invasive method to monitor the PSII photoinactivation. Their chlorophyll fluorescence approach is based on the calculation of the parameter qP_d, "*photochemical quenching measured in the dark*." qP_d assesses the onset of PSII photoinactivation by comparing two values of minimum fluorescence (F_0'): (a) the actual minimum fluorescence measured after a short far-red stimulation ($F_{0'act}$) and (b) the value of F_0' calculated according to Oxborough and Baker (1997), which is an estimate of F_0' as a function of NPQ ($F_{0'calc}$). qP_d varies theoretically between 0 and 1; in the absence of photoinactivation, $F_{0'calc}$ matches $F_{0'act}$, and correspondingly $qP_d = 1$. The occurrence of photoinactivation affects only $F_{0'act}$, whereas $F_{0'calc}$ does not account for it; hence, $F_{0'calc}$ underestimates F_0' (i.e., $F_{0'calc} < F_{0'act}$), and qP_d drops consequently below 1. The theoretical lower limit $qP_d = 0$ could be only reached when all the PSII reaction centers are closed and photoinactivated. qP_d values are monitored during experiments in which a plant sample is exposed to subsequent steps with increasing irradiance (light curves). Ruban and Murchie (2012) empirically fixed $qP_d \leq 0.98$ as the threshold to assess the onset of PSII photoinactivation during a light curve. Accordingly, the effectiveness of photoprotection provided by NPQ to PSII corresponds to the last value of NPQ that allows a qP_d value above 0.98. This method was developed and broadly validated in Alexander Ruban's Laboratory in the model angiosperm *Arabidopsis thaliana*, including mutants, chemical treatments, and acclimation to contrasting light regimes (Giovagnetti & Ruban, 2015; Ruban & Belgio, 2014; Tian et al., 2017; Townsend et al., 2018; Ware et al., 2015, 2016; Wilson & Ruban, 2019, 2020b). More recently, the qP_d method was also applied to other photosynthetic organisms, such as the spring ephemeral *Bertereoa incana*, *Prunus cerasifera*, *Oryza sativa*, and the algal reef builder *Neogoniolithon* sp. (Gefen-Treves et al., 2020; Lo Piccolo et al., 2020; Okegawa et al., 2020; Wilson & Ruban, 2020a). However, the *phototropin 2* mutant of *A. thaliana*, which is unable to produce light-avoidance chloroplast movements, was found to be completely insensitive to photoinhibition according to the qP_d method (Wilson & Ruban, 2020b), while it is instead known to be extremely prone to

photobleaching (Cazzaniga et al., 2013). Consequently, Bassi and Dall'Osto (2021) consider the qP_d method insufficiently validated, that is, not always leading to results consistent with independent methods.

In *S. martensii*, the variability in PSII photoprotection is expected from an ecophysiological point of view, but it seems hardly compatible with the constancy of NPQ and qE amplitudes across L, M, and H plants. The use of the qP_d method in the lycophyte *S. martensii* may potentially unveil whether the long-term acclimation to contrasting light regimes influences the PSII photoprotection capacity. Given the recent introduction of the method and the non-angiosperm plant species, the qP_d method was checked for consistency with a direct assessment of PSII quantum yield loss upon light exposure. The present study shows that the photoprotective capacity of NPQ well matches the growth light regime in *S. martensii*. Moreover, the qP_d method indicates the relevance of antenna uncoupling in PSII photoprotection, suggesting a physiological role for the abundant and invariable amount of LHCII in ancient vascular plants.

2 | MATERIALS AND METHODS

2.1 | Plant material and growth conditions

Selaginella martensii Spring (Selaginellaceae) plants were cultivated in a humid greenhouse of the Botanical Garden of Ferrara, Italy (N 44°50′30″, E 11°37′22″), at 25–30°C and subjected to the natural photoperiod. Deep-shade plants (L) were grown in conditions of natural shade, with light sheltered by upper-broadleaved plants. During the daytime, the irradiance maximum was below 10 μmol m^{-2} s^{-1} of photosynthetic photon fluence rate (PPFR). A second group of plants (M) was long-term acclimated to the mid-shade light regime (PPFR <80 μmol m^{-2} s^{-1}), that is, the typical light environment experienced by *S. martensii* in its natural habitat. Finally, high-light grown plants (H) were exposed to direct sunlight, which provided typically a maximal PPFR higher than 800 μmol m^{-2} s^{-1}. Subsequent biochemical and fluorometric analyses were performed on the terminal branches after at least 3 weeks of acclimation to each light regime.

2.2 | Thylakoid isolation and blue-native gel electrophoresis

Branches of *S. martensii* plants were dark acclimated for 1 h. Terminal branches were harvested and grinded in an ice-cold (−20°C) mortar in the presence of a grinding buffer (Järvi et al., 2011). The whole thylakoid isolation was performed according to Järvi et al., 2011. Extracted thylakoids were promptly frozen and stored in liquid nitrogen until use. For quantification of pigments, thylakoids were solubilized in 90% (v/v) acetone buffered with HEPES-KOH (pH 7.8) and analyzed using a spectrophotometer Ultrospec 2000 (Pharmacia Biotech). Chlorophyll *a* and *b* content were determined according to Ritchie (2006), while Wellburn's equation (Wellburn, 1994) was used to determine the carotenoid content. For electrophoresis, thylakoid solubilization was performed according to Järvi et al. (2011) using 1.5% β-dodecylmaltoside. Blue-native gel electrophoresis (BN-PAGE) was performed according to Järvi et al. (2011), with modifications as in Giovanardi et al. (2018), maintaining the electrophoretic chamber at 0°C.

2.3 | Chlorophyll fluorescence measurements

Modulated chlorophyll fluorescence was measured using a Walz Junior PAM (Walz) on independent samples previously dark-acclimated for 30 min. All the measurements were performed in the morning to avoid the presence of photoinhibition, especially in H plants. Light curves were recorded applying a simplified version of the method described by Ruban and Murchie (2012). Before light exposure, minimum (F_0) and maximum (F_m) fluorescence levels in the dark were measured with the saturating pulse (SP, 0.6 s) method, and the variable fluorescence was calculated as $F_v = F_m - F_0$. $F_v/F_m > 0.75$ was imposed as the minimum acceptable value of PSII quantum yield: plants with lower F_v/F_m were excluded from the analysis. This first measurement was followed by 12 steps of actinic light illumination from 25 to 1500 μmol m^{-2} s^{-1}, each lasting 5 min to reach quasi-steady-state conditions. Maximum fluorescence level of the quenched, light-acclimated state (F_m') was measured at the end of each actinic light step upon applying an SP. The minimum fluorescence level in the light-adapted state ($F_{0'act}$) was determined as the lowest value when applying a 7-s-long far red-light pulse with the actinic light switched off (Van Kooten & Snel, 1990). Quantum yields of actual PSII photochemistry [Y(II)], non-regulatory energy loss [Y(NO)], and regulatory thermal dissipation [Y(NPQ)] were calculated according to Hendrickson et al. (2004). The 1-qP parameter was calculated as an indicator of the excitation pressure inside PSII according to Schreiber et al. (1986). F_m quenching to F_m' following the onset of light-induced thermal dissipation was quantified using the Stern-Volmer NPQ parameter (Bilger & Björkman, 1990). NPQ equals the Y(NPQ)/Y(NO) ratio (Ferroni et al., 2014; Lazár, 2015).

In addition to the light curves, induction curves were also recorded at fixed independent irradiances. After the 30-min dark-acclimation, the samples were exposed to 19 min of continuous actinic light illumination (24, 45, 65, 90, 125, 190, 285, 420, 625, and 820 μmol m^{-2} s^{-1}), each followed by 38 min and 30 s of dark relaxation. F_m' and F_0' fluorescence levels were measured every minute during the light induction and at intervals with increasing length during the dark relaxation (30 s, 1 min, 2 min, 5 min, 10 min, and 20 min). The PSII quantum yield loss because of photoinhibition, Y(qI), was calculated as the difference between the PSII quantum yields in the dark-acclimated sample before the induction curve (F_v/F_m) and at the end of the dark-relaxation period.

2.4 | qP_d parameter and photoprotective NPQ quantification

qP_d parameter was calculated at the end of each actinic light illumination step according to Ruban and Murchie (2012). Briefly, qP_d

compares the actual and calculated values of minimal fluorescence of the light-adapted state samples as it follows:

$$qP_d = \frac{F'_m - F'_{0\,act}}{F'_m - F'_{0\,calc}}$$

where $F_0'_{act}$ is the measured minimum fluorescence level, and $F_0'_{calc}$ is the theoretical minimum fluorescence level according to Oxborough and Baker (1997). However, because at low-medium irradiances qP_d was generally found >1, $F_0'_{calc}$ values were corrected as described by Ware et al. (2015) accounting for uncoupled and loosely coupled PSII antenna, thus obtaining the new estimate of $F_0'_{calc}$ in the case of a heterogeneous antenna, $F_0'_{het}$:

$$F'_{0\,het} = \left(\frac{1}{nF_0 + F} - \frac{1}{F_m} + \frac{(NPQ+1)(mNPQ+1)}{F_m[n(mNPQ+1) + (1-n)(NPQ+1)]}\right)^{-1}$$

where F_0 and F_m are the entry constants and NPQ is the independent variable. *n* (fraction of coupled antenna), *m* (relative NPQ amplitude of the uncoupled antenna), and *F* (relative fluorescence emission of the uncoupled antenna) are fitting parameters. We further define the fraction of uncoupled antenna *U* as 1-*n*. The fitting procedure was performed using Origin software v. 2020b or 2021 (OriginLab Corporation, USA). $F_0'_{het}$ values were used in the qP_d equation allowing the estimation of qP_d in the case of a heterogeneous antenna system of *S. martensii* ($qP_{d\ het}$) as described by Ware et al. (2015):

$$qP_{d\,het} = \frac{F'_m - F'_{0\,act}}{F'_m - F'_{0\,het}}$$

pNPQ was determined according to Ruban and Murchie (2012) as the last value of NPQ corresponding to $qP_{d\ het} > 0.98$. pNPQ values relative to the independent samples were used to obtain the average pNPQ values for each plant group.

2.5 | Light-tolerance curves

Light tolerance curves were determined for each plant group plotting the fraction of photoinactivated samples at a given irradiance (those with $qP_{d\ het} < 0.98$) with the light intensity as described by Ware et al. (2015). Instead of the Hill equation used by Ware et al. (2015), regression curves were produced fitting the data with the following logistic equation using Origin software:

$$\text{photoinactivated samples fraction} = 1 - \frac{1}{1 + \left(\frac{I_x}{I_{50}}\right)^p}$$

where I_{50} is the irradiance responsible for the photoinactivation of half the samples and I_X is the irradiance corresponding to a given fraction of photoinactivated samples. The fitting parameter *p* can be related to the intrinsic propensity of the specific plant group to PSII photoinactivation.

2.6 | Data treatment

Statistical analyses and graphical representations were performed using Origin software. Statistical differences were tested by ANOVA followed by a post-hoc Tukey test, using a threshold of $P < 0.05$.

3 | RESULTS

Thermal dissipation capacity in *S. martensii* acclimated to different light regimes

Compared to L and M plants, the leaf pigmentation was visibly more yellow-green in H, as a consequence of the carotenoid accumulation, while only limited changes affected the chlorophyll *a/b* ratio (Figure 1A and Figure S1). BN-PAGE gel analysis confirmed the low abundance of PSII-LHCII supercomplexes, especially in H plants. The LHCII free trimers formed the most intense band in all the three plant groups without apparent differences (Figure S2; Ferroni et al., 2016). The Y(II) drop with light intensity was expectedly more marked in L plants than in M or H (Figure 1B). The higher photochemical capacity of H plants suggested a higher tolerance to PSII photoinactivation compared to the other plant groups. Such differences were more important at the early-intermediate steps of the light curves, converging toward similarly low values at the end of the light exposure (Figure 1B). In parallel, Y(NO) was higher in L plants at low-intermediate irradiances, confirming the lower efficiency of this plant group in light energy management (Figure 1C). The higher effectiveness in recovering Y(NO) to stable low values under increasing irradiances in H plants indicated an improved ability to control the plastoquinone pool reduction state compared with L and M plants (Tikkanen et al., 2015). This contributed to a lower excitation pressure inside PSII (1-qP) in H plants (Figure 1E). At higher irradiances Y(NO) stabilized to a plateau value both in M and H plants, while in L plants, it decreased continuously, suggesting, in the latter, the occurrence of an additional mechanism responsible for a decrease in the electron inflow into the chain (Figure 1C). Finally, the differences in Y(NPQ) trend were relatively minor, indicating that the thermal dissipation mechanisms had a similar amplitude in the three plant groups. To the scope of the qP_d method, the thermal dissipation was quantified using NPQ.

The steep rise in NPQ at the initial irradiances was very similar in all three groups, while the curves diverged at 125 μmol m^{-2} s^{-1} when NPQ was more intense in H plants than in M and L (Figure 2A). Such divergence was maintained between H and M plants up to the highest irradiance when it approached a plateau. Differently, in L plants NPQ increased strongly over the entire range of irradiance because of the decrease in Y(NO). The maximum capacity of thermal dissipation (NPQ_{MAX}) spanned a relatively small range of values in L, M, and H plants (4.39–5.45; Figure 2B).

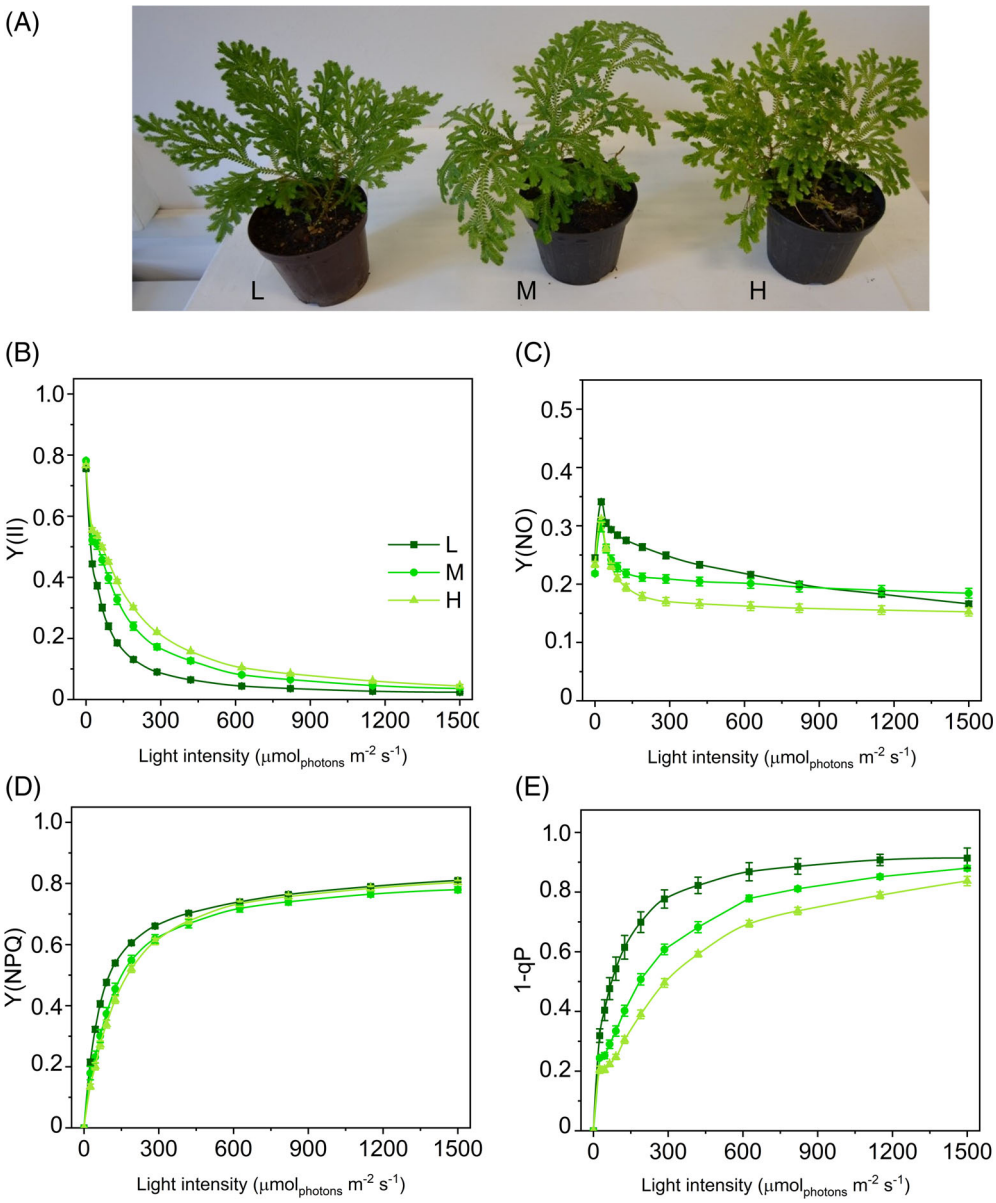

FIGURE 1 Long-term light-acclimation features of photosynthesis in *Selaginella martensii* acclimated to three natural light regimes. (A) Plants grown in deep shade (L, left), intermediate shade (M, center), and high light (H, right). Light curves relative to: (B) actual quantum yield of PSII photochemistry Y(II), (C) quantum yield of constitutive energy dissipation Y(NO), (D) quantum yield of regulatory thermal dissipation Y(NPQ), and (E) excitation energy pressure inside PSII (1-qP). Average values ±standard error for $n = 12$ (L), 16 (M), 18 (H)

3.1 | In sun plants PSII photoprotection is higher and accompanied by PSII antenna uncoupling

Given the similar NPQ_{MAX} in all plants, we used the qP_d method to investigate whether the photoinhibition was likewise weakly related to the light-acclimation regime. A drop in qP_d below the 0.98 thresholds indicates the onset of PSII photoinhibition and identifies at which irradiance the PSII photoprotective mechanisms start becoming less effective (Ruban & Murchie, 2012). Average qP_d-light response curves pointed out that the PSII sensitivity to photoinhibition could depend on the light regime (Figure 3A–C). In L plants, qP_d was less than 0.98 at lower irradiance (90 μmol m^{-2} s^{-1}) compared to M (190 μmol m^{-2} s^{-1}) and even more H (625 μmol m^{-2} s^{-1}) plants. Similarly, the covariation of qP_d and NPQ seemed to indicate a big difference in the photoprotection offered by NPQ in H, M, and L plants, where the still photoprotective NPQ values could be around 4.7, 2.7, and 1.7, respectively (Figure 3D–F). Unfortunately, the application of the qP_d method in its original formulation was evidently affected by an important shortcoming since the qP_d values were consistently above 1 at the lower irradiances in all the plant groups. This observation strongly indicated that the two basic processes to which the qP_d variations are attributed (NPQ and PSII photoinactivation) were not sufficient to explain qP_d trends in *S. martensii*. In particular, the qP_d method postulates a homogeneous antenna system. However, the occurrence of PSII antenna uncoupling can produce distortions in photoinhibition monitoring using qP_d. A modified calculation protocol allows accounting for the antenna uncoupling to obtain reliable qP_d in the hypothesis of antenna heterogeneity, $qP_{d\ het}$ (Ware et al., 2015). According to the heterogeneous antenna model, uncoupled and loosely coupled PSII antennae are responsible for the increase in qP_d above 1 observed at the early stages of the light

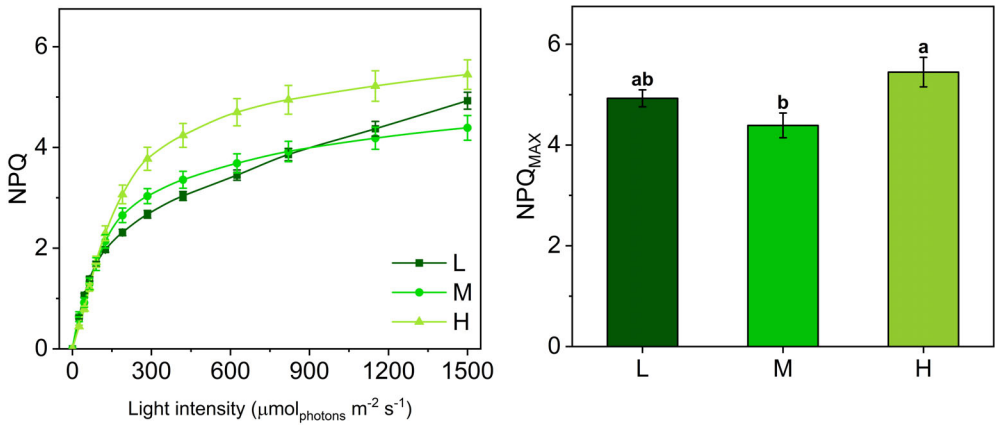

FIGURE 2 NPQ light-response curves and maximum NPQ values in *Selaginella martensii* acclimated to three natural light regimes. (A) NPQ-light response curves of deep shade (L, dark green), intermediate shade (M, green), and high light (H, pale green) plants during 60-min exposure to increasing actinic light intensities. Average values ±standard error for $n = 12$ (L), 16 (M), 18 (H). (B) Maximum NPQ values (NPQ_{MAX}) reached at the end of the light curve. Histogram represents average values ±standard error for $n = 12$ (L), 16 (M), 18 (H); different letters indicate a significant difference at $P < 0.05$, as determined using one-factor ANOVA followed by Tukey's test

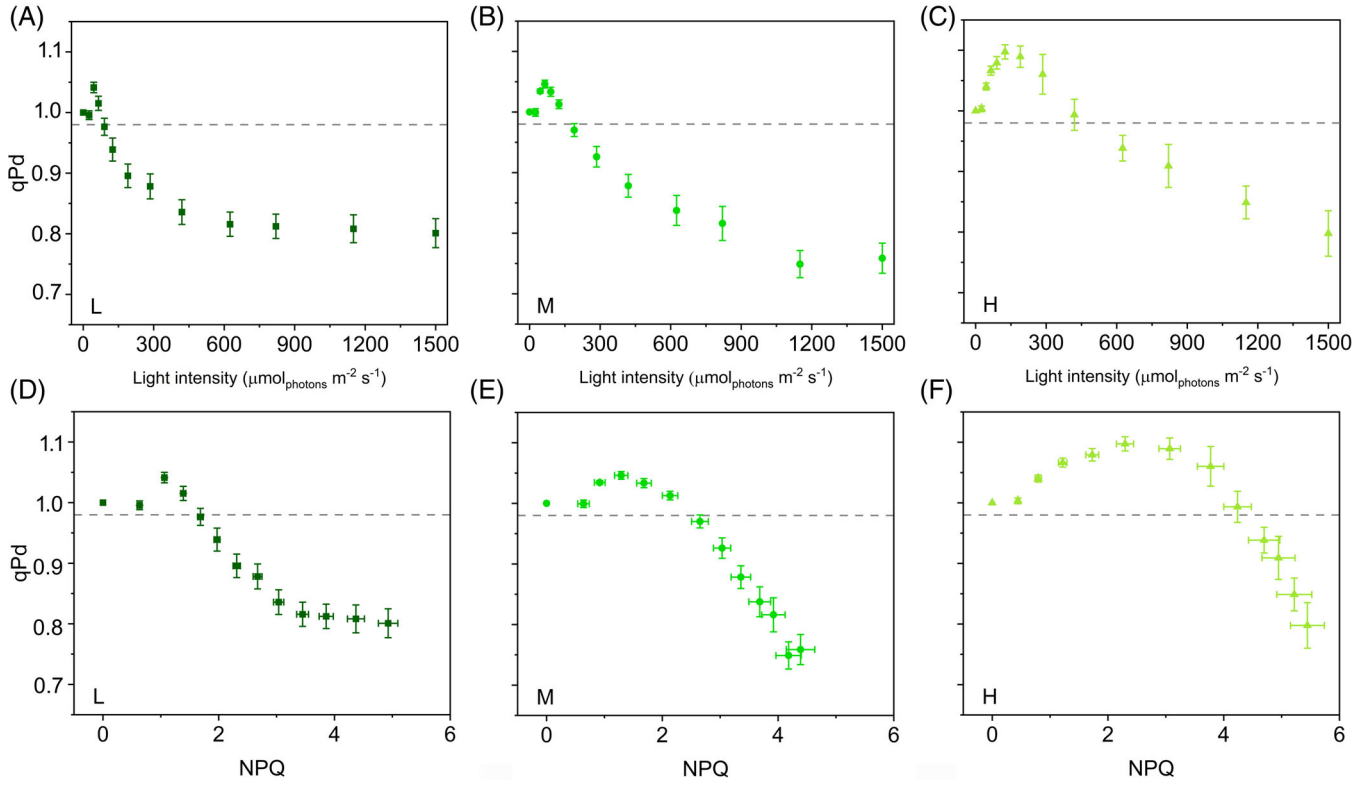

FIGURE 3 Photochemical quenching measured in the dark (qP_d) in the hypothesis of a homogeneous antenna system in *Selaginella martensii* acclimated to three natural light regimes. (A–C) qP_d-light response curves of deep shade (L, dark green), intermediate shade (M, green), and high light (H, pale green) plants during 60-min exposure to increasing actinic light intensities. (D–F) qP_d versus NPQ curves of L, M, and H plants. In all cases, some data points correspond to $qP_d > 1$, excluding the correctness of the homogeneous antenna model. Dashed-gray horizontal line represents the photoinactivation threshold of $qP_d = 0.98$. Average values ± standard error for $n = 12$ (L), 16 (M), 18 (H)

curve. This distortion is caused by an underestimation of the NPQ-dependent $F_0'_{calc}$ (Oxborough & Baker, 1997) and can be compensated by applying a correction to the $F_0'_{calc}$ formula (see Materials and Methods for details). Such correction is exemplified for the average $F_0'_{act}$-NPQ curves in Figure S3. $F_0'_{act}$ was fitted with a hyperbolic function of NPQ to obtain new $F_0'_{calc}$ values ($F_0'_{het}$) that be almost superimposable to $F_0'_{act}$ at least at the lower values of NPQ (i.e., at NPQ values corresponding to $qP_d > 1$ as in

Figure 3D–F). The fitting procedure re-established qP_d ca. 1 at the low irradiances and depended on three parameters: *m*, *F*, *U*.

m and *F* represent the relative NPQ amplitude produced by uncoupled antennae and their relative fluorescence, respectively. They can be considered as "structural" parameters of the antenna system. According to Ware et al. (2015), *m* was fixed to 2, accepting estimates by Belgio et al. (2012) of a doubled quenching capacity by uncoupled antennae compared to the coupled in *Arabidopsis thaliana*. Ware et al. (2015) assumed a constant *F* equal to 0.5. Differently, we let *F* vary freely between 0 and 1: *F* was quite uniform in the three plant groups, fluctuating between 0.21 and 0.29 (Figure 4A). These lower values may indicate a structurally lower fluorescence emission by uncoupled antennae in the phylogenetically distant *S. martensii*. However, the correctness of *m* and *F* strongly depends on the validity of the assumption of the heterogeneous antenna model proposed by Ware et al. (2015). For instance, in an artificial system, the quenching capacity by uncoupled antennae was found to be similar or even smaller than that of the coupled antennae (Tian et al., 2015). However, in our study, fitting tests using different combinations of *F* and *m*, for example, closer to the value of 1, were unproductive. Conversely, the Ware's heterogeneous antenna model is internally consistent and indicated that the apparent differences among plant groups were almost exclusively due to the parameter *U*. This is the fraction of uncoupled antenna and can vary between 0 (all antenna is coupled with PSII) and 1 (all antenna is uncoupled from PSII). L plants had $U = 0.22$, a value close to what estimated by Ware et al. (2015) in *A. thaliana* grown under low light (0.15–0.20; Figure 4B). In striking contrast, the M and H samples uncoupled ca. 2 and 3 times more antenna, respectively, reaching in the latter an outstanding level of PSII antenna uncoupling (Figure 4B).

qP_d values were corrected replacing $F_{0'\,calc}$ with $F_{0'\,het}$ in the qP_d equation, leading to the new parameter $qP_{d\ het}$. $qP_{d\ het}$ did not increase above 1 during the early steps of the light routine and was suitable for the quantification of the photoprotection offered by NPQ during 55 min of increasing actinic light illumination. pNPQ is now defined as the last value of

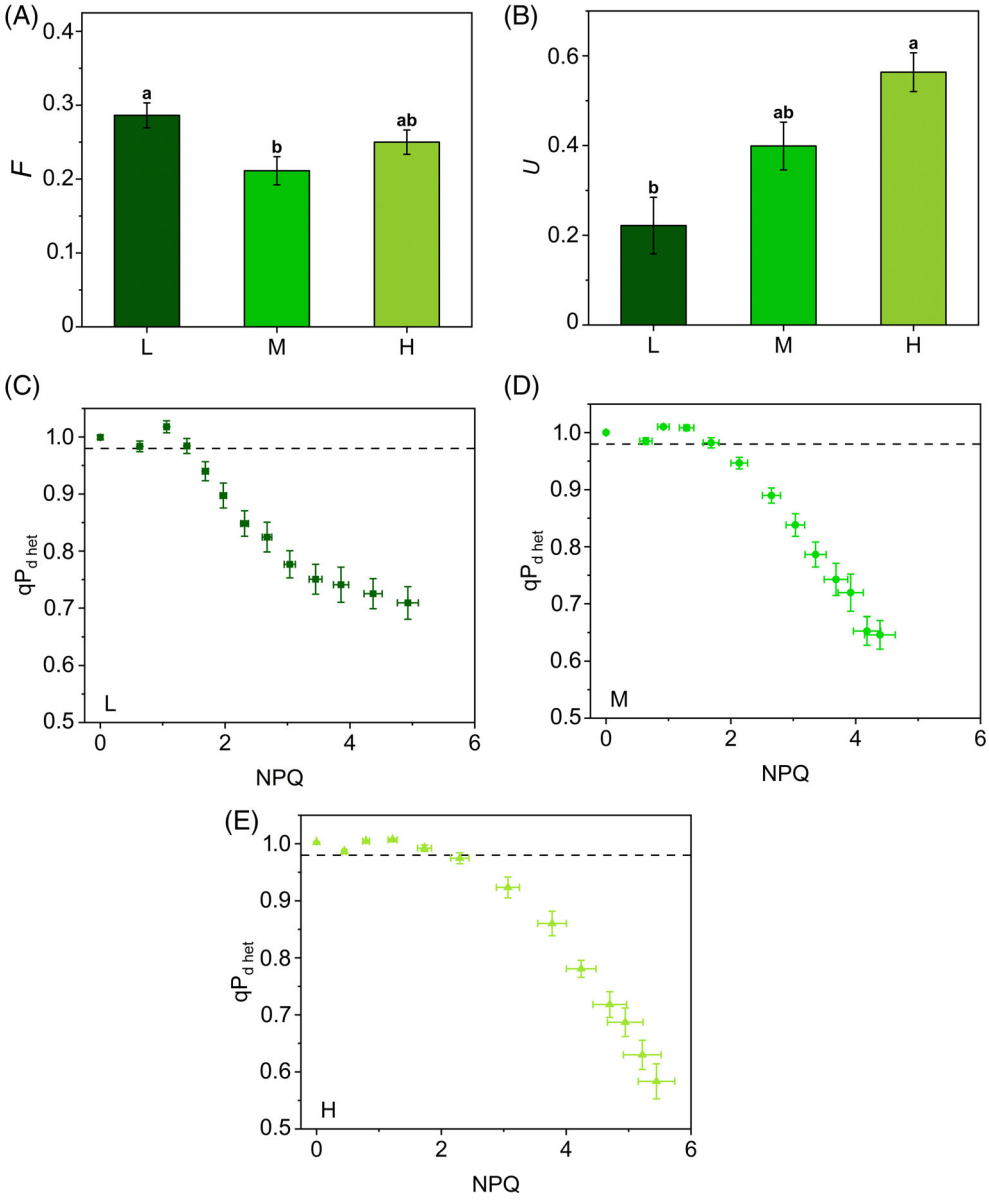

FIGURE 4 Photochemical quenching measured in the dark in context of a heterogeneous antenna system ($qP_{d\ het}$) in *Selaginella martensii* acclimated to three natural light regimes. Fitting parameters (calculated as described in Material and methods): (A) the relative fluorescence F emitted by uncoupled antenna and (B) the fraction U of PSII uncoupled antenna in deep shade (L, dark green), intermediate shade (M, green) and high light (H, pale green) plants. Histograms show average values ± standard error for n = 12 (L), 16 (M), 18 (H); different letters indicate a significant difference at $P < 0.05$, as determined using one-factor ANOVA followed by Tukey's test. (C–E) $qP_{d\ het}$ versus NPQ curves of L (C), M (D) and H (E) plants during 60-min exposure to increasing actinic light intensities. Note the effectiveness of the F and U parameters determination in reestablishing $qP_d \leq 1$. Dashed-gray horizontal line represents the photoinactivation threshold of $qP_{d\ het} = 0.98$. Average values ± standard error for $n = 12$ (L), 16 (M), 18 (H)

NPQ that maintains $qP_{d\ het}$ above the 0.98 threshold (Ware et al., 2015). $qP_{d\ het}$ was maintained above 0.98 for higher NPQ values in H plants than in M and L, showing a higher photoprotective capacity in the former, although to a well-reduced extent as compared to the estimates from uncorrected qP_d (see Figure 3A–C and 4C–E for comparison). H plants benefitted from 29% and 38% more pNPQ than M and L, respectively (Figure 5A). Photoinhibitory irradiances were re-determined as 70, 90, and 120 μmol m^{-2} s^{-1} for L, M, and H, respectively. Although pNPQ estimation can be strongly dependent on the light treatment (length, number, and intensity of the light intervals), pNPQ was strongly consistent with the growth light regime, in contrast to what observed for NPQ_{MAX} (Figure 2B). The pNPQ/NPQ_{MAX} ratio reported in Figure 5B indicated that ca. 40% of NPQ_{MAX} was photoprotective in H and M plants, while in L plants the photoprotective fraction was reduced to 29%.

3.2 | Validation of qP_d sensitivity to the onset of PSII photoinhibition

The light curves account for cumulative light-related effects occurring on the same sample exposed to increasing light intensities, but cannot allow a direct comparison of qP_d and PSII photoinhibition. To this aim, the qP_d method was also applied on the data obtained after independent light inductions to stable irradiances, followed by dark relaxation (see induction curves of NPQ, Figure S4A–J).

To allow an easier comparison of results obtained with two protocols (light curve or individual inductions), the qP_d values were sampled during the light induction based on the total number of photons conveyed to the sample. For instance, at the end of the step of 190 μmol m^{-2} s^{-1} in the light curve, 2700 μmol m^{-2} photons had been directed to the sample; during the induction curve at 190 μmol m^{-2} s^{-1}, a very close number of photons (2660 μmol m^{-2}) reached the sample after 14 min. The qP_d trends obtained from the induction curves were overall consistent with those derived from the light curves, including $qP_d > 1$ at low-medium irradiance (Figure S5 and Figure 5A–C). Similar to the original light-curve-based method, the actual level of PSII photoinhibition remained unknown.

Because the link between qP_d and photoinhibition is of vital importance to a well-grounded use of qP_d in *S. martensii*, $qP_{d\ het}$ values were then calculated at the end of the induction curves to compare them with the recovered F_v/F_m after the dark relaxation. The lost PSII yield is photoinhibition per definition, Y(qI). The preliminary fitting procedure of $F_0'_{act}$ values allowed the estimation of increasing *U* from L to M and H plants (0.39, 0.61, and 0.82). Higher *U* values compared to the light-curve experiment could be due to the different protocol used and the longer natural photoperiod experienced by the plants in the greenhouse (14 vs. 9 h day^{-1}). The resulting $qP_{d\ het}$-light curves revealed that, for stable and low values of Y(qI) (0.02), $qP_{d\ het}$ remained constantly and consistently above 0.98 (Figure 6A–C). Subsequently, when Y(qI) started to increase, $qP_{d\ het}$ dropped below 0.98, but, as expected, at lower light intensities in L plants compared to M and H (approximately 65, 125, and 125 μmol m^{-2} s^{-1}, respectively, Figure 6A–C). Therefore, despite the strong assumptions in the interpretation of qP_d, even stronger in context of antenna heterogeneity, we obtained empirical evidence of the link between $qP_{d\ het}$ decay and the onset of PSII photoinhibition in *S. martensii*. Importantly, $qP_{d\ het} < 0.98$ characterized the absence of photoinhibition, that is, the effectiveness of photoprotection. Again, higher levels of photoprotection were linked to higher values of *U*. Notwithstanding the different experimental setup, the irradiances determining the start of photoinhibition were close to those obtained in the original protocol of the $qP_{d\ het}$ experiment.

3.3 | $qP_{d\ het}$ decreasing phase under high light reveals a surprisingly strict control of photoinhibition in L plants

The second phase of the $qP_{d\ het}$ curves ($qP_{d\ het} < 0.98$) was characterized by a monotonous decay of $qP_{d\ het}$, which generally does not add further information about PSII photoprotection, as confirmed in M

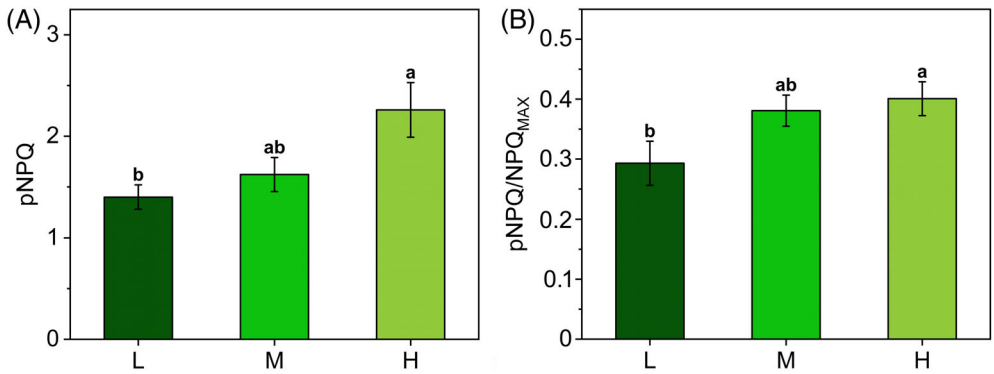

FIGURE 5 Quantification of photoprotection offered by the non-photochemical quenching (NPQ) in *Selaginella martensii* acclimated to deep shade (L, dark green), intermediate shade (M, green), and high light (H, pale green). (A) Photoprotective NPQ (pNPQ) in L, M, and H plants calculated following $qP_{d\ het}$ versus NPQ curves analysis as in Figure 4. (B) Ratio between pNPQ and maximum NPQ (NPQ_{MAX}). Histograms represent average values ± standard error for $n = 12$ (L), 16 (M), and 18 (H); different letters indicate a significant difference at $P < 0.05$, as determined using one-factor ANOVA followed by Tukey's test

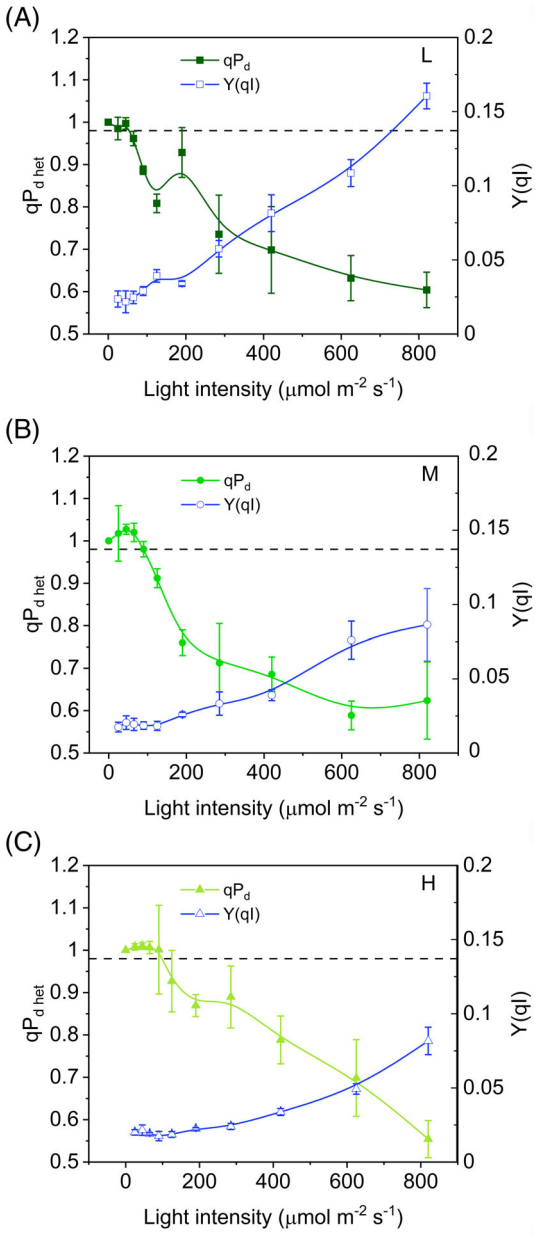

FIGURE 6 Comparison between photochemical quenching measured in the dark in context of a heterogeneous antenna system ($qP_{d\ het}$) and quantum yield of PSII photoinhibition (Y(qI)) as functions of the light intensity in *Selaginella martensii* acclimated to three natural light regimes—deep shade (A), intermediate shade (B) and high light (C) (see the text for details). In all plants, stable and low values of Y(qI) correspond to stable $qP_{d\ het}$ around 1. The increment in Y(qI) corresponds to a drop in $qP_{d\ het}$. Average values ± standard error for $n = 3–5$

and H *S. martensii* plants (Figure 4D–E). Surprisingly, $qP_{d\ het}$ decay in L plants tended instead to stabilize at the highest irradiances, remarkably diverging from the simpler trends observed in M and H, and resulting in higher $qP_{d\ het}$ final values (Figure 4C), that is, a mitigation of the PSII photoinhibition rate had occurred at the end of the light routine. The stabilization of $qP_{d\ het}$ values might be credited to the NPQ action. The slowing down the $qP_{d\ het}$ decay in L plants was due to the linear decrease in $F_{0'act}$ as a function of NPQ (Figure S3). In particular, the quenching of $F_{0'act}$ can be assigned to the marked NPQ increase occurring during the late stages of the light curve, characterizing specifically the L plants (Figure 2A). This result shows that enhanced thermal dissipation processes could effectively contribute to mitigate PSII photoinhibition rate in L plants at irradiance levels > 400 μmol m^{-2} s^{-1} (Figure 4C–E).

3.4 | Light tolerance curves offer an alternative and consistent quantification of phototolerance

To further substantiate the results of comparative photoprotection in *S. martensii* plants, light tolerance curves were built on the same datasets and used as an approach independent from the pNPQ quantification. Plots of light intensity against the respective fraction of photoinactivated samples (those yielding $qP_{d\ het} < 0.98$)were fitted with a logistic function: an increased steepness of the curve indicates a higher propension of plants to PSII photoinactivation. Phototolerance was estimated by I_{50} parameter, that is, the light intensity causing the PSII inactivation in half the analyzed samples. The sensitivity of PSII to photoinactivation decreased from shade to sun acclimation (Figure 7A–C). However, despite the strongly contrasting light regimes, the difference in I_{50} between the two extremes was of only 74 μmol m^{-2} s^{-1} (72 vs. 146 μmol m^{-2} s^{-1} in L and H plants, respectively; Figure 7D).

Phototolerance trends revealed by I_{50} resembled the gradient previously observed for pNPQ (Figures 5A and 7D). Because there was no obvious relationship between pNPQ and NPQ_{MAX}, it was interesting to find out how the I_{50} and pNPQ positioned on the NPQ-light curves. For each type of long-term acclimation, the position of pNPQ marked the end of the linear growth of NPQ in response to increasing irradiance; for NPQ > pNPQ (or irradiance>I_{50}) the linear response with light intensity was lost, that is, NPQ increased more slowly (Figure 8A–C). This scenario was uniform in all the analyzed samples and indicated that PSII photoprotection was efficient until NPQ increased linearly as a function of light intensity.

4 | DISCUSSION

The present study demonstrates that in the ancient vascular plant *S. martensii* the pNPQ is not proportional to the total NPQ amplitude (NPQ_{MAX}) inducible in plants acclimated to strongly contrasting light regimes. Instead, the PSII photoprotection effectiveness is strongly dependent on the light regime, with a remarkable increase in pNPQ from L to H plants (Figure 5A). Developmental acclimation to higher light availability results indeed in a higher phototolerance to increasing irradiance (Figure 7). The inconsistency between pNPQ and NPQ_{MAX} finds its major explanation in the special regulation of excitation energy management in deep-shade plants when exposed to exceedingly high light.

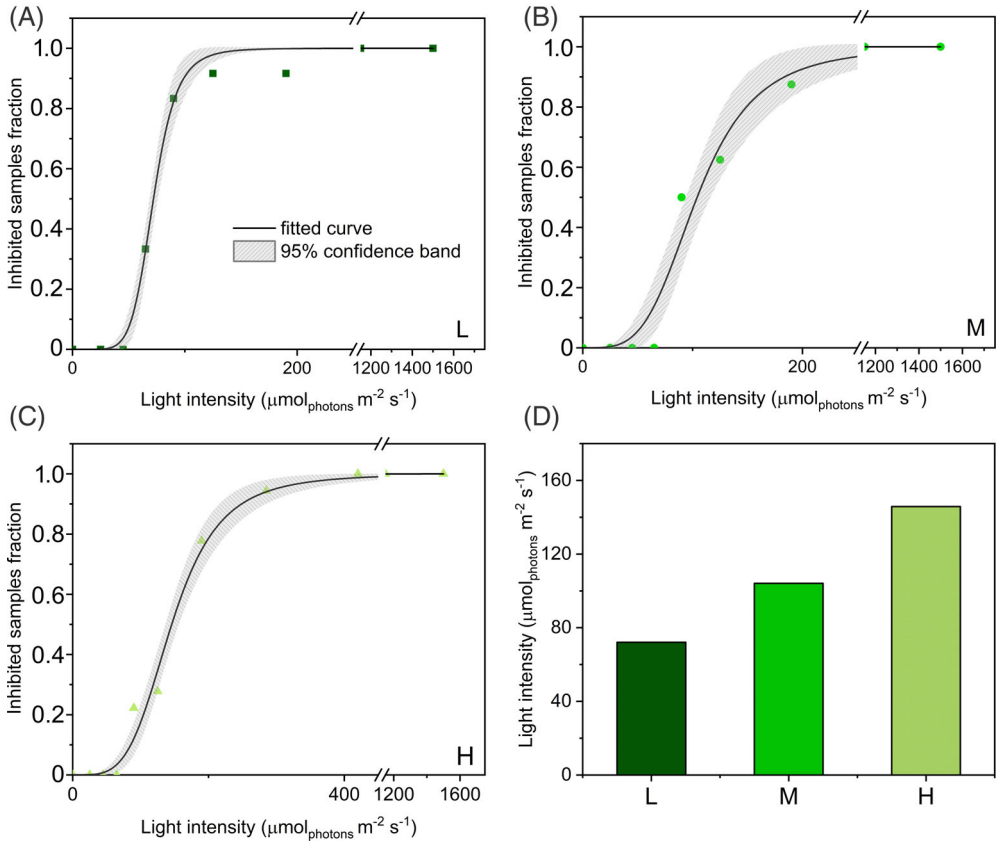

FIGURE 7 Tolerance to photoinhibition in *Selaginella martensii* acclimated to different natural light regimes. (A–C) Light tolerance curves of plants acclimated to deep shade (L, dark green), intermediate shade (M, green) and high light (H, pale green); fitting curves (black lines) were obtained with the logistic equation and are reported with 95% confidence bands. (D) Values of half-inhibiting samples irradiance (I_{50}) obtained with the logistic fitting

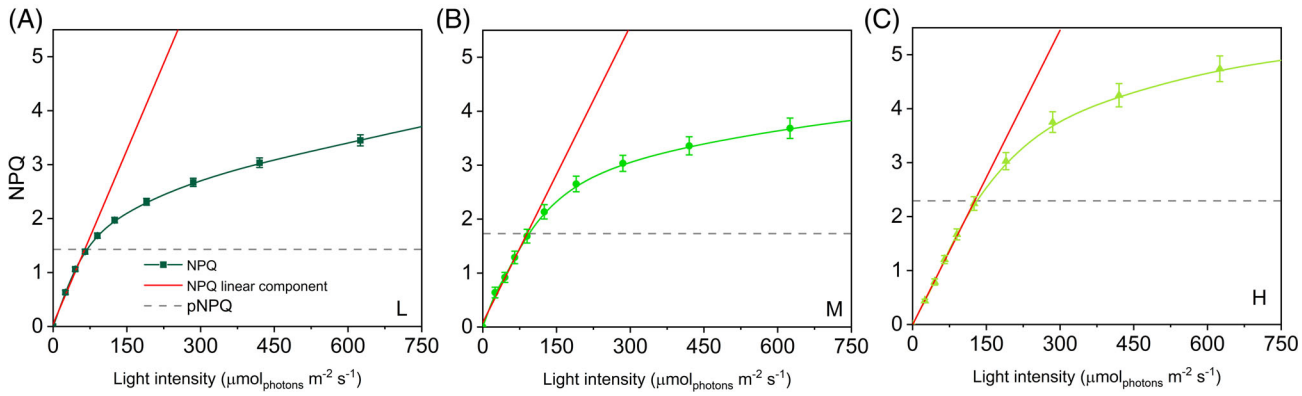

FIGURE 8 Light-tolerance and photoprotective NPQ (pNPQ) in *Selaginella martensii* acclimated to different natural light regimes. Linear fitting (red lines) relative to the first, steepest increasing phase of NPQ-light curves (green lines) in L (A), M (B), and H (C) plants. Gray-dashed horizontal lines indicate the photoprotection offered by thermal dissipation to PSII (pNPQ) in each plant group (see Figure 5). NPQ loses its linear response to light at NPQ > pNPQ. Each point represents average value ± standard error for $n = 12$ (L), 16 (M), and 18 (H)

According to Ruban (2016), pNPQ is mainly due to qE. Because in angiosperms qE is more induced in sun-grown plants, it can be satisfying to explain the variations in photoprotective capacity upon long-term light-acclimation (Anderson & Aro, 1994; Demmig-Adams et al., 2015; Mathur et al., 2018; Mishra et al., 2012; Park II et al., 1997; Schumann et al., 2017). Differently, in *S. martensii*, qE is only slightly variable between L, M, and H plants (Ferroni et al., 2016). A different view about the PSII photoprotection offered by NPQ was presented by Lambrev et al. (2012), based on ultrafast time-resolved fluorescence measurement in *A. thaliana*. Although qE contributes largely to the total NPQ amplitude, it was not considered the main component of photoprotective NPQ, but qZ was instead proposed as the prevailing mechanism that brings photoprotection to PSII (Lambrev et al., 2012). However, the interpretation of the same kinetic NPQ component as qZ in *S. martensii* is quite questionable (Ferroni, Colpo, et al., 2021). In fact, rather than depending on zeaxanthin, this component, termed qX, seems to be triggered by a reduced electron transport chain and to exploit PSI as a thermal quencher to

prevent PSII photodamage (Ferroni et al., 2018; Ferroni, Colpo, et al., 2021). qX activity is deemed related to PSII interactions with PSI as mediated by LHCII (Ferroni et al., 2014), not only the formation of the state transition complex (Galka et al., 2012; Pesaresi et al., 2009; Wood & Johnson, 2020), but also the assembly of PSI-LHCII-PSII megacomplexes responsible for an extensive connectivity between photosystems, including the chance for energy spillover of excitation energy from PSII to PSI (Barber, 1980; Grieco et al., 2015; Jajoo et al., 2014; Järvi et al., 2011; Tiwari et al., 2016; Yokono et al., 2015). Currently, energy spillover in megacomplexes is considered relevant to effective PSII photoprotection (Yokono et al., 2019).

Because the gradient in pNPQ cannot be explained by variations of qE/qZ in *S. martensii*, alternative explanations could be related to other regulatory functions of the antenna system. According to the qP_d method, pNPQ determination is based on the comparison between the ideal $F_0'_{calc}$ and the measured $F_0'_{act}$, leading to qP_d values lower than 1 as a mark for photoinhibition onset. More problematic are qP_d values above 1. Any distortion in $F_0'_{act}$ could be in principle due to the PSII photoinhibition: in fact, only $F_0'_{act}$ determination is affected by PSII photoinhibition, while $F_0'_{calc}$ should be insensitive (Oxborough & Baker, 1997). If this were the case, we should observe a rise in the measured values of $F_0'_{act}$ compared to the calculated, while the results show a completely opposite scenario in which $F_0'_{act}$ is lower than $F_0'_{calc}$. Moreover, negligible values of Y(qI) during the qP_d rise are a straightforward demonstration that $qP_d > 1$ cannot be due to photoinhibition. Such lower-than-expected $F_0'_{act}$ suggests instead the occurrence of quenching mechanisms of F_0' in addition to the direct effect of NPQ. According to the interpretation of average quenching properties of uncoupled antennae offered by Belgio et al. (2014) and Ware et al. (2015), the role of additional F_0' quenchers could be played by the antennae uncoupled from PSII. These hypothetical quenchers would be characterized by an enhanced NPQ capacity and by a lower fluorescence emission than the coupled population. At present, this is the only well-modeled interpretation of qPd > 1 and, as such, it was used in our work. Accordingly, *S. martensii* would be characterized by a larger population of uncoupled/loosely coupled antenna than the angiosperms, in particular *A. thaliana* (Ware et al., 2015). In the latter, the antenna uncoupling distorting the qP_d trends is specific to the low light-grown plants and related to the acclimative accumulation of LHCII (Ware et al., 2015). It is not surprising that the shade-tolerant lycophyte *S. martensii* is affected by similar distortions, because of the great amount of LHCII as compared to PSII (Ferroni et al., 2014, 2016). However, with respect to the developmental acclimation to light, *S. martensii* behaves exactly the opposite of *A. thaliana*: *U* markedly increases from L to H plants, suggesting a massive use of LHCII antenna uncoupling. In H plants, the invariant quantity of free LHCII trimers becomes accordingly overabundant in comparison with the reduced amount of PSII reaction centers (Ferroni et al., 2016). Therefore, in *S. martensii* the involvement of uncoupled quenched antennae in qP_d determination seems well grounded from a biochemical point of view. However, considering that the excitation quenching capacity by uncoupled LHCII is a debated issue, other explanations are possible (Tian et al., 2015). Another reason for a too low $F_0'_{act}$ at non-photoinhibitory irradiances could be the reduction in PSII absorption cross-section due to state-transition-like antenna detachment. Interestingly, in M plants the maximum divergence between $F_0'_{act}$ and $F_0'_{calc}$—that is, the peak in qP_d—is in very good agreement with the peak of LHCII phosphorylation previously reported (Ferroni et al., 2018). Both events occur approximately at the irradiance of growth (50–100 μmol m^{-2} s^{-1}). If the qP_d increase is a reflection of state-transition-like processes, the antenna uncoupling plays again a pivotal role. This inference allows the interpretation of qP_d in the more general frame of the multiple roles assigned to the free LHCII in the thylakoid membrane, including the regulation of PSI-PSII interaction at the grana margins (Grieco et al., 2015; Wientjes et al., 2013; Wood & Johnson, 2020; Zivcak et al., 2014). It is very probable that a more complete interpretation of qP_d should also take into account the photoprotective contribution by PSI, together with mixed populations of uncoupled LHCII, which could be "functionally isolated" from PSII (quenched or unquenched) and/or connected to PSI.

Among PSII uncoupled antennae, a consistent fraction probably serves as qE quenching site (Holzwarth et al., 2009; Miloslavina et al., 2011; Ruban, 2016). Because in *S. martensii* the qE amplitude is almost invariable irrespective of the light regime (Ferroni et al., 2016), the remaining, non-qE-related fraction of uncoupled antenna must be responsible for the increased photoprotection from L to H plants, for example, via interactions involving PSI as a photochemical or non-photochemical quencher (Brestic et al., 2015; Tiwari et al., 2016; Wood & Johnson, 2020; Yokono et al., 2019). In *S. martensii* the amount of PSI and PSI-LHCII-PSII megacomplexes increases under high light (Ferroni et al., 2016) and the assembly of the latter requires the recruitment of free LHCII trimers to mediate labile interactions between PSII and PSI (Grieco et al., 2015). Terashima et al. (2021) suggested that the energy spillover process could be particularly important in shade-tolerant plants to confer them resistance against strong sunflecks. In a lycophyte with invariable LHCII amount and low carbon fixation capacity (Ferroni et al., 2016; Ferroni, Brestič, et al., 2021), the extensive PSII antenna uncoupling can allow an emphasized exploitation of PSI-linked photoprotection also upon long-term acclimation to high light. Conversely, in the complete absence of sunflecks, the photoprotective role of uncoupled antennae and PSI seems diminished, potentially exposing the small PSI pool of L plants to photodamage upon short-term exposure to even moderate light (Brestic et al., 2015). Because PSI is particularly sensitive to donor-side over-reduction (Takagi et al., 2017), its photoprotection primarily depends on a reduced inflow of electrons from PSII into the membrane (Yamamoto & Shikanai, 2019). The $qP_{d\ het}$ results suggest that in L plants of *S. martensii* the safe accumulation of a stable population of photoinactivated PSII under moderate/high light may serve to the scope of downregulating the electron flow and preserve PSI (Tikkanen et al., 2015). Beside photoprotective thermal dissipation mechanisms, PSII photoinactivation is also counteracted by the repair cycle of PSII based on the D1 core protein turnover (Keren et al., 1995, Baena–González & Aro, 2002, Kato & Sakamoto, 2009, Nath et al., 2013). The PSII repair cycle requires the migration of

photodamaged PSII to the non-appressed grana margins, where the turnover takes place (Anderson & Aro, 1994; Järvi et al., 2015; Li et al., 2018; Kirchhoff, 2014). D1 turnover is more active in sun plants, whose thylakoid membranes are enriched in grana margins (Anderson & Aro, 1994). Differently, shade plants are characterized by a higher grana stacking, further increased when exposed to high irradiance; the extensive thylakoid appression hinders the PSII turnover, so that the grana contain a kind of reservoir of inactive PSII (Anderson & Aro, 1994; Mathur et al., 2018; Matsubara & Chow, 2004; Tietz et al., 2015). The accumulation of photoinactivated PSII upon increasing irradiances also occurs in *S. martensii*, starting from relatively low light intensities (see I_{50} values, Figure 7D). However, in L plants—the richest in PSII—qP_d surprisingly slows its drop at the highest irradiances, indicating the achievement of a constant ratio between intact and photoinactivated PSII (Figure 4C). A stable reservoir of photoinactivated PSII in long appressed pseudo-lamellar thylakoids may have an important photoprotective role, because they safely dissipate the excess of absorbed energy, preventing the photoinactivation of the remaining, active PSII, but also restricting the electron inflow directed to PSI (Mathur et al., 2018; Matsubara & Chow, 2004). According to Ruban (2016), qI does not contribute to pNPQ. However, the qP_d method indirectly evidences the physiological function of qI in mitigating the PSII photoinactivation, although the small qI extent (5%–10% of total NPQ amplitude, Ferroni et al., 2016) could not explain per se the constant increase in NPQ at high irradiances observed in L plants (Figure 2A). A possible interpretation of this phenomenon can be related to an additional thermal dissipation mechanism produced by PSII cores (Nicol et al., 2019), more relevant in L plants because of their higher content in PSII.

In conclusion, although qE might still represent the main component of pNPQ as postulated by Ruban (2016), in *S. martensii* the pNPQ could also strongly depend on the PSII antenna uncoupling and the relative amount of PSII and PSI. After the correction for the antenna heterogeneity, $qP_{d\ het}$ is confirmed as a very precise indicator of incipient PSII photoinhibition. Furthermore, the example of *S. martensii* suggests that the qP_d method can be sensitive to PSI-related mechanisms and to the PSII core-related thermal dissipation. A sustained PSII photoinhibition can have a photoprotective function to increase physiologically a low PSI/PSII ratio (Shimakawa & Miyake, 2019). Evidence for the importance of such processes is quite sparse in the literature regarding angiosperms. The results obtained in *S. martensii* may indicate that processes collateral to qE, and often considered as minor, can have had a special relevance for thylakoid membrane photoprotection in ancient land plants, which do not modulate extensively the LHCII total content (Gerotto et al., 2019; Lei et al., 2021). However, any evolutionary conclusion should be cautious taking into consideration millions of years of parallel evolution of *Selaginella*, making it difficult to define a certain physiological trait as primitive or derived. For instance, some properties evidenced in *S. martensii* could be shared by other shade plants because of convergent evolution. This study invites the validation (or not) of the qP_d method and its conclusions emerging in a lycophyte in other plants sharing the same deep-shade habitat and long-term invariable LHCII amount.

ACKNOWLEDGMENTS

This work was performed with the contribution of the University of Ferrara (Fondo per l'Incentivazione alla Ricerca - FIR 2020 granted to LF) and the Ministry of University and Research of Italy (Finanziamento Attività Ricerca di Base granted to LF). We are grateful to Fausto Molinari (Botanical Garden of the University of Ferrara) for his careful cultivation of the plants used in this experiment. Ilaria Corelli is kindly thanked for her technical assistance for BN-PAGE analysis.

Open Access Funding provided by Universita degli Studi di Ferrara within the CRUI-CARE Agreement.

AUTHOR CONTRIBUTIONS

Lorenzo Ferroni conceived and supervised the experiment; Andrea Colpo planned and performed the experiments; Andrea Colpo and Alessandra Sabia performed the data analysis; Andrea Colpo, Costanza Baldisserotto, Simonetta Pancaldi, Lorenzo Ferroni analyzed and interpreted the results; Andrea Colpo and Lorenzo Ferroni wrote the manuscript; all authors edited the manuscript.

DATA AVAILABILITY STATEMENT

The data supporting the findings of this study are available from the corresponding author Lorenzo Ferroni, upon request.

ORCID

Andrea Colpo https://orcid.org/0000-0002-7278-7063
Costanza Baldisserotto https://orcid.org/0000-0002-8710-558X
Simonetta Pancaldi https://orcid.org/0000-0002-2077-3268
Alessandra Sabia https://orcid.org/0000-0003-3850-5496
Lorenzo Ferroni https://orcid.org/0000-0002-5694-2078

REFERENCES

Albanese, P., Manfredi, M., Marengo, E., Saracco, G. & Pagliano, C. (2019) Structural and functional differentiation of the light-harvesting protein Lhcb4 during land plant diversification. *Physiologia Plantarum*, 166(1), 336–350.

Anderson, J.M. & Aro, E.M. (1994) Grana stacking and protection of photosystem II in thylakoid membranes of higher plant leaves under sustained high irradiance: an hypothesis. *Photosynthesis Research*, 41(2), 315–326.

Aro, E.M., McCaffery, S. & Anderson, J.M. (1993) Photoinhibition and D1 protein degradation in peas acclimated to different growth irradiances. *Plant Physiology*, 103(3), 835–843.

Baena–González, E. & Aro, E.M. (2002) Biogenesis, assembly and turnover of photosystem II units. *Philosophical Transactions of the Royal Society of London. Series B: Biological Sciences*, 357(1426), 1451–1460.

Ballottari, M., Dall'Osto, L., Morosinotto, T. & Bassi, R. (2007) Contrasting behavior of higher plant photosystem I and II antenna systems during acclimation. *Journal of Biological Chemistry*, 282(12), 8947–8958.

Barber, J. (1980) An explanation for the relationship between salt-induced thylakoid stacking and the chlorophyll fluorescence changes associated with changes in spillover of energy from photosystem II to photosystem I. *FEBS Letters*, 118(1), 1–10.

Bassi, R. & Dall'Osto, L. (2021) Dissipation of light energy absorbed in excess: the molecular mechanisms. *Annual Review of Plant Biology*, 72, 47–76.

Belgio, E., Johnson, M.P., Jurić, S. & Ruban, A.V. (2012) Higher plant photosystem II light-harvesting antenna, not the reaction center, determines the excited-state lifetime—both the maximum and the nonphotochemically quenched. *Biophysical Journal*, 102(12), 2761–2771.

Belgio, E., Kapitonova, E., Chmeliov, J., Duffy, C.D., Ungerer, P., Valkunas, L., et al. (2014) Economic photoprotection in photosystem II that retains a complete light-harvesting system with slow energy traps. *Nature Communications*, 5(1), 1–8.

Bilger, W. & Björkman, O. (1990) Role of the xanthophyll cycle in photoprotection elucidated by measurements of light-induced absorbance changes, fluorescence and photosynthesis in leaves of *Hedera canariensis*. *Photosynthesis Research*, 25(3), 173–185.

Brestic, M., Zivcak, M., Kunderlikova, K., Sytar, O., Shao, H., Kalaji, H.M. et al. (2015) Low PSI content limits the photoprotection of PSI and PSII in early growth stages of chlorophyll b-deficient wheat mutant lines. *Photosynthesis Research*, 125(1), 151–166.

Campbell, D.A. & Tyystjärvi, E. (2012) Parameterization of photosystem II photoinactivation and repair. *Biochimica et Biophysica Acta (BBA)-Bioenergetics*, 1817(1), 258–265.

Cazzaniga, S., Dall'Osto, L., Kong, S.G., Wada, M. & Bassi, R. (2013) Interaction between avoidance of photon absorption, excess energy dissipation and zeaxanthin synthesis against photooxidative stress in Arabidopsis. *The Plant Journal*, 76(4), 568–579.

Chow, W.S., Hope, A.B. & Anderson, J.M. (1991) Further studies on quantifying photosystem II in vivo by flash-induced oxygen yield from leaf discs. *Functional Plant Biology*, 18(4), 397–410.

Delieu, T.J. & Walker, D.A. (1983) Simultaneous measurement of oxygen evolution and chlorophyll fluorescence from leaf pieces. *Plant Physiology*, 73(3), 534–541.

Demmig-Adams, B. (1998) Survey of thermal energy dissipation and pigment composition in sun and shade leaves. *Plant and Cell Physiology*, 39(5), 474–482.

Demmig-Adams, B., Cohu, C.M., Muller, O. & Adams, W.W. (2012) Modulation of photosynthetic energy conversion efficiency in nature: from seconds to seasons. *Photosynthesis Research*, 113(1), 75–88.

Demmig-Adams, B., Muller, O., Stewart, J.J., Cohu, C.M. & Adams, W.W., III. (2015) Chloroplast thylakoid structure in evergreen leaves employing strong thermal energy dissipation. *Journal of Photochemistry and Photobiology B: Biology*, 152, 357–366.

Ferroni, L., Angeleri, M., Pantaleoni, L., Pagliano, C., Longoni, P., Marsano, F. et al. (2014) Light-dependent reversible phosphorylation of the minor photosystem II antenna Lhcb6 (CP 24) occurs in lycophytes. *The Plant Journal*, 77(6), 893–905.

Ferroni, L., Suorsa, M., Aro, E.M., Baldisserotto, C. & Pancaldi, S. (2016) Light acclimation in the lycophyte *Selaginella martensii* depends on changes in the amount of photosystems and on the flexibility of the light-harvesting complex II antenna association with both photosystems. *New Phytologist*, 211(2), 554–568.

Ferroni, L., Cucuzza, S., Angeleri, M., Aro, E.M., Pagliano, C., Giovanardi, M. et al. (2018) In the lycophyte *Selaginella martensii* is the "extra-qT" related to energy spillover? Insights into photoprotection in ancestral vascular plants. *Environmental and Experimental Botany*, 154, 110–122.

Ferroni, L., Brestič, M., Živčak, M., Cantelli, R. & Pancaldi, S. (2021) Increased photosynthesis from a deep-shade to high-light regime occurs by enhanced CO_2 diffusion into the leaf of *Selaginella martensii*. *Plant Physiology and Biochemistry*, 160, 143–154.

Ferroni, L., Colpo, A., Baldisserotto, C. & Pancaldi, S. (2021) In an ancient vascular plant the intermediate relaxing component of NPQ depends on a reduced stroma: evidence from dithiothreitol treatment. *Journal of Photochemistry and Photobiology B: Biology*, 215, 112114.

Flannery, S.E., Hepworth, C., Wood, W.H., Pastorelli, F., Hunter, C.N., Dickman, M.J. et al. (2021) Developmental acclimation of the thylakoid proteome to light intensity in Arabidopsis. *The Plant Journal*, 105(1), 223–244.

Galka, P., Santabarbara, S., Khuong, T.T.H., Degand, H., Morsomme, P., Jennings, R.C. et al. (2012) Functional analyses of the plant photosystem I–light-harvesting complex II supercomplex reveal that light-harvesting complex II loosely bound to photosystem II is a very efficient antenna for photosystem I in state II. *The Plant Cell*, 24(7), 2963–2978.

Gefen-Treves, S., Kedem, I., Weiss, G., Wagner, D., Tchernov, D. & Kaplan, A. (2020) Acclimation of a rocky shore algal reef builder *Neogoniolithon* sp. to changing illuminations. *Limnology and Oceanography*, 65(1), 27–36.

Gerotto, C., Alboresi, A., Giacometti, G.M., Bassi, R. & Morosinotto, T. (2011) Role of PSBS and LHCSR in *Physcomitrella patens* acclimation to high light and low temperature. *Plant, Cell & Environment*, 34(6), 922–932.

Gerotto, C., Trotta, A., Bajwa, A.A., Mancini, I., Morosinotto, T. & Aro, E.M. (2019) Thylakoid protein phosphorylation dynamics in a moss mutant lacking SERINE/THREONINE PROTEIN KINASE STN8. *Plant Physiology*, 180(3), 1582–1597.

Giovagnetti, V. & Ruban, A.V. (2015) Discerning the effects of photoinhibition and photoprotection on the rate of oxygen evolution in Arabidopsis leaves. *Journal of Photochemistry and Photobiology B: Biology*, 152, 272–278.

Giovanardi, M., Pantaleoni, L., Ferroni, L., Pagliano, C., Albanese, P., Baldisserotto, C. et al. (2018) In pea stipules a functional photosynthetic electron flow occurs despite a reduced dynamicity of LHCII association with photosystems. *Biochimica et Biophysica Acta (BBA)-Bioenergetics*, 1859(10), 1025–1038.

Grieco, M., Suorsa, M., Jajoo, A., Tikkanen, M. & Aro, E.M. (2015) Light-harvesting II antenna trimers connect energetically the entire photosynthetic machinery—including both photosystems II and I. *Biochimica et Biophysica Acta (BBA)-Bioenergetics*, 1847(6–7), 607–619.

Haferkamp, S., Haase, W., Pascal, A.A., van Amerongen, H. & Kirchhoff, H. (2010) Efficient light harvesting by photosystem II requires an optimized protein packing density in grana thylakoids. *Journal of Biological Chemistry*, 285(22), 17020–17028.

Hendrickson, L., Furbank, R.T. & Chow, W.S. (2004) A simple alternative approach to assessing the fate of absorbed light energy using chlorophyll fluorescence. *Photosynthesis Research*, 82(1), 73–81.

Holzwarth, A.R., Miloslavina, Y., Nilkens, M. & Jahns, P. (2009) Identification of two quenching sites active in the regulation of photosynthetic light-harvesting studied by time-resolved fluorescence. *Chemical Physics Letters*, 483(4–6), 262–267.

Horton, P., Wentworth, M. & Ruban, A.V. (2005) Control of the light harvesting function of chloroplast membranes: the LHCII-aggregation model for non-photochemical quenching. *FEBS Letters*, 579(20), 4201–4206.

Jajoo, A., Mekala, N.R., Tongra, T., Tiwari, A., Grieco, M., Tikkanen, M. et al. (2014) Low pH-induced regulation of excitation energy between the two photosystems. *FEBS Letters*, 588(6), 970–974.

Järvi, S., Suorsa, M., Paakkarinen, V. & Aro, E.M. (2011) Optimized native gel systems for separation of thylakoid protein complexes: novel super-and mega-complexes. *Biochemical Journal*, 439(2), 207–214.

Järvi, S., Suorsa, M. & Aro, E.M. (2015) Photosystem II repair in plant chloroplasts—Regulation, assisting proteins and shared components with photosystem II biogenesis. *Biochimica et Biophysica Acta (BBA)-Bioenergetics*, 1847(9), 900–909.

Johnson, M.P., Goral, T.K., Duffy, C.D., Brain, A.P., Mullineaux, C.W. & Ruban, A.V. (2011) Photoprotective energy dissipation involves the reorganization of photosystem II light-harvesting complexes in the grana membranes of spinach chloroplasts. *The Plant Cell*, 23(4), 1468–1479.

Kato, Y. & Sakamoto, W. (2009) Protein quality control in chloroplasts: a current model of D1 protein degradation in the photosystem II repair cycle. *Journal of Biochemistry*, 146(4), 463–469.

Kato, Y., Sun, X., Zhang, L. & Sakamoto, W. (2012) Cooperative D1 degradation in the photosystem II repair mediated by chloroplastic proteases in Arabidopsis. *Plant Physiology*, 159(4), 1428–1439.

Keren, N., Gong, H. & Ohad, I. (1995) Oscillations of reaction center II-D1 protein degradation in vivo induced by repetitive light flashes. *Journal of Biological Chemistry*, 270(2), 806–814.

Kirchhoff, H. (2014) Structural changes of the thylakoid membrane network induced by high light stress in plant chloroplasts. *Philosophical*

Transactions of the Royal Society B: Biological Sciences, 369(1640), 20130225.

Lambrev, P.H., Miloslavina, Y., Jahns, P. & Holzwarth, A.R. (2012) On the relationship between non-photochemical quenching and photoprotection of photosystem II. *Biochimica et Biophysica Acta (BBA)-Bioenergetics*, 1817(5), 760–769.

Lazár, D. (2015) Parameters of photosynthetic energy partitioning. *Journal of Plant Physiology*, 175, 131–147.

Lei, Y.B., Xia, H.X., Chen, K., Plenković-Moraj, A., Huang, W. & Sun, G. (2021) Photosynthetic regulation in response to fluctuating light conditions under temperature stress in three mosses with different light requirements. *Plant Science*, 311, 111020.

Li, L., Aro, E.M. & Millar, A.H. (2018) Mechanisms of photodamage and protein turnover in photoinhibition. *Trends in Plant Science*, 23(8), 667–676.

Lichtenthaler, H.K., Ač, A., Marek, M.V., Kalina, J. & Urban, O. (2007) Differences in pigment composition, photosynthetic rates and chlorophyll fluorescence images of sun and shade leaves of four tree species. *Plant Physiology and Biochemistry*, 45(8), 577–588.

Lo Piccolo, E., Landi, M., Massai, R., Remorini, D. & Guidi, L. (2020) Girled-induced anthocyanin accumulation in red-leafed *Prunus cerasifera*: effect on photosynthesis, photoprotection and sugar metabolism. *Plant Science*, 294, 110456.

Malnoë, A. (2018) Photoinhibition or photoprotection of photosynthesis? Update on the (newly termed) sustained quenching component qH. *Environmental and Experimental Botany*, 154, 123–133.

Mathur, S., Jain, L. & Jajoo, A. (2018) Photosynthetic efficiency in sun and shade plants. *Photosynthetica*, 56(1), 354–365.

Matsubara, S. & Chow, W.S. (2004) Populations of photoinactivated photosystem II reaction centers characterized by chlorophyll a fluorescence lifetime in vivo. *Proceedings of the National Academy of Sciences*, 101(52), 18234–18239.

Mattila, H., Mishra, K.B., Kuusisto, I., Mishra, A., Novotná, K., Šebela, D. et al. (2020) Effects of low temperature on photoinhibition and singlet oxygen production in four natural accessions of Arabidopsis. *Planta*, 252(2), 1–17.

Miloslavina, Y., de Bianchi, S., Dall'Osto, L., Bassi, R. & Holzwarth, A.R. (2011) Quenching in *Arabidopsis thaliana* mutants lacking monomeric antenna proteins of photosystem II. *Journal of Biological Chemistry*, 286, 36830–36840.

Mishra, Y., Jänkänpää, H.J., Kiss, A.Z., Funk, C., Schröder, W.P. & Jansson, S. (2012) Arabidopsis plants grown in the field and climate chambers significantly differ in leaf morphology and photosystem components. *BMC Plant Biology*, 12(1), 1–18.

Nath, K., Jajoo, A., Poudyal, R.S., Timilsina, R., Park, Y.S., Aro, E.M. et al. (2013) Towards a critical understanding of the photosystem II repair mechanism and its regulation during stress conditions. *FEBS Letters*, 587(21), 3372–3381.

Nicol, L., Nawrocki, W.J. & Croce, R. (2019) Disentangling the sites of non-photochemical quenching in vascular plants. *Nature Plants*, 5(11), 1177–1183.

Nilkens, M., Kress, E., Lambrev, P., Miloslavina, Y., Müller, M., Holzwarth, A.R. et al. (2010) Identification of a slowly inducible zeaxanthin-dependent component of non-photochemical quenching of chlorophyll fluorescence generated under steady-state conditions in Arabidopsis. *Biochimica et Biophysica Acta (BBA)-Bioenergetics*, 1797(4), 466–475.

Okegawa, Y., Basso, L., Shikanai, T. & Motohashi, K. (2020) Cyclic electron transport around PSI contributes to photosynthetic induction with thioredoxin f. *Plant Physiology*, 184(3), 1291–1302.

Öquist, G., Chow, W.S. & Anderson, J.M. (1992) Photoinhibition of photosynthesis represents a mechanism for the long-term regulation of photosystem II. *Planta*, 186(3), 450–460.

Oxborough, K. & Baker, N.R. (1997) Resolving chlorophyll a fluorescence images of photosynthetic efficiency into photochemical and non-photochemical components–calculation of qP and F_v/F_m; without measuring F_o. *Photosynthesis Research*, 54(2), 135–142.

Park, Y., II, Chow, W.S. & Anderson, J.M. (1997) Antenna size dependency of photoinactivation of photosystem II in light-acclimated pea leaves. *Plant Physiology*, 115(1), 151–157.

Pesaresi, P., Hertle, A., Pribil, M., Kleine, T., Wagner, R., Strissel, H. et al. (2009) Arabidopsis STN7 kinase provides a link between short-and long-term photosynthetic acclimation. *The Plant Cell*, 21(8), 2402–2423.

Pribil, M., Labs, M. & Leister, D. (2014) Structure and dynamics of thylakoids in land plants. *Journal of Experimental Botany*, 65(8), 1955–1972.

Ritchie, R.J. (2006) Consistent sets of spectrophotometric chlorophyll equations for acetone, methanol and ethanol solvents. *Photosynthesis Research*, 89(1), 27–41.

Roach, T. & Krieger-Liszkay, A. (2014) Regulation of photosynthetic electron transport and photoinhibition. *Current Protein and Peptide Science*, 15(4), 351–362.

Ruban, A.V. (2016) Nonphotochemical chlorophyll fluorescence quenching: mechanism and effectiveness in protecting plants from photodamage. *Plant Physiology*, 170(4), 1903–1916.

Ruban, A.V. & Belgio, E. (2014) The relationship between maximum tolerated light intensity and photoprotective energy dissipation in the photosynthetic antenna: chloroplast gains and losses. *Philosophical Transactions of the Royal Society B: Biological Sciences*, 369(1640), 20130222.

Ruban, A.V. & Murchie, E.H. (2012) Assessing the photoprotective effectiveness of non-photochemical chlorophyll fluorescence quenching: a new approach. *Biochimica et Biophysica Acta (BBA)-Bioenergetics*, 1817(7), 977–982.

Ruban, A.V., Johnson, M.P. & Duffy, C.D. (2012) The photoprotective molecular switch in the photosystem II antenna. *Biochimica et Biophysica Acta (BBA)-Bioenergetics*, 1817(1), 167–181.

Schansker, G. & van Rensen, J.J. (1999) Performance of active photosystem II centers in photoinhibited pea leaves. *Photosynthesis Research*, 62(2), 175–184.

Schreiber, U., Schliwa, U. & Bilger, W. (1986) Continuous recording of photochemical and non-photochemical chlorophyll fluorescence quenching with a new type of modulation fluorometer. *Photosynthesis Research*, 10(1), 51–62.

Schumann, T., Paul, S., Melzer, M., Dörmann, P. & Jahns, P. (2017) Plant growth under natural light conditions provides highly flexible short-term acclimation properties toward high light stress. *Frontiers in Plant Science*, 8, 681.

Shimakawa, G. & Miyake, C. (2019) What quantity of photosystem I is optimum for safe photosynthesis? *Plant Physiology*, 179(4), 1479–1485.

Shukla, M.K., Watanabe, A., Wilson, S., Giovagnetti, V., Moustafa, E.I., Minagawa, J. et al. (2020) A novel method produces native light-harvesting complex II aggregates from the photosynthetic membrane revealing their role in nonphotochemical quenching. *Journal of Biological Chemistry*, 295(51), 17816–17826.

Stewart, J.J., Adams, W.W., Cohu, C.M., Polutchko, S.K., Lombardi, E.M. & Demmig-Adams, B. (2015) Differences in light-harvesting, acclimation to growth-light environment, and leaf structural development between Swedish and Italian ecotypes of *Arabidopsis thaliana*. *Planta*, 242(6), 1277–1290.

Takagi, D., Amako, K., Hashiguchi, M., Fukaki, H., Ishizaki, K., Goh, T. et al. (2017) Chloroplastic ATP synthase builds up a proton motive force preventing production of reactive oxygen species in photosystem I. *The Plant Journal*, 91(2), 306–324.

Terashima, I., Matsuo, M., Suzuki, Y., Yamori, W. & Kono, M. (2021) Photosystem I in low light-grown leaves of Alocasia odora, a shade-tolerant plant, is resistant to fluctuating light-induced photoinhibition. *Photosynthesis Research*, 1–14.

Tian, L., Dinc, E. & Croce, R. (2015) LHCII populations in different quenching states are present in the thylakoid membranes in a ratio that depends on the light conditions. *The Journal of Physical Chemistry Letters*, 6(12), 2339–2344.

Tian, Y., Sacharz, J., Ware, M.A., Zhang, H. & Ruban, A.V. (2017) Effects of periodic photoinhibitory light exposure on physiology and productivity of Arabidopsis plants grown under low light. *Journal of Experimental Botany*, 68(15), 4249–4262.

Tietz, S., Puthiyaveetil, S., Enlow, H.M., Yarbrough, R., Wood, M., Semchonok, D.A. et al. (2015) Functional implications of photosystem II crystal formation in photosynthetic membranes. *Journal of Biological Chemistry*, 290(22), 14091–14106.

Tikkanen, M., Rantala, S. & Aro, E.M. (2015) Electron flow from PSII to PSI under high light is controlled by PGR5 but not by PSBS. *Frontiers in Plant Science*, 6, 521.

Tiwari, A., Mamedov, F., Grieco, M., Suorsa, M., Jajoo, A., Styring, S. et al. (2016) Photodamage of iron–sulphur clusters in photosystem I induces non-photochemical energy dissipation. *Nature Plants*, 2(4), 1–9.

Townsend, A.J., Ware, M.A. & Ruban, A.V. (2018) Dynamic interplay between photodamage and photoprotection in photosystem II. *Plant, Cell & Environment*, 41(5), 1098–1112.

Van Kooten, O. & Snel, J.F. (1990) The use of chlorophyll fluorescence nomenclature in plant stress physiology. *Photosynthesis Research*, 25(3), 147–150.

Ware, M.A., Belgio, E. & Ruban, A.V. (2015) Photoprotective capacity of non-photochemical quenching in plants acclimated to different light intensities. *Photosynthesis Research*, 126(2), 261–274.

Ware, M.A., Dall'Osto, L. & Ruban, A.V. (2016) An in vivo quantitative comparison of photoprotection in Arabidopsis xanthophyll mutants. *Frontiers in Plant Science*, 7, 841.

Wellburn, A.R. (1994) The spectral determination of chlorophylls a and b, as well as total carotenoids, using various solvents with spectrophotometers of different resolution. *Journal of Plant Physiology*, 144(3), 307–313.

Wientjes, E., van Amerongen, H. & Croce, R. (2013) LHCII is an antenna of both photosystems after long-term acclimation. *Biochimica et Biophysica Acta (BBA)-Bioenergetics*, 1827(3), 420–426.

Wilson, S. & Ruban, A.V. (2019) Quantitative assessment of the high-light tolerance in plants with an impaired photosystem II donor side. *Biochemical Journal*, 476(9), 1377–1386.

Wilson, S. & Ruban, A.V. (2020a) Enhanced NPQ affects long-term acclimation in the spring ephemeral *Berteroa incana*. *Biochimica et Biophysica Acta (BBA)-Bioenergetics*, 1861(4), 148014.

Wilson, S. & Ruban, A.V. (2020b) Rethinking the influence of chloroplast movements on non-photochemical quenching and photoprotection. *Plant Physiology*, 183(3), 1213–1223.

Wood, W.H. & Johnson, M.P. (2020) Modeling the role of LHCII-LHCII, PSII-LHCII, and PSI-LHCII interactions in state transitions. *Biophysical Journal*, 119(2), 287–299.

Yamamoto, H. & Shikanai, T. (2019) PGR5-dependent cyclic electron flow protects photosystem I under fluctuating light at donor and acceptor sides. *Plant Physiology*, 179(2), 588–600.

Yokono, M., Nagao, R., Tomo, T. & Akimoto, S. (2015) Regulation of excitation energy transfer in diatom PSII dimer: how does it change the destination of excitation energy? *Biochimica et Biophysica Acta (BBA)-Bioenergetics*, 1847(10), 1274–1282.

Yokono, M., Takabayashi, A., Kishimoto, J., Fujita, T., Iwai, M., Murakami, A. et al. (2019) The PSI–PSII megacomplex in green plants. *Plant and Cell Physiology*, 60(5), 1098–1108.

Zivcak, M., Brestic, M. & Kalaji, H.M. (2014) Photosynthetic responses of sun-and shade-grown barley leaves to high light: is the lower PSII connectivity in shade leaves associated with protection against excess of light? *Photosynthesis Research*, 119(3), 339–354.

SUPPORTING INFORMATION

Additional supporting information may be found in the online version of the article at the publisher's website.

How to cite this article: Colpo, A., Baldisserotto, C., Pancaldi, S., Sabia, A. & Ferroni, L. (2022) Photosystem II photoinhibition and photoprotection in a lycophyte, *Selaginella martensii*. *Physiologia Plantarum*, 174(1), e13604. Available from: https://doi.org/10.1111/ppl.13604

Photosystem II photoinhibition and photoprotection in a lycophyte, *Selaginella martensii*

Andrea Colpo, Costanza Baldisserotto, Simonetta Pancaldi, Alessandra Sabia, Lorenzo Ferroni

Department of Environmental and Prevention Sciences, University of Ferrara, Corso Ercole I d'Este 32, 44121 Ferrara, Italy.

Supporting information

Fig. S1. Photosynthetic pigments quantification in *Selaginella martensii* acclimated to deep shade (L), intermediate shade (M) and full sunlight (H).

Fig. S2. Native thylakoid composition in *Selaginella martensii* acclimated to deep shade (L), intermediate shade (M) and full sunlight (H).

Fig. S3. Examples of minimum fluorescence as a function of Non-Photochemical Quenching (NPQ) in *Selaginella martensii.*

Fig. S4. NPQ kinetics curves of *S. martensii* plants recorded at different light intensities.

Fig.S5. Photochemical quenching measured in the dark in *S. martensii* plants acclimated to deep shade (L), intermediate shade (M) and full sunlight (H) upon independent exposure to increasing irradiances.

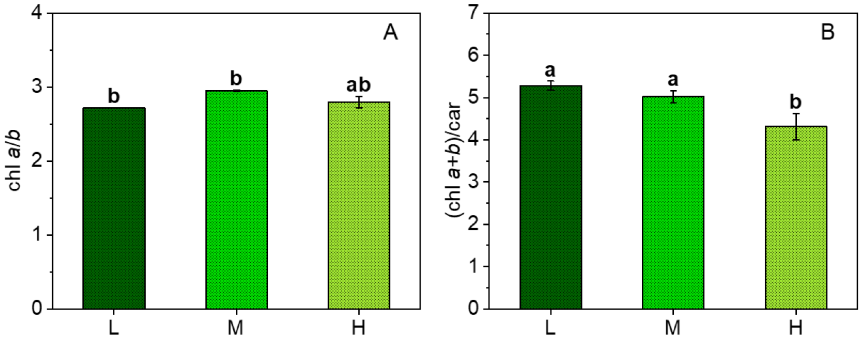

Fig. S1. Photosynthetic pigments quantification in *Selaginella martensii* acclimated to deep shade (L), intermediate shade (M) and full sunlight (H). Pigment ratios in isolated thylakoids are reported as the molar ratio between chlorophyll (chl) *a* and *b* content (A) and chlorophyll *a*+*b* and carotenoids (B). Histograms represent average values ±Standard Error for *n*=3. Different letters indicate a significant difference determined with ANOVA followed by Tukey's test at $p<0.05$.

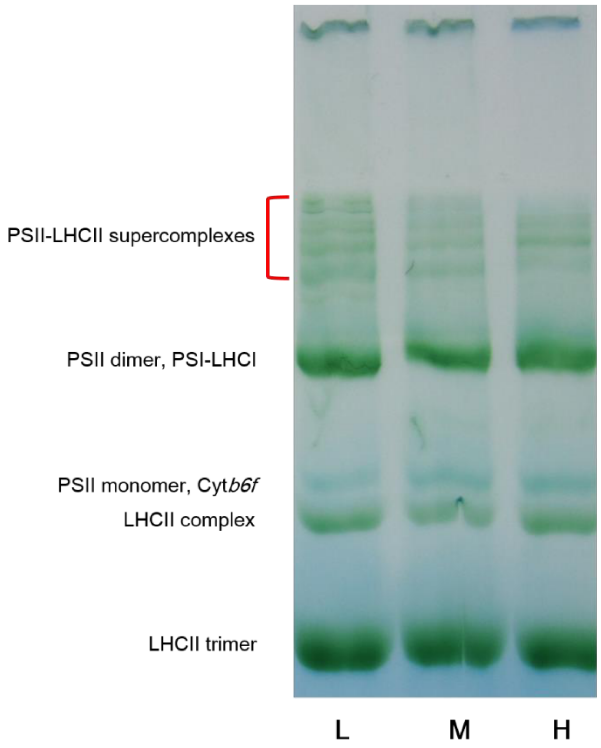

Fig. S2. Native thylakoid composition in *Selaginella martensii* acclimated to deep shade (L), intermediate shade (M) and full sunlight (H). Thylakoids corresponding to 8 mg of chlorophyll were solubilized with 1.5% β-dodecylmaltoside to a final chlorophyll concentration of 0.5 mg ml^{-1} and subjected to Blue-Native Polyacrylamide gel Electrophoresis (BN-PAGE). Electrophoretic bands were identified according to Järvi *et al*. (2011) and Ferroni *et al*. (2014). The heavy PSII-LHCII supercomplexes are more abundant in L plants than in M or H plants. In contrast, the intensity of the band corresponding to the LHCII trimers is almost invariable in the three types of plants. The thylakoid organization in the plant material used for the fluorometric experiments is therefore uniform to that used in Ferroni *et al*. (2016).

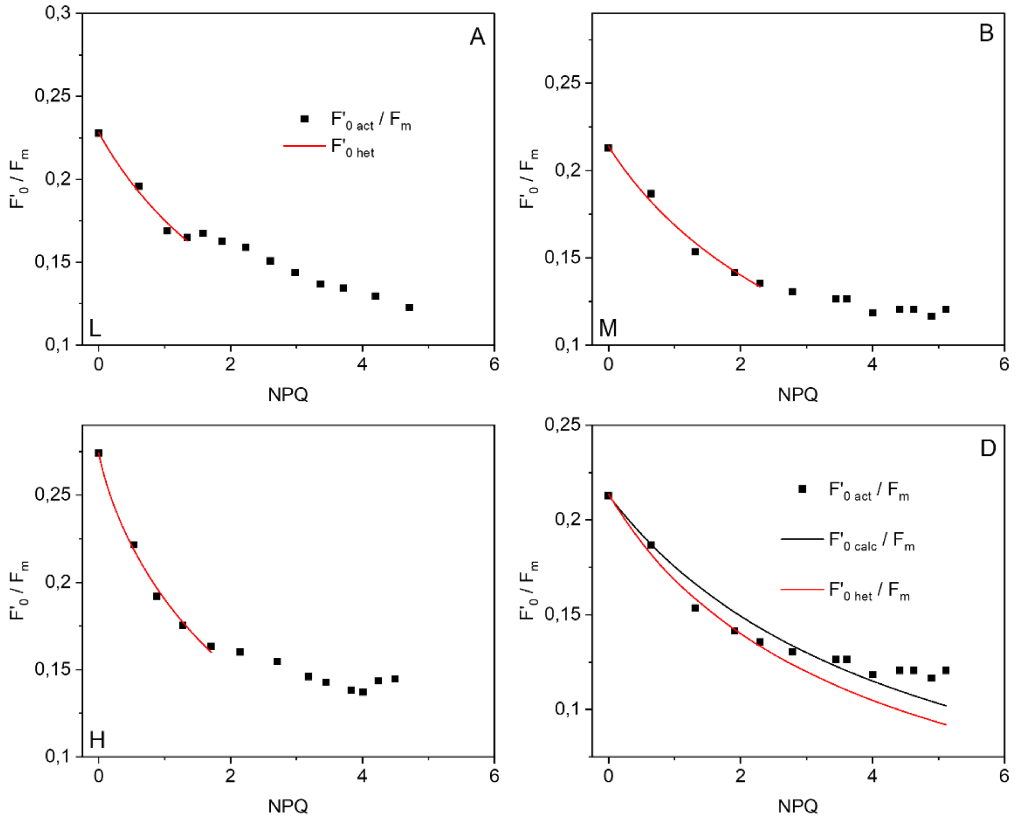

Fig. S3. Examples of minimum fluorescence as a function of Non-Photochemical Quenching (NPQ) in *Selaginella martensii* acclimated to deep shade (L), intermediate shade (M) and full sunlight (H). F'_0 is expressed relative to its respective maximum fluorescence level (F_m). (A-C) experimental, actual values of minimum fluorescence (F'_0, black squares) together with the fitting function of F'_0 accounting for a heterogeneous antenna (red line) in the three light regimes. The fitting procedure involves only the values of $F'_{0\ act}$ in the absence of photoinhibition (qP_d>0.98), according to what postulated by Ware *et al*. (2015). Note that the subsequent $F'_{0\ act}$ drop as a function of NPQ is still approximately hyperbolic only in M and H plants (A-B), while the decrease in L plants is linear (C). (D) Example of $F'_{0\ act}$ (black squares), $F'_{0\ calc}$ (black line, homogeneous antenna, Oxborough and Baker 1997) and $F'_{0\ het}$ (red line, heterogeneous antenna, Ware *et al*. 2015) relative to the sample in (B).

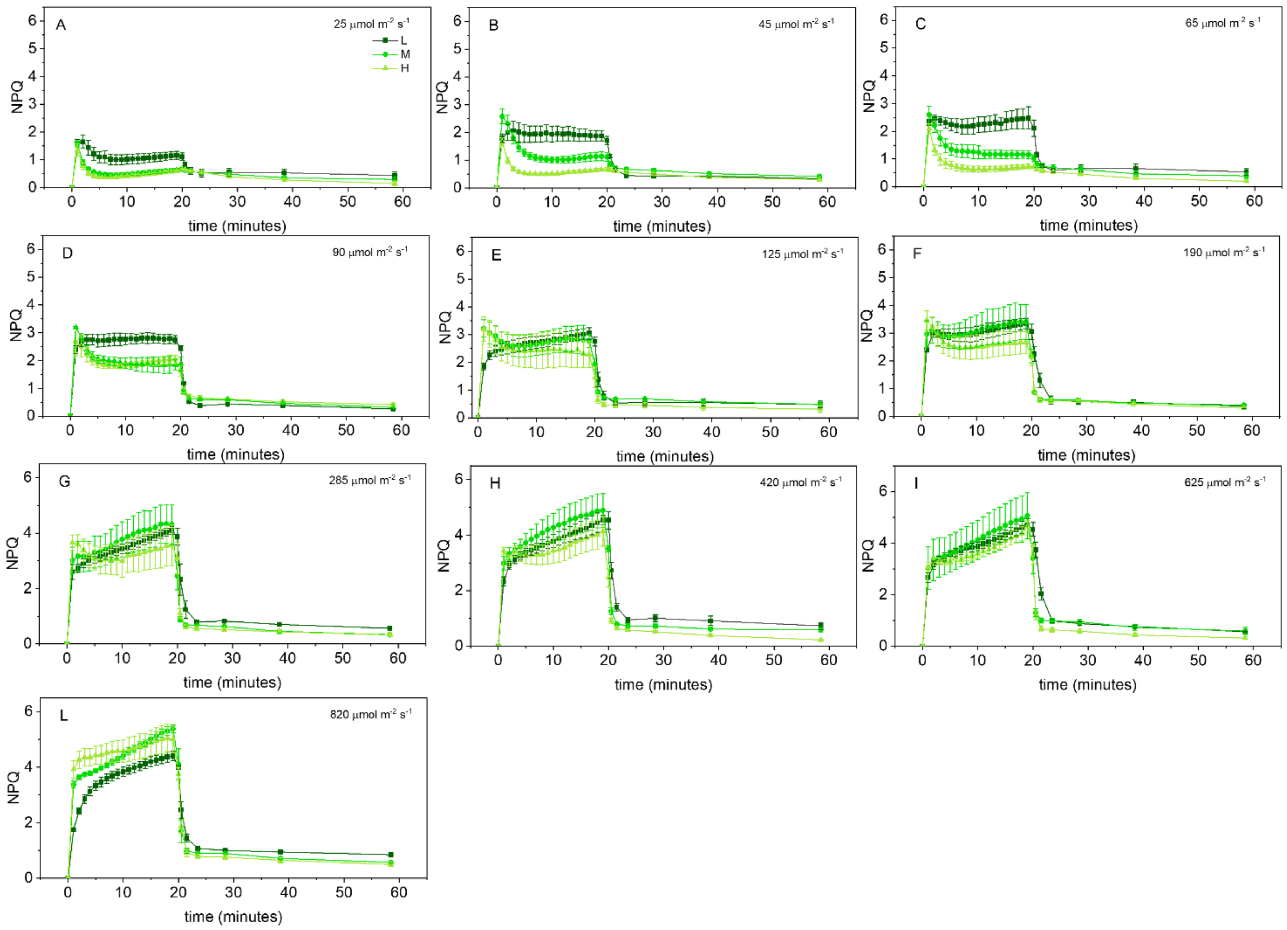

Fig. S4. Kinetic curves of NPQ during 19 minutes of continuous actinic light illumination followed by 40 minutes of dark relaxation in *Selaginella martensii* plants acclimated to deep shade (L), intermediate shade (M) and full sunlight (H). Levels of light intensity: 25, 45, 65, 90, 125, 190, 285, 420, 625, 820 μmol m^{-2} s^{-1}. Average values ±Standard Error for n = 3-6.

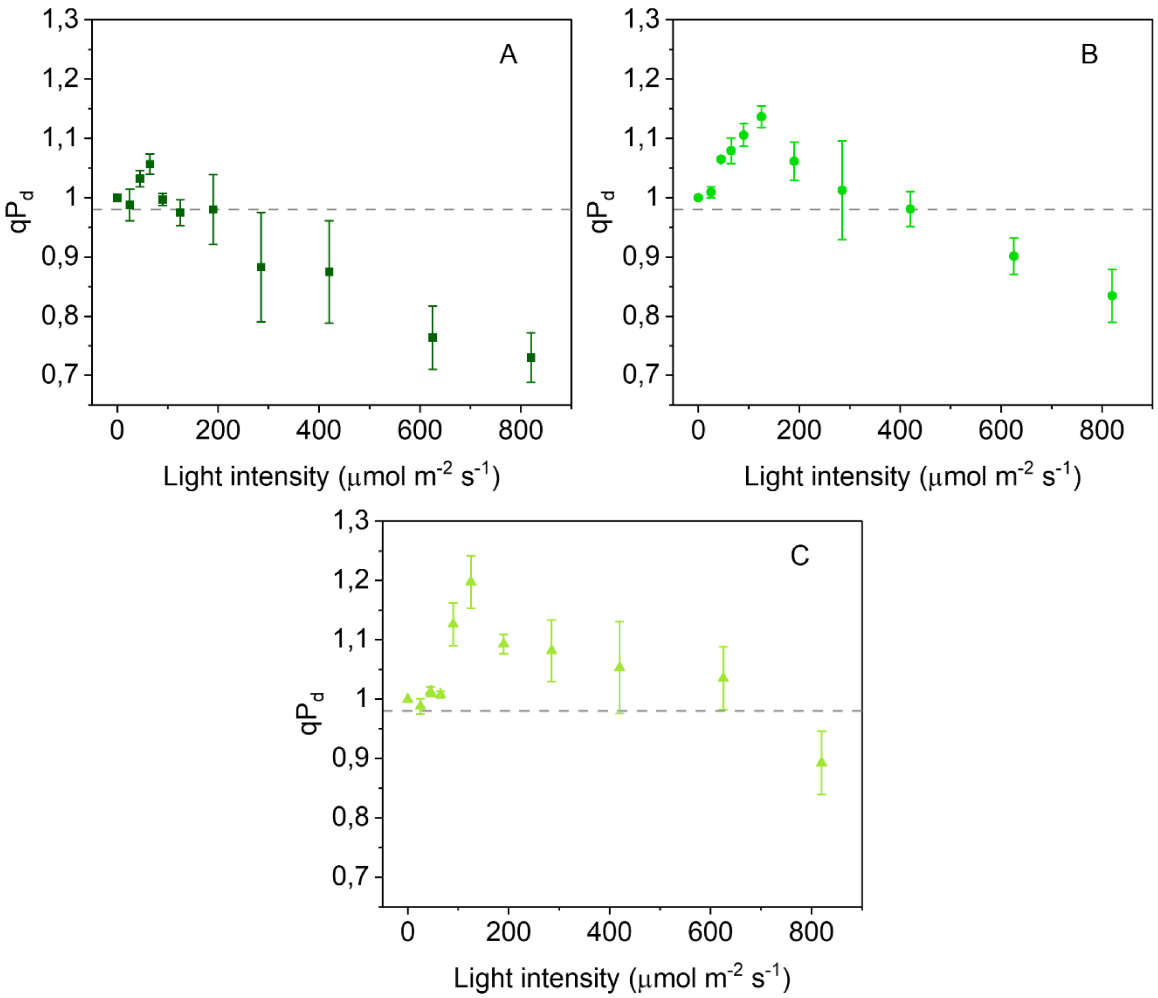

Fig. S5. Light curves of qP_d as function of light intensity. qP_d was calculated according to Ruban and Murchie (2012) in *Selaginella martensii* plants acclimated to deep shade (L), intermediate shade (M) and full sunlight (H). qP_d values were selected at specific times of the induction curve in order to closely match the number of photons that reached the samples at the end of each light interval of the light curve (the one treated in the paragraph "In sun plants higher photoprotection is accompanied by extensive PSII antenna uncoupling")

References

Ferroni, L., Angeleri, M., Pantaleoni, L., Pagliano, C., Longoni, P., Marsano, F., et al. (2014). Light-dependent reversible phosphorylation of the minor photosystem II antenna Lhcb6 (CP 24) occurs in lycophytes. *The Plant Journal*, 77(6), 893-905.

Järvi, S., Suorsa, M., Paakkarinen, V., & Aro, E.M. (2011). Optimized native gel systems for separation of thylakoid protein complexes: novel super-and mega-complexes. *Biochemical Journal*, 439(2), 207-214.

Oxborough, K., & Baker, N.R. (1997). Resolving chlorophyll a fluorescence images of photosynthetic efficiency into photochemical and non-photochemical components–calculation of qP and Fv/Fm; without measuring Fo'. *Photosynthesis Research*, 54(2), 135-142.

Ware, M.A., Belgio, E., & Ruban, A.V. (2015). Photoprotective capacity of non-photochemical quenching in plants acclimated to different light intensities. *Photosynthesis Research*, 126(2), 261-274.

Chapter 2:

Thylakoid membrane appression in the giant chloroplast of the shade-adapted lycophyte *Selaginella martensii* Spring (Lycopodiophyta)

Introduction

Selaginellaceae, with the only genus *Selaginella*, are a rich family of lycophytes, the diminutive early divergent group of vascular plants, sister clade of the euphyllophytes (Weststrand and Korall 2016). Most *Selaginella* species are found in the lower vegetation layers of tropical and subtropical forests, where the plant life would be impossible without special adaptations to deep shade. Light reaches the understorey after having been attenuated by the upper canopy, which not only strongly reduces irradiance, but also modifies the spectral composition of the light available to photosynthesis, determining a relative enrichment in green and far-red wavelengths. Moreover, understorey plants are exposed to unpredictable fluctuations in both light intensity and quality because of the sunflecks filtering through the canopy. The morphological adaptations of species adapted to deep shade are known for some time and include all levels of biological organization from the plant habit to the leaf anatomy, from the cell shape to the thylakoid system architecture inside the chloroplasts (Kozlowski and Pallardy 1997, Anderson et al. 1988, Mathur et al. 2018).

The most characterizing morphological feature of the thylakoid system is the segregation of the membranes into granal and stromal lamellar domains, which is biochemically related to the uneven distribution of photosystem I (PSI) in the stroma-exposed domains and photosystem II (PSII) in the appressed domains (Andersson and Anderson 1980). A granum can be defined as an approximately cylindrical stack with a diameter of ca. 400-600 nm and formed by at least three thylakoids, usually 5 to 25, depending on species and light conditions (Rantala et al. 2020; Mazur et al. 2021). Magnificent three-dimensional renderings of the granum structure and its connections with the stroma lamellae are currently available for model angiosperms (Austin and Staehelin 2011, Bussi et al. 2019; for a historical review on thylakoid architecture modelling, see Staehelin and Paolillo 2020). The thylakoid stacking depends on one hand on the vertical interactions of the supramolecular complexes formed by PSII and its light-harvesting complex LHCII in the appressed regions (Barber 1980, Albanese et al. 2020); on the other hand, it depends on the exclusion of PSI and the ATP synthase from the grana cores because of their stromal protrusions, which cannot be accommodated in the stromal gap of the grana partitions (Miller and Staehelin 1976, Daum et al. 2010, Nevo et al. 2012). The regions found at the interface between the appressed and non-appressed domains are called the “grana margins” (Rantala et al. 2020). The grana curvature areas are another thylakoid domain enriched in membrane curvature factors which regulate the granum size (Armbruster et al. 2013, Trotta et al. 2019). Inside the chloroplasts of shade-adapted plants, particularly angiosperms, the thylakoid system is very abundant, and the grana stacks are irregularly orientated and made up of several tens of thylakoids, even up to hundreds (e.g., *Alocasia macrorrhiza*, Anderson et al. 1973; *Anoectochilus roxburghii*, Shao et al. 2014; *Monstera deliciosa*, Demmig-Adams et al. 2015). The large amount of LHCII compared to PSII typically leads to low chlorophyll (Chl) *a*/*b* molar ratios (2.3-2.7) compared to sun-adapted plants (2.9-3.6; Lichtenthaler and Babani 2004, Anderson et al. 2012). The PSI/PSII ratio in shade plants is a conflicting issue, with contradictory reports also by the same authors (e.g., Melis and Harvey 1981, Anderson et al. 1988, Chow et al. 1990, Fan et al. 2007, Anderson et al. 2012). Given the exclusion of PSI from the grana cores and the need of understorey plants for balancing the over-excitation

of PSI due to the enrichment in far-red light, it is logical that, in the natural shade of the understorey, a high degree of thylakoid appression is accompanied by a low PSI/PSII ratio (Walters and Horton 1994, Pantaleoni et al. 2009).

Broadening the perspective to non-angiosperms, the structural diversity of the chloroplasts in shade plants is not limited to the size of the grana stacks. The striking ultrastructural shade adaptations in *Selaginella* species are instructive of an evolution of shade-adaptation traits that occurred independently of that better-characterized in angiosperms. In the very small and thin microphylls of rainforest *Selaginella* species the upper epidermal cells are usually the main location of photosynthesis (Jagels 1970, Sheue et al. 2007, Ferroni et al. 2016). The upper epidermal cells are roughly conical and, in many species, host only one giant chloroplast per cell, generally lying at the cell bottom to collect as much light as possible through a very extensive thylakoid system (Liu et al. 2020). Light harvesting is helped by the convex upper tangential cell wall, sometimes ornamented with silica bodies, which focuses light downwards to the chloroplast (lens effect; Liu et al. 2020, Shih et al. 2022). At the same time, the funnel-shape of the cell allows multiple light reflections inside the protoplast to possibly enable light harvesting also by less exposed thylakoids (light-pipe effect; Liu et al. 2020). In the *Selaginella* species adapted to the deepest shade (subgenus *Stachygynandrum*, Liu et al. 2020), the thylakoid system can differentiate into two structural zones, an upper region with parallel long lamellae formed by 2-4 appressed thylakoids and a lower granal structure (Sheue et al. 2007, 2015, Ferroni et al. 2016, Liu et al. 2020). In such "bizonoplast", the upper thylakoid lamellae are deemed responsible for blue iridescence, a phenomenon also observed in some deep-shade angiosperms, such as many *Begonia* species and *Phyllogatis rotundifolia* (Gould and Lee 1996, Pao et al. 2018, Masters et al. 2018, Castillo et al. 2021). In the most characterized species *S. erythropus*, the lower chloroplast region contains grana formed on average by 18 stacked thylakoids with a diameter of ca. 600 nm (Sheue et al. 2007). Therefore, despite the adaptation to deep shade, the granal structure lays within common ranges of grana size variation with respect to the granum height, and at the upper limit of the granum diameter (Kirchhoff 2019, Rantala et al. 2020). In the related species *S. martensii*, the upper epidermal cells host likewise a bizonoplast, although the thylakoid zonation is less pronounced than in *S. erythropus* (Ferroni et al. 2016) or was also reported to lack (Liu et al. 2020). In the prevailing granal region, occupying the major part of the chloroplast, the thylakoid stacking degree appears very variable inside the same organelle (Ferroni et al. 2016).

Because a high degree of thylakoid stacking is a very characterising morphological trait in the cell biology of shade-adapted species, in this report we aimed at testing if this assumption can be supported quantitatively in *S. martensii*. The thylakoid stacking extent was analysed using complementary morphometric (electron microscopy) and biochemical (differential thylakoid solubilisation) approaches, in combination with the electron paramagnetic resonance determination of the PSI/PSII ratio and the *in vivo* simultaneous analysis of prompt Chl *a* fluorescence and PSI oxidation state.

Materials and Methods

Plant material

The plant material used in this research was sampled from a colony of *Selaginella martensii* Spring (Selaginellaceae) kept under stable environmental conditions in the warm humid greenhouse at the Botanical Garden of the University of Ferrara (44°50'30'' N, 11°37'21''E). The temperature was maintained at 25-30°C and the relative humidity was always above 60%. The greenhouse reproduces the natural shade of the lower vegetation layers in a dense forest formation, where the *S. martensii* plants grow in a low-intensity, far-red enriched environment. All over the year, the maximum incident light intensity is less than 80 μmol photons m^{-2} s^{-1} and is enriched in far red (red/far red quantum ratio, 0.7). For analyses, terminal branches (2-3 ramifications from the apex) were sampled at the end of the night and all manipulations were done under a dim green safe light.

Transmission electron microscopy

Small portions of branches were cut and transferred into a 10-mL syringe. Soon after, 3 mL of a fixing solution were added (3% glutaraldehyde in 0.1 M K-Na phosphate buffer, pH 7.2, kept at 4°C) and air in intercellular spaces was removed creating a slight vacuum with the syringe plunger. The syringe was then covered with aluminium foil and fixation was allowed for 4 h at room temperature. After several washings with phosphate buffer, the samples were recovered in a vial and post-fixed with 1% OsO_4 in the same buffer over night at 4°C (Ferroni et al. 2016). After dehydration in a graded acetone series, the samples were infiltrated with Durcupan ACM epoxy resin. The ultrathin sections were contrasted with lead citrate and uranyl acetate and, for observation, a Zeiss EM910 transmission electron microscope was used (Electron Microscopy Centre, University of Ferrara).

For morphometric determinations of the thylakoid system, micrographs were analysed using the free processing package Fiji (https://imagej.net/software/fiji/). The ratio between appressed and stroma-exposed thylakoid membranes was determined in micrographs taken at 31.500×.

Thylakoid isolation

For thylakoid isolation the protocol described in Pantaleoni et al. (2009) was used with modifications as follows. At the end of the night, the terminal branches were cut and immediately transferred to a cold mortar (-20°C). The cold (4°C) grinding buffer was added (50 mM Tricine/KOH – pH 7.6, 330 mM sorbitol, 2 mM Na_2EDTA, 5 mM $MgCl_2$, 2.5 mM ascorbate, 0.05% bovine serum albumin, 10 mM NaF). After addition of sand quartz, the sample was quickly homogenized with a cold pestle and the homogenate was filtered through two layers of Miracloth (Calbiochem) and collected in a tube kept in ice. After centrifugation at 150 *g* for 5 min at 4°C to remove cell debris and residual quartz, the supernatant was collected and centrifuged at 18.000 *g* for 5 min at 4°C. The pellet, containing the chloroplasts, was subjected to hypoosmotic stress by resuspending in a cold shock buffer (50 mM Tricine/KOH – pH 7.6, 5 mM sorbitol, 2 mM Na_2EDTA, 5 mM $MgCl_2$, 10 mM

NaF). Centrifugation at 18.000 *g* for 5 min at 4°C allowed to collect the isolated thylakoids in the pellet, which were resuspended in storage buffer (100 mM Tricine/KOH – pH 7.6, 5 mM sorbitol, 2 mM Na_2EDTA, 5 mM $MgCl_2$, 10 mM NaF) to a final Chl concentration of ca. 1-2 mg mL^{-1}. The Chl concentration in the thylakoid suspension was determined after extraction with 80% (v/v) buffered acetone (2.5 mM Hepes/NaOH, pH 7.5) and quantitated as described by Porra et al. (1989). Subsequently, the samples were stored in liquid nitrogen until used for analyses.

Electron paramagnetic resonance

The protocol for the detection of the PSI and PSII signals was adapted from Danielsson et al. (2004) and Fan et al. (2007). The isolated thylakoids were pelleted by centrifugation at 18.000 g at 4°C for 5 min, the supernatant was discarded and the thylakoid pellet was resuspended with a MES [2-(N-morpholino)ethanesulfonic acid] buffer having the following composition: 15 mM MES/NaOH pH 6.5, 15 mM NaCl, 300 mM sucrose, to give a final Chl concentration of 3-4 mg mL^{-1} in a volume of 250 mL inside a 1.5 mL microtube. The thylakoid suspension was maintained on ice in darkness and used for electron paramagnetic resonance (EPR) measurements.

For EPR measurements, a Bruker ER200 MRD spectrometer equipped with a TE201 resonator (microwave frequency of 9.4 GHz) was used. The instrument was calibrated by using α,α'-diphenylpicrylhydrazyl (dpph). The sample to be analyzed (250 μL) was put in a flat quartz cell and the EPR spectrum was recorded for the blank constituted by a 5mM solution of $K_3[Fe(CN)_6]$ prepared in MES buffer. The radical-cation $P700^+$ in PSI (one radical spin per reaction centre) was chemically generated by addition of freshly prepared $K_3[Fe(CN)_6]$ to the thylakoid suspension to give a final concentration of 5 mM. After a dark incubation period of 10 min at room temperature, the sample was put in the flat cell for the EPR measurement of $P700^+$ signal. After the record, the flat cell was recovered from the cavity and exposed to white fluorescent light (ca. 30 μmol photons m^{-2} s^{-1}) for 60 s at room temperature. Then, the cell was reinserted into the cavity for the detection of the light-induced, dark-stable Tyrosine D radical in PSII reaction centre ($YD^{\cdot}$, one radical spin per reaction centre). Readjustment of the resonance conditions in the cavity corresponded to a waiting time of ca. 5 min prior to $YD^{\cdot}$ signal registration. For spectra elaboration, Origin™ version 2022 (OriginLab, Northampton, MA, USA) was used. The $P700^+$ signal was obtained by subtracting the $K_3[Fe(CN)_6]$ blank signal to avoid the disturbance due to Fe. Because the $P700^+$ signal is a single narrow line (Fan et al. 2007), it was easily identified nearby the G value typical of radicals; a line was drawn manually intersecting the signal centre tangential to the basal outline in the neighbourhood of the $P700^+$ line. The drawn line was used as baseline for integration, thus assigning to the signal centre the value of zero in the derivative, i.e., the maximum in the resulting quasi-Gaussian primitive curve. The intensity of the PSI signal was determined as the area subtended under the latter curve. For PSII, the $YD^{\cdot}$ signal overlapped on that of $P700^+$ (+ $K_3[Fe(CN)_6]$) and therefore was obtained by subtraction. The derivative $YD^{\cdot}$ signal is larger than that of $P700^+$ and consists of composite lines (Fan et al. 2007), therefore giving rise to a complex primitive curve; nevertheless, the signal centre was recognizable, and the same analytical procedure was applied as per the $P700^+$ signal, obtaining the signal intensity of $YD^{\cdot}$. Both

radical signals are equimolar to the respective photosystems, and the $YD^{\cdot}/P700^{+}$ area ratio was used as an estimate of the PSII/PSI stoichiometry.

Comparative thylakoid solubilization

The methods used were adapted from Rantala et al. (2017). Aliquots of thylakoid suspensions corresponding to 8 µg Chl were collected by centrifugation at 18.000 *g* for 5 min at 4°C and the supernatant was discarded. The pellet was then treated in one of the three following alternatives for solubilisation, in all cases operating in very dim light.

(1) Solubilisation with β-dodecylmaltoside (β-DM; Sigma-Aldrich) in BTH buffer [25 mM BisTris/HCl – pH 7.0, 20% (w/v) glycerol, 0.25 mg ml^{-1} Pefabloc, 10 mM NaF], on ice for 10 min with very slow mixing.
(2) Solubilisation with digitonin (Calbiochem) in BTH buffer, at room temperature (23°C) for 30 min with continuous gentle mixing.
(3) Solubilisation with digitonin in ACA buffer [50 mM BisTris/HCl – pH 7.0, 375 mM e-aminocaproic acid, 1 mM Na_2EDTA, 0.25 mg ml^{-1} Pefabloc, 10 mM NaF], at room temperature (23°C) for 30 min with continuous gentle mixing.

Operatively, the pellets were first resuspended in the buffer (BTH or ACA) and an equal volume of detergent solution (in BTH or ACA buffer) was added to obtain the final detergent concentrations of 0 (insolubilized control), 0.75, 1.50, 2.50%. After solubilization, the insolubilized material was pelleted by centrifugation at 18.000 *g* at 4°C for 20 min. The solubilized and insolubilized fractions were used to determine the respective Chl content as described in the previous paragraph. Alternatively, they were treated for SDS-PAGE separation of thylakoid proteins on a resolving gel with 15% acrylamide and 6 M urea (Laemmli 1970). Gels were silver stained using routine protocols.

Simultaneous analysis of P700 redox state and Chl a *fluorescence*

A Dual PAM-100 (Walz, Germany) was used for the measurement of the fast Chl *a* fluorescence induction and the P700 redox state (Klughammer and Schreiber 1994, Živčak et al. 2014a, Ferroni et al. 2022). Uncut terminal branches of dark-acclimated plants were positioned in the measuring head of the instrument, allowing a further dark-acclimation for ca. 2 minutes before analysis. Subsequently, the sample was exposed to a 600 ms-long saturation pulse with intensity of 10.000 µmol photons m^{-2} s^{-1}. During the pulse, the Chl *a* fluorescence emission signal and the $P700^{+}$ absorption signal (dual wavelength 830/875 nm) were recorded simultaneously at a high frequency (0.3 ms intervals).

Results

Thylakoid ultrastructure and morphometrics

To simplify the characterization of the thylakoid system in *S. martensii* giant chloroplasts, the plant material was sampled at the end of the night. The rationale for this choice was to promote the disappearance of the assimilatory starch grains and obtain better views of the thylakoid system. At the same time, in the long-term dark-acclimated chloroplast, the thylakoid system generally emphasizes the lateral heterogeneity of the photosynthetic complexes, i.e., a stricter segregation of PSII and PSI in grana cores or stroma-exposed domains, respectively (Rantala et al. 2020). Under these conditions, the appression degree should reflect more closely the PSI/PSII ratio.

At the end of the night, in the upper epidermal cells of *S. martensii* the giant chloroplast was cup-shaped and laid at the cell bottom, opposite to the large vacuole (Fig. 1A). Despite several hours of darkness and opposite to expectations, the organelle was still filled with many starch granules. Different from previous observations, no thylakoid dimorphism could be observed between the upper and lower region of the chloroplast, without any trace of the upper elongated lamellae (Ferroni et al. 2016). The very abundant thylakoid system was exclusively organized in grana stacks connected by stroma thylakoids all over the organelle and quite uniformly distributed around the starch granules (Fig. 1B). At a first glance, the degree of thylakoid appression was high, but the size of the grana stacks was extremely heterogeneous (Fig. 1C). In the same organelle, grana stacks formed several tens of thylakoids were found along with small stacks of only a few thylakoids (Fig. 1C). In some cases, the granum appeared as an individual unit well separated from the neighbouring grana (Fig. 1D). The appressed domains represented by the dark grana partitions (or stromal gaps) occupied the granum core. The non-appressed domains included mainly the stroma thylakoids and the top and bottom layers of each stack (end membranes). Laterally, the continuity domains of the granal thylakoids with the stroma lamellae in the region interfacing the appressed and non-appressed membranes, i.e., the grana margins, were well visible (Fig. 1E; Rantala et al. 2020). Relatively less easy was the observation the bended edges of the stacked thylakoids, i.e., the curvature areas the granum border (Trotta et al. 2019, Rantala et al. 2020). In addition, the identification of the borders of an individual granum was sometimes difficult, because the thylakoid system in *S. martensii* was quite frequently organized in a continuity of the appressed thylakoids from one stack to the other (Fig. 1F). Especially in these last cases, at the stack borders the clear prevalence of the grana margin regions over the curvature areas was appreciated; the stroma lamellae in continuity with the grana thylakoids tended to maintain a well-ordered parallel arrangement (Fig. 1G).

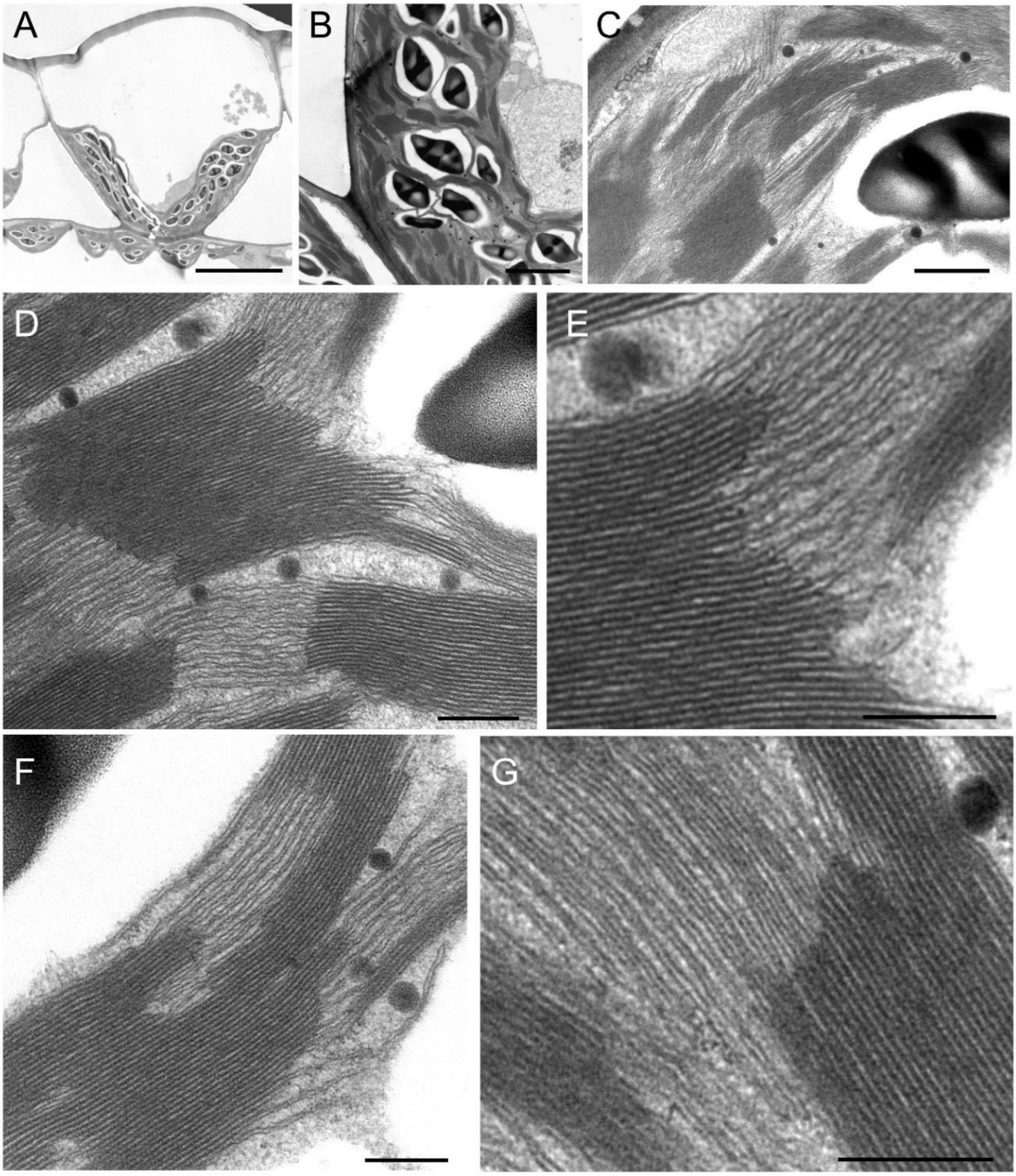

Figure 1 Electron micrographs of the giant chloroplast and thylakoid system in microphylls of *Selaginella martensii* at the end of the night. (A) A cell of the upper epidermis showing the cup-shaped giant chloroplast. (B) The thylakoid system appears abundant; note the abundance of starch grains. (C) Heterogeneity of the thylakoid stacking extent exemplified by the different height of grana in the same field of observation. (D) An example of large granum with several tens of appressed thylakoids. (E) A detail of the granum border in D showing the grana margins alternating with curvature areas. (F) An example of the direct continuity of neighbouring stacks, mediated not only by stroma lamellae, but also by appressed thylakoids, hardly reconciled with the model of a cylindrical granum. (G) Detail of a granum border from which almost all thylakoids originate parallelly arranged stroma lamellae. Scale bars: (A) 10 μm; (B) 2 μm; (C) 0.5 μm; (D-G) 0.2 μm.

The complicate distribution of the thylakoid system in *S. martensii* giant chloroplast, always influenced by the abundant interspersed starch granules, challenged its morphometric analysis. Within the single giant chloroplasts, the measurements were focussed on selected areas at a magnification offering a good compromise between rich-in-thylakoid field and sufficient resolution of the membranes, sectioned parallel to the stack axis. Heterogeneity of thylakoid stacking emerged clearly from the large variability of two morphometric parameters used to characterize the grana. The distribution of the number of thylakoids per granum was within a range of [5-86] and resulted in an average of 26 ± 19 (SD), corresponding to a coefficient of variation of 73% (Fig. 2A). Though the statistical distribution could be approximated as normal, its asymmetry was evident (skewness 1.43). The median of 21 thylakoids per granum was indeed smaller than the average and extreme stacking degree (>50 thylakoids/granum) was a relatively rare occurrence. The length of the grana partitions was also distributed in the quite wide range of [308-1026] nm and resulted in an average of 673 ± 157 (SD) nm, corresponding to a coefficient of variation of 23% (Fig. 2B). The distribution was symmetric (median 686 nm, skewness -0.45).

As emerging from the representative micrographs shown in Fig. 1, the non-appressed thylakoid domains (stroma lamellae, granum end membranes, curvature areas and grana margins) were well represented in *S. martensii* chloroplasts. The non-appressed domains accounted for 46.1% ± 5.2 (SD, with $N = 11$) of the membranes. Therefore, the thylakoid appression degree was quantified by the total length ratio between appressed/non-appressed thylakoid domains as 1.20 ± 0.27 (SD, with $N = 11$), i.e., a value much lower than expected for plants adapted to the shade (4-5; Andersson and Anderson 1988, Pancaldi et al. 1998).

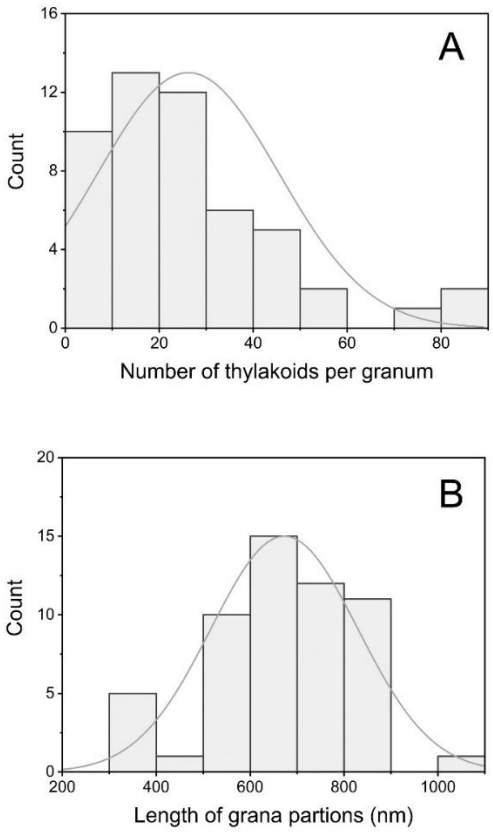

Figure 2 Morphometric analyses of thylakoid stacks in *Selaginella martensii* at the end of the night. (A) Histogram with the number of thylakoids per granum ($N = 51$). (B) Histogram with the length of grana partitions ($N = 55$). In both cases, the Gaussian curve approximating the distribution is shown.

Chl a/b *ratio and PSI/PSII ratio*

Prompted by the results of morphometric analyses, we analyzed two major determinants of the thylakoid stacking, i.e., the abundance of the antenna system and the PSII/PSI ratio. The Chl *a*/*b* molar ratio is a very good absolute marker to define the shade adaptation degree of vascular plants and is inversely proportional to the relative abundance of LHCII (Lichtenthaler and Babani 2004, Anderson 2012). Shade-adapted plants have an expected Chl *a*/*b* ratio within a range of [2.3-2.8]. In buffered acetonic extracts, the Chl *a*/*b* ratio of *S. martensii* thylakoids, sampled in different periods of the year, was within the interval [2.43-2.85] with a mean of 2.63±0.14 (SD, *n*=16).

EPR spectroscopy is an elective method for the precise determination of the PSI/PSII reaction centre stoichiometry (Danielsson et al. 2004, Fan et al. 2007, Ermakova et al. 2021). Preliminarily to each replicate analysis, the region of DPPH resonance was centred at 3457 G. In general, operating at conditions comparable to the relevant literature, the EPR signals of photosystems in *S. martensii* thylakoids had an extremely low intensity, which was symptomatic of the low concentration of reaction centres in the thylakoid membranes.

The P700+ signal of PSI was a single line centred at ca. 3466 G; the YD˙ signal was less defined and larger, centred at ca. 3462 G (Fig. 3). The average PSI/PSII ratio estimated from five independent biological replicates was 0.31 ± 0.04 (SE of the mean), indicating that PSII was in a large excess of PSI in S. martensii thylakoids. Therefore, notwithstanding the relative abundance in stroma-exposed membranes, Chl a/b and PSI/PSII ratios were in line with the shade-adaptation of this species, particularly the abundance of antennae in response to a low light availability and the low amount of PSI in response to the enrichment in far red.

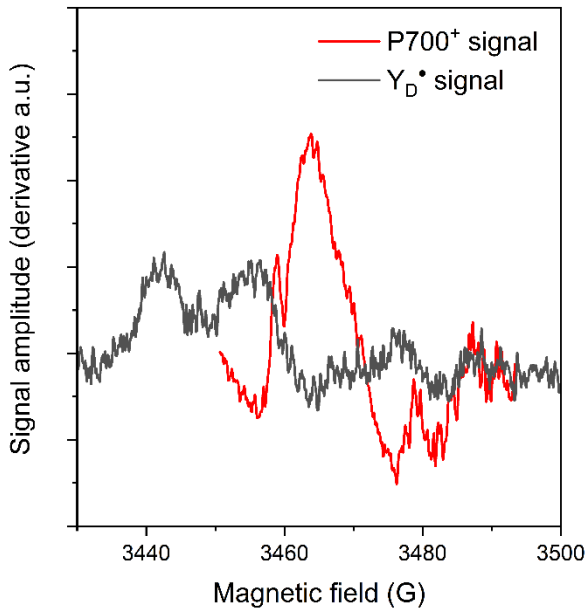

Figure 3 Spectra of EPR signals associated with tyrosine D radical Y_D˙ in PSII and $P700^+$ radical cation in PSI in thylakoids isolated from *Selaginella martensii*.

Differential solubilization of the thylakoid membranes

A method complementary to the ultrastructural analysis for the evaluation of the degree of thylakoid appression is based on selective thylakoid solubilization with non-ionic detergents. The isolated thylakoid membranes were solubilized using three different mild detergents at three concentrations, following the rationale exposed by Rantala et al. (2017).

β-DM is a very commonly used non-ionic detergent, releasing almost all protein complexes from the thylakoid membrane network (Aro et al. 2005; Järvi et al. 2011). This detergent is able to effectively penetrate the grana cores, destroying the weak hydrophobic interactions keeping together the LHCII lake with PSII and PSI (Grieco et al. 2015). β-DM in BTH buffer allows a quantitative and non-selective solubilization of thylakoids, and therefore it was used in this experiment as a control. In the absence of detergent, the BTH buffer alone did not lead to any measurable release of Chl-containing complexes. The solubilization yield, approaching 90%,

did not differ significantly between the three β-DM concentrations, although slightly higher at 1.5 and 2.5%. (Fig. 4). The Chl *a*/*b* molar ratio was determined in the solubilized and non-solubilized fractions and their weighted means were compared for consistency with the Chl *a*/*b* ratio of the entire thylakoids of origin. Expectedly, the β-DM-solubilized fractions had a Chl *a*/*b* ratio very similar to that of the entire thylakoid system. The 10% non-solubilized fraction did not differ significantly from that of the solubilized fraction (Table 1).

In order to assess biochemically the degree of thylakoid appression, the thylakoids were treated with increasing concentrations on digitonin using the same BTH buffer as for β-DM. Digitonin is an amphipathic molecule as β-DM but is bulkier and cannot penetrate the grana cores, i.e., digitonin solubilizes only the stroma-exposed thylakoid domains (Järvi et al. 2011, Suorsa et al. 2015). With *S. martensii* thylakoids, the solubilization yield with digitonin in BTH buffer was approximately the same independent of the detergent concentration, on average 24% (Fig. 4). The mean Chl *a*/*b* ratio of the solubilized fraction was 3.2, significantly higher than 2.5 in the insoluble fraction (Student's *t* test, $P<10^{-7}$), indicating the selective action of digitonin on the thylakoid system, although the difference between the two ratios was relatively small, only 0.7 (Table 1). Particularly, the Chl *a*/*b* ratio in the insoluble fraction was in line with reported values of the grana core of angiosperms (ca. 2.5; Danielsson et al. 2004, Rantala et al. 2017, Koochak et al. 2019). Conversely, in the soluble fraction the 3.2 ratio was markedly lower than expected, i.e., ca. 4.5 reported in digitonin-solubilized stroma-exposed thylakoid domains of angiosperms (Danielsson et al. 2004, Rantala et al. 2017).

As a further control, the digitonin solubilization was carried out in ACA buffer. Rantala et al. (2017) reported that digitonin in ACA buffer can solubilize the entire thylakoid system with an efficiency comparable to that of β-DM, i.e., losing the selectivity of this detergent towards appressed and non-appressed domains. As with BTH, ACA buffer alone did not lead to significant thylakoid solubilization. Different from expected, we could not reach ca. 90% solubilization as with β-DM and increasing doses of digitonin even decreased the solubilization yield. At the intermediate concentration of 1.5% digitonin, only half of the membranes had been solubilized (Fig. 4). The Chl *a*/*b* ratio in the fractions was similar to that of the original entire thylakoids of origin (Table 1).

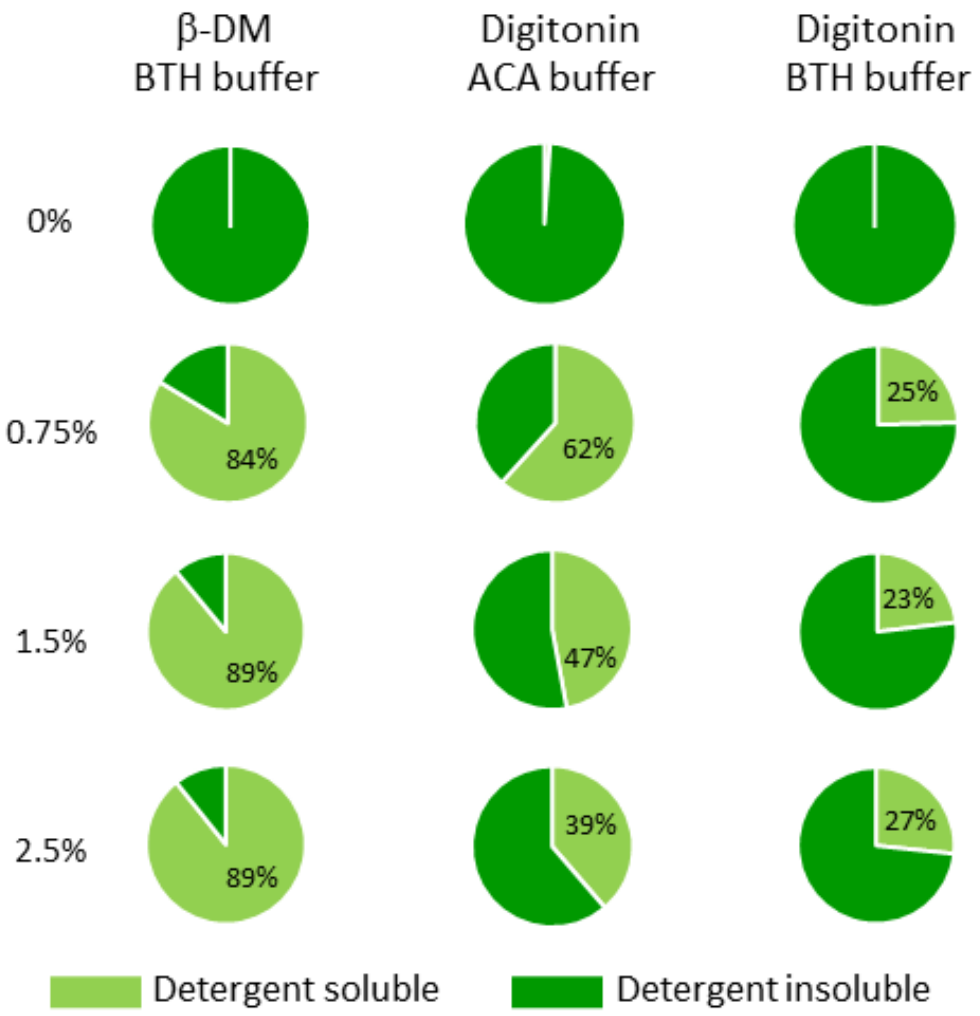

Figure 4 Solubilization of thylakoids isolated from *Selaginella martensii* at the end of the night with different detergent treatments. Thylakoid membranes were solubilized with different concentrations of β-dodecyl maltoside (β-DM) in bis-tris-HCl (BTH) buffer, or digitonin in BTH, or digitonin in aminocaproic acid buffer (ACA). The insolubilized membranes were pelleted by centrifugation. The chlorophyll content was determined in solubilized fraction (detergent-soluble supernatant) and insolubilized fraction (detergent-insoluble pellet). Each diagram represents the mean of 3-5 independent replicates.

Table 1 The chlorophyll *a/b* molar ratio in the detergent-soluble and insolubilized fraction of thylakoids isolated from *Selaginella martensii* at the end of the night and treated with different detergents. Thylakoid membranes were solubilized with different concentrations of β-dodecyl maltoside (β-DM) in bis-tris-HCl (BTH) buffer, or digitonin in BTH, or digitonin in aminocaproic acid buffer (ACA). The insolubilized membranes were pelleted by centrifugation. For each treatment, the weighted mean between the two fractions was calculated based on the yields of solubilization as in Fig. 4. The results are means of *N*=3-5 independent experiments, with SD. Asterisk mark a significant difference between the two fractions according to Student's *t*-test with $P<0.05$.

Sample	**Solubilized fraction**	**Non-solubilized fraction**	**Weighted mean**
Solubilization with β-DM in BTH buffer			
Thylakoids		2.55 ± 0.07	
BTH - 0% β-DM		2.56 ± 0.06	
BTH - 0.75% β-DM	2.54 ± 0.04	2.45 ± 0.13	2.53 ± 0.02
BTH - 1.5% β-DM	2.54 ± 0.07	2.28 ± 0.36	2.51 ± 0.10
BTH - 2.5% β-DM	2.52 ± 0.07	2.40 ± 0.71	2.51 ± 0.06
Solubilization with digitonin in BTH buffer			
Thylakoids		2.61 ± 0.17	
BTH - 0% digitonin		2.70 ± 0.20	
BTH - 0.75% digitonin	3.33 ± 0.10*	2.39 ± 0.04	2.62 ± 0.03
BTH - 1.5% digitonin	3.13 ± 0.22*	2.43 ± 0.03	2.59 ± 0.04
BTH - 2.5% digitonin	3.17 ± 0.24*	2.55 ± 0.20	2.71 ± 0.18
Solubilization with digitonin in ACA buffer			
Thylakoids		2.75 ± 0.04	
ACA - 0% digitonin		2.71 ± 0.07	
ACA - 0.75% digitonin	2.67 ± 0.08	2.84 ± 0.34	2.70 ± 0.11
ACA - 1.5% digitonin	2.73 ± 0.07	2.78 ± 0.10	2.75 ± 0.02
ACA - 2.5% digitonin	2.82 ± 0.07	2.73 ± 0.16	2.75 ± 0.12

The relatively low Chl *a*/*b* ratio in the digitonin-BTH-soluble fraction and the incomplete solubilization with digitonin-ACA were two most interesting results from the solubilization experiments with respect to the thylakoid domain differentiation. The thylakoid protein profile in the fractions was compared using SDS-PAGE. The identification of major proteins of *S. martensii* thylakoids was based on apparent molecular weight and previous detailed reports on the thylakoid composition in the same species (Ferroni et al. 2014, 2016, 2018). Because *S. martensii* thylakoids are particularly rich in antenna complexes, as also evident from the low Chl *a*/*b* ratio, gels were silver-stained allowing a short stain development to analyse comparatively the relative abundance of the major LHCII, in particular of its subunits Lhcb1-3 (Fig. 5A). Almost all LHCII was solubilized by β-DM; with digitonin-BTH, although a major part of LHCII remained in the insoluble fraction, a significant population of LHCII was also solubilized. The treatment with digitonin-ACA led to a nearly equal repartition of LHCII between the two fractions. Therefore, the distribution of LHCII between soluble and insoluble fractions closely followed the yield of solubilization for each detergent treatment (Fig. 5A).

Allowing a longer stain development, the band intensity of LHCII tended to saturate, and the main subunits of the major thylakoid complexes appeared (Fig. 5B). Information about the selectivity of digitonin was primarily obtained from the distribution of the ATP-β subunit of the ATP synthase, which marks undoubtedly only the stroma-exposed thylakoid domains. ATP-β originated an easily recognizable band with an apparent molecular weight of ca. 54 kDa. Almost all ATP-β was found in the soluble fraction after digitonin-BTH treatment, confirming the access of the detergent to only non-appressed domains. A similar enrichment in ATP-β also occurred in the digitonin-ACA-solubilized fraction. The stroma-exposed domains were expected to be also enriched in PSI. In the original thylakoids, the PsaA/B subunits of the PSI core were recognized as a single band at ca. 66 kDa; all samples presented a faint band in the same region. Although PsaA/B formed a quite well-defined band in the soluble fraction obtained with digitonin-BTH, it was also present in the corresponding insoluble fraction, which therefore included, along with the grana cores, a significant amount of stroma-exposed membranes. The use of digitonin-ACA enriched the amount of PsaA/B found in the soluble fraction, therefore allowing a better access of the detergent to the non-appressed membranes. The main four subunits of the PSII core are D1 and D2 of the reaction centre, at ca. 30 and 33 kDa, respectively, and the two inner Chl *a*-binding antenna proteins CP43 and CP47, at ca. 43 and 47 kDa, respectively. The CP43 band was less sharp than that of CP47 probably because in *S. martensii* it occurs in phosphorylated and non-phosphorylated forms even in darkness (Ferroni et al. 2014, 2018). The PSII core subunits were largely found in the digitonin-BTH-insoluble fraction, which was in line with the enrichment in grana cores. However, some PSII core subunits, particularly CP47 and D2, were also contained in the corresponding soluble fraction. The less evident CP43 indicated the presence of a CP43-less PSII subpopulation. Using digitonin-ACA, the release of the PSII core subunits was clearly more marked than with the BTH buffer; however, while some PSII core subunits, especially D2, were enriched in the soluble fraction, CP47 appeared equally distributed between the soluble and insoluble fractions. Given the expected equimolar presence of CP47 and D2, none of which directly involved in PSII repair cycle (different from D1 and CP43), their differential abundance in soluble and

insoluble fractions was indicative of an artefactual reorganization of the complexes using digitonin in ACA buffer.

Overall, the membrane that was promptly accessible to digitonin-BTH solubilization was approximately half of the stroma-exposed domains as evaluated from the morphometrics. A thylakoid fractionation closer to the result of the latter was obtained using digitonin-ACA, which improved the solubilization of PSI, but also extracted a significant amount of PSII from the thylakoids. Noticeably, LHCII was evenly distributed in the thylakoid membrane.

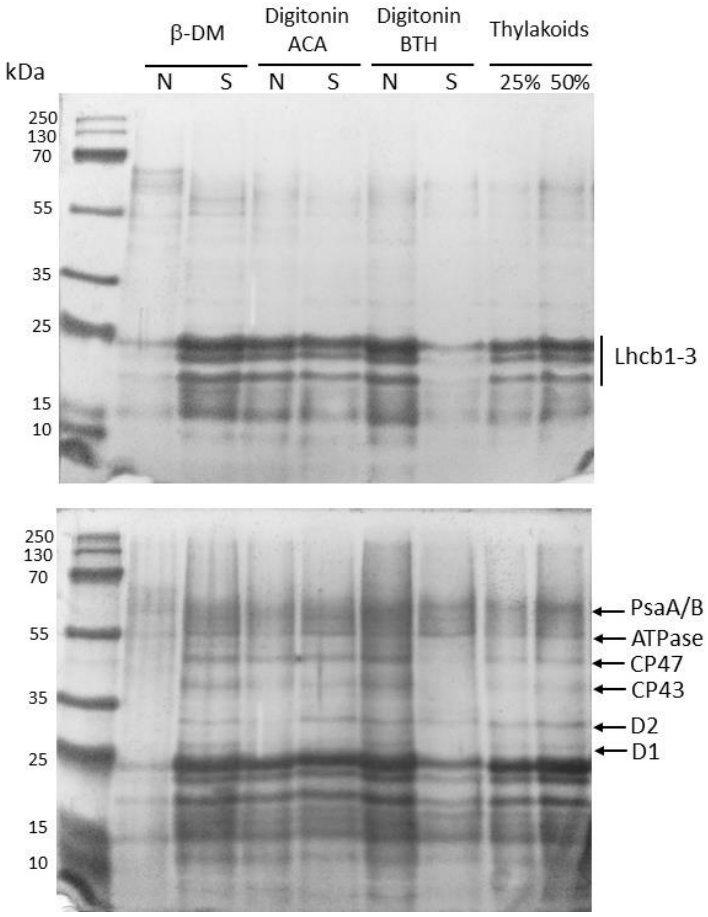

Figure 5 Proteins of the thylakoid membranes of *Selaginella martensii* solubilized with different detergents and separated on SDS-PAGE. Thylakoid membranes were solubilized with different 1.5% β-dodecyl maltoside (β-DM) in bis-tris-HCl (BTH) buffer, or 1.5% digitonin in BTH, or 1.5% digitonin in aminocaproic acid buffer (ACA). For reference, entire thylakoids were also loaded in the same gel. Bands were silver stained, and proteins were assigned based on Ferroni et al. (2014, 2016). N, detergent-insoluble fraction; S, detergent-soluble fraction. Upper and lower gel differ with respect to the stain development.

Fast Chl a *fluorescence induction and P700 oxidation state*

The analytical methods used to characterize the thylakoid appression in *S. martensii* gave results not easily matching with each other, particularly the low Chl *a*/*b* and PSI/PSII ratios in a thylakoid system characterized instead by a regular appression degree. To obtain further information, we analysed the *in vivo* fast Chl *a* fluorescence transient (OJIP) upon the microphyll excitation with a saturating pulse. When visualized on a logarithmic timescale, the OJIP transient appears polyphasic: starting from a minimum value of fluorescence at step O, it shows a first fast increase up to an inflection at step J, followed by a second rise and a new inflection at step I, before reaching the plateau P, corresponding to the maximum fluorescence emitted by PSII (for review, Stirbet and Govindjee 2011). Using a modulated fluorometer, in *S. martensii* the J and I steps were reached after approx. 4 and 40 ms from the onset of the pulse, respectively (Fig. 6A). The amplitude of relative fluorescence at I step ($\Delta V_{I\text{-}P}$) depends on the activity of PSI that moves electrons from the reduced intersystem electron carriers to its end acceptors (ferredoxin and ferredoxin-$NADP^+$-oxido-reductase) and is an indirect indicator of the PSI/PSII stoichiometry (Schansker et al. 2005, Ceppi et al. 2012; for relevant exceptions see Zivcak et al. 2015 and Ferroni et al. 2022). In seed plants, the value is generally within a range of [0.18-0.35] (e.g., Zivcak et al. 2014b, Pollastrini et al. 2016, 2020, Umar et al. 2019, Killi et al. 2020, Filacek et al. 2022). The OJIP transient of *S. martensii* was evidently characterized by a very small I-P amplitude: the $\Delta V_{I\text{-}P}$ value of 0.119±0.009 (SE, $N = 5$) supported a very low abundance of PSI relative to PSII.

We also analysed the changes in P700 oxidation state in PSI reaction centre simultaneous with the Chl fluorescence rise. During the first 3-4 ms, the $P700^+$ signal increased very rapidly nearly approaching its maximum (Fig. 6A). The cause for the $P700^+$ accumulation was the lack of reduced electron transporters during the O-J phase, which is dominated by the reduction of the primary electron acceptor Q_A in PSII reaction centre, up to reaching a transitionary equilibrium with the Q_A^- oxidation by forward electron transport to the plastoquinone pool at step J. Again, the very prompt and nearly complete oxidation of P700 in just a few ms was indicative of a small relative amount of PSI. During the subsequent J-I phase, the plastoquinone pool was progressively reduced (Tóth et al. 2007), starting to make electrons available to the re-reduction of P700 through the plastocyanin. In angiosperms, $P700^+$ still markedly accumulates during the J-I phase, approaching a transitionary steady state after 7-10 ms from the onset of the pulse – this testifies to an effective supply of electrons leading to a balance between P700 oxidation and re-reduction (Zivcak et al. 2014a, Tsimilli-Michael 2020, Guo et al. 2020, Ferroni et al. 2022). In *S. martensii* the increase in $P700^+$ was instead marginal during the J-I phase and the maximum $P700^+$ (a quite sharp peak rather than a quasi-plateau) was reached in correspondence of the I step at ca. 40 ms (Fig. 6). Subsequently, the complete re-reduction of $P700^+$ took approx. 350 ms, with the exhaustion of the oxidized end electron acceptors of PSI (Fig. 3B). For reference, in Fig. 3C, the $P700^+$ kinetics is shown comparatively in *S. martensii* and in the angiosperm *Triticum durum*, where the re-reduction of P700 was achieved in some 100-150 ms. Therefore, in *S. martensii*, the electrons were made very slowly available to the reduction of $P700^+$.

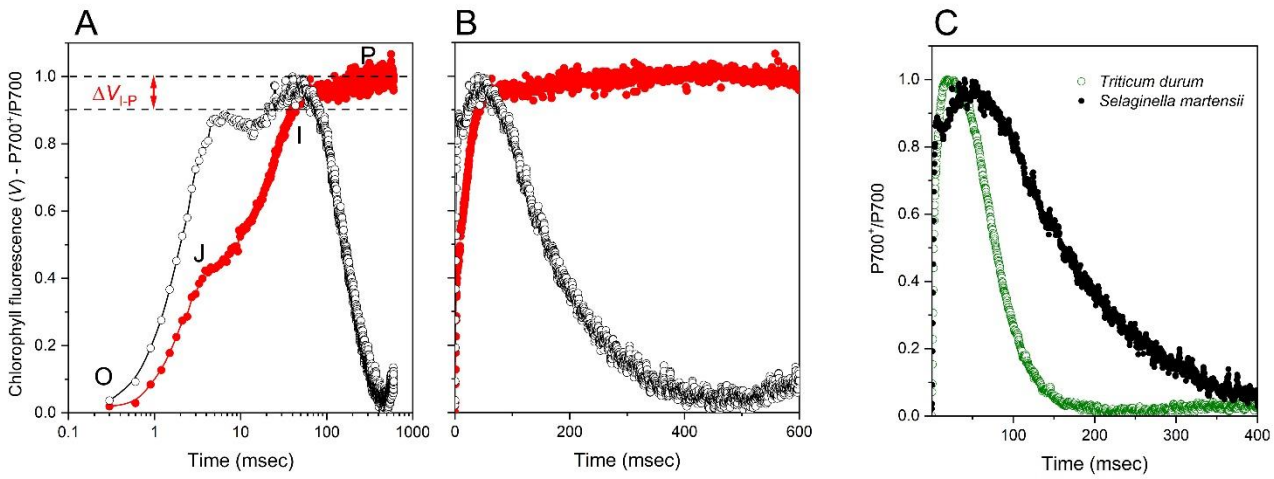

Figure 6 Kinetics of chlorophyll *a* fluorescence induction and P700 oxidation kinetics in *Selaginella martensii* microphylls. (A) Simultaneous kinetics represented on a logarithmic timescale and double normalized between maximum and minimum. The noticeable steps of the fluorescence transient (red) are indicated as the origin O, the first inflection J, the second inflection I, and the final value P. The relative amplitude of the I-P phase is indicated as $\Delta V_{I\text{-}P}$. The P700 oxidation kinetics is shown in black. Notice that the I step marks the final rise of fluorescence and also the re-reduction of P700. (B) The same as in A, represented in a linear timescale. (C) Comparative P700 oxidation kinetics in *S. martensii* (green) and in *Triticum durum* (durum wheat, black). Notice the extremely slow re-reduction of P700 in the lycophyte.

Discussion

Within the lineage of Viridiplantae, starting from a seeming random alternation of appressed and non-appressed thylakoid domains in green algae, the three-dimensional architecture of the thylakoid system evolved in land plants and originated the highly structured multiple membrane layers known as grana (Gunning and Schwartz 1999, Gu et al. 2022). However, the granum structure formed by thylakoid membranes with the same diameter and almost perfectly aligned laterally to build a cylinder (Staehelin and Paolillo 2020) is an idealization, which does not account for the irregular grana shapes observed in most plant species (Mazur et al. 2021). The structural diversity of the thylakoid system in vascular plants has long been interpreted in terms of adaptation to the growth light regime (sun-to-shade gradient; Andersson and Anderson 1988, Anderson et al. 2012). Very interestingly, as compared to euphyllophytes, the sister clade of lycophytes has explored an extreme variability of chloroplast structures, particularly through the species belonging to Selaginellaceae (Liu et al. 2020). The limitations of the granum structural model are evident from the properties of the thylakoid system in the chloroplast of *Selaginella martensii*.

Paradigm of the shade adaptation of the thylakoid system, as derived mainly from angiosperms, is the high membrane extension associated with the enhancement of thylakoid stacking, which is meant as the vertical granum development, or the number of stacked thylakoids per granum, up to the construction of giant grana (Anderson et al. 1973, Lichtenthaler and Babani 2004, Anderson et al. 2012, Shao et al. 2014, Demmig-Adams et al. 2015). Interestingly, despite the shade adaptation and the night incubation, in *S. martensii* the non-appressed/appressed ratio is close to 1 and the occurrence of giant grana in the chloroplast of *S. martensii* is only sporadic. Regular size stacks largely prevail, in line with morphometrics previously reported for the related, shade-tolerant species *S. erythropus* (Sheue et al. 2007). Nonetheless, the Chl *a/b* and PSI/PSII ratios are clear biochemical markers of the deep-shade adaptation of *S. martensii* thylakoids. A PSI/PSII ratio of 0.31 is lower than values reported for angiosperms grown in a far-red-enriched environment (0.4-0.5; Fan et al. 2007) but higher than that of grana preparations (0.125-0.25; Danielsson et al. 2004, Koochak et al. 2019). Although our EPR determination can be affected by errors due to the small concentration of reaction centres in *S. martensii* thylakoids, the very low PSI/PSII ratio is independently supported by the Chl *a* prompt fluorescence transient, featuring a minute amplitude of the I-P phase: $\Delta V_{\text{I-P}}$ around 0.10 were reported in sciaphilous angiosperms, such as rainforest bromeliads (Souza et al. 2019, Martins et al. 2021). Therefore, *S. martensii* thylakoids are confirmed to possess the typical biochemical hallmarks of shade adaptation.

Contrasting with the structural paradigm of thylakoid shade-adaptation in angiosperms, *S. martensii* privileges the lateral extension of thylakoid appressions in place of the vertical development of grana, leading to a thylakoid system dominated by an extreme stacking heterogeneity. A geometrical feature, somehow grounding the cylindrical granum model of angiosperms, is the very narrow variation range of the thylakoid disk diameter, consistently reported in a range of 400-600 nm (Kaftan et al. 2022, Shimoni et al. 2005, Fristedt et al. 2009, Daum et al. 2010, Armbruster et al. 2013, Pfeiffer and Krupinska 2005, Kouril et al. 2011, Wood et al. 2019). Using *Arabidopsis thaliana* mutants lacking thylakoid curvature factors, Höhner et al. (2020) showed that

oversized appressed domains cause a restricted plastocyanin diffusion from cytochrome b_6f to PSI. Accordingly, they interpret the restriction of the granum diameter to less than 500 nm as the result of a strong evolutionary pressure facilitating the linear electron flow. A mean grana partition diameter of 594 nm as in *S. erythropus* (Sheue et al. 2007) and even more of 673 nm in *S. martensii* – in both species including appressions as long as 1000 nm – suggests that the evolutionary trajectory fixing the threshold for the lateral development of grana to 500 nm is specific to angiosperms, and maybe can be generalized to euphyllophytes, but certainly *not to lycophytes*. Nonetheless, in agreement with Höhner et al. (2020), our analysis of $P700^+$ reduction kinetics confirms that an extensive lateral development of thylakoid appressions, while very likely emphasises light harvesting, limits the long-range diffusion of plastocyanin, making the re-reduction of P700 very slow. Therefore, the overall thylakoid function in *Selaginella* chloroplasts will require compensation for the slowness of the linear electron flow determined by structural constraints. For example, the high capacity of thermal dissipation of excess absorbed energy documented in *S. martensii* and quite unusual for a deep-shade species can be considered one of such mechanisms (Ferroni et al. 2014, 2018, 2021, Colpo et al. 2022). In addition, the high percentage of stroma-exposed membranes, again unusual in shade-adapted plants, suggests an extensive use of cyclic electron flow around PSI, in alternative or combination with other mechanisms ensuring the safe oxidized state of PSI in understorey plants (Sun et al. 2020, Terashima et al. 2021).

If we aim at a less reductionist representation of *S. martensii* thylakoid system, going beyond the mere grana-intergrana antithesis, electron micrographs suggest a particularly complex tridimensionality of the thylakoid architecture in *S. martensii*. Mazur et al. (2020) recently pointed out that the cylindric granum model does not catch the complexity of grana in angiosperms, where irregularity is more the rule than the exception. Views of the thylakoid system in *Selaginella* species document how relevant this caveat is in a lycophyte (Sheue et al. 2007, Ferroni et al. 2016, Ghaffar et al. 2018, Liu et al. 2020). Two structural features increase the complexity of the thylakoid organization in *S. martensii*. The first is the frequent granum confluence into the neighbouring one(s), which can be interpreted as an individual, but very irregular, granum, formed by layers with highly variable diameters (Mazur et al. 2020). However, granum irregularity in *S. martensii* is not limited to the lateral sliding apart of the thylakoid layers but is also complicated by the connecting stromal thylakoids: images such as that in Fig. 1F suggest that some regions formed by parallel stroma thylakoids can be partly embedded in the granum body. A complex tridimensional arrangement of the thylakoid system can conceivably limit the accessibility of the stroma-exposed membranes to a selective detergent like digitonin.

The quantification of non-appressed membranes was strongly divergent between the digitonin (25%) and morphometric (46%) approaches. Because of the small hydrophobic moiety represented by the sterol part, the action of digotonin is limited to the outer leaflet of a membrane bilayer (Fan and Heerklotz 2017). At the same time the hydrophilic oligosaccharidic part is too bulky and cannot penetrate the narrow stromal gaps (Järvi et al. 2011, Suorsa et al. 2015). Consequently, digitonin-soluble fractions are considered representative of the non-appressed thylakoid domains, which reorganize into lipid-protein-digitonin micelles preserving a very close-to-native organization of the thylakoid megacomplexes (for review, Rantala et al. 2020). Previous

application of this method to *S. martensii* thylakoids evidenced the existence of abundant and large PSII–LHCII–PSI–LHCI megacomplexes (Ferroni et al. 2016). The low Chl *a/b* ratio in digitonin-BTH-soluble fraction, much lower than expected for stroma thylakoids (4.5-7.1; Rantala et al. 2017, Koochak et al. 2019), suggests a very extensive use of LHCII as an antenna serving PSI in *S. martensii*. Importantly, this result obtained in the dark-acclimated state endorses an emerging idea in angiosperms about the stable association of a population of LHCII to PSI also in the dark (Chukhutsina et al. 2020), a property that could be exploited more intensely in lycophytes and deserving further studies. However, it remains that the digitonin-BTH-soluble fraction, though highly enriched in ATP synthase, offers only a partial picture of the stroma-exposed domains in *S. martensii*, because a large part of PSI is instead still found in the insoluble fraction (Fig. 6). Owing to its 5 nm stromal protrusion, PSI cannot be accommodated in the grana partitions for steric reasons (Nevo et al. 2012), and therefore in the lycophyte the digitonin-BTH-insoluble fraction contains not only the grana cores, but also a considerable amount of non-appressed thylakoid membranes. A fraction such of the non-appressed thylakoids can be the most "hidden" inside the grana network and represent approx. one half of the stroma-exposed membranes, which resolves the divergence between the morphometric and biochemical result. Our findings also indicate that in *S. martensii* the stroma-exposed membranes are not uniform with respect to the distribution of photosynthetic complexes, particularly the ATP synthase. Conceivably, the "hidden" non-appressed regions cannot be reached by digitonin unless the grana partitions are open to allow the detergent access. Rantala et al. (2017) reported that, through an unknown mechanism, the use of a buffer with a high concentration of aminocaproic acid allows digitonin to enter the tightly appressed grana partitions. In *A. thaliana* the thylakoid solubilisation was almost complete and showed a very high level of preservation of native associations of photosynthetic complexes (Rantala et al. 2017). In *S. martensii* the digitonin-ACA-soluble fraction accounted for approx. half of the thylakoids and was richer in PSI than the digitonin-BTH-soluble fraction, indicating that a significant part of the "hidden" non-appressed membranes was also solubilized. Therefore, most, but not all, of the non-appressed domains can be solubilised by digitonin-ACA and these membranes host a relative LHCII amount like that of the grana cores, but in the presence of both PSI and PSII. We notice that the result obtained with *S. martensii* thylakoids is heavily contrasting with that reported with the model angiosperm *A. thaliana* – actually the only species in which the method has been used up to date (Rantala et al. 2017, 2022). The reason is almost certainly to be sought in the tridimensional complexity of the thylakoid system and/or the unusually high lateral extension of the appressed domains in *S. martensii*, which hinders the capacity of digitonin penetration into the granum network even in the presence of ACA. Moreover, the inverse dose dependence (more digitonin leads to less solubilisation; Fig. 4) and the altered distribution of PSII subunits between the fractions (Fig. 6) indicate a direct strong interference of the detergent with the membrane complexes. Therefore, different to *A. thaliana* (Rantala et al. 2017, 2022), in *S. martensii* there is a lack of prerequisites for using the digitonin-ACA method for the comprehensive isolation of native megacomplexes from the entire thylakoid system.

The level of structural complexity of the thylakoid system in *Selaginella* species can be higher than described in this work. A unique thylakoid zonation into elongated lamellae formed by a few thylakoids and, underneath,

the granal system is an ultrastructural trait shared by the deep-shade species included in subgenus *Stachygynandrum* (Liu et al. 2020), which includes *S. martensii* (Ferroni et al. 2016). This intra-organelle dimorphism is interpreted as a special adaptation to deep shade and seems a very stable structural feature (Sheue et al. 2015, Ghaffar et al. 2018). In *S. martensii* the absence of the elongated lamellae after a night-long dark incubation was an unexpected finding, and a somehow fortunate event to allow the study in a simplified only-granal system. Interestingly, in their extensive comparative analysis of chloroplasts in *Selaginella* species, Liu et al. (2020) could not find any thylakoid zonation in *S. martensii*. Our observation suggests that the differentiation of the lamellar region is inducible in the short-term in *S. martensii* and requires the exposure to light.

In conclusion, the evolution of chloroplast adaptive traits to deep shade has occurred in parallel in lycophytes and in euphyllophytes, up to the most recent lineage of angiosperms. Under the same environmental pressure including low light intensity, far red enrichment, and unpredictable sunflecks, the two lineages underwent a convergent evolution of some basic traits, e.g., the extension of the thylakoid system and the enlargement of the antenna complement. However, a closer look also highlights significant elements of divergence, particularly the vertical development of grana in angiosperms and, conversely, the lateral widening of thylakoid appressions in lycophytes. The structural divergence lays its foundation in the supramolecular organisation of the thylakoid complexes, known in detail in angiosperms (Kirchhoff 2019, Rantala et al. 2020), but still very limitedly in lycophytes (Ferroni et al. 2014, 2016). Breaking some well-established or emerging relations between structure and function of thylakoids, *S. martensii* illustrates that, despite a very low PSI/PSII ratio and very abundant LHCII, a thylakoid system can be build with a high fraction of non-appressed domains – which however contain a large part of PSI and PSII in a wide lake of antennae. It also demonstrates that the 500 nm is not an upper threshold to the stacked thylakoid diameter in lycophytes.

Acknowledgements

Prof. Alessandra Molinari (Department of Chemical, Pharmaceutical and Agricultural Sciences, University of Ferrara) is kindly thanked for the EPR measurements. Prof. Ing. Marian Brestić and Prof. Ing. Marek Živčák are kindly thanked for the use of the DUAL-PAM fluorometer at the Slovak University of Agriculture in Nitra (SK).

References

Albanese, P., Tamara, S., Saracco, G., Scheltema, R. A., & Pagliano, C. (2020). How paired PSII–LHCII supercomplexes mediate the stacking of plant thylakoid membranes unveiled by structural mass-spectrometry. *Nature Communications*, 11(1), 1-14.

Anderson, J. M., Chow, W. S., & Goodchild, D. J. (1988). Thylakoid membrane organisation in sun/shade acclimation. *Functional Plant Biology*, 15(2), 11-26.

Anderson, J. M., Goodchild, D. J., & Boardman, N. K. (1973). Composition of the photosystems and chloroplast structure in extreme shade plants. *Biochimica et Biophysica Acta (BBA)-Bioenergetics*, 325(3), 573-585.

Anderson, J. M., Horton, P., Kim, E. H., & Chow, W. S. (2012). Towards elucidation of dynamic structural changes of plant thylakoid architecture. *Philosophical Transactions of the Royal Society B: Biological Sciences*, 367(1608), 3515-3524.

Andersson, B., & Anderson, J. M. (1980). Lateral heterogeneity in the distribution of chlorophyll-protein complexes of the thylakoid membranes of spinach chloroplasts. *Biochimica et Biophysica Acta (BBA)-Bioenergetics*, 593(2), 427-440.

Armbruster, U., Labs, M., Pribil, M., Viola, S., Xu, W., Scharfenberg, M., et al. (2013). *Arabidopsis* CURVATURE THYLAKOID1 proteins modify thylakoid architecture by inducing membrane curvature. *The Plant Cell*, 25(7), 2661-2678.

Aro, E. M., Suorsa, M., Rokka, A., Allahverdiyeva, Y., Paakkarinen, V., Saleem, A., et al. (2005). Dynamics of photosystem II: a proteomic approach to thylakoid protein complexes. *Journal of Experimental Botany*, 56(411), 347-356.

Austin, J. R., & Staehelin, L. A. (2011). Three-dimensional architecture of grana and stroma thylakoids of higher plants as determined by electron tomography. *Plant Physiology*, 155(4), 1601-1611.

Barber, J. (1980). An explanation for the relationship between salt-induced thylakoid stacking and the chlorophyll fluorescence changes associated with changes in spillover of energy from photosystem II to photosystem I. *FEBS letters*, 118(1), 1-10.

Bussi, Y., Shimoni, E., Weiner, A., Kapon, R., Charuvi, D., Nevo, R., et al. (2019). Fundamental helical geometry consolidates the plant photosynthetic membrane. *Proceedings of the National Academy of Sciences*, 116(44), 22366-22375.

Castillo, M. A., Wardley, W. P., & Lopez-Garcia, M. (2021). Light-dependent morphological changes can tune light absorption in iridescent plant chloroplasts: a numerical study using biologically realistic data. *ACS Photonics*, 8(4), 1058-1068.

Ceppi, M. G., Oukarroum, A., Çiçek, N., Strasser, R. J., & Schansker, G. (2012). The IP amplitude of the fluorescence rise OJIP is sensitive to changes in the photosystem I content of leaves: a study on plants exposed to magnesium and sulfate deficiencies, drought stress and salt stress. *Physiologia Plantarum*, 144(3), 277-288.

Chow, W. S., Anderson, J. M., & Melis, A. (1990). The photosystem stoichiometry in thylakoids of some Australian shade-adapted plant species. *Functional Plant Biology*, 17(6), 665-674.

Chukhutsina, V. U., Liu, X., Xu, P., & Croce, R. (2020). Light-harvesting complex II is an antenna of photosystem I in dark-adapted plants. *Nature Plants*, 6(7), 860-868.

Colpo, A., Baldisserotto, C., Pancaldi, S., Sabia, A., & Ferroni, L. (2022). Photosystem II photoinhibition and photoprotection in a lycophyte, *Selaginella martensii*. *Physiologia Plantarum*, 174(1), e13604.

Danielsson, R., Albertsson, P. Å., Mamedov, F., & Styring, S. (2004). Quantification of photosystem I and II in different parts of the thylakoid membrane from spinach. *Biochimica et Biophysica Acta (BBA)-Bioenergetics*, 1608(1), 53-61.

Daum, B., Nicastro, D., Austin, J., McIntosh, J. R., & Kühlbrandt, W. (2010). Arrangement of photosystem II and ATP synthase in chloroplast membranes of spinach and pea. *The Plant Cell*, 22(4), 1299-1312.

Demmig-Adams, B., Muller, O., Stewart, J. J., Cohu, C. M., & Adams III, W. W. (2015). Chloroplast thylakoid structure in evergreen leaves employing strong thermal energy dissipation. *Journal of Photochemistry and Photobiology B: Biology*, 152, 357-366.

Ermakova, M., Bellasio, C., Fitzpatrick, D., Furbank, R. T., Mamedov, F., & von Caemmerer, S. (2021). Upregulation of bundle sheath electron transport capacity under limiting light in C4 *Setaria viridis*. *The Plant Journal*, 106(5), 1443-1454.

Fan, D. Y., Hope, A. B., Smith, P. J., Jia, H., Pace, R. J., Anderson, J. M., & Chow, W. S. (2007). The stoichiometry of the two photosystems in higher plants revisited. *Biochimica et Biophysica Acta (BBA)-Bioenergetics*, 1767(8), 1064-1072.

Fan, H. Y., & Heerklotz, H. (2017). Digitonin does not flip across cholesterol-poor membranes. *Journal of Colloid and Interface Science*, 504, 283-293.

Ferroni, L., Angeleri, M., Pantaleoni, L., Pagliano, C., Longoni, P., Marsano, F., et al. (2014). Light-dependent reversible phosphorylation of the minor photosystem II antenna Lhcb6 (CP 24) occurs in lycophytes. *The Plant Journal*, 77(6), 893-905.

Ferroni, L., Colpo, A., Baldisserotto, C., & Pancaldi, S. (2021). In an ancient vascular plant the intermediate relaxing component of NPQ depends on a reduced stroma: Evidence from dithiothreitol treatment. *Journal of Photochemistry and Photobiology B: Biology*, 215, 112114.

Ferroni, L., Cucuzza, S., Angeleri, M., Aro, E. M., Pagliano, C., Giovanardi, M., et al. (2018). In the lycophyte *Selaginella martensii* is the "extra-qT" related to energy spillover? Insights into photoprotection in ancestral vascular plants. *Environmental and Experimental Botany*, 154, 110-122.

Ferroni, L., Suorsa, M., Aro, E. M., Baldisserotto, C., & Pancaldi, S. (2016). Light acclimation in the lycophyte *Selaginella martensii* depends on changes in the amount of photosystems and on the flexibility of the light-harvesting complex II antenna association with both photosystems. *New Phytologist*, 211(2), 554-568.

Ferroni, L., Živčak, M., Kovar, M., Colpo, A., Pancaldi, S., Allakhverdiev, S. I., & Brestič, M. (2022). Fast chlorophyll a fluorescence induction (OJIP) phenotyping of chlorophyll-deficient wheat suggests that an enlarged acceptor pool size of Photosystem I helps compensate for a deregulated photosynthetic electron flow. *Journal of Photochemistry and Photobiology B: Biology*, 234, 112549.

Filacek, A., Zivcak, M., Barboricova, M., Misheva, S. P., Pereira, E. G., Yang, X., & Brestic, M. (2022). Diversity of responses to nitrogen deficiency in distinct wheat genotypes reveals the role of alternative electron flows in photoprotection. *Photosynthesis Research*, 154(3), 259-276.

Fristedt, R., Willig, A., Granath, P., Crevecoeur, M., Rochaix, J. D., & Vener, A. V. (2009). Phosphorylation of photosystem II controls functional macroscopic folding of photosynthetic membranes in Arabidopsis. *The Plant Cell*, 21(12), 3950-3964.

Ghaffar, R., Weidinger, M., Mähnert, B., Schagerl, M., & Lichtscheidl, I. (2018). Adaptive responses of mature giant chloroplasts in the deep-shade lycopod *Selaginella erythropus* to prolonged light and dark periods. *Plant, Cell and Environment*, 41(8), 1791-1805.

Gould, K. S., & Lee, D. W. (1996). Physical and ultrastructural basis of blue leaf iridescence in four Malaysian understory plants. *American Journal of Botany*, 83(1), 45-50.

Grieco, M., Suorsa, M., Jajoo, A., Tikkanen, M., & Aro, E. M. (2015). Light-harvesting II antenna trimers connect energetically the entire photosynthetic machinery—including both photosystems II and I. *Biochimica et Biophysica Acta (BBA)-Bioenergetics*, 1847(6-7), 607-619.

Gu, L., Grodzinski, B., Han, J., Marie, T., Zhang, Y. J., Song, Y. C., & Sun, Y. (2022). Granal thylakoid structure and function: explaining an enduring mystery of higher plants. *New Phytologist*, 236(2), 319-329.

Gunning, B. E. S., & Schwartz, O. M. (1999). Confocal microscopy of thylakoid autofluorescence in relation to origin of grana and phylogeny in the green algae. *Functional Plant Biology*, 26(7), 695-708.

Guo, Y., Lu, Y., Goltsev, V., Strasser, R. J., Kalaji, H. M., Wang, H., et al. (2020). Comparative effect of tenuazonic acid, diuron, bentazone, dibromothymoquinone and methyl viologen on the kinetics of Chl a fluorescence rise OJIP and the MR820 signal. *Plant Physiology and Biochemistry*, 156, 39-48.

Höhner, R., Pribil, M., Herbstová, M., Lopez, L. S., Kunz, H. H., Li, M., et al. (2020). Plastocyanin is the long-range electron carrier between photosystem II and photosystem I in plants. *Proceedings of the National Academy of Sciences*, 117(26), 15354-15362.

Jagels, R. (1970). Photosynthetic apparatus in *Selaginella*. II. Changes in plastid ultrastructure and pigment content under different light and temperature regimes. Canadian Journal of Botany, 48(10), 1853-1860.

Järvi, S., Suorsa, M., Paakkarinen, V., & Aro, E. M. (2011). Optimized native gel systems for separation of thylakoid protein complexes: novel super-and mega-complexes. *Biochemical Journal*, 439(2), 207-214.

Kaftan, D., Brumfeld, V., Nevo, R., Scherz, A., & Reich, Z. (2002). From chloroplasts to photosystems: in situ scanning force microscopy on intact thylakoid membranes. *The EMBO journal*, 21(22), 6146-6153.

Killi, D., Raschi, A., & Bussotti, F. (2020). Lipid peroxidation and chlorophyll fluorescence of photosystem II performance during drought and heat stress is associated with the antioxidant capacities of C3 sunflower and C4 maize varieties. *International Journal of Molecular Sciences*, 21(14), 4846.

Kirchhoff, H. (2019). Chloroplast ultrastructure in plants. *New Phytologist*, 223(2), 565-574.

Klughammer, C., & Schreiber, U. (1994). Saturation pulse method for assessment of energy conversion in PS I. *Planta*, 192, 261-268.

Koochak, H., Puthiyaveetil, S., Mullendore, D. L., Li, M., & Kirchhoff, H. (2019). The structural and functional domains of plant thylakoid membranes. *The Plant Journal*, 97(3), 412-429.

Kouřil, R., Oostergetel, G. T., & Boekema, E. J. (2011). Fine structure of granal thylakoid membrane organization using cryo electron tomography. *Biochimica et Biophysica Acta (BBA)-Bioenergetics*, 1807(3), 368-374.

Kozlowski, T. T., & Pallardy, S. G. (1997). Growth control in woody plants. Elsevier.

Laemmli, U. K. (1970). Cleavage of structural proteins during the assembly of the head of bacteriophage T4. *Nature*, 227(5259), 680-685.

Lichtenthaler, H. K., & Babani, F. (2004). Light adaptation and senescence of the photosynthetic apparatus. Changes in pigment composition, chlorophyll fluorescence parameters and photosynthetic activity. In Chlorophyll *a* fluorescence: A signature of Photosynthesis (pp. 713-736). Springer, Dordrecht.

Liu, J. W., Li, S. F., Wu, C. T., Valdespino, I. A., Ho, J. F., Wu, Y. H., et al. (2020). Gigantic chloroplasts, including bizonoplasts, are common in shade-adapted species of the ancient vascular plant family *Selaginellaceae*. *American Journal of Botany*, 107(4), 562-576.

Martins, J. P. R., Moreira, S. W., Braga, P. C. S., Conde, L. T., Cipriano, R., Falqueto, A. R., & Gontijo, A. B. P. L. (2021). Photosynthetic apparatus performance and anatomical modulations of *Alcantarea imperialis* (Bromeliaceae) exposed to selenium during in vitro growth. *Photosynthetica*, 59(4), 529-537.

Masters, N. J., Lopez-Garcia, M., Oulton, R., & Whitney, H. M. (2018). Characterization of chloroplast iridescence in *Selaginella erythropus*. *Journal of the Royal Society Interface*, 15(148), 20180559.

Mathur, S., Jain, L., & Jajoo, A. (2018). Photosynthetic efficiency in sun and shade plants. *Photosynthetica*, 56(1), 354-365.

Mazur, R., Mostowska, A., & Kowalewska, Ł. (2021). How to measure grana–ultrastructural features of thylakoid membranes of plant chloroplasts. *Frontiers in Plant Science*, 12.

Melis, A., & Harvey, G. W. (1981). Regulation of photosystem stoichiometry, chlorophyll a and chlorophyll b content and relation to chloroplast ultrastructure. *Biochimica et Biophysica Acta (BBA)-Bioenergetics*, 637(1), 138-145.

Miller, K. R., & Staehelin, L. A. (1976). Analysis of the thylakoid outer surface. Coupling factor is limited to unstacked membrane regions. *The Journal of Cell Biology*, 68(1), 30-47.

Nevo, R., Charuvi, D., Tsabari, O., & Reich, Z. (2012). Composition, architecture and dynamics of the photosynthetic apparatus in higher plants. *The Plant Journal*, 70(1), 157-176.

Pancaldi, S., Bonora, A., Gualandri, R., Gerdol, R., Manservigi, R., & Fasulo, M. P. (1998). Intra-tissue characteristics of chloroplasts in the lamina and petiole of mature winter leaf of *Arum italicum* Miller. *Botanica acta*, 111(4), 261-272.

Pantaleoni, L., Ferroni, L., Baldisserotto, C., Aro, E. M., & Pancaldi, S. (2009). Photosystem II organisation in chloroplasts of *Arum italicum* leaf depends on tissue location. *Planta*, 230(5), 1019-1031.

Pao, S. H., Tsai, P. Y., Peng, C. I., Chen, P. J., Tsai, C. C., Yang, E. C., et al. (2018). Lamelloplasts and minichloroplasts in Begoniaceae: iridescence and photosynthetic functioning. *Journal of Plant Research*, 131(4), 655-670.

Pfeiffer, S., & Krupinska, K. (2005). Chloroplast ultrastructure in leaves of *Urtica dioica* L. analyzed after high-pressure freezing and freeze-substitution and compared with conventional fixation followed by room temperature dehydration. *Microscopy research and technique*, 68(6), 368-376.

Pollastrini, M., Holland, V., Brüggemann, W., Bruelheide, H., Dănilă, I., Jaroszewicz, B., et al. (2016). Taxonomic and ecological relevance of the chlorophyll a fluorescence signature of tree species in mixed European forests. *New Phytologist*, 212(1), 51-65.

Pollastrini, M., Salvatori, E., Fusaro, L., Manes, F., Marzuoli, R., Gerosa, G., et al. (2020). Selection of tree species for forests under climate change: is PSI functioning a better predictor for net photosynthesis and growth than PSII?. *Tree Physiology*, 40(11), 1561-1571.

Rantala, M., Ivanauskaite, A., Laihonen, L., Kanna, S. D., Ughy, B., & Mulo, P. (2022). Chloroplast acetyltransferase GNAT2 is involved in the organization and dynamics of thylakoid structure. *Plant and Cell Physiology*, 63(9), 1205-1214.

Rantala, M., Rantala, S., & Aro, E. M. (2020). Composition, phosphorylation and dynamic organization of photosynthetic protein complexes in plant thylakoid membrane. *Photochemical and Photobiological Sciences*, 19(5), 604-619.

Rantala, M., Tikkanen, M., & Aro, E. M. (2017). Proteomic characterization of hierarchical megacomplex formation in *Arabidopsis* thylakoid membrane. *The Plant Journal*, 92(5), 951-962.

Schansker, G., Tóth, S. Z., & Strasser, R. J. (2005). Methylviologen and dibromothymoquinone treatments of pea leaves reveal the role of photosystem I in the Chl a fluorescence rise OJIP. *Biochimica et Biophysica Acta (BBA)-Bioenergetics*, 1706(3), 250-261.

Shao, Q., Wang, H., Guo, H., Zhou, A., Huang, Y., Sun, Y., & Li, M. (2014). Effects of shade treatments on photosynthetic characteristics, chloroplast ultrastructure, and physiology of *Anoectochilus roxburghii*. *PloS One*, 9(2), e85996.

Sheue, C. R., Liu, J. W., Ho, J. F., Yao, A. W., Wu, Y. H., Das, S., et al. (2015). A variation on chloroplast development: the bizonoplast and photosynthetic efficiency in the deep-shade plant *Selaginella erythropus*. *American Journal of Botany*, 102(4), 500-511.

Sheue, C. R., Sarafis, V., Kiew, R., Liu, H. Y., Salino, A., Kuo-Huang, L. L., et al. (2007). Bizonoplast, a unique chloroplast in the epidermal cells of microphylls in the shade plant *Selaginella erythropus* (Selaginellaceae). *American Journal of Botany*, 94(12), 1922-1929.

Shih, M. C., Xie, P. J., Chen, J., Chesson, P., & Sheue, C. R. (2022). Size always matters, shape matters only for the big: potential optical effects of silica bodies in *Selaginella*. *Journal of the Royal Society Interface*, 19(192), 20220204.

Shimoni, E., Rav-Hon, O., Ohad, I., Brumfeld, V., & Reich, Z. (2005). Three-dimensional organization of higher-plant chloroplast thylakoid membranes revealed by electron tomography. *The Plant Cell*, 17(9), 2580-2586.

Souza, A. F. C., Martins, J. P. R., Gontijo, A. B. P. L., & Falqueto, A. R. (2019). Selenium improves the transport dynamics and energy conservation of the photosynthetic apparatus of in vitro grown *Billbergia zebrina* (Bromeliaceae). *Photosynthetica*, 57(4), 931-941.

Staehelin, L. A., & Paolillo, D. J. (2020). A brief history of how microscopic studies led to the elucidation of the 3D architecture and macromolecular organization of higher plant thylakoids. *Photosynthesis Research*, 145(3), 237-258.

Stirbet, A., & Govindjee (2011). On the relation between the Kautsky effect (chlorophyll a fluorescence induction) and photosystem II: basics and applications of the OJIP fluorescence transient. *Journal of Photochemistry and Photobiology B: Biology*, 104, 236-257.

Sun, H., Zhang, S. B., Liu, T., & Huang, W. (2020). Decreased photosystem II activity facilitates acclimation to fluctuating light in the understory plant *Paris polyphylla*. *Biochimica et Biophysica Acta (BBA)-Bioenergetics*, 1861(2), 148135.

Suorsa, M., Rantala, M., Mamedov, F., Lespinasse, M., Trotta, A., Grieco, M., et al. (2015). Light acclimation involves dynamic re-organization of the pigment–protein megacomplexes in non-appressed thylakoid domains. *The Plant Journal*, 84(2), 360-373.

Terashima, I., Matsuo, M., Suzuki, Y., Yamori, W., & Kono, M. (2021). Photosystem I in low light-grown leaves of *Alocasia odora*, a shade-tolerant plant, is resistant to fluctuating light-induced photoinhibition. *Photosynthesis Research*, 149(1), 69-82.

Tóth, S. Z., Schansker, G., & Strasser, R. J. (2007). A non-invasive assay of the plastoquinone pool redox state based on the OJIP-transient. *Photosynthesis Research*, 93(1), 193-203.

Trotta, A., Bajwa, A. A., Mancini, I., Paakkarinen, V., Pribil, M., & Aro, E. M. (2019). The role of phosphorylation dynamics of CURVATURE THYLAKOID 1B in plant thylakoid membranes. *Plant Physiology*, 181(4), 1615-1631.

Tsimilli-Michael, M. (2020). Revisiting JIP-test: An educative review on concepts, assumptions, approximations, definitions and terminology. *Photosynthetica*, 58, 275-292.

Umar, M., Uddin, Z., & Siddiqui, Z. S. (2019). Responses of photosynthetic apparatus in sunflower cultivars to combined drought and salt stress. *Photosynthetica*, 57(2), 627-639.

Walters, R. G., & Horton, P. (1994). Acclimation of *Arabidopsis thaliana* to the light environment: changes in composition of the photosynthetic apparatus. *Planta*, 195(2), 248-256.

Weststrand, S., & Korall, P. (2016). A subgeneric classification of *Selaginella* (Selaginellaceae). *American Journal of Botany*, 103(12), 2160-2169.

Wood, W. H., Barnett, S. F., Flannery, S., Hunter, C. N., & Johnson, M. P. (2019). Dynamic thylakoid stacking is regulated by LHCII phosphorylation but not its interaction with PSI. *Plant Physiology*, 180(4), 2152-2166.

Zivcak, M., Brestic, M., Kalaji, H. M, Govindjee (2014b). Photosynthetic responses of sun-and shade-grown barley leaves to high light: is the lower PSII connectivity in shade leaves associated with protection against excess of light?. *Photosynthesis Research*, 119(3), 339-354.

Zivcak, M., Brestic, M., Kunderlikova, K., Olsovska, K., & Allakhverdiev, S. I. (2015). Effect of photosystem I inactivation on chlorophyll a fluorescence induction in wheat leaves: does activity of photosystem I play any role in OJIP rise?. *Journal of Photochemistry and Photobiology B: Biology*, 152, 318-324.

Zivcak, M., Kalaji, H. M., Shao, H. B., Olsovska, K., & Brestic, M. (2014a). Photosynthetic proton and electron transport in wheat leaves under prolonged moderate drought stress. *Journal of Photochemistry and Photobiology B: Biology*, 137, 107-115.

Chapter 3:

Long-term alleviation of the functional phenotype in chlorophyll-deficient wheat and impact on productivity: a semi-field phenotyping experiment

Premise

According to several studies, the chlorophyll content of leaves could be unnecessarily high compared to the actual energy requirements of a plant (Jin and Jihua 2016, Wang et al. 2018). It is assumed that a low chlorophyll concentration in leaves would already be sufficient in itself to achieve an optimal photosynthetic rate to meet the metabolic and growth needs of the plant. Furthermore, in a plant, the apical leaves absorb most of the light and, consequently, shade the lower ones, suggesting that a reduced chlorophyll accumulation in the leaves would promote growth due to increased light transmission and its efficient utilisation throughout the shoot (Song et al. 2017, Friedland et al. 2019). Another argument in favour of the hypothesis of excessive chlorophyll concentration in leaves is the fact that most of the absorbed light energy is actually dissipated in thermal form (NPQ) and not used for photosynthesis. In addition to this, chlorophyll is a rather expensive molecule to synthesise because of its high nitrogen content (Nunes-Nesi et al. 2010): excess chlorophyll synthesis potentially subtracts nutrients and energy that could be channelled elsewhere (Genesio et al. 2020). If, at least theoretically, leaves contain too much chlorophyll, then the question arises as to the evolutionary reason why the pigment is in such large quantities.

By comparing sun and shade plants, it is clear that high amounts of chlorophylls are required in shady environments and that most chlorophylls are hosted in the appressed membranes of the grana. Thus, the simplest explanation for the hypothetical excess of chlorophylls is that it evolved as a response to shade. Terrestrial plants are derived from green algae, which originally evolved in competition with cyanobacteria. These autotrophic prokaryotic microorganisms are characterised by a light-harvesting protein complex, the phycobilisome, consisting of phycobiliproteins with absorption peaks in the green region of the solar spectrum. After the ancestral endosymbiosis event, the cyanobacterium-derived chloroplast lost its phycobilisomes: in their place, the green algae developed different membrane-intrinsic antenna systems with chlorophylls and xanthophylls. This led to the development of the multigene family that encodes for the subunits of the LHC light-harvesting complexes (Engelken et al. 2010), maximising photon capture in a surface water environment characterised by high irradiance and full solar spectrum. According to Mullineaux (2005), after the loss of the phycobilisomes, the origin of the thylakoid stacks responded to the need for restoring an antenna system sufficiently wide to also ensure photosynthesis in light-limited environments. Land plants form vegetation consortia, in which the different species must in fact photosynthesise by exploiting the light available with varying intensity and quality. However, it should be stressed that the entire evolutionary line of the *Viridiplantae* is characterised by the bipartite structure of the thylakoid system into appressed and non-appressed thylakoids, even though this finds its greatest expression in the grana-intergrana system of land plants. For this reason, it is unclear why shade adaptation may have dominated the evolution of grana and high chlorophyll contents, given that the shade environment presupposes the existence of a plant cover by sun plants, which likewise have granal thylakoids and chlorophyll in seeming excess (Gu et al. 2022). It has been proposed that the benefits of the existence of granal thylakoids accumulated during the evolution of plants to

the condition we know today and that it would now be impossible to trace back the primary cause of their appearance, which actually predates the emergence of plants from water (Nevo et al. 2012). According to the most recent hypothesis, formulated by Gu et al. (2022), the advantage of the grana-intergrana system, which would have evolutionarily fixed this ultrastructure in land plants, is related not so much to the availability of light, but to fluctuations in water availability and the control of electron transport allowed by changes in water content in the lumen of the thylakoid. Nonetheless, this hypothesis does not go into the chlorophyll content of the thylakoids.

Wheat belongs to the genus *Triticum* (Poaceae) and among its most commercially relevant species are the hexaploid *T. aestivum* and tetraploid *T. durum*. Due to its global importance, increasing wheat productivity has always been a desirable goal through the selection of new genotypes. Improving photosynthetic efficiency is one of the possible ways proposed to increase the yield potential of wheat crops (Long et al., 2015). Specifically, following the popular hypothesis of "too much chlorophylls in leaves", reducing the concentration of chlorophyll in leaves has been suggested as a method to improve light distribution and the efficiency of its utilisation within crops (Ort et al. 2011, Zhu et al. 2010). This has renewed interest in *chlorina* mutants, characterised by a yellow-green phenotype due to lower chlorophyll content than wild-type (WT) genotypes. The analysis of *chlorina* mutants has a long history, especially in studies aimed at elucidating chlorophyll metabolism, photosynthetic physiology, thylakoid organisation and grana function in crops and other model plants (Falbel et al. 1996, Niedermaier et al. 2020). In contrast to WT plants, wheat mutants with reduced leaf chlorophyll content could in fact allow a better vertical light distribution due to increased transmittance (Long et al. 2006). In fact, however, *chlorina* mutants of several species, including wheat, generally experience growth retardation. Their retarded growth is believed to be the consequence of inadequate regulation of photosynthetic electron flow due to the unbalanced excitation rate of PSI and PSII (Andrews et al. 1995, Terao and Katoh 1996). Consequently, a biochemical feature commonly present in all *chlorina* mutants is a lower PSI/PSII ratio than the corresponding WTs (Ghirardi et al. 1988, Andrews et al. 1995, Terao et al. 1996, Brestič et al. 2015). The antenna size of PSII is indeed small compared to those of the PSI (Harrison et al. 1993, Andrews et al. 1995). However, more recent studies carried out on different species re-propose that mutants or transformants with lower total chlorophylls, or specifically chlorophyll *b*, or antenna proteins, would benefit from having less chlorophyll and smaller antennae (Wang et al. 2017, Friedland et al. 2019, Bielczynski et al. 2020, Wang et al. 2022).

The typical *chlorina* mutants of wheat are stress-sensitive and have a very low yield capacity under field conditions, which is why they are excluded from agricultural use. To obtain accessions with better productivity, mutations were transferred from donor genotypes to the genome of some high-yielding cultivars. In the resulting genotypes, the phenotype was less severe, and consequently growth and productivity were more developed, despite the still lower chlorophyll concentration (Watanabe and Koval 2003). In general, the *chlorina* phenotype of wheat depends on recessive mutations in the *cn* loci present on chromosome 7 of one of the A or B subgenomes and consists of a partial reduction in chlorophyll synthesis (Zivcak et al. 2019), particularly chlorophyll *b*. Possible candidates for the mutation are the magnesium chelatase subunits, which

catalyse the addition of Mg^{2+} in protoporphyrin IX (Falbel et al. 1996, Watanabe and Koval, 2003, Kosuge et al. 2011, Wang et al. 2018, Jiang et al. 2019), causing untargeted down-sizing of the antennae (Falbel et al. 1996, Kosuge et al. 2011, Wu et al. 2018). As chlorophyll *a* is less abundant due to the genetic defect, it is primarily used for the core of the two photosystems – which ensure photochemistry – and only to a lesser extent for chlorophyll *b* synthesis. The homoeologs in subgenomes A, B or D are healthy and, as the plant develops, they progressively compensate for the defect, until a WT phenotype is reported to be restored in mature plants. Consistently, the high chlorophyll *a/b* ratio present initially decreases with growth (Brestic et al. 2015, Zivcak et al. 2019). The CO_2 assimilation rate is relatively low in *chlorina* mutants, particularly in ANDW-7B, compared to WT (Zivcak et al. 2019). However, this difference is not proportional to the decrease in chlorophyll content, which means that the photosynthetic rate per chlorophyll is much higher than in the WT lines (Lin et al. 2003, Brestic et al. 2008). These results explain the growth characteristics of *chlorina* mutants, which is initially slow but then becomes similar to that of WT.

The mutants exhibit impaired photosynthetic electron transport, with a specific deficit in cyclic electron transport (Zivcak et al. 2019, Ferroni et al. 2020). As a consequence, they tend to induce less proton-motor force and have less capacity to dissipate excess absorbed energy thermally (Ferroni et al. 2020). Defects in controlling the redox state of the membrane are particularly evident when plants are exposed to a rapid increase in irradiance (Ferroni et al. 2020). Some mutants, particularly those having the *cn*-1B mutated locus, are more sensitive to a fluctuating light regime (Ferroni et al. 2020). Light fluctuations challenge the electron flow regulation because of the recurrent electron bursts occurring at each lightfleck (Pearcy et al. 1996, Morales and Kaiser 2020). Lightflecks are especially dangerous for the integrity of PSI, which is prone to oxidative damage when it is reached by more electrons than it can allow to flow out the membrane (Ferroni et al, 2020, Niedermeier et al. 2020, Ferroni et al, 2022). Concerted mechanisms operate upstream and downstream of PSI to promote the safe oxidized state of PSI (Tikhonov et al. 2014, Tikkanen et al. 2015, Shimakawa et al. 2018, Miyake, 2018, Furutani et al. 2023).

The best characterized among the *chlorina sensu lato* wheat mutants is ANK-32A durum wheat. Despite a quite severe defect in electron flow regulation, it acclimates effectively to a fluctuating light regime, developing a better ability to control electron transport (Ferroni et al. 2020). The same scenario occurs under thermal stress, for temperatures between 31 and 35°C (Fischer, 2011, Brestič et al. 2016, Barboričova et al. 2022). Despite its pronounced sensitivity to acute thermal stress, ANK-32A, when pre-acclimated to elevated temperatures, develops a good thermal resistance capacity, probably due to increased PSI activity (Filaček et al. 2022). These experimental results indicate that ANK-32A has the ability to implement compensatory responses to the electron transport defect, such as the utilisation of alternative electron sinks for photosynthesis and the accumulation of intrachain electron transporters (Ferroni et al. 2022). The thylakoid architecture is modified in ANK-32A: the overall amount of thylakoids decreases, but large grana persist along with long, straight and parallel thylakoid arrays, especially under a fluctuating light regime, (Ferroni et al. 2020).

This Chapter examines the problem of the photosynthetic regulation in chlorophyll-deficient wheat mutants exploiting modulated and prompt chlorophyll *a* fluorescence, looking for correlations with grain yields. The chapter proposes the manuscript submitted to the journal *Plants*, prepared according to the journal template and provisionally accepted pending revision:

Colpo, A., Demaria, S., Baldisserotto, C., Pancaldi, S., Brestic, M., Zivcak, M., & Ferroni, L. (2023). Long-term alleviation of the functional phenotype in chlorophyll-deficient wheat and impact on productivity: a semi-field phenotyping experiment. *Plants.*

References

Andrews, J. R., Fryer, M. J., & Baker, N. R. (1995). Consequences of LHC II deficiency for photosynthetic regulation in chlorina mutants of barley. *Photosynthesis Research*, *44*, 81-91.

Bielczynski, L. W., Schansker, G., & Croce, R. (2020). Consequences of the reduction of the Photosystem II antenna size on the light acclimation capacity of *Arabidopsis thaliana*. *Plant, Cell & Environment*, *43*(4), 866-879.

Barboričová, M., Filaček, A., Vysoká, D. M., Gašparovič, K., Živčák, M., & Brestic, M. (2022). Sensitivity of fast chlorophyll fluorescence parameters to combined heat and drought stress in wheat genotypes. *Plant, Soil and Environment*, *68*(7), 309-316.

Brestic, M., Zivcak, M., Kunderlikova, K., Sytar, O., Shao, H., Kalaji, H. M., & Allakhverdiev, S. I. (2015). Low PSI content limits the photoprotection of PSI and PSII in early growth stages of chlorophyll *b*-deficient wheat mutant lines. *Photosynthesis Research*, *125*, 151-166.

Brestic, M., Zivcak, M., Kunderlikova, K., & Allakhverdiev, S. I. (2016). High temperature specifically affects the photoprotective responses of chlorophyll b-deficient wheat mutant lines. *Photosynthesis research*, *130*, 251-266.

Brestic, M., Zivcak, M., Olsovska, K., & Repkova, J. (2008). Functional study of PS II and PS I energy use and dissipation mechanisms in barley wild type and chlorina mutants under high light conditions. In *Photosynthesis. Energy from the Sun: 14th International Congress on Photosynthesis* (pp. 1407-1411). Springer Netherlands.

Engelken, J., Brinkmann, H., & Adamska, I. (2010). Taxonomic distribution and origins of the extended LHC (light-harvesting complex) antenna protein superfamily. *BMC Evolutionary Biology*, *10*, 1-15.Friedland, N., Negi, S., Vinogradova-Shah, T., Wu, G., Ma, L., Flynn, S., Kumssa, T., Lee, C. H., & Sayre, R. T. (2019). Fine-tuning the photosynthetic light harvesting apparatus for improved photosynthetic efficiency and biomass yield. Scientific Reports, 9(1), 13028.

Falbel, T. G., Meehl, J. B., & Staehelin, L. A. (1996). Severity of mutant phenotype in a series of chlorophyll-deficient wheat mutants depends on light intensity and the severity of the block in chlorophyll synthesis. *Plant Physiology*, *112*(2), 821-832.

Ferroni, L., Živčak, M., Kovar, M., Colpo, A., Pancaldi, S., Allakhverdiev, S. I., & Brestič, M. (2022). Fast chlorophyll *a* fluorescence induction (OJIP) phenotyping of chlorophyll-deficient wheat suggests that an enlarged acceptor pool size of Photosystem I helps compensate for a deregulated photosynthetic electron flow. *Journal of Photochemistry and Photobiology B: Biology*, *234*, 112549.

Ferroni, L., Živčak, M., Sytar, O., Kovár, M., Watanabe, N., Pancaldi, S., Baldisserotto, C., & Brestič, M. (2020). Chlorophyll-depleted wheat mutants are disturbed in photosynthetic electron flow regulation but can retain an acclimation ability to a fluctuating light regime. *Environmental and Experimental Botany*, *178*, 104156.

Filaček, A., Živčák, M., Ferroni, L., Barboričová, M., Gašparovič, K., Yang, X., ... & Brestič, M. (2022). Pre-acclimation to elevated temperature stabilizes the activity of photosystem I in wheat plants exposed to an episode of severe heat stress. *Plants*, *11*(5), 616.

Fischer, R. A. (2011). Wheat physiology: a review of recent developments. *Crop and Pasture Science*, *62*(2), 95-114.

Furutani, R., Wada, S., Ifuku, K., Maekawa, S., & Miyake, C. (2023). Higher Reduced State of Fe/S-Signals, with the Suppressed Oxidation of P700, Causes PSI Inactivation in Arabidopsis thaliana. *Antioxidants*, *12*(1), 21.

Genesio, L., Bright, R. M., Alberti, G., Peressotti, A., Delle Vedove, G., Incerti, G., Toscano, P., Rinaldi, M., Muller, O., & Miglietta, F. (2020). A chlorophyll-deficient, highly reflective soybean mutant: radiative forcing and yield gaps. Environmental Research Letters, 15(7), 074014.

Ghirardi, M. L., & Melis, A. (1988). Chlorophyll b deficiency in soybean mutants. I. Effects on photosystem stoichiometry and chlorophyll antenna size. *Biochimica et Biophysica Acta (BBA)-Bioenergetics*, *932*, 130-137.

Gu, L., Grodzinski, B., Han, J., Marie, T., Zhang, Y. J., Song, Y. C., & Sun, Y. (2022). Granal thylakoid structure and function: explaining an enduring mystery of higher plants. *New Phytologist*, *236*(2), 319-329.

Harrison, M. A., Nemson, J. A., & Melis, A. (1993). Assembly and composition of the chlorophyll *ab* light-harvesting complex of barley (*Hordeum vulgare* L.): Immunochemical analysis of chlorophyll *b*-less and chlorophyll *b*-deficient mutants. *Photosynthesis Research*, *38*, 141-151.

Jiang, H. B., Wang, N., Jian, J. T., Wang, C. S., & Xie, Y. Z. (2019). Rapid mapping of a *chlorina* mutant gene cn-A1 in hexaploid wheat by bulked segregant analysis and single nucleotide polymorphism genotyping arrays. *Crop and Pasture Science*, *70*(10), 827-836.

Jin, X., & Jihua, M. (2016). Overview on estimating crop chlorophyll content with remote sensing. Remote Sensing Technology and Application, 31(1), 74-85.

Kosuge, K., Watanabe, N., & Kuboyama, T. (2011). Comparative genetic mapping of homoeologous genes for the chlorina phenotype in the genus Triticum. *Euphytica*, *179*, 257-263.

Lin, Z. F., Peng, C. L., Lin, G. Z., Ou, Z. Y., Yang, C. W., & Zhang, J. L. (2003). Photosynthetic characteristics of two new chlorophyll *b*-less rice mutants. *Photosynthetica*, *41*, 61-67.

Long, S. P., Marshall-Colon, A., & Zhu, X. G. (2015). Meeting the global food demand of the future by engineering crop photosynthesis and yield potential. *Cell*, *161*(1), 56-66.

Long, S. P., Zhy, X. G., Naidu, S. L., & Ort, D. R. (2006). Can improvement in photosynthesis increase crop yields?. *Plant, Cell & Environment*, *29*(3), 315-330.

Miyake, C. (2020). Molecular mechanism of oxidation of P700 and suppression of ROS production in photosystem I in response to electron-sink limitations in C3 plants. *Antioxidants*, *9*(3), 230.

Morales, A., & Kaiser, E. (2020). Photosynthetic acclimation to fluctuating irradiance in plants. *Frontiers in Plant Science*, *11*, 268.

Mullineaux, C. W. (2005). Function and evolution of grana. *Trends in Plant Science*, *10*(11), 521-525.

Nevo, R., Charuvi, D., Tsabari, O., & Reich, Z. (2012). Composition, architecture and dynamics of the photosynthetic apparatus in higher plants. *The Plant Journal*, *70*(1), 157-176.

Niedermaier, S., Schneider, T., Bahl, M. O., Matsubara, S., & Huesgen, P. F. (2020). Photoprotective acclimation of the *Arabidopsis thaliana* leaf proteome to fluctuating light. *Frontiers in Genetics*, *11*, 154.

Nunes-Nesi, A., Fernie, A. R., & Stitt, M. (2010). Metabolic and signaling aspects underpinning the regulation of plant carbon nitrogen interactions. Molecular Plant, 3(6), 973-996.

Ort, D. R., Zhu, X., & Melis, A. (2011). Optimizing antenna size to maximize photosynthetic efficiency. *Plant Physiology*, *155*(1), 79-85.

Pearcy, R. W., Krall, J. P., & Sassenrath-Cole, G. F. (1996). Photosynthesis in fluctuating light environments. *Photosynthesis and the Environment*, 321-346.

Shimakawa, G., Shaku, K., & Miyake, C. (2018). Reduction-induced suppression of electron flow (RISE) is relieved by non-ATP-consuming electron flow in *Synechococcus elongatus* PCC 7942. *Frontiers in Microbiology*, *9*, 886.

Song, L., Ma, Q., Zou, Z., Sun, K., Yao, Y., Tao, J., Kaleri, N. A., & Li, X. (2017). Molecular link between leaf coloration and gene expression of flavonoid and carotenoid biosynthesis in *Camellia sinensis* cultivar 'Huangjinya'. *Frontiers in Plant Science*, *8*, 803.

Terao, T., & Katoh, S. (1996). Antenna sizes of photosystem I and photosystem II in chlorophyll *b*-deficient mutants of rice. Evidence for an antenna function of photosystem II centers that are inactive in electron transport. *Plant and Cell Physiology*, *37*(3), 307-312.

Tikhonov, A. N. (2014). The cytochrome b6f complex at the crossroad of photosynthetic electron transport pathways. *Plant Physiology and Biochemistry*, *81*, 163-183.

Tikkanen, M., Rantala, S., & Aro, E. M. (2015). Electron flow from PSII to PSI under high light is controlled by PGR5 but not by PSBS. *Frontiers in Plant Science*, *6*, 521.

Wang, G., Zeng, F., Song, P., Sun, B., Wang, Q., & Wang, J. (2022). Effects of reduced chlorophyll content on photosystem functions and photosynthetic electron transport rate in rice leaves. *Journal of Plant Physiology*, *272*, 153669.

Wang, S. A., Wang, P., Gao, L., Yang, R., Li, L., Zhang, E., Wang, Q., Li, Y., & Yin, Z. (2017). Characterization and complementation of a chlorophyll-less dominant mutant GL1 in *Lagerstroemia indica*. *DNA and Cell Biology*, *36*(5), 354-366.

Wang, Y., Zheng, W., Zheng, W., Zhu, J., Liu, Z., Qin, J., & Li, H. (2018). Physiological and transcriptomic analyses of a yellow-green mutant with high photosynthetic efficiency in wheat (*Triticum aestivum* L.). *Functional & Integrative Genomics*, *18*, 175-194.

Watanabe, N., & Koval, S. F. (2003). Mapping of chlorina mutant genes on the long arm of homoeologous group 7 chromosomes in common wheat with partial deletion lines. *Euphytica*, *129*, 259-265.

Wu, H., Shi, N., An, X., Liu, C., Fu, H., Cao, L., Feng, Y., Sun, D., & Zhang, L. (2018). Candidate genes for yellow leaf color in common wheat (*Triticum aestivum* L.) and major related metabolic pathways according to transcriptome profiling. *International Journal of Molecular Sciences*, *19*(6), 1594.

Zhu, X. G., Long, S. P., & Ort, D. R. (2010). Improving photosynthetic efficiency for greater yield. *Annual Review of Plant Biology*, *61*, 235-261.

Zivcak, M., Brestic, M., Botyanszka, L., Chen, Y. E., & Allakhverdiev, S. I. (2019). Phenotyping of isogenic chlorophyll-less bread and durum wheat mutant lines in relation to photoprotection and photosynthetic capacity. *Photosynthesis research*, *139*, 239-251.

plants

MDPI

Article

Long-term alleviation of the functional phenotype in chlorophyll-deficient wheat and impact on productivity: a semi-field phenotyping experiment

Andrea Colpo[1], Sara Demaria[1], Costanza Baldisserotto[1], Simonetta Pancaldi[1], Marian Brestič[2], Marek Živčak[2,*] and Lorenzo Ferroni[1,*]

[1] Department of Environmental and Prevention Sciences, University of Ferrara, Corso Ercole I d'Este 32, 44100 Ferrara, Italy; andrea.colpo@unife.it (A.C.), sara.demaria@unife.it (S.D.), costanza.baldisserotto@unife.it (C.B.), simonetta.pancaldi@unife.it (S.P.)

[2] Institute of Plant and Environmental Sciences, Slovak University of Agriculture, Trieda A. Hlinku 2, 949 76 Nitra, Slovakia; marian.brestic@uniag.sk (M.B.)

* Correspondence: forenzo.ferroni@unife.it (L.F.); marek.zivcak@uniag.sk (M.Ž.); Tel: +39-0532-293785 (L.F.); +421-37-6414-821 (M.Ž.)

Abstract: Wheat mutants with a reduced chlorophyll synthesis are affected by a defective control of the photosynthetic electron flow but tend to recover a wild-type phenotype. The sensitivity of some mutants to light fluctuations suggested that cultivation outdoors could significantly impact productivity. Six mutant lines of *Triticum durum* or *Triticum aestivum* with their respective wild-type cultivars were cultivated with a regular seasonal cycle (October-May) in a semi-field experiment. Leaf chlorophyll content and fluorescence parameters were analysed at the early (November) and late (May) developmental stages and checked for correlation with morphometric and grain production parameters. The mitigation of the phenotype severity concerned primarily the recovery of the photosynthetic membrane functionality, while it was marginal with respect to the chlorophyll content. The accumulation of interchain electron carriers was a primary acclimative response towards the naturally fluctuating environment, maximally exploited by the mature durum wheat mutants. The mutation itself and/or the energy-consuming compensatory mechanisms markedly influenced the plant morphogenesis, especially leading to reduced tillering, which in turn resulted in lower grain production per plant. Consistently with the interrelation between early photosynthetic phenotype and grain yield per plant, chlorophyll fluorescence indexes related to the level of photoprotective thermal dissipation (pNPQ), photosystem II antenna size (ABS/RC), and pool of electron carriers (Sm) are proposed as good candidates for the in-field phenotyping of chlorophyll-deficient wheat.

Keywords: acclimation; antenna size; chlorophyll fluorescence; electron transport; photoprotection; photosynthesis; photosystem II; wheat

Citation: Colpo, A.; Demaria, A.; Baldisserotto, C.; Pancaldi, S.; Brestič, M.; Živčak, M.; Ferroni, L. Long-term alleviation of the functional phenotype in chlorophyll-deficient wheat and impact on productivity: a semi-field phenotyping experiment. *Plants* **2023**, *11*, x. https://doi.org/10.3390/xxxxx

Academic Editor: Firstname Lastname

Received: date
Accepted: date
Published: date

1. Introduction

Plant phenotyping is prospected as a key tool to increase crop productivity and understand the impact of biotic and abiotic stresses on plant fitness [1]. Application of these wide-ranging techniques requires a fine-tuning process in controlled environments, such as laboratory-scale cultivations, climate chambers or phenotyping units, in order to build the foundation for future exploitation of research results in the field [1-3]. A proper translation of information from controlled environments to the open field is critical to produce meaningful insights into crop behaviour in real agricultural contexts. Basic physiological processes and their link to plant productivity can be profitably studied under semi-field conditions as an intermediate step between controlled laboratory environments and the open field. This approach is quite popular in (agro)ecology to verify predictions emerging

from laboratory findings in an easily monitored near-natural environment, where the experimental material is exposed to realistic climatic conditions [4].

Among the approaches used in plant phenotyping, the characterization of photosynthesis is an important tool [5], mainly for two reasons. First, photosynthesis is the process that enables the plant to produce the building blocks for its growth and development by converting solar energy into chemical bonds. Consequently, increasing a crop's photosynthetic efficiency plays a key role in improving productivity. Second, photosynthesis can be measured by various techniques also in the field, for example analysing the leaf gas exchange or the chlorophyll fluorescence emission. Especially the measurements of chlorophyll fluorescence are advantageous because they are quick to perform and non-invasive, allowing the collection of a large amount of data while preserving samples [6].

Most of the work produced in recent decades in photosynthetic plant phenotyping has converged on the hypothesis that decreasing the leaf chlorophyll content could help improve crop productivity. The two basic concepts underlying this hypothesis can be summarized as: (a) most of the light absorbed in the harvesting process is not used to produce charge separation in photosystems but is thermally dissipated; (b) the photosynthetic activity of the canopy is not homogeneous and is mainly due to the upper leaves, which shade the lower leaves. For these reasons, reducing the chlorophyll content, especially in the upper leaves, could theoretically reduce the amount of dissipated light energy and increase the light availability for the lower leaves, potentially leading to higher photosynthetic efficiency and, consequently, biomass production [7]. One may expect that many decades of breeding would have indirectly favoured plants with a lower leaf chlorophyll content. A detailed comparison of 26 winter wheat cultivars released during 1940-2010 in China has shown that breeding has accidentally influenced the stoichiometry of some photosynthetic proteins and modified some anatomical traits related to the light distribution in the canopy [8]. However, no significant decrease in chlorophyll content emerged from the research [8].

Several mutants characterized by different degrees of chlorophyll depletion in model plants and crops have been produced. These mutants often exhibit peculiar features in their photosynthetic membranes, among which an altered stoichiometry between photosystem I and II (PSI and PSII); this, in turn, causes an imbalance in the excitation rate between PSI and PSII, an abnormal organization of the thylakoids, changes in the spatial distribution of the two photosystems, and reduced control of photosynthetic electron flow, resulting in delayed/reduced growth and increased sensitivity to environmental factors [9-14]. Nevertheless, especially recent studies have reported that some mutants or transformants with an overall reduced leaf chlorophyll content [15, 16], or a specific reduction in chlorophyll *b* [17] or depleted in specific antenna proteins [18], could potentially have a growth benefit.

Among the mutants for chlorophyll synthesis, there are wheat lines derived from wild-type cultivars of *Triticum durum* L. (durum wheat LD222) and *Triticum aestivum* L. (bread wheat Novosibirskaya 67, NS67), which have been extensively characterized for the structure, organization, and functionality of their photosynthetic apparatus. Such mutants were used in the present study: ANDW-7A, ANDW-8A and ANDW-7B (7A, 8A, 7B) for durum wheat, ANBW-4A, ANBW-4B and ANK-32A (4A, 4B, 32A) for bread wheat (Table A1). At the seedling stage of indoor cultivation, these mutants are characterized by a reduction in total chlorophyll content between 40% and 70%, along with an increase in chlorophyll *a*/*b* ratio; the most severe mutant phenotype was found in 7B and 32A [9, 10]. Similarly, the rate of CO_2 assimilation decreases in mutants with different degrees of severity, but the photosynthetic rate per chlorophyll unit is higher than that of the respective wild types [9]. This observation could support the original hypothesis about a potentially higher productivity in chlorophyll-depleted wheat. The differences in carbon assimilation flatten out in the later stages of development for plants grown indoors [9]. In contrast, plants grown outdoors (March-June) tended to retain the typical characteristics of the chlorophyll-depleted phenotype, particularly in durum wheat mutants [9]. It was

proposed that their growth in the open field may exacerbate an already compromised control of linear electron flow (LEF), caused by an insufficient cyclic electron flow (CEF). This in turn causes a reduced capacity of energy dissipation, ATP synthesis, and photoprotection. The combination of these alterations is responsible for a tendency to the overreduction of the acceptor side of PSI, potentially leading to a significant rate of PSI inactivation [19]. A chronic overreduction of the electron transport chain can be extremely harmful for plants and even mine their survival [20]. Nevertheless, the chlorophyll-depleted wheat mutants are evidently able to cope with this deregulation of the electron flow. Two relevant mechanisms alleviating the stress due to excess of photosynthetic electrons have been documented, i.e., primarily the accumulation of PSI end electron acceptor (ferredoxin and ferredoxin-$NADP^+$-oxido-reductase, FNR) and in addition the enhancement of electron sinks alternative to photosynthesis and photorespiration [10, 11]. These compensative adjustments inevitably affect the biomass yield of the mutants, which is generally lower than that of their wild-type lines [10]. In an indoor experiment, the plant growth under a fluctuating light regime aggravated this condition specifically in the 7B and 4B mutants compared with their respective wild-type lines; this response was attributed to the recurrent electron bursts caused by a fluctuating light regime, which requires a perfect tuning of the electron flow [21]. However, and surprisingly, the 4A mutant seemed to benefit instead from the fluctuating light regime and its biomass yield was even higher than that of NS67.

Up to now, the relevant information about this collection of mutants for potential field cultivation can be summarized as follows:

1) the phenotype severity tends to decrease during the life cycle of the plants cultivated indoors, i.e., the leaf chlorophyll content recovers to wild-type-like levels [9];

2) the phenotype alleviation is incomplete outdoors with a short (March-June) life cycle [9];

3) the phenotype alleviation can be incomplete indoors if plants are cultivated under fluctuating light [10-11].

Nevertheless, the contrasting results obtained with mutants sharing similar degrees of chlorophyll depletion (e.g., 7B and 7A) make the outcome of an open-field cultivation basically unpredictable.

The present work aims to elucidate how outdoor cultivation of chlorophyll-depleted wheat mutants affects the photosynthetic characteristics at the early (November) and late (May) developmental stages when wheat is cultivated in a normal seasonal cycle. Based on observations from previous work, two alternatives were considered possible: (a) the direct outdoor sowing in October could exacerbate the phenotype of chlorophyll-depleted mutants because of the everchanging environmental conditions, including light fluctuations; (b) alternatively, the overwintering cultivation, necessary to the tillering phase, allows for an effective long-term acclimation, for instance emphasizing the compensatory mechanisms previously described. In both cases, it was interesting to assess whether the mutants were affected by a substantial loss in grain yield and whether the functional phenotyping parameters already proposed for the characterization of the mutants could be validated and/or implemented with other chlorophyll fluorescence-derived parameters. The study was carried out in small soil parcels at the Botanical Garden of Ferrara, in a position exposed to direct sunlight for a major part of the day, but also subjected to significant light fluctuations (Figure 1). The easy access to the Botanical Garden allowed for the concept of a semi-field experiment, in which in-field continuous excitation chlorophyll fluorescence analyses were successfully integrated with modulated chlorophyll fluorescence measurements of samples collected in the field and promptly analysed in the laboratory without any significant delay.

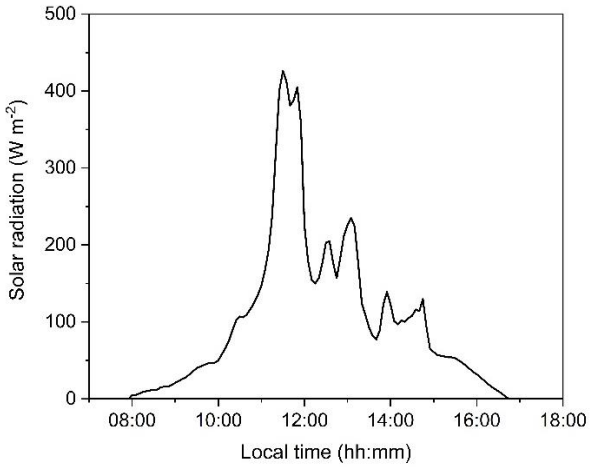

Figure 1. Example of a daily variation in solar radiation reaching the experimental site as assessed on November 20, 2020, through the Meteorological Observatory of the Botanical Garden of Ferrara, Italy.

2. Results

2.1 Pigment content in young and mature plants

Total chlorophyll content and chlorophyll *a*/*b* molar ratio are markers for the phenotype severity in both durum and bread wheat mutants [9-11]. Total chlorophyll content was consistent with the severity gradient already observed in young and mature plants grown indoors [9-11] (Figure 2); the two wild-type lines, LD222 and NS67, were the richest in chlorophyll, followed by two intermediate mutants (7A and 8A in durum, 4A and 4B in bread) and the more severe phenotype of 7B for durum wheat and 32A for bread wheat. All genotypes showed an increased chlorophyll content in the leaves of the mature plants compared to the young, though much more marked in bread wheat (almost doubled) than in durum wheat (+15%, Figure 2). The increase was homogeneous across genotypes, so the severity gradient was maintained.

The chlorophyll *a*/*b* ratio is inversely proportional to the size of the PSII antenna system, the light-harvesting complex II (LHCII), which hosts most chlorophyll *b*. In young durum wheat mutants, it was significantly higher than in the wild-type LD222, while bread wheat 4A and 4B were intermediate between NS67 and 32A (Figure 2). Plant maturation tended to maintain the differences between the mutant and the wild-type lines in both species; only in the bread wheat mutant 32A, the chlorophyll *a*/*b* ratio was approx. 30% higher in the mature compared to the young plants.

The relative variations in the total chlorophyll/carotenoids molar ratio were roughly similar to the trends observed for chlorophyll (*a*+*b*), but the range of variation was obviously much narrower (Figure 2). This result revealed a tendency of the mutants to adjust their leaf carotenoid content already in the young leaves, thus minimizing the mismatch between the syntheses of the two types of photosynthetic pigments. It was particularly evident in 32A: despite a halved chlorophyll content, the chlorophyll/carotenoids ratio only decreased by 13%.

Overall, based on the pigment analysis, the expected recovery of a wild-type-like pigmentation phenotype [10] occurred only partially in mature plants as compared to the young, or even it did not occur at all (32A).

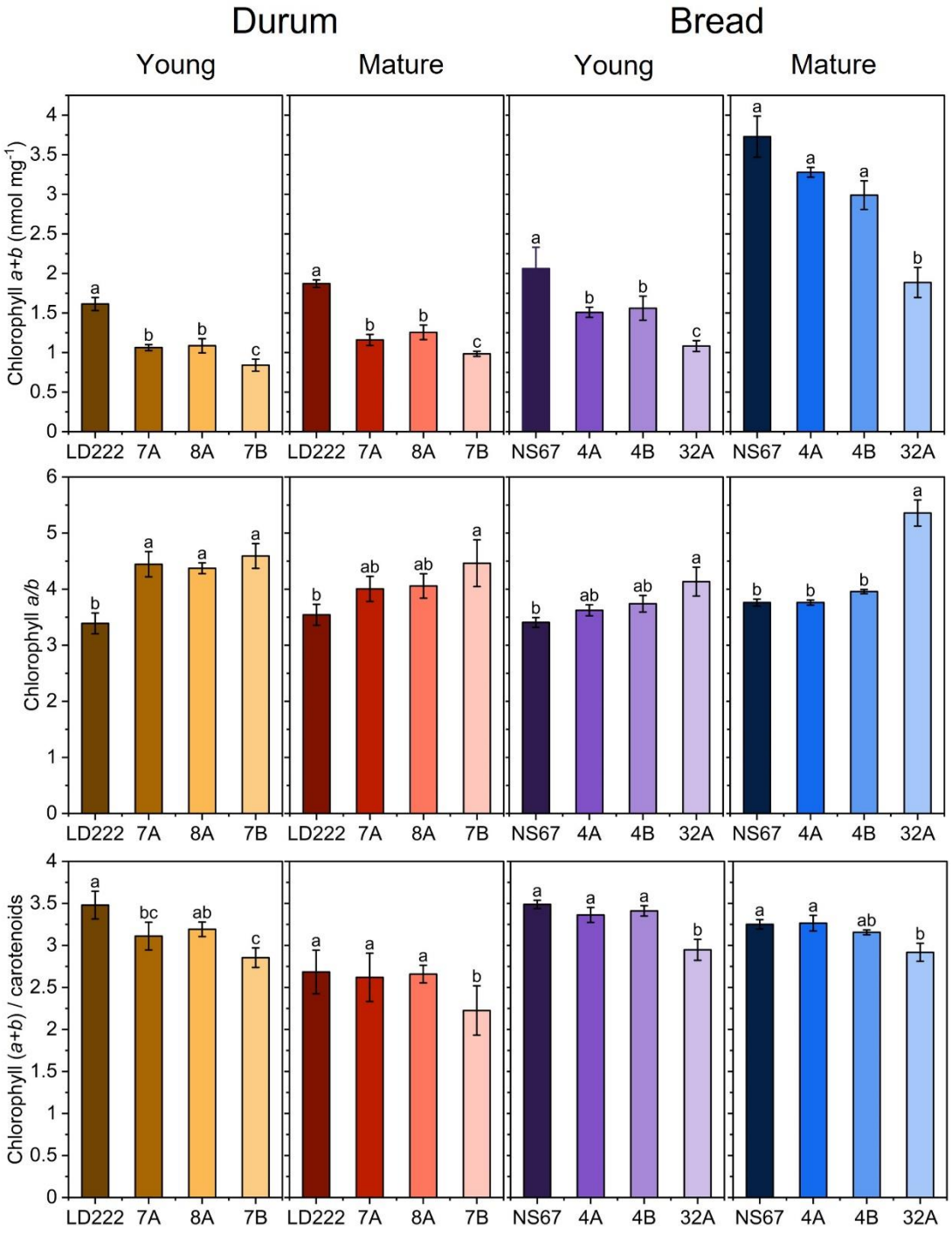

Figure 2. Photosynthetic pigments quantification in leaves of young and mature plants of durum and bread wheat. Histograms represent average values ± Standard Deviation for n=5-8; different letters indicate a significant difference at $P < 0.05$, as determined using one-factor ANOVA followed by Tukey's test.

2.2 Irradiance-dependence of PSII quantum yields

PSII quantum yields of photochemistry [Y(II)], constitutive energy loss [Y(NO)] and thermal dissipation [Y(NPQ)] were recorded during the induction of photosynthesis with increasing irradiance to monitor quasi-steady-state values of PSII photochemical activity

and obtain information on the redox state of the electron transport chain and on the energy dissipation capacity.

Starting from the reference value in the dark-acclimated state (corresponds to F_V/F_M), Y(II) underwent a progressive decay at increasing irradiance, which depends on the combined effect of the strength of electron sinks, primarily the Calvin-Benson-Bassham cycle, and the regulation of the LEF from PSII to PSI [22] (Figure 3A-D). A tendency to slightly higher Y(II) was visible especially in the most severe mutants and in the young leaves, in line with previous reports [9-11] (Figure 3A,C). In mature plants, this effect on Y(II) was still observed in durum wheat, while in bread wheat, the curves were nearly overlapping (Figure 3B,D).

Y(NO) can be used as a straightforward parameter to assess defects in the regulation of the plastoquinone redox state [23], and was accordingly proposed as the main phenotyping index for chlorophyll-depleted wheat [10]. The Y(NO)-irradiance dependence in the wild-type lines showed a typical behaviour, in which Y(NO) rose to a peak at the lowest light intensity related to the functioning of only LEF (Figure 3E-H); subsequently, at higher irradiance, it decreased because of the activation of the CEF [24-27] and the related regulatory processes known as the photosynthetic control operated at the Cytochrome b_6f complex [28-29]. The major divergences in Y(NO) were observed in young plants of mutant durum wheat, which reflected the inefficiency in regulating LEF and resulted in an impaired capacity to keep the plastoquinone pool in a sufficiently oxidized state (Figure 3E,G). The most affected mutant was 7B, emphasizing the divergence from the LD222 at increasing irradiance (Figure 3E). Nevertheless, at the mature stage, all durum wheat mutants were able to regulate the electron poise properly (Figure 3F). In bread wheat 4A and 4B, LEF was generally well regulated (Figure 3H). The leaves of young 32A mutant tended instead to diverge from the wild type at the highest irradiances, and this physiological trait worsened in the mature plants (Figure 3H). Persisting high Y(NO) values up to intermediate irradiances marked a delay in the activation of CEF. After the peak, Y(NO) decreased but maintained higher values than NS67, indicating that in mature plants of 32A, the control of the electron flow could not be recovered to a wild-type level (Figure 3H).

The third quantum yield, Y(NPQ), illustrates the progressive activation of photoprotective regulatory processes leading to the thermal dissipation of excess absorbed energy [30]. Y(NPQ) well reflected the phenotype severity in young durum wheat mutants and showed their lower efficiency in inducing thermal dissipation compared to LD222 (Figure 3I). In the leaves of the mature plants, the tendency to approach a wild-type behaviour was evident (Figure 3J,L). The Y(NPQ)-light curves of young 4A and 4B overlapped with that of NS67, and only 32A exhibited a defective induction of thermal dissipation (Figure 3K). The lesser ability to drive energy to regulatory dissipation did not improve in mature 32A. Interestingly, the mature 4B appeared better regulated than NS67, with lower Y(NO) and higher Y(NPQ) (Figure 3L).

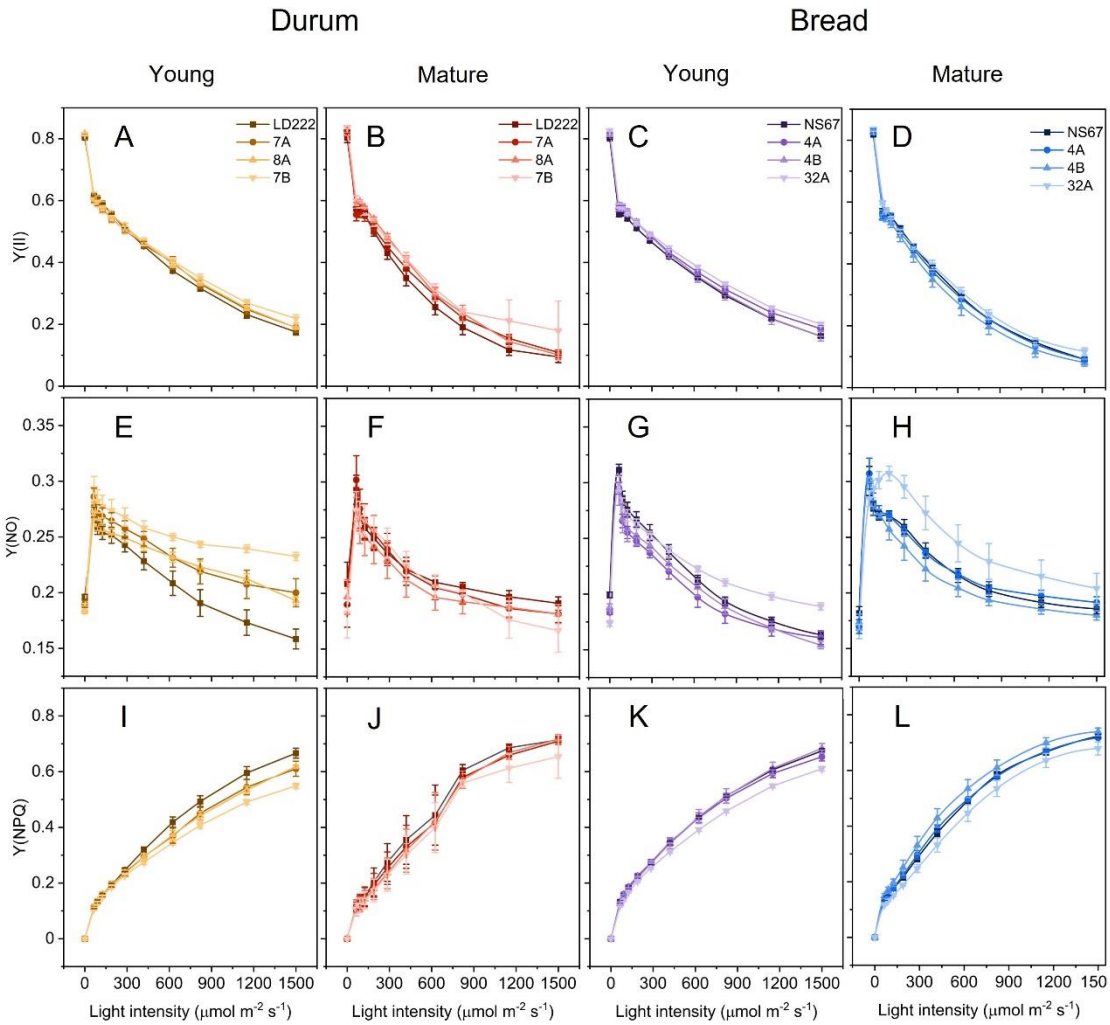

Figure 3. Long-term light-acclimation features of photosynthesis in young and mature bread wheat plants. Light-response curves relative to: (A-D) actual quantum yield of PSII photochemistry Y(II), (E-H) quantum yield of constitutive, non-regulatory energy dissipation Y(NO), and (I-L) quantum yield of regulatory thermal dissipation Y(NPQ). The curves were recorded during 60 minutes of exposure to increasing actinic light intensities. Average values ± Standard Deviation for n= 4-6.

2.3 NPQ and PSII photoprotection

Stern-Vollmer NPQ is the standard parameter to quantify the overall thermal dissipation in quenching analysis [31-32]. Light-induced thermal dissipation in young plants was dependent on the plant genotype, especially in durum wheat (Figure 4A,C). Up to 300 µmol m^{-2} s^{-1}, the NPQ rise occurred in LD222 and its mutants to the same extent (Figure 4A). For higher light intensity, the initially tiny differences between durum wheat lines were progressively magnified, reaching the maximum NPQ value (NPQ_{MAX}) at the end of the induction, but without approaching any plateau. NPQ_{MAX} exactly matched the phenotype severity being 25% less in the intermediate chlorophyll-depleted mutants, 7A and 8A, and almost halved in the most severe mutant 7B (Figure 4A). In young bread wheat plants, differences in NPQ induction were less apparent than in durum wheat, and only the most severe mutant 32A started to diverge from the others around 300 µmol m^{-2} s^{-1} (Figure 4C).

Unlike young plants, mature plants tended to reach a plateau value of NPQ at the highest irradiances (Figure 4B,D). In durum wheat, differences between the genotypes were negligible (Figure 4B); in mature bread wheat, the ineffective NPQ induction was confirmed in 32A, although less severe than in young plants (Figure 4D). The mutant 4B was surprisingly the most effective in inducing NPQ in response to the increasing light intensity (Figure 4B).

Higher values of NPQ are commonly or implicitly associated with a higher photoprotective ability against PSII photodamage [33-35]. However, NPQ is recognized as the reflection of a multiplicity of processes that are non-photochemical in origin [36-37], including the energy dissipation by the damaged PSII centers themselves. It means that the extent of NPQ and the level of PSII photoprotection are not always linearly related and high levels of NPQ may not correspond to high levels of PSII photoprotection [38]. In the case of chlorophyll-deficient wheat mutants, while lower levels of NPQ could conceivably allow lower PSII protection, a conclusion could not be drawn with a sufficient degree of confidence for mutants developing NPQ to the same extent as the wild-type lines. To discriminate between the photoprotective and non-photoprotective components of NPQ, the parameter pNPQ calculated according to the "qP_d model" was introduced by Ruban and Murchie [39]. The theoretical fundament of the "qP_d model" is based on the comparison between the actual minimum fluorescence F'_0 measured after far-red light exposure ($F'_{0\,act}$) and the theoretical F'_0 calculated according to Oxborough and Baker ($F'_{0\,calc}$) [40]. Since the latter is insensitive to PSII photoinhibition, their comparison at the different steps of a light-response curve allows one to verify the presence of PSII photoinhibition and its extent [39, 41-43]. The F'_0-derived qP_d parameter lies between 0 (all PSII are photoinactivated) and 1 (all PSII are active). In the model, the threshold used to assess the occurrence of PSII photoinhibition was set at qP_d=0.98; the NPQ associated to the last qP_d>0.98 is pNPQ. In case qP_d assumes values above 1 because of significant PSII antenna uncoupling, the determination of pNPQ is still possible with suitable corrections [44-45]. The result of this calculation applied to the wheat lines allowed a comparative evaluation of pNPQ. The photoprotection offered by NPQ in young plants was maximum in the two wild-type lines and in 4A, independent of the plant age (Figure 4E,G). Less pNPQ was developed by all young durum wheat mutants, as well as in 4B and 32A (Figure 4E,G). In the leaves of mature plants, the alleviation of the impaired pNPQ phenotype was complete in 7A and 8A, but not even partial in the other mutants (Figure 4F,H). Despite mature 7B and 32A tended to approach NPQ_{MAX} values identical or closer to their wild-type lines, their capacity for PSII photoprotection remained very low (Figure 4F,H). Although the mature 4B was capable of inducing higher NPQ than NS67, it did not gain a superior PSII photoprotective capacity (Figure 4H).

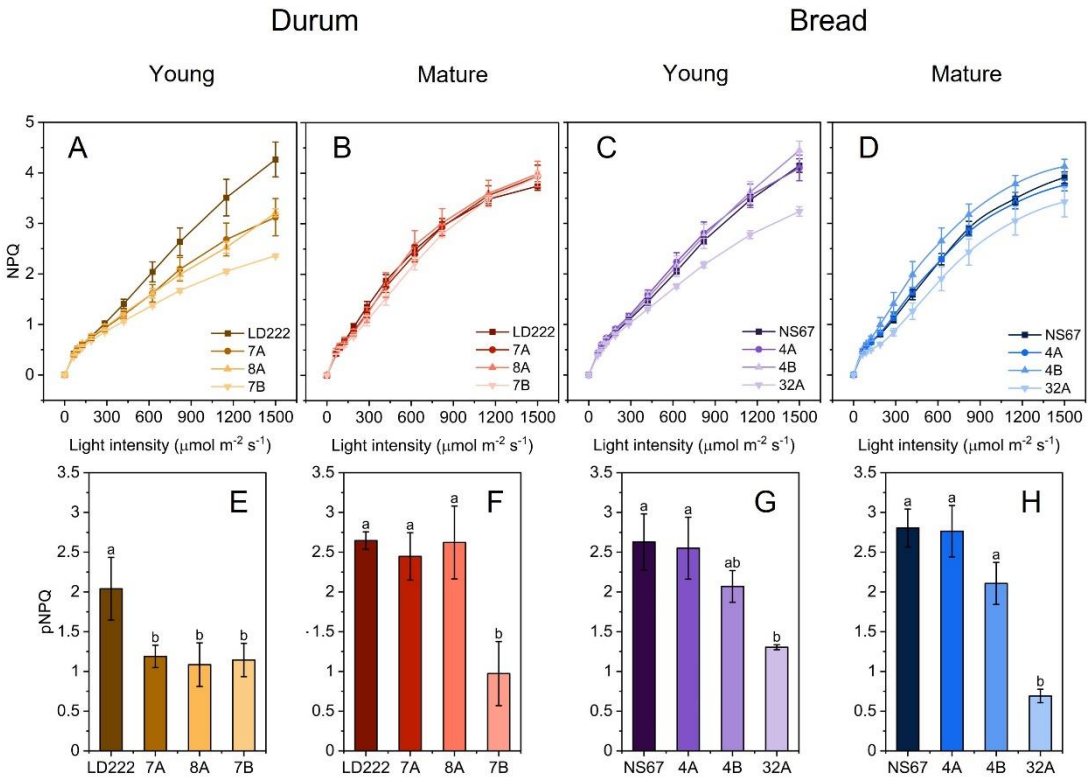

Figure 4. NPQ light-response curves and photoprotective NPQ (pNPQ) in young and mature plants of bread and durum wheat. (A-D) NPQ-light response curves of young-durum (A), mature durum (B), young bread (C) and mature bread (D) plants during 60 minutes exposure to increasing actinic light intensities. Average values ± Standard Deviation for n=4-6. (E-H) pNPQ values obtained after applying the "qP_a method". Histograms represent average values ± Standard Error for n=4-6; different letters indicate a significant difference at $P < 0.05$, as determined using one-factor ANOVA followed by Tukey's test.

2.4 Fast chlorophyll a *fluorescence transients and JIP test parameters*

Analysis of the fast chlorophyll *a* fluorescence emission (OJIP transient) was recently shown to offer a set of powerful indexes for the functional phenotyping of chlorophyll-depleted wheat lines [11]. In young plants, the OJIP transients were indeed clearly influenced by the plant genotype (Figure 5A,C). F_0 values in the two wild-type lines were obviously higher, with the biggest differences found for the durum wheat mutants (Figure 5A). For a qualitative comparison of the mutants, the fluorescence transients were first double normalized between F_0 (step O) and F_M (plateau P, Figure 5E-H)). The two inflections at approx. 2 ms (step J) and 30 ms (step I) were variably affected in the mutants. The geometrical features of the transients were used to calculate technical parameters (Sm), quantum yields and probabilities (φPo, ψETo, ψREo and δREo) and specific energy fluxes per reaction center (ABS/RC, TRo/RC, ETo/RC, REo/RC, DIo/RC) according to the model by Strasser et al. [46] and Stibert and Govindjee [47]. The definitions of the parameters are reported in Appendix B (Table B1), and the results are comparatively shown in the diagrams of Figure 5.

In the young plants, the initial exponential rise of chlorophyll *a* fluorescence was slightly slower in the mutants compared to their wild-type counterparts (Figure 5A,C); this feature can be attributed to a smaller PSII antenna size in the mutants, which was quantified by significantly lower ABS/RC values (Figure 6A,C). Such slower increase was uniform among mutants, without apparent relation with phenotype severity as assessed by pigment analysis. The same samples also showed a tendency to higher φPo (Figure

6A,C); although this is the most common parameter used to estimate the maximum PSII quantum yield, formally equivalent to F_V/F_M, in the mutants its increase is due to a lower PSI/PSII ratio rather than a genuine increase in PSII photochemical activity [11]. In young durum wheat mutants and in 32A, Sm, ψETo, ψREo and δREo were enhanced as compared to the corresponding wild type lines (Figure 6A). Particularly, higher ψREo and δREo values have already been associated with 7A, 8A, 7B and 32A mutant phenotypes in controlled growth conditions, indicating a more abundant relative pool of electron carriers downstream of PSI [11, 48]. In the semi-field condition of this experiment, the same mutants also underwent an increase in ψETo – related to the probability that an electron is accepted by the plastoquinone, and thus the pool size of the latter [46-47, 49] (Figure 6A). This response was in line with the tendency to accumulate more electron carriers per PSII-PSI chain unit, as evidenced by generalized higher Sm values. Noticeably, in previous indoor study the relative enhancement of the down-stream electron flow (δREo) was found as a phenotypic trait shared by all mutants under controlled conditions, but the Sm increase was specific to bread wheat [11]. Conversely, in young plants here grown outdoors, the increased number of interchain electron carriers became an important feature also of the durum wheat mutants (Figure 6A).

In the young plants of mutants, all energy fluxes, except REo/RC, per active PSII center were depressed in comparison with the corresponding wild-type lines (Figure 6A,C). Given the dependency of these parameters on the normalized initial slope of the OJIP transient, a response such clearly descended from the smaller PSII antenna size of the mutants (Figure 5A,C; Figure 6A,C). The most affected flux was that related to the untrapped energy dissipation per active PSII (DIo/RC), which was reduced between 25 and 50% depending on the mutant. The decrease in DIo/RC was easily related to the seeming gain in PSII photochemical efficiency, φPo, which, however and as already mentioned, is merely the reflection of a lower relative amount of PSI. A noticeable parameter was REo/RC: in young durum wheat mutants and 32A it was similar to the wild-type values, while in 4A and 4B it was lower (Figure 6B). REo/RC describes the energy flux from Q_B to PSI end acceptors, therefore high values were consistent with the increased probability of electron transfer from Q_B to PSI end acceptors (ψREo) in these mutants (Figure 6B).

Measurements performed at the end of the season revealed a generalized alleviation of the mutant functional phenotype (Figure 6B,D). In particular, F_0 and the specific energy fluxes became more similar between wild-type and mutant lines compared to the young plants. However, some peculiarities were found with respect to the electron transfer probabilities and Sm. In durum wheat mutants the number of interchain electron carriers increased considerably following the gradient of phenotype severity (Figure 6B). This response was absent in the intermediate mutants of bread wheat (4A, 4B), whereas it was apparent in 32A (Figure 6D). ψREo and δREo similarly increased in the same mutants, suggesting that the mutants benefitted from a compensative mechanism that relied on the accumulation of PSI end electron acceptors, as already suggested [11].

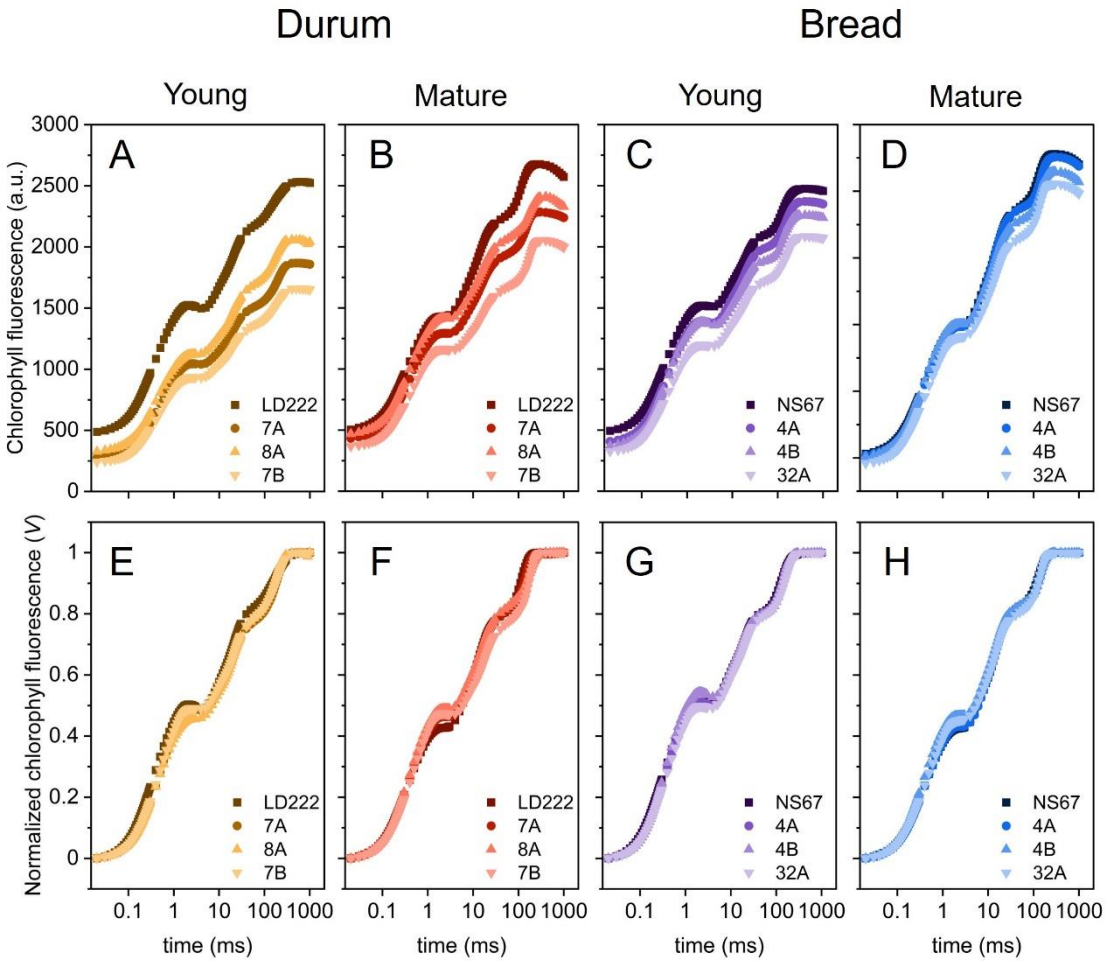

Figure 5. Prompt chlorophyll *a* fluorescence emission in young and mature plants of durum and bread wheat. (A-D) Average OJIP transients on logarithmic timescale. (E-H) Average OJIP transient normalized between F_0=$F_{20\mu s}$ and F_M on logarithmic timescale.

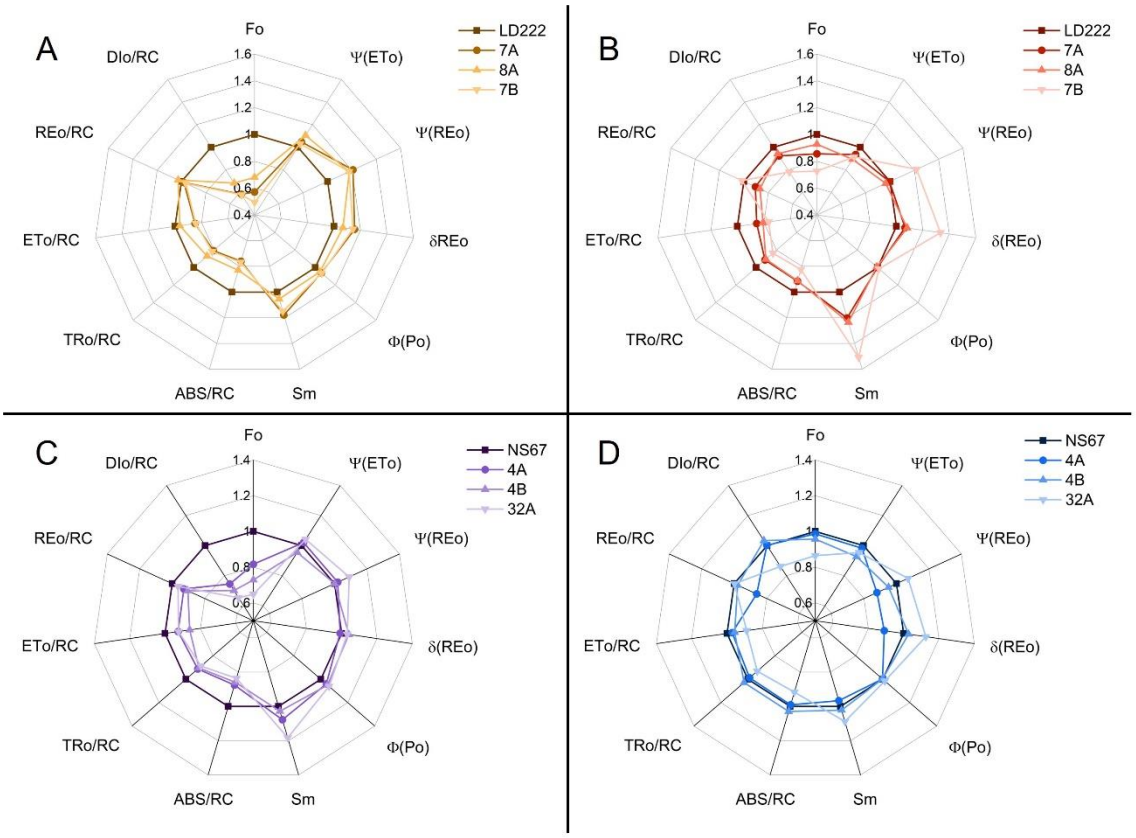

Figure 6. Spider plots of selected fast-chlorophyll-*a*-fluorescence-derived parameters calculated according to the "Energy Fluxes" model in young and mature leaves of durum and bread wheat plants. Each point represents the average value normalized on the respective average value of the wild-type line (LD222 in durum wheat, NS67 in bread wheat) for n=8-12 replicates. (A-B) Spider plots of young (A) and mature (B) durum wheat lines. (C-D) Spider plots of young (C) and mature (D) bread wheat lines. For the definition of the parameters, see Appendix B.

2.5 Productivity estimation, morphometric measurements, and correlation analysis

At the end of the 2020 and 2021 seasons (3rd week of May) morphometric and productivity measurements were performed after harvesting the grains. Morphometric measurements like plant height, ear number and spikelet length did not show major differences between the genotypes, except for a reduced plant height in 8A, 4A and 32A in comparison to their wild-type lines (Table C1); moreover, the spikelet in 32A was significantly shorter compared to the other bread wheat genotypes (Table C1). Conversely, the tillering degree (number of stems per plant) was very sensitive to the genotype: in durum wheat significant differences were found between LD222 and 7B, whereas in bread wheat all the mutants were characterized by a smaller tillering degree (Figure 7C,G). The number of grains per ear was reduced only in durum wheat mutants 7A and 7B (Figure 7A,E). The weight of a single grain was more affected by the severity of the phenotype, being lower in the most severe mutants 7B and 32A (Figure 7B,F). The product of the number of grains per ear by the weight of a single grain and the tillering degree resulted in the synthetic parameter termed "single plant productivity", which summarizes the potential in plant productivity for each wheat line (Figure 7D,H). Compared to LD222, durum wheat mutants were clearly less productive: in 8A the productivity was 1/3 less, in 7A it was halved and in 7B more than halved (60% decrease, Figure 7D). Smaller differences were instead observed between bread wheat lines, although the mutants were generally less productive (Figure 7H). As compared to NS67, 4B performed quite well, with a reduction in productivity by only 10%, while 4A single plant productivity was reduced by ca. 25%. The most

severe mutant, 32A was the least productive line with less than half grain production compared to NS67.

The ambition of crop photosynthetic phenotyping is to support predictions of plant productivity. A correlation matrix was built to check the presence of significant correlations between photosynthetic parameters recorded in young plants and productivity/morphometric parameters obtained at the end of the season when mature grains were harvested (Figure 8). Morphometric parameters such as plant height, spikelet number and length did not display any significant correlation with the photosynthetic parameters. Conversely, several correlations were found between photosynthetic and grain productivity parameters. The parameters derived from the pigment analyses are the standard to describe the phenotype severity in chlorophyll-depleted mutants. However, the individual morphometric/productivity parameters showed weak correlations with the pigment parameters, with only two exceptions (total chlorophylls *vs.* tillering degree; chlorophyll/carotenoid ratio *vs.* single grain weight). Much more interesting was the strong correlation between all pigment parameters and the synthetic index of the productivity of a single plant. A considerable number of correlations was found with fluorometric parameters as well. The number of grains per ear was negatively correlated with $Y(NO)_{MAX}$ (i.e., the highest value of Y(NO) recorded during a light-response curve); the single grain weight was negatively correlated with Sm, and the tillering degree with pNPQ. However, taking again the single plant productivity as the most informative about the plant performance, the most sensitive fluorometric parameters were NPQ_{MAX}, pNPQ, Sm, ABS/RC, and TRo/RC.

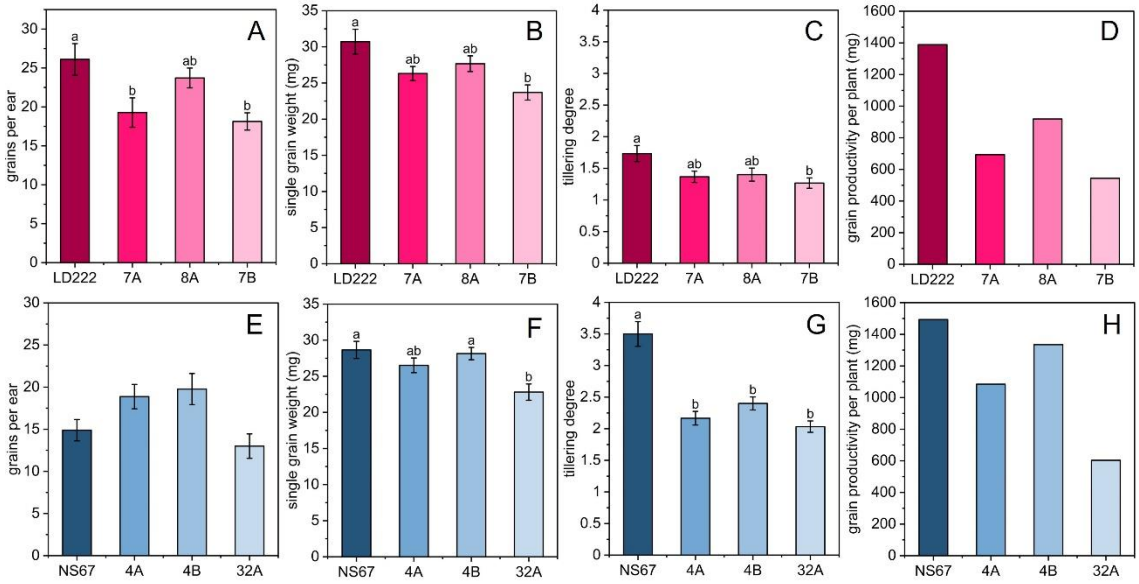

Figure 7. Productivity parameters measured at the end of the season in durum and bread wheat mature plants. (7A,E) represent the average number of grains per ear (n_{ears}=10) in durum and bread wheat, respectively. (7B,F) report the average weight of a single grain harvested from the 10 ears used in the previous measurement. Tillering degree (7C,G) is the average tillering degree in durum and bread wheat (n=30). Histograms represent average values ± Standard Error; different letters indicate a significant difference at $P < 0.05$, as determined using one-factor ANOVA followed by Tukey's test. (7D,H) Grain productivity per plant, a synthetic parameter that combines the previous three and estimates the mass of grains that was produced by a single plant for each wheat line.

	grains per ear	single grain weight	plant height	spikelets number	spikelets length	tillering degree	single plant productivity
Chlorophyll (*a*+*b*)	-0.017	0.705	0.228	0.087	0.684	0.875	0.937
Chlorophyll *a*/*b*	-0.099	-0.684	-0.292	-0.027	-0.621	-0.736	-0.900
Chlorophyll (a+b) / carotenoids	0.364	0.899	0.382	0.256	0.490	0.620	0.970
NPQ MAX	0.199	0.737	0.203	0.093	0.624	0.660	0.908
Y(NO)MAX	-0.900	-0.361	-0.631	-0.250	0.632	0.734	0.075
pNPQ	-0.078	0.538	-0.005	0.131	0.686	0.805	0.827
Fo	0.742	0.641	0.782	0.239	-0.527	-0.278	0.252
ψ(ETo)	0.556	0.173	0.578	-0.264	-0.790	-0.610	-0.206
ψ(REo)	-0.389	-0.722	-0.287	-0.218	-0.123	-0.305	-0.618
δ(REo)	-0.688	-0.649	-0.610	0.005	0.492	0.226	-0.290
φ(Po)	-0.361	-0.574	-0.536	-0.306	0.226	-0.125	-0.356
Sm	-0.494	-0.903	-0.525	0.006	-0.162	-0.376	-0.818
ABS/RC	0.104	0.758	0.435	0.001	0.364	0.713	0.833
TRo/RC	0.026	0.708	0.345	-0.086	0.482	0.774	0.855
ETo/RC	0.454	0.638	0.693	-0.263	-0.258	0.075	0.451
REo/RC	-0.451	-0.111	0.021	-0.373	0.388	0.479	0.184
DIo/RC	0.227	0.724	0.529	0.159	0.088	0.484	0.654

Figure 8. Matrix of Pearson's *r* correlation coefficients of photosynthetic parameters *vs.* productivity parameters in durum and bread wheat lines. Correlations were constructed with average values of the measurements performed in the young plants using Microsoft Office Excel™ (Microsoft). Green color marks significant positive correlations, red the negative ($P < 0.05$).

3. Discussion

In previous experiments, the indoor cultivation of the chlorophyll-deficient wheat mutants evidenced their tendency to recover a wild-type phenotype with respect to the leaf chlorophyll content, emphasizing the impact of the genomic context, particularly which subgenome (A or B) hosted the mutated locus and the condition of hexaploidy (bread wheat) *vs*. tetraploidy (durum wheat) [9-10]. Moreover, the differential susceptibility of the mutants to light fluctuations underlined the relevance of the growth environment in shaping their phenotype [10-11]. The metabolic energy investment in compensatory responses capable of limiting the detrimental effects of a disturbed photosynthetic electron flow was proposed to be the main cause for a lower biomass accumulation. Whether this conclusion could also hold true under a normal life cycle in the field needed testing, looking at phenotypic traits in association with the grain yields: under a naturally fluctuating environment, does the phenotype recover to wild type? Is the mutant severity series confirmed? Has the mutation a significant impact on grain production?

In general, the young plants confirmed previous findings, showing the phenotype severity in the order 7B>7A=8A>LD222 and 32A>4A=4B>NS67 [9], with the functional defects quite well matching the chlorophyll depletion level. However, overwintering

outdoor cultivation of durum and bread wheat did not lead to the expected recovery of a wild-type-like leaf chlorophyll content (Figure 2). More interestingly, the mutants underwent an effective *long-term acclimation of the functional traits* related to photosynthesis. In mature plants, the alleviation of the functional phenotype was evident from the restored ability to control the photosynthetic electron poise (Figure 3,4), as well as the tendency to more regular spider plots of OJIP-derived parameters (Figure 6). Especially in durum wheat mutants, but also in 32A, the importance of accumulating interchain electron carriers and PSI end acceptors, as represented by Sm, emerges even more strongly than in previous indoor experiment [11].

The results collected in this semi-field experiment suggest the predictive power of the early biochemical and functional traits with respect to grain productivity (Figure 8). The genetic lesion in chlorophyll-deficient wheat lines is attributed to a decreased activity of the Mg-chelatase, which impairs chlorophyll accumulation, particularly chlorophyll *b* [50-52]. Despite recurrent reports on highly productive chlorophyll-deficient crops, wheat included [15], the less-than-normal chlorophyll content in wheat mutants causes several alterations of the photosynthetic membrane function and structure [9-11, 19, 53-54]. The picture we get from previous studies and the current research is that most of the efforts of the chlorophyll-deficient wheat plants are devoted to reach a compensation for the genetic defect: this is certainly helped by the healthy homoeologous genes in other subgenome(s), but it also benefits from energy-consuming adjustments of the photosynthetic electron flow [10-11]. The consequence is that the chlorophyll synthesis mutation has a pleiotropic effect, including significant long-term impacts on plant morphogenesis and reproduction. Accordingly, we show that in this collection of chlorophyll-depleted mutants, it is possible to discriminate between different degrees of productivity by performing fast and non-invasive chlorophyll fluorescence measurements at the initial stages of plant development. Interestingly, input phenotyping data were mostly correlated with the synthetic parameter "single plant productivity" (Figure 8). This observation reveals that increasing degrees of chlorophyll depletion do not result in an unambiguously identifiable, single, impaired productive trait, such as the grains per ear or the spike length (see also [54]), but rather lead to an overall depression of the capacity of producing grains by the single plant. In the over-wintering experiment, a significant contribution to such decrease is due to the lowered tillering of the mutants, indicating that, directly or indirectly, the genetic defect influences productivity by limiting the emergence of axillary shoots well before the reproductive phase (Figure 7). This response is interesting because a low number of tillers is usually a shade-avoidance response in wheat cultivated in a dense canopy and is counterbalanced by investment in plant height [55-56]. According to the principle equating a low-chlorophyll phenotype with an improved light interception [7, 57], lower plants (a tendency visible in Table C1) but with many tillers would have been expected. We can suggest that in chlorophyll-deficient wheat, the potential benefit of a higher light transmittance through the canopy is overcome by the energy-demanding adjustment of an altered photosynthetic electron transport chain.

Based on previous research, Y(NO) and NPQ obtained from modulated-chlorophyll emission data were deemed to be the most sensitive to chlorophyll depletion in mutants [9-10], and, thus, good correlative candidates to productivity. These parameters derive from dynamic measuring protocols – the light-response curves – and are suited to a correlative analysis if expressed as synthetic phenotypic indexes. Given the different light-dependency of Y(NO) and NPQ in the wheat lines, we extracted $Y(NO)_{MAX}$ and NPQ_{MAX} from the light curves (Figure 3,4). The former proves a defective electron transport control, the latter a reduction in thermal dissipation capacity, i.e., two main physiological traits characterizing the mutants [9-10]. $Y(NO)_{MAX}$ correlated negatively only with the number of grains per ear (Figure 8); therefore, in this outdoor experiment, $Y(NO)_{MAX}$ did not appear to be a much straightforward index to the correlative scope. Y(NO) certainly changes with light intensity, but its maximum value, representative of a quasi-steady state, can be not very informative (see [10]). More interesting was NPQ_{MAX}, which in young plants was

clearly dependent on the phenotype severity, correlating with a single plant's productivity (Figure 4). In the mutants, a lower capacity to develop NPQ is a physiological trait related to an insufficient proton pumping into the thylakoid lumen, which was interpreted as a side effect of the defective CEF [9-10]. It was previously shown that the parallel up-regulation of the ATP synthase activity allows a sufficient ability of these mutants to sustain ATP synthesis [10]. Despite the defective CEF, ensuring an adequate supply of ATP is permissive to the stability of the photosystems, e.g., supporting the repair of photodamaged PSII [25]. However, NPQ_{MAX}, as a technical parameter, is complex in origin and includes not only ΔpH-dependent de-excitation processes ("high-energy quenching", qE), but also other components, e.g., related to the plastid redox state or the integrity of photosystems [36-37, 58-62]. Not all NPQ components have a primary photoprotective meaning, and indeed the photoprotective fraction of NPQ – pNPQ – was a robust phenotyping index, strongly correlating with the tillering degree and the single plant productivity (Figure 8). As also shown in another experimental system [45], a high capacity to develop NPQ is not necessarily accompanied by a superior PSII photoprotection. Interestingly, a comparison of NPQ_{MAX} and pNPQ makes it clear that the former may underestimate the severity of the photosynthetic regulation defect, particularly in the "intermediate" mutants 7A and 7B, or also 4B (Figure 4). The phenotype alleviation occurring during the life cycle of outdoors-grown plants includes at least a partial recovery of NPQ_{MAX} to wild-type values, in one case – 4B – even exceeding them (Figure 4A-D). However, a comparative analysis of the corresponding pNPQ invites to be particularly cautious about conclusions because a reduced PSII photoprotection capacity remains in 7B and 32A, which may be expected, but also in 4B as a tendency (Figure 4).

A reduced PSII photoprotection *per se* can be insufficient to explain the decreased productivity in the mutants: it is well established that a high PSII photoprotection can also cause losses in PSII quantum yield and, in turn, a lower maximum yield in carbon assimilation [35, 63-64]. Although it is necessary to prevent yield losses due to excessive PSII photodamage, the qE-induced PSII photoprotection must be quickly reversible to allow a rapid switch from high to low light [35, 63-66]. The semi-field condition is a perfect example of an everchanging light environment, in which fast responsiveness of photoprotective mechanisms to fluctuating light is fundamental to maintain an optimal carbon assimilation capacity. Therefore, given the decreased ability of the mutants to promptly control the balance between LEF and CEF [9-11], it is conceivable that the most compromised mutants were not only less photoprotected, but also slower in the adaptation to natural light fluctuations. In the incomplete recovery of a wild-type-like functionality in 7B and 4B, we envisage a sign of the higher severity of a mutation at locus *cn*B1-d, shared by the two mutants and making them more prone to fluctuating light [10]. Lower productivity also affects the mutant 4A (mutated locus *cn*A1-d as in 7A), which, however, already in the young plant appeared indistinguishable from the wild-type NS67 as far as pNPQ is concerned. The complementary approach of the OJIP transient analysis offers hints to understand why an apparently well-regulated mutant like 4A can be nonetheless poorly productive.

Prompt-chlorophyll *a* fluorescence parameters are among the most suited to implement future large-scale phenotyping studies because they allow the collection of considerable amounts of data in a fast and non-invasive way [6, 11, 46-47, 67-68]. Single plant productivity in wheat was correlated with three JIP-test-derived parameters, catching different facets of the light energy conversion in the mutants: ABS/RC, TRo/RC and Sm (Figure 8). ABS/RC and TRo/RC are energy flux parameters describing the functional PSII antenna size and the maximum trapped energy in PSII [46-47]. The down-sizing of the PSII antenna was an expected consequence of the reduced availability of chlorophyll *a* and *b* to assemble the LHCII, shared by all mutants at their young stage (Figure 6A,B). The reduced trapping ability in active PSII was also expected and consistent with the smaller antenna of the photosystem, despite a tendency of the mutants to higher φPo [11]. In the previous indoor experiment, ABS/RC tended to very effectively recover to wild-

type values, making it a weak phenotyping index [11]. In the case of the outdoor, overwintering wheat growth, the reduction of the PSII antenna size appears to be a more persistent trait, perfectly in line with the severity gradient in the chlorophyll *a*/*b* ratio still observed in mature plants (Figure 2). It was previously proposed that the chlorophyll-deficient wheat lines may have an intrinsic ability to adjust the PSII antenna system under the unfavourable supply of chlorophylls [11]. This regulation, whose molecular backgrounds are unknown, may help mitigate an unbalanced excitation distribution between PSII and PSI. Evidently, outdoor cultivation is less permissive to such regulation, which occured effectively only in 4A and 4B (Figure 6). In other mutants, we observed instead enhanced accumulation of electron transporters. A similar response was observed in the previous indoor experiment, but it was more linked to the relative pool size of the end acceptors of PSI (ferredoxin and FNR), represented by δREo, than to the overall abundance of electron carriers, Sm [11]. Sm values were indicators of the chlorophyll-depleted phenotype severity in bread wheat mutants but not in the durum lines. In the semi-field experiment, the increase in Sm occurred in all young mutant plants. Subsequently, while Sm tended to revert to wild-type in bread wheat mutants, the differences between durum wheat genotypes were magnified at the end of the season, up to the excessive Sm increase characterizing 7B (Figure 6B,D). A compensative meaning against the membrane over-reduction was assigned to the seeming excess of end transporters [11], supported by findings about the role of FNR as a buffer for electrons to keep PSI in a safe oxidized state and prevent the accumulation of reactive oxygen radicals [69-70]. A relevant hypothesis denoted as the "ultrastructural control" of photosynthetic electron transport was proposed by Gu and coworkers (2022) [71]. They attribute the role of electron reservoirs to all mobile electron carriers, i.e., plastoquinone, plastocyanin and ferredoxin, to cushion the light fluctuations causing variations of the thylakoid lumen swelling [71]. The electron buffering activity demonstrated for FNR [70] suggests including this enzyme in the model. In the JIP test, the concept of Sm includes all mobile pools and the enhancement of Sm in the mutant wheat lines can be interpreted consistently within the ultrastructural control hypothesis to offer an extended buffering system against the recurrent electron bursts caused by lightflecks in a fluctuating light regime [11]. In a natural environment, where the light fluctuations are combined with other variables and the re-sizing of the PSII antennae cannot be reached completely, the Sm increase emerges as possibly the main compensation mechanism of the electron flow defects in chlorophyll-deficient mutants. More intense exploitation of this response in durum wheat than in bread wheat is in line with the acclimative advantage offered by hexaploidy in the latter [9, 72]. In most mature plants, the achievement of an electron flow regulation similar to the wild-type lines, as seen for Y(NO), testifies to the success of the defect compensation. However, the investment in electron carriers is energy-demanding and conceivably diverts a part of the metabolic energy from vegetative growth and reproduction to the acclimation of photosynthesis. Therefore, a strong negative correlation links the single plant productivity and Sm, which can be proposed as a robust potential marker in plant phenotyping projects in the open field and aimed to increase grain production in chlorophyll-deficient durum and bread wheat lines. For example, the early screening of chlorophyll-deficient mutants for excessive Sm may help discard low productive lines.

Although not correlating with the plant productivity, the JIP-test parameters DIo/RC was the most affected parameter in young plants and showed the best relief in mature plants. The lack of correlation is due to the absence of a clear correspondence with the phenotype severity series. Two factors concur to lowering the DIo/RC – the reduced PSII antenna size and the seemingly increased PSII photochemical activity – making it difficult to assess if the DIo/RC decrease can be truly symptomatic of a reduced ability of energy dissipation in PSII unit [73].

4. Conclusion

In the semi-field overwintering experiment, the mitigation of the phenotype severity of chlorophyll-deficient wheat primarily concerned the recovery of the photosynthetic membrane functionality, but only marginally the leaf chlorophyll content. The efforts for acclimating photosynthesis towards a fluctuating environment are already visible in the young plants and include a compensatory mechanism against the defective control of the electron flow, i.e., the accumulation of interchain electron carriers and PSI end acceptors. Such a mechanism, already proposed from indoor experiments, is here shown to be maximally exploited in mature plants of durum wheat mutants, which probably relates to their less efficient acclimative potential than bread wheat. The tillering phase had a substantial effect in reducing the single plant's grain productivity, indicating that the mutation itself or the energy-consuming compensatory mechanisms significantly influence plant morphogenesis. Consistently with the interrelation between early photosynthetic phenotype and grain yield per plant, some chlorophyll fluorescence-derived parameters are proposed as good candidates for future phenotyping applications in the open field.

5. Materials and Methods

5.1 Plant material and cultivation

The wheat lines used in this work were the same as described by Živčak et al. [9]. Four lines were used for *Triticum durum* L.: the wild-type LD222 and three derived chlorophyll-depleted mutants, namely ANDW-7A, ANDW-8A and ANDW-7B. Similarly, four lines were used for *T. aestivum* L. the wild-type Novosibirskaya 67 (NS67) and three derived chlorophyll-depleted mutants, namely ANBW-4A, ANBW-4B and ANK-32A. Main characteristics of the wheat lines are reported in Table A1. Plants were sown in parcels (30 seeds per parcel) of the Botanical Garden of the University of Ferrara (44.841912 N, 11.622454 E) in October for two subsequent seasons (2020-21 and 2021-22), following the regular schedule for sowing *T. durum* and *T. aestivum*, and therefore allowing the plants to overwinter and go through the tillering phase in outdoor conditions. The general meteorological conditions, including solar radiation, are publicly available through the website of the Meteorological Observatory of the Botanical Garden of Ferrara (http://www.meteosystem.com/dati/ortofe/index.php), and a graphical summary of the weather features during the experimental seasons is reported in Appendix D (Figure D1). The first round of analyses was performed during the first weeks after plant germination, following the appearance of the third leaf in all lines. The second round of analyses was performed on the flag leaf during the second week of May.

5.2 Morphometric measurements and grain productivity estimation

Morphometric indexes consisting of plant height, spikelet number per spike, spike length, and tillering degree were measured after the complete emergency of the spike. At the end of the season, mature ears were harvested, and grain productivity was estimated by counting the number of grains in each ear with ten random replicates per genotype. The grains of each ear were counted and weighed to obtain the average number of grains per ear and the average weight of a single grain. The synthetic parameter and best estimator of plant productivity, namely "grain productivity per plant", was calculated by multiplying the average weight of a single grain by the number of grains per ear and the tillering degree.

5.3 Quantification of photosynthetic pigments

Leaf segments (2 cm^2) were cut from the 3rd leaf of young plants and the flag leaf of mature plants. The segments were subsequently weighed, reduced to smaller pieces, and placed in glass tubes containing 3 mL of 80% (v/v) acetone buffered with HEPES-KOH (pH 7.8). Extraction was performed at -20 °C for 3 days until complete depigmentation of the leaf samples. Extracts were analysed using a spectrophotometer, Ultrospec 2000 (Pharmacia Biotech); chlorophyll *a* and *b* content in the extract were determined according to Ritchie [74], while total carotenoids were calculated using the equation by Wellburn [75].

5.4 Modulated chlorophyll a *fluorescence measurements*

Modulated chlorophyll *a* fluorescence was measured in leaves dark-acclimated for 30 minutes in the laboratory using a Junior-PAM (Walz) fluorometer. Measurements were performed as described in Colpo et al. [45] with some modifications. Minimum and maximum fluorescence (F_0 and F_M, respectively) were measured before starting the light-response curve experiment. Ten irradiance intervals (actinic light from 65 to 1500 μmol photons m^{-2} s^{-1}), each with 7 minutes length, were applied to the sample. To avoid leaf dehydration, the samples were placed on top of a humid piece of filter paper during the whole measuring routine. Saturation pulses were 0.6 s long, each followed by 5 s exposure to far-red light to determine F_0'. Quantum yields of actual PSII photochemistry [Y(II)], non-regulatory energy loss [Y(NO)], and regulatory thermal dissipation [Y(NPQ)] were calculated according to Hendrickson et al. [30]. Photoprotective thermal dissipation (pNPQ) was calculated by applying the qP_d protocol as described by Ruban and Murchie [39], with modifications as detailed by Colpo et al. [45].

5.5 Prompt chlorophyll a *fluorescence measurements*

Prompt chlorophyll *a* fluorescence was measured directly in the field on the 3rd or flag leaf, according to the growth stage. After 30 minutes of dark-acclimation in the leaf clip, the fluorescence emission was recorded using a portable HandyPEA (Hansatech) fluorometer. For analysis, a 1-s-long saturating pulse was applied to the sample with an intensity of 3500 μmol photons m^{-2} s^{-1} (650 nm light provided by the LEDs integrated in the measuring head of the device). The derived OJIP transients were analyzed according to the energy fluxes model as reported by Strasser et al. [46] and Stirbet and Govindjee [47], allowing the calculation of selected basic and derived parameters with the Biolyzer software (Fluoromatic Software). F_0 value was sampled at 20 μs. The list of the parameters and their phenomenological meaning is reported in Appendix B, Table B1.

5.6 Data analysis and correlation matrix

Data obtained from each set of measurements were analyzed using the Microsoft Office Excel™ (Microsoft) software for the preliminary elaborations. Graphs and statistical analyses were carried out using Origin™ version 2022 (OriginLab). Statistical comparison between the replicates of each group (durum and bread wheat) was performed using ANOVA one-factor test with $\alpha = 0.05$ significant threshold, followed by the post hoc Tukey's test ($\alpha = 0.05$) for means comparison. The Pearson's *r* correlation matrix between productivity values, morphometric indexes, and photosynthetic phenotyping data was built with Microsoft Office Excel.

Author Contributions: Conceptualization, A.C. and L.F.; validation, M.Z. and M.B.; formal analysis, A.C. and S.D.; investigation, A.C., S.D., C.B., L.F.; data curation, A.C. and S.D.; writing—original draft preparation, A.C.; writing—review and editing, L.F. and M.Z.; supervision, L.F., M.B., S.P. All authors have read and agreed to the published version of the manuscript.

Funding: This research was funded by the University of Ferrara, "Fondo per l'Incentivazione alla Ricerca - FIR 2020" (granted to L.F.), "Fondo di Ateneo per la Ricerca scientifica" (FAR2020 and FAR2021, granted to L.F.), as well as by the Ministry of Education, Science, Research and Sport of the Slovak Republic, Project No. VEGA 1-0664-22 (granted to M.B.) and by the Slovak Research and Development Agency, Project No. APVV-18-465 (granted to M.B.).

Data Availability Statement: Raw data that support the findings of this study are made available on request.

Acknowledgments: The authors are grateful to Professor Nobuyoshi Watanabe (Ibaraki University, Japan) for the kind gift of the wheat lines used in this study. The authors acknowledge the careful assistance by Fausto Molinari and Roberta Marchesini (Botanical Garden of the University of Ferrara) for the cultivation of the plants used for experiments.

Conflicts of Interest: The authors declare no conflict of interest.

Appendix A

Table A1. Main characteristics of the wheat lines used in this study.

Wheat line	Mutated locus	Chlorophyll Level (% wild-type)[1]	Effect of fluctuating light[2]
NS67	Wild-type	--	Slightly negative
ANBW-4A	*cn*A1-d	10-40%	Positive
ANBW-4B	*cn*B1-d	0-50%	Very negative
ANK-32A	*cn*A1-a	30-70%	Insensitive
LD222	Wild-type	--	Slightly negative
ANDW-7A	*cn*A1-d	40-60%	Slightly negative
ANDW-7B	*cn*B1-d	35-65%	Very negative
ANDW-8A	unknown	10-45%	Insensitive

[1]Variation ranges based on Živčak et al. and Ferroni et al. [9-11]
[2]Based on aboveground biomass as reported by Ferroni et al. [10]

Appendix B

Table B1. Measured and calculated parameters from the fast chlorophyll *a* fluorescence transients.

Parameter	Definition[1]
Descriptive parameters of the OJIP transient	
F_0	Minimum fluorescence value at 20 μs
F_K	Fluorescence value at 0.3 ms
F_J	Fluorescence value at 2 ms
F_I	Fluorescence value at 30 ms
F_M	Maximum fluorescence value at plateau
$F_V = F_M - F_0$	Variable PSII fluorescence
$V_t = (F_t - F_0)/(F_M - F_0)$	Relative variable fluorescence at time t (V_J at 2 ms, V_I at 30 ms)
$Mo = \Delta V/\Delta t$	Approximate value of the initial slope (trait 20-300 μs) of the relative variable fluorescence curve V_t
Sm	Normalized area, proportional to the number of electron carriers per electron transport chain
Quantum yields and probabilities	
φPo = $(F_M - F_0)/F_M = F_V/F_M$	Estimate of PSII maximum quantum yield
ψETo = $\Delta V_J = 1 - V_J$	Estimate of the oxidized plastoquinone size, or the probability with which a PSII trapped electron is transferred from reduced Q_A to Q_B
ψREo = $\Delta V_I = 1 - V_I$	Estimate of the relative size of the pool of PSI end electron acceptors, or the probability with which a PSII trapped electron is transferred from reduced Q_A to PSI final acceptors (ferredoxin, ferredoxin-NADP+ oxido-reductase)
δREo = $\Delta V_I / \Delta V_J$	Pool of PSII electron acceptors relative to the pool of plastoquinone, or the probability with which an electron is transferred from reduced Q_B to PSI final acceptors
Specific energy fluxes per active PSII reaction center	
ABS/RC = Mo / (V_J · φPo)	Flux of light absorption per PSII, or apparent antenna size of an active PSII
TRo/RC = (Mo/V_J)	Maximum trapped exciton flux per PSII
ETo/RC = (Mo/V_J) · ψETo	Electron transport flux from Q_A to Q_B per PSII
REo/RC = (Mo/V_J) · ψREo	Electron transport flux from Q_A to final PSI acceptors per PSII
DIo/RC = (Mo/V_J) · F_M/F_0	Flux of energy dissipation per active PSII

[1] For reference, see [46-47, 67].

Appendix C

Figure C1. Average morphometric measurements of durum and bread wheat selected features with the corresponding standard deviations (n=10). Different letters indicate a significant difference at $P < 0.05$, as determined using one-factor ANOVA followed by Tukey's test.

Wheat line	Plant height (cm)	Spike length (cm)	Spikelets number
LD222	162.2±9.7 (a)	6.81±1.16	19.8±3.2
7A	156.9±13.1 (a)	6.79±0.55	21.7±1.9
8A	143.7±8.5 (b)	6.52±1.17	19.1±1.8
7B	160.9±5.8 (a)	6.79±1.01	20.3±1.4
NS67	151.3±5.0 (a)	9.37±0.45 (a)	20.2±2.7
4A	141.5±4.6 (b)	8.12±1.19 (ab)	20.8±1.5
4B	146.5±4.5 (ab)	9.39±1.15 (a)	20.5±1.4
32A	144.2±3.4 (b)	7.80±1.34 (b)	18.8±2.3

Appendix D

Figure D1. Meteorological data derived from the Meteorological Observatory of the Botanical Garden of Ferrara, Italy, relative to the two experimental cultivation seasons (2020-2021, 2021-2022).

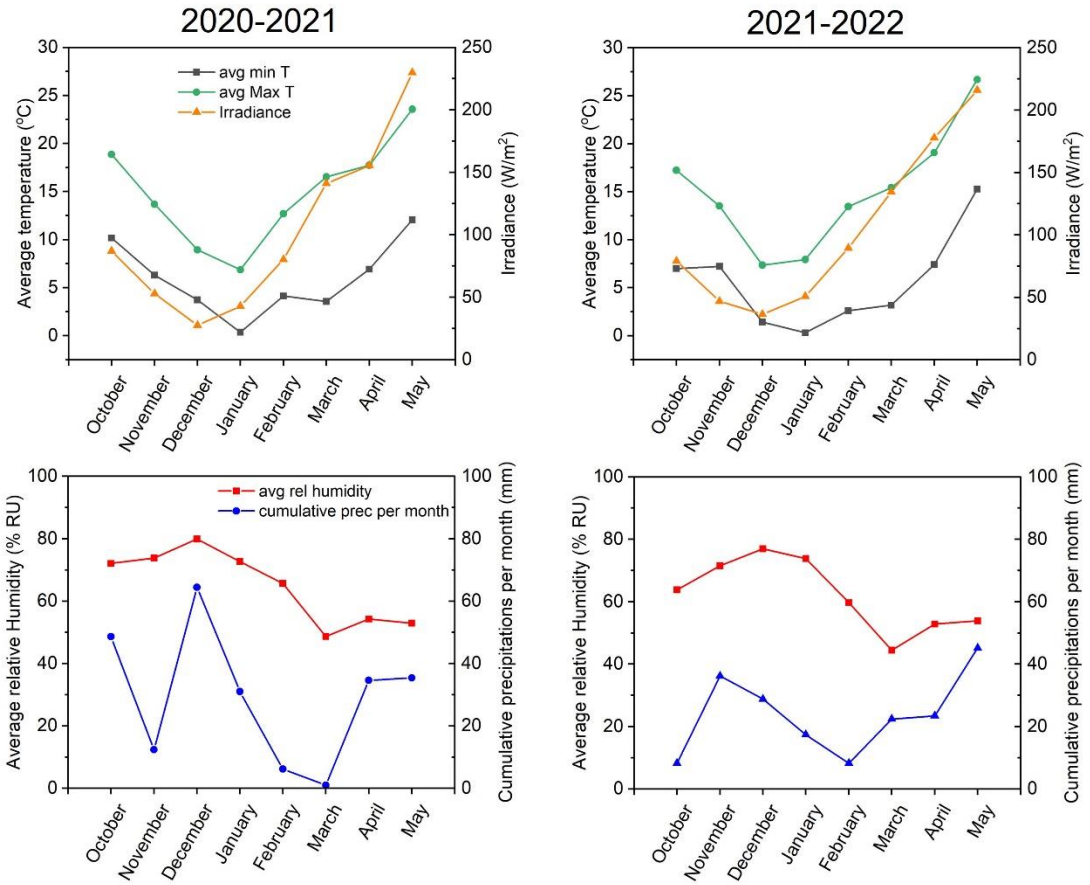

References

1. Song, P.; Wang, J.; Guo, X.; Yang, W.; Zhao, C. High-throughput phenotyping: Breaking through the bottleneck in future crop breeding. *The Crop Journal* **2021**, *9*(3), 633-645. https://doi.org/10.1016/j.cj.2021.03.015.
2. Yang, W.; Feng, H.; Zhang, X.; Zhang, J.; Doonan, J. H.; Batchelor, W. D.; Xiong, L.; Yan, J. Crop phenomics and high-throughput phenotyping: past decades, current challenges, and future perspectives. *Molecular Plant* **2020**, *13*(2), 187-214. https://doi.org/10.1016/j.molp.2020.01.008.
3. Pratap, A.; Gupta, S.; Nair, R. M.; Gupta, S. K.; Schafleitner, R.; Basu, P. S.; Singh, C.M.; Prajapati, U.; Gupta, A.K.; Nayyar, H.; Mishra, A.K.; Baek; K. H. Using plant phenomics to exploit the gains of genomics. *Agronomy* **2019**, *9*(3), 126. https://doi.org/10.3390/agronomy9030126.
4. Gielen, R.; Põldmaa, K.; Tammaru, T. In search of ecological determinants of fungal infections: A semi-field experiment with folivorous moths. *Ecology and Evolution* **2022**, *12*(5), e8926. https://doi.org/10.1002/ece3.8926.
5. Van Bezouw, R. F.; Keurentjes, J. J.; Harbinson, J.; Aarts, M. G. Converging phenomics and genomics to study natural variation in plant photosynthetic efficiency. *The Plant Journal* **2019**, *97*(1), 112-133. https://doi.org/10.1111/tpj.14190.
6. Kalaji, H. M.; Schansker, G.; Brestič, M.; Bussotti, F.; Calatayud, A.; Ferroni, L.; Goltsev, V.; Guidi, L.; Jajoo, A.; Li, P.; Losciale, P.; Mishra, V.K.; Misra, A.N.; Nebauer, S.G.; Pancaldi, S.; Penella, C.; Pollastrini, M.; Suresh, K.; Tambussi, E.; Yanniccari, M.; Živčak, M.; Cetner, M.D.; Samborska, I.A.; Stirbet, A.; Olsovska, K.; Kunderlikova, K.; Shelonzek, H.; Rusinowski, S.; Bąba, W. (2017). Frequently asked questions about chlorophyll fluorescence, the sequel. *Photosynthesis Research* **2017**, *132*(1), 13-66. https://doi.org/10.1007/s11120-016-0318-y.
7. Ort, D.; Merchant, S. S.; Alric, J.; Barkan, A.; Blankenship, R.E.; Bock, R.; Croce, R.; Hanson, M. R.; Hibberd, J. M.; Long, S. P.; Moore, T. A.; Moroney, J.; Niyogi, K. K.; Parry, M. A. J.; Peralta-Yahya, P. P.; Prince, R. C.; Redding, K. E.; Spalding, M. H.; van Wijk, K. J.; Vermaas, W. F. J.; von Caemmerer S.; Weber, A. P. M.; Yeates T. O.; Yuan, J. S.; Zhu, X. G. Redesigning photosynthesis

to sustainably meet global food and bioenergy demand. *Proceedings of the National Academy of Sciences* **2015**, *112*(28), 8529-8536. https://doi.org/10.1073/pnas.142403111.

8. Li, Y. T.; Li, Y.; Song, J. M.; Guo, Q. H.; Yang, C.; Zhao, W. J.; Wang, J.Y.; Luo, J.; Xu, Y.N., Zhang, Q.; Ding, X.Y.; Liang, Y.; Li, Y.N.; Feng, Q.L.; Liu, P.; Gao, H.Y.; Li, G.; Zhao, S.J.; Zhang, Z. S. Has breeding altered the light environment, photosynthetic apparatus, and photosynthetic capacity of wheat leaves?. *Journal of Experimental Botany* **2022**, *73*(10), 3205-3220. https://doi.org/10.1093/jxb/erab495.
9. Živčak, M.; Brestič, M.; Botyanszka, L.; Chen, Y. E.; Allakhverdiev, S. I. Phenotyping of isogenic chlorophyll-less bread and durum wheat mutant lines in relation to photoprotection and photosynthetic capacity. *Photosynthesis Research* **2019**, *139*(1), 239-251. https://doi.org/10.1007/s11120-018-0559-z.
10. Ferroni, L.; Živčak, M.; Sytar, O.; Kovar, M.; Watanabe, N.; Pancaldi, S.; Baldisserotto, C.; Brestič, M. Chlorophyll-depleted wheat mutants are disturbed in photosynthetic electron flow regulation but can retain an acclimation ability to a fluctuating light regime. *Environmental and Experimental Botany* **2020**, *178*, 104156. https://doi.org/10.1016/j.envexpbot.2020.104156.
11. Ferroni, L.; Živčak, M.; Kovar, M.; Colpo, A.; Pancaldi, S.; Allakhverdiev, S. I.; Brestič, M. Fast chlorophyll *a* fluorescence induction (OJIP) phenotyping of chlorophyll-deficient wheat suggests that an enlarged acceptor pool size of Photosystem I helps compensate for a deregulated photosynthetic electron flow. *Journal of Photochemistry and Photobiology B: Biology* **2022**, *234*, 112549. https://doi.org/10.1016/j.jphotobiol.2022.112549.
12. Andrews, J. R.; Fryer, M. J.; Baker, N. R. Consequences of LHC II deficiency for photosynthetic regulation in chlorina mutants of barley. *Photosynthesis Research* **1995**, *44*(1), 81-91. https://doi.org/10.1007/BF00018299.
13. Terao, T.; Sonoike, K.; Yamazaki, J. Y.; Kamimura, Y.; Katoh, S. Stoichiometries of photosystem I and photosystem II in rice mutants differently deficient in chlorophyll *b*. *Plant and Cell Physiology* **1996**, *37*(3), 299-306. https://doi.org/10.1093/oxfordjournals.pcp.a028946.
14. Terao, T.; Katoh, S. Antenna sizes of photosystem I and photosystem II in chlorophyll *b*-deficient mutants of rice. Evidence for an antenna function of photosystem II centers that are inactive in electron transport. *Plant and Cell Physiology* **1996**, *37*(3), 307-312. https://doi.org/10.1093/oxfordjournals.pcp.a028947.
15. Wang, Y.; Zheng, W.; Zheng, W.; Zhu, J.; Liu, Z.; Qin, J.; Li, H. Physiological and transcriptomic analyses of a yellow-green mutant with high photosynthetic efficiency in wheat (*Triticum aestivum* L.). *Functional & Integrative Genomics* **2018**, *18*(2), 175-194. https://doi.org/10.1007/s10142-017-0583-7.
16. Wang, G.; Zeng, F.; Song, P.; Sun, B.; Wang, Q.; Wang, J. Effects of reduced chlorophyll content on photosystem functions and photosynthetic electron transport rate in rice leaves. *Journal of Plant Physiology* **2022**, *272*, 153669. https://doi.org/10.1016/j.jplph.2022.153669.
17. Friedland, N.; Negi, S.; Vinogradova-Shah, T.; Wu, G.; Ma, L.; Flynn, S.; Kumssa, T.; Lee, C.H.; Sayre, R. T. Fine-tuning the photosynthetic light harvesting apparatus for improved photosynthetic efficiency and biomass yield. *Scientific Reports* **2019**, *9*(1), 1-12. https://doi.org/10.1038/s41598-019-49545-8.
18. Bielczynski, L. W.; Schansker, G.; Croce, R. Consequences of the reduction of the Photosystem II antenna size on the light acclimation capacity of *Arabidopsis thaliana*. *Plant, Cell & Environment* **2020**, *43*(4), 866–879. https://doi.org/10.1111/pce.13701
19. Brestič, M.; Živčak, M.; Kunderlikova, K.; Sytar, O.; Shao, H.; Kalaji, H. M.; Allakhverdiev, S. I. Low PSI content limits the photoprotection of PSI and PSII in early growth stages of chlorophyll *b*-deficient wheat mutant lines. *Photosynthesis Research* **2015**, *125*(1), 151-166. https://doi.org/10.1007/s11120-015-0093-1.
20. Furutani, R.; Wada, S.; Ifuku, K.; Maekawa, S.; Miyake, C. Higher Reduced State of Fe/S-Signals, with the Suppressed Oxidation of P700, Causes PSI Inactivation in Arabidopsis thaliana. Antioxidants 2023, 12, 21. https://doi.org/10.3390/antiox12010021
21. Yamori, W. Photosynthetic response to fluctuating environments and photoprotective strategies under abiotic stress Journal of Plant Research **2016**, *129*(3), 379–395. https://doi.org/10.1007/s10265-016-0816-1.
22. Joliot, P.; Johnson, G. N. Regulation of cyclic and linear electron flow in higher plants. *Proceedings of the National Academy of Sciences* **2011**, *108*(32), 13317-13322. https://doi.org/10.1073/pnas.1110189108.
23. Tikkanen, M.; Rantala, S.; Grieco, M.; Aro, E. M. Comparative analysis of mutant plants impaired in the main regulatory mechanisms of photosynthetic light reactions-From biophysical measurements to molecular mechanisms. *Plant Physiology and Biochemistry* **2017**, *112*, 290-301. https://doi.org/10.1016/j.plaphy.2017.01.014.
24. Huang, W.; Zhang, S. B.; Cao, K. F. Stimulation of cyclic electron flow during recovery after chilling-induced photoinhibition of PSII. *Plant and Cell Physiology* **2010**, *51*(11), 1922-1928. https://doi.org/10.1093/pcp/pcq144.
25. Huang, W.; Yang, Y. J.; Zhang, S. B.; Liu, T. Cyclic electron flow around photosystem I promotes ATP synthesis possibly helping the rapid repair of photodamaged photosystem II at low light. *Frontiers in Plant Science* **2018**, *9*, 239. https://doi.org/10.3389/fpls.2018.00239.
26. Shi, Q.; Zhang, S. B.; Wang, J. H.; Huang, W. Pre-illumination at high light significantly alleviates the over-reduction of photosystem I under fluctuating light. *Plant Science* **2021**, *312*, 111053. https://doi.org/10.1016/j.plantsci.2021.111053.
27. Tan, S. L.; Liu, T.; Zhang, S. B.; Huang, W. Balancing light use efficiency and photoprotection in tobacco leaves grown at different light regimes. *Environmental and Experimental Botany* **2020**, *175*, 104046. https://doi.org/10.1016/j.envexpbot.2020.104046.
28. Yamamoto, H.; Shikanai, T. PGR5-dependent cyclic electron flow protects photosystem I under fluctuating light at donor and acceptor sides. *Plant Physiology* **2019**, *179*(2), 588-600. https://doi.org/10.1104/pp.18.01343.
29. Tikkanen, M.; Rantala, S.; Aro, E. M. Electron flow from PSII to PSI under high light is controlled by PGR5 but not by PSBS. *Frontiers in Plant Science* **2015**, *6*, 521. https://doi.org/10.3389/fpls.2015.00521.

30. Hendrickson, L.; Furbank, R. T.; Chow, W. S. A simple alternative approach to assessing the fate of absorbed light energy using chlorophyll fluorescence. *Photosynthesis Research* **2004**, *82*(1), 73-81. https://doi.org/10.1023/B:PRES.0000040446.87305.f4.
31. Bilger, W.; Björkman, O. Role of the xanthophylls cycle, fluorescence and photosynthesis in *Hedera canariensis*. *Photosynthesis Research* **1990**, *25*(5), 173-185. https://doi.org/10.1007/BF00033159.
32. Kalaji, H. M.; Schansker, G.; Ladle, R. J.; Goltsev, V.; Bosa, K.; Allakhverdiev, S. I.; Brestič, M.; Bussotti, F.; Calatayud, A.; Dąbrowski, P.; Elsheery, N.I.; Ferroni, L.; Guidi, L.; Hogewoning, S. W.; Jajoo, A.; Misra, A. N.; Nebauer, S. G.; Pancaldi, S.; Penella, C.; Poli, D.B.; Pollastrini, M.; Romanowska-Duda, Z. B.; Rutkowska, B.; Serodio, J.; Suresh, K.; Szulc, W.; Tambussi, E.; Yanniccari, M.; Živčak, M. Frequently asked questions about in vivo chlorophyll fluorescence: practical issues. *Photosynthesis Research* **2014**, *122*(2), 121-158. https://doi.org/10.1007/s11120-014-0024-6.
33. Demmig-Adams, B.; Adams III, W. W.; Heber, U.; Neimanis, S.; Winter, K.; Krüger, A.; Czygan, F.C.; Bilger, W., Bjorkman, O. Inhibition of zeaxanthin formation and of rapid changes in radiationless energy dissipation by dithiothreitol in spinach leaves and chloroplasts. *Plant Physiology* **1990**, *92*(2), 293-301. https://doi.org/10.1104/pp.92.2.293.
34. Demmig-Adams, B.; Adams III, W. W. Photoprotection in an ecological context: the remarkable complexity of thermal energy dissipation. *New Phytologist* **2006**, *172*(1), 11-21. https://doi.org/10.1111/j.1469-8137.2006.01835.x.
35. Long, S. P.; Taylor, S. H.; Burgess, S. J.; Carmo-Silva, E.; Lawson, T.; De Souza, A. P.; Leonelli, L.; Wang, Y. Into the shadows and back into sunlight: photosynthesis in fluctuating light. *Annual Review of Plant Biology* **2022**, *73*, 617-648. https://doi.org/10.1146/annurev-arplant-070221-024745.
36. Ruban, A. V. Nonphotochemical chlorophyll fluorescence quenching: mechanism and effectiveness in protecting plants from photodamage. *Plant Physiology* **2016**, *170*(4), 1903-1916. https://doi.org/10.1104/pp.15.01935.
37. Malnoë, A. Photoinhibition or photoprotection of photosynthesis? Update on the (newly termed) sustained quenching component qH. *Environmental and Experimental Botany* **2018**, *154, 123-133*. https://doi.org/10.1016/j.envexpbot.2018.05.005.
38. Lambrev, P. H.; Miloslavina, Y.; Jahns, P.; Holzwarth, A. R. On the relationship between non-photochemical quenching and photoprotection of photosystem II. *Biochimica et Biophysica Acta (BBA)-Bioenergetics* **2012**, *1817*(5), 760-769. https://doi.org/10.1016/j.bbabio.2012.02.002.
39. Ruban, A. V.; Murchie, E. H. Assessing the photoprotective effectiveness of non-photochemical chlorophyll fluorescence quenching: a new approach. *Biochimica et Biophysica Acta (BBA)-Bioenergetics* **2012**, *1817*(7), 977-982. https://doi.org/10.1016/j.bbabio.2012.03.026.
40. Oxborough, K.; Baker, N.R. Resolving chlorophyll *a* fluorescence images of photosynthetic efficiency into photochemical and non-photochemical components–calculation of qP and Fv/Fm; without measuring Fo. *Photosynthesis Research* **1997**, *54*(2), 135-142. https://doi.org/10.1023/A:1005936823310.
41. Wilson, S.; Ruban, A. V. Rethinking the influence of chloroplast movements on non-photochemical quenching and photoprotection. *Plant Physiology* **2020**, *183*(3), 1213-1223. https://doi.org/10.1104/pp.20.00549.
42. Giovagnetti, V.; Ware, M. A.; Ruban, A. V. Assessment of the impact of photosystem I chlorophyll fluorescence on the pulse-amplitude modulated quenching analysis in leaves of *Arabidopsis thaliana*. *Photosynthesis Research* **2015**, *125*(1), 179-189. https://doi.org/10.1007/s11120-015-0087-z.
43. Ware, M. A.; Dall'Osto, L.; Ruban, A. V. An in vivo quantitative comparison of photoprotection in *Arabidopsis* xanthophyll mutants. *Frontiers in Plant Science* **2016**, 7, 841. https://doi.org/10.3389/fpls.2016.00841.
44. Ware, M. A.; Belgio, E.; Ruban, A. V. Photoprotective capacity of non-photochemical quenching in plants acclimated to different light intensities. *Photosynthesis Research* **2015**, *126*(2), 261-274. https://doi.org/10.1007/s11120-015-0102-4.
45. Colpo, A.; Baldisserotto, C.; Pancaldi, S.; Sabia, A.; Ferroni, L. Photosystem II photoinhibition and photoprotection in a lycophyte, *Selaginella martensii*. *Physiologia Plantarum* **2022**, *174*(1), e13604. https://doi.org/10.1111/ppl.13604.
46. Strasser, R. J.; Tsimilli-Michael, M.; Srivastava, A. Analysis of the chlorophyll *a* fluorescence transient. In Chlorophyll *a* fluorescence: a signature of photosynthesis. Advances in Photosynthesis and Respiration; Papageorgiou, G., Govindjee (Eds.), Springer: Dordrecht, Germany; 2004, pp. 321-362.
47. Stirbet, A.; Govindjee. On the relation between the Kautsky effect (chlorophyll a fluorescence induction) and photosystem II: basics and applications of the OJIP fluorescence transient. *Journal of Photochemistry and Photobiology B: Biology* **2011**, *104*(1-2), 236-257. https://doi.org/10.1016/j.jphotobiol.2010.12.010.
48. Živčak, M.; Brestič, M.; Kunderlikova, K.; Olsovska, K.; Allakhverdiev, S. I. Effect of photosystem I inactivation on chlorophyll a fluorescence induction in wheat leaves: does activity of photosystem I play any role in OJIP rise? *Journal of Photochemistry and Photobiology B: Biology* **2015**, *152*, 318-324. https://doi.org/10.1016/j.jphotobiol.2015.08.024.
49. Tóth, S. Z.; Schansker, G.; Strasser, R. J. A non-invasive assay of the plastoquinone pool redox state based on the OJIP-transient. *Photosynthesis Research* **2007**, *93*(1), 193-203. https://doi.org/10.1007/s11120-007-9179-8.
50. Falbel, T. G.; Meehl, J. B.; Staehelin, L.A. Severity of mutant phenotype in a series of chlorophyll-deficient wheat mutants depends on light intensity and the severity of the block in chlorophyll synthesis. *Plant Physiology* **1996**, *112*(2), 821–832. https://doi.org/10.1104/pp.112.2.821.
51. Jiang, H. B.; Wang, N.; Jian, J. T.; Wang, C. S.; Xie, Y. Z. Rapid mapping of a chlorina mutant gene *cn*-A1 in hexaploid wheat by bulked segregant analysis and single nucleotide polymorphism genotyping arrays. *Crop and Pasture Science* **2019**, *70*(10), 827. https://doi.org/10.1071/CP19165.

52. Wu, H.; Shi, N.; An, X.; Liu, C.; Fu, H.; Cao, L.; Feng, Y.; Sun, D.; Zhang, L. Candidate genes for yellow leaf color in common wheat (*Triticum aestivum* L.) and major related metabolic pathways according to transcriptome profiling. *International Journal of Molecular Sciences* **2018**, *19*(6), 1594. https://doi.org/10.3390/ijms19061594.
53. Brestič, M.; Živčak, M.; Kunderlikova, K.; Allakhverdiev, S.I. High temperature specifically affects the photoprotective responses of chlorophyll *b*-deficient wheat mutant lines. *Photosynthesis Research* **2016**, *130*(1), 251–266. https://doi.org/10.1007/s11120-016-0249-7.
54. Li, N.; Jia, J.; Xia, C.; Liu, X.; Kong, X. Characterization and mapping of novel chlorophyll deficient mutant genes in durum wheat. *Breeding Science* **2013**, *63*(2): 169–175. https://doi.org/10.1270/jsbbs.63.169.
55. Evers, J. B.; Vos, J.; Andrieu, B.; Struik, P. C. Cessation of tillering in spring wheat in relation to light interception and red:far-red ratio. *Annals of Botany* **2006**, *97*(4), 649-658. https://doi.org/10.1093/aob/mcl020.
56. Moeller, C.; Evers, J. B.; Rebetzk, G. Canopy architectural and physiological characterization of near-isogenic wheat lines differing in the tiller inhibition gene tin. *Frontiers in Plant Science* **2014**, *5*, 617. https://doi.org/10.3389/fpls.2014.00617.
57. Genesio, L.; Bassi, R.; Miglietta, R. Plants with less chlorophyll: A global change perspective. *Global Change Biology* **2021**, *27*(5), 959-967. https://doi.org/10.1111/gcb.15470.
58. Ferroni, L.; Colpo, A.; Baldisserotto, C.; Pancaldi, S. In an ancient vascular plant the intermediate relaxing component of NPQ depends on a reduced stroma: Evidence from dithiothreitol treatment. *Journal of Photochemistry and Photobiology B: Biology* **2021**, *215*, 112114. https://doi.org/10.1016/j.jphotobiol.2020.112114.
59. Nilkens, M.; Kress, E.; Lambrev, P.; Miloslavina, Y.; Müller, M.; Holzwarth, A. R.; Jahns, P. Identification of a slowly inducible zeaxanthin-dependent component of nonphotochemical quenching of chlorophyll fluorescence generated under steady state-conditions in *Arabidopsis*. *Biochimica et Biophysica Acta* **2010**, *1797*, 466–475. https://doi.org/10.1016/j.bbabio.2010.01.001.
60. Aro, E.-M.; Virgin, I.; Andersson, B. Photoinhibition of photosystem II. Inactivation, protein damage and turnover. *Biochimica et Biophysica Acta* **1993**, 1143, 113–134. https://doi.org/10.1016/0005-2728(93)90134-2.
61. Tiwari, A.; Mamedov, F.; Grieco, M.; Suorsa, M.; Jajoo, A.; Styring, S.; Tikkanen, M.; Aro, E.-M. Photodamage of iron-sulphur clusters in photosystem I induces nonphotochemical energy dissipation. *Nature Plants* **2016**, *2*, 16035. https://doi.org/10.1038/nplants.2016.35.
62. Nawrocki, W. J.; Liu, X.; Raber, B.; Hu, C.; de Vitry, C.; Bennett, D. I. G.; Croce, R. Molecular origins of induction and loss of photoinhibition-related energy dissipation qI. *Science Advances* **2021**, 7, eabj0055. https://doi.org/10.1126/sciadv.abj0055.
63. Long, S. P.; Humphries, S.; Falkowski, P. G. Photoinhibition of photosynthesis in nature. *Annual Review of Plant Biology* **1994**, *45*(1), 633-662. https://doi.org/10.1146/annurev.pp.45.060194.003221.
64. Zhu, X. G.; Ort, D. R.; Whitmarsh, J.; Long, S. P. The slow reversibility of photosystem II thermal energy dissipation on transfer from high to low light may cause large losses in carbon gain by crop canopies: a theoretical analysis. *Journal of Experimental Botany* **2004**, *55*(400), 1167-1175. https://doi.org/10.1093/jxb/erh141.
65. Kromdijk, J.; Głowacka, K.; Leonelli, L.; Gabilly, S. T.; Iwai, M.; Niyogi, K. K.; Long, S. P. Improving photosynthesis and crop productivity by accelerating recovery from photoprotection. *Science* **2019**, *354*(6314), 857-861. https://doi.org/10.1126/science.aai8878.
66. Murchie, E. H.; Niyogi, K. K. Manipulation of photoprotection to improve plant photosynthesis. *Plant Physiology* **2011**, *155*(1), 86-92. https://doi.org/10.1104/pp.110.168831.
67. Tsimilli-Michael, M. Revisiting JIP-test: An educative review on concepts, assumptions, approximations, definitions and terminology. *Photosynthetica* **2020**, *58*, 275-292. https://doi.org/10.32615/ps.2019.150.
68. Khan, N.; Essemine, J.; Hamdani, S.; Qu, M.; Lyu, M.-J. A.; Perveen, S.; Stirbet, A.; Govindjee; Zhu, X.-G. Natural variation in the fast phase of chlorophyll *a* fluorescence induction curve (OJIP) in a global rice minicore panel. *Photosynthesis Research* **2021**, *150*(1-3), 137-158. https://doi.org/10.1007/s11120-020-00794-z.
69. Rodriguez, R. E.; Lodeyro, A.; Poli, H. O.; Zurbriggen, M.; Peisker, M.; Palatnik, J. F.; Tognetti, V. B.; Tschiersch, H.; Hajirezaei, M.R.; Valle, E. M.; Carrillo, N. Transgenic tobacco plants overexpressing chloroplastic ferredoxin-NADP(H) reductase display normal rates of photosynthesis and increased tolerance to oxidative stress. *Plant Physiology* **2007**, *143*, 639–649. https://doi.org/10.1104/pp.106.090449.
70. Rodriguez-Heredia, M.; Saccon, F.; Wilson, S.; Finazzi, G.; Ruban, A.V.; Hanke, G. T. Protection of photosystem I during sudden light stress depends on ferredoxin:NADP(H) reductase abundance and interactions. *Plant Physiology* **2022**, *188*, 1028–1042. https://doi.org/10.1093/plphys/kiab550.
71. Gu, L.; Grodzinski, B.; Han, J.; Marie, T.; Zhang, Y.-J.; Song, Y. C.; Sun, Y. Granal thylakoid structure and function: explaining an enduring mystery of higher plants. *New Phytologist* **2022**, *236*(2), 319-329. https://doi.org/10.1111/nph.18371.
72. Chovancek, E.; Živčak, M.; Brestič, M.; Hussain, S.; Allahkverdiev, S. I. The different patterns of post-heat stress responses in wheat genotypes: the role of the transthylakoid proton gradient in efficient recovery of leaf photosynthetic capacity. *Photosynthesis Research* **2021**, *150*, 179–193. https://doi.org/10.1007/s11120-020-00812-0.
73. Force, L.; Critchley, C.; Van Rensen, J. J. New fluorescence parameters for monitoring photosynthesis in plants. *Photosynthesis Research* **2003**, *78*(1), 17-33. https://doi.org/10.1023/A:1026012116709.
74. Ritchie, R. J. Consistent sets of spectrophotometric chlorophyll equations for acetone, methanol and ethanol solvents. *Photosynthesis Research* **2006**, *89*(1), 27-41. https://doi.org/10.1007/s11120-006-9065-9.

75. Wellburn, A. R. (1994). The spectral determination of chlorophylls a and b, as well as total carotenoids, using various solvents with spectrophotometers of different resolution. *Journal of Plant Physiology* **1994**, *144*(3), 307-313. https://doi.org/10.1016/S0176-1617(11)81192-2.

Chapter 4:
Phenotyping of photosynthetic traits to support the selection of strawberry accessions resistant to salt stress

Introduction

Soil salinization is a major threat to agriculture production affecting around 20% of irrigated lands worldwide (Qadir et al. 2014). Natural and anthropogenic causes concur in exacerbating the increase in soil salt concentrations. Natural causes, such as the occurrence of salty rainfalls and the contamination from parental rocks and seawater, are mainly responsible for the salinization of coastal environments (Mahajan and Tuteja 2005, Jajoo 2013). Differently, anthropogenic causes indiscriminately affect different types of ecosystems, with the worst effects occurring in arid and semi-arid regions of the world (Wallender and Tanji 2011, Cuevas et al. 2019). Anthropogenic soil salinization occurs when the balance between freshwater supply (from rainfalls and irrigation) and soil transpiration is altered in favor of the latter because of bad irrigation practices, such as waterlogging, use of unlined canals and vegetation clearing (Qadir et al. 2014, Ritzema 2016, Cuevas et al. 2019). To keep the pace with increasing soil degradation and worldwide food demand it becomes necessary to improve crops' water use efficiency and salt tolerance (Jajoo 2013).

The major player in salinity stress is sodium chloride (NaCl), with Cl^- being the most toxic in plants tissues of the two ions (Ferreira et al. 2019). Plants cope with salinity stress adopting a complex network of acclimation and adaptation strategies. Plants naturally adapted to live and proliferate in salty soils are termed halophytes: these species adopt different mechanisms, such as selective ion uptake, compartmentalization of Na^+, tight regulation of ion homeostasis, production of osmolytes, development of salt glands and bladders, and enhanced antioxidant activity (Flowers et al. 2008, Platel et al. 2020, Rahman et al. 2021). The study of these plants is extremely important to unveil the metabolic pathways needed to inhabit environments characterized by high salt concentrations, because the most widespread crops are conversely sensitive or extremely sensitive to high levels of NaCl in the soil (Rahman et al. 2021).

Plants respond to salinity stress in two ways at the shoot level: ion-independent responses and ion-dependent responses (Negrão et al. 2017). The ion-independent response occurs as primary response within minutes to days and is deemed to be triggered by Na^+ sensing and signaling (Gilroy et al. 2014, Roy et al. 2014); side effects produced by this response are stomatal closure and inhibited (Munns and Termaat 1986). The ion-dependent response develops over days to weeks and depends on the accumulation of ions up to toxic concentrations, which cause premature leaf senescence, reduced plant yield or even plant death (Negrão et al. 2017). Plants avoid the most negative outcomes by excluding ions from the shoot, segregating toxic ions into specific tissues, cells and organelles, and maintaining growth and water uptake rates independently of the accumulation of Na^+ (Negrão et al. 2017).

However, crops are usually sensitive to salt stress, therefore side effects appear even when tolerance responses are developed to some extent. General effects of salinity comprise the inhibition of seed germination and progressive dehydration, reduced growth, metabolic disfunctions, enzymes inactivation and altered protein

synthesis, impairment of membrane permeability and reduction of photosynthetic activity (Jajoo 2012, Zörb et al. 2018, Hernández 2019, Rahjabi Dehnavi et al. 2020, Arif et al. 2021). The depression of the photosynthetic activity is a fundamental concern for crops productivity because photosynthesis is necessary to sustain plant development and growth. At the photosynthetic level, two main types of effects are activated when plants are subjected to salinity stress: osmotic effects and ion effects (Jajoo 2012, Chen et al. 2015, Dąbrowski et al. 2016). Osmotic effects are responsible of the progressive dehydration of the plant tissues, leading to reduction of stomatal conductance and therefore of the intracellular CO_2 concentration, depression of RuBisCO activity, sucrose accumulation, changes in PSII antenna heterogeneity, reduction of chlorophyll content, and significant ultrastructural alterations of the chloroplast (Hernández et al. 1999, James et al. 2002, Munns and Tester 2008, Jajoo 2012, Arif et al. 2021). Conversely, ion effects are related to ion imbalance and consequently to the direct alteration of the thylakoid membrane organization, for example the induction of increased grana stacking, the inhibition at the donor and acceptor side of PSII due to increased production of Oxygen Reactive Species (ROS), the over-reduction of the photosynthetic electron transport chain and, consequently, the depression of the electron transport (Hernandez et al. 1999, Mitsuya et al. 2000, Strasser et al. 2010, Metha et al. 2010a-b, Yaghubi et al. 2016, Pan et al. 2021).

In view of the strong sensitivity of the photosynthetic machinery to salt stress, especially the methods based on chlorophyll fluorescence emission are considered elective for monitoring the occurrence of detrimental effects caused by salt stress, as well as for screening plants with respect to their ability to exploit effective acclimative responses (Perez-Bueno et al. 2019, Van Bezouw et al. 2019). The chlorophyll fluorescence measurements suited to the scope of plant phenotyping are neither time demanding nor destructive, therefore they are the perfect deal to collect much useful information about the photosynthetic functionality in medium-to-large screening experiments approaching the plant responses to a variety of stresses, salt stress included (Baker and Rosenqvist 2004, Lazar et al. 2006, Borawska-Jarmułowicz et al. 2014, Humplik et al. 2015). Major advances have occurred in the last decades, including the use of phenotyping facilities to maintain a controlled environment and perform automated measurements on samples (Song et al. 2021). The control of environmental conditions in growth chambers and in the whole phenotyping infrastructure allows the maximization of the samples homogeneity and, therefore, emphasizes the differential effect produced by a given stress, such as salinity stress, on a panel of cultivars or accessions (Van Bezouw et al. 2019, Song et al. 2021)

The present experiment is an application of chlorophyll fluorescence techniques operated in an automated plant phenotyping facility and aims to screen five strawberries market cultivars for their salinity stress tolerance. Strawberry is a valuable crop cultivated worldwide and is particularly sensitive to salinity stress (Ferreira et al. 2019, Esmaeilizadeh et al. 2021). According to Grieve et al. (2012) the salinity tolerance threshold for strawberry is 1 mS cm^{-1}, after which the plant yield decreases by 33% per every unit increase in electric conductivity. Both NaCl and KCl induce leaf scorching after four weeks of irrigation with water at 1 mS cm^{-}

[1], while severe leaf damages appear at electric conductivity > 5 mS cm^{-1} (Martinez-Barroso and Alvarez 1997). The selection of less salt-sensitive strawberry accessions has been pursed for some time with the main scope of extending the cultivation of this crop to harsher land, particularly in the Mediterranean area (Ondrašek et al. 2006, Al-Shorafa et al. 2014, Cardeñosa et al. 2015, Bani et al. 2021). The awareness of the rising salinization of soils has progressively increased to interest in screening programs of strawberry selections that exhibit an enhanced salt tolerance. The five cultivars used in this experiment (Table 1) were provided by the Consorzio Italiano Vivaisti (C.I.V., Comacchio, Italy, https://civ.it), a high profile and internationally recognized research center specialized, among others, in obtaining new market varieties of strawberry and investigating their potential for cultivation in different environmental contexts, including marginal land prone to salt stress. The plant material has been studied at the Slovak PlantScreen™ Phenotyping Unit (SPPU) of the Slovak University of Agriculture in Nitra (SK), which allowed us to set precise environmental conditions and perform automated RGB morphometric and chlorophyll fluorescence monitoring of the plants. Together with a regularly irrigated control group, two different treatments have been applied by enriching the control water with NaCl in order to reach the electric conductivity values of 2 and 4 mS cm^{-1}. Such levels were chosen to enable the onset of moderate (2 mS cm^{-1}) and severe (4 mS cm^{-1}) salinity stress in agreement with previous reports (Martinez-Barroso and Alvarez 1997, Grieve et al. 2012, Bani et al. 2021). Moreover, based on indications by C.I.V., these values well approximated real salinity records in irrigation waters during the summer period in the coastal zone of the Ferrara Province, Northern Italy, where strawberry is widely cultivated.

Beside the specific scientific objective of the strawberry minipanel screening for salt stress sensitivity, this work also aims at fostering a methodological advancement by exploiting an advanced phenotyping protocol. The state-of-art technology proposed in this research can potentially support future strawberry breeding programs, shortening the time needed for selection and overcoming the limitations of the routine visual inspection (late emergence of sufferance signs, subjectivity of evaluations) using quantitative automated analyses (Van Bezouw et al. 2019, Yang et al. 2020, Song et al. 2021). Particularly, two screening methods have been investigated and compared for their effectiveness to enable the early detection of salt stress effects. The first is based on morphometric parameters obtained through red-green-blue (RGB) imaging, which allows a gain in objectivity with regard to the plant symptoms evaluation at the whole shoot level. The second, hypothesized to be more sensitive, in based on the physiological information derived from chlorophyll *a* fluorescence emission signals, according to the principles of modulated fluorometry and quenching analysis (Schreiber 2004, Klughammer and Schreiber 2008, Linn et al. 2021).

Materials and methods

Plant material and growth conditions

Five market varieties of strawberry (*Fragaria* × *ananassa* Duch.) were made available by C.I.V. All of them are day-neutral, ever-bearing cultivars with a high requirement for cold. The main characteristics of each variety are listed in Table1. Immediately after delivering to the Slovak University of Agriculture in Nitra (SK), the rooted plantlets were temporary stored in darkness at 4 ºC until planting in pots containing 100 g sand as an inert substrate. The pots were placed in a growth chamber for one week to restart the vegetative growth and acclimate the plants (180 µmol photons m^{-2} s^{-1} cool white light, photoperiod 14:10h day:night, temperature 24 ºC / 18 ºC day/night, thermoperiod 14:10h day:night) watering them with Hoagland solution in the first day and with tap water on the subsequent days. Subsequently, 18 to 21 plants per variety were moved to the SPPU phenotyping facility (Photon System Instruments, Czech Republic), placed in individual trays, and registered into the PlantScreen™ system (Photon System Instruments, Czech Republic).

A photoperiod of 16:8 h (day:night) was set with continuous illumination provided by cool-white LED panels. The daily lighting protocol included the simulation of sunrise up to a plateau photosynthetically active radiation (PAR) of 900 µmol photons m^{-2} s^{-1}; after four hours exposure to constant PAR, light intensity decreased progressively to simulate sunset, as exemplified in Fig. 1. Temperature ranged from 17 ºC in the night to 23 ºC in the daytime, with constant 40% relative humidity.

Table 1. Main characteristics of the strawberry cultivars examined in this research. Source of information about plants and fruits is Consorzio Italiano Vivaisti (www.civ.it). Notice that the term "fruit" is used for the sake of brevity, while in *Fragaria* species it is a pseudocarp.

	Plant	**Fruits**
Vivara^{pbr}	Medium to high vigor. Very high and constant productivity.	Heart shape. Regular medium-large caliber. Good flavor, medium sugar values. High shelf life.
Murano^{pbr}	Plant of good vigor with upright. Very high productivity.	Conical shape. High and constant caliber. Excellent flavor, with high and constant Brix. Excellent shelf life.
Ania® (CIVRH612^{pbr})	Hardy plant of medium vigor, upright habit. Good productivity.	Heart shape. Medium and constant caliber. Excellent organoleptic characteristics with high Brix levels. Excellent shelf life.
Cantus® (CIVRH621^{pbr})	Hardy plant with medium-high vigor and semi-erect habit. High productivity.	Conical shape. Optimal and constant caliber. Pleasant taste, good Brix level. Very good shelf life.
Edwina® (CIVRH295*)	Ever-bearing middle-low vigor plant, low branching of inflorescence. Medium productivity, lower compared to the other varieties.	Large caliber. Excellent shelf life. Pleasant taste. Very good shelf life.

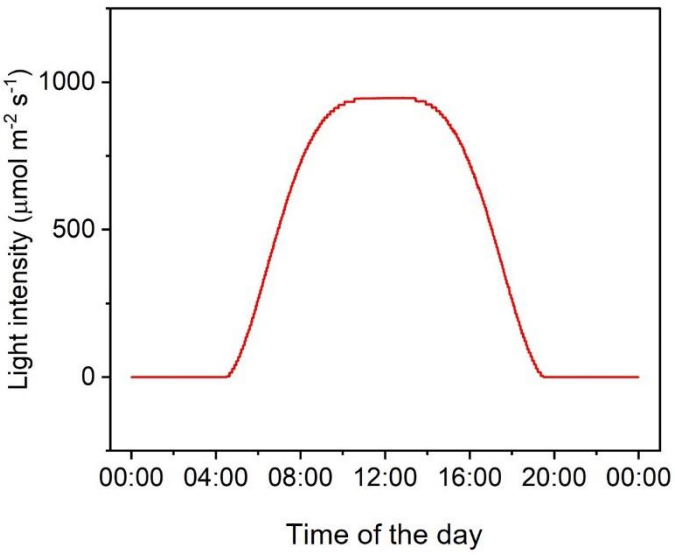

Figure 1. Example of the daily light routine used in the experiment.

Plant irrigation and salt treatments

Irrigation was provided daily to the control plants using the automated watering system included in the SPPU phenotyping unit. In treated plants, the daily irrigation with tap water added with NaCl was performed manually. To impose the intermediate salt stress (S1 group, water electric conductivity = 2.0 mS cm^{-1}), 651 mg L^{-1} of NaCl were added to the solution, while for severe salt stress (S2, electric conductivity = 4.0 mS cm^{-1}) 1702 mg L^{-1} were added.

Automated plant phenotyping measurements

For shoot image-based phenotyping, the plant-to-sensor, automated PlantScreen™ system operating at SPPU was used. Measurements were performed before the beginning of treatment (day 0) and subsequently after 3, 6, 10, 14, 19, 30, 34 and 41 days of treatment. The routine started with the measurements of chlorophyll *a* fluorescence, obtained using the modulated chlorophyll fluorescence imaging unit in PlantScreen™ systems, which quantifies the reemitted light upon excitation with red light. PSII maximum quantum yield of photochemistry (F_V/F_M) was measured after the application of a saturating pulse (800 ms cool white light, 3287 μmol photons m^{-2} s^{-1}). F_V/F_M measurement was followed by 70 seconds of exposure to a high intensity of actinic light (cool white light, 496 μmol photons m^{-2} s^{-1}), which allowed the photosynthetic apparatus to approach a quasi-steady state (ss). Steady state values for non-regulatory energy loss quantum yield Y(NOss), quantum yield of thermal dissipation Y(NPQss), Stern-Volmer parameter of non-photochemical quenching NPQss and Lichtenthaler's vitality index R_{Fd} were calculated as reported in Table 2. Immediately after the induction protocol, the plants were allowed to dark relaxate the fluorescence parameters and the recovered F_V/F_M value was determined applying a saturation pulse after 100 seconds. The difference between initial and recovered F_V/F_M was assigned to the photoinhibitory quantum yield loss of PSII Y(qI). The overall fluorescence analysis routine is reported in Fig. 2.

After the measurement in the fluorescence cabin, the trays moved to the RGB cabin. Morphometric measurements were performed automatically using an RGB camera mounted above the passing trays. The RGB values were converted to synthetic morphometric parameters representative of the whole shoot and listed in Table 3, with the corresponding meaning according to the manufacturer (see also Gao et al. 2020).

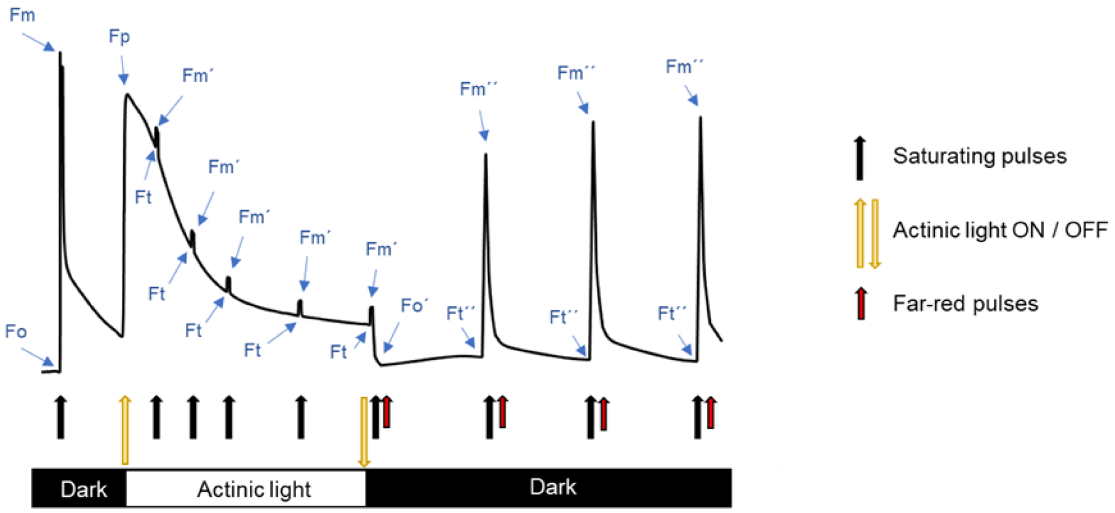

Figure 2. Example of fluorescence analysis routine. Fo was measured in dark acclimated samples, while upon the application of a saturating pulse (800 ms cool white light, 3287 mmol photons m^{-2} s^{-1}) maximum fluorescence yield Fm was measured. After 17 seconds of dark acclimation, actinic light (cool white light, 496 mmol photons m^{-2} s^{-1}) was switched on, allowing the measurement of the fluorescence peak during the initial phase of the Kautsky effect (Fp). Actinic light illumination, yielding a fluorescence value Ft, was spaced by five saturating pulses at regular intervals to measure the quenching of maximum fluorescence (Fm'). The illumination with actinic light was maintained for 70 seconds, followed by 100 seconds of dark relaxation. After switching off the actinic light, three saturating pulses were applied to the plant. Each saturating pulse was followed by a 2 seconds exposure to far-red light to measure the minimum fluorescence Fo'. The fluorescence values measured at the end of the recovery were used to calculate PSS photoinhibition.

Table 2. List of fluorometric parameters with their formula and description.

PARAMETER	FORMULA	DESCRIPTION
Fo	measured	Minimum fluorescence level for the dark-adapted state
Fm	measured	Maximum fluorescence level for the dark-adapted state
Fp	measured	Fluorescence peak during the initial phase of the Kautsky effect
Fm'	measured	Maximum fluorescence level for the light-adapted state
Ft	measured	Instantaneous fluorescence level at time t
Fv/Fm	(Fm-Fo)/Fm	Maximum PSII quantum yield of photochemistry for the light adapted state
Y(NOss)	Ft/Fm	Quantum yield of PSII non-regulatory energy loss for the light-adapted state (Hendrickson et al. 2004)
Y(NPQss)	(Ft/Fm´)-(Ft/Fm)	Quantum yield of PSII thermal dissipation for the light-adapted state (Hendrickson et al. 2004)
NPQss	Y(NPQss)/Y(NOss)	Non-photochemical quenching which estimates the rate constant for PSII thermal dissipation (Lazar 2006)
R_{Fd}	(Fp-Ft)/Ft	Vitality index or ratio of fluorescence decay (Lichtenthaler et al. 2005)
Y(qI)	(Fv/Fm)-(Fv/Fm after dark recovery)	Quantum yield of PSII photoinhibition

Table 3. List of morphometric parameters with their meaning and units.

PARAMETER	DESCRIPTION	UNIT
Area	Total area covered with plant	pixel
Roundness	Ratio between area and perimeter or its convex hull	dimensionless
Isotropy	Ratio between area and surface of convex hull	dimensionless
Compactness	Difference between convex hull area and circle which has center in plant centroid and radius proportional to area weighted by compactness	dimensionless
Eccentricity	Ratio between the distance of the foci of the ellipse with same variance as a plant and its major axis length	dimensionless
Rotational Mass Symmetry (RMS)	Ratio between squared sum of leaf lengths and area	dimensionless
Slenderness Of Leaves (SOL)	Ratio between squared sum of leaf lengths and area	dimensionless

Data treatment

Raw data were exported from the PlantScreen™ system and analyzed using Microsoft Office Excel software (Microsoft, USA). Scatter/line and spider plots were obtained after processing the data using Origin software version 2022 (OriginLab Corporation, USA).

Results and discussion

Effect of salt treatment on morphometric parameters

Morphometric measurements were performed on the whole plant shoot at various time intervals over an extended period of 41 days. Area parameter was used to obtain the plant growth curve. In four of the control, water-irrigated cultivars (Vivara, Murano, Ania and Cantus), the growth continued during the entire experiment approaching a plateau between 20-30 days, while in Edwina a decrease in the Area was observed at the last sampling time (Fig. 3). The cause for the late Area decrease in Edwina was the tendency of plants to die after 30 days of cultivation. Exposure to the intermediate salt concentration (S1) did not affect negatively the growth curve until the 19th day, and surprisingly in Murano and Cantus the growth was even higher than in the respective controls (Fig. 3). However, in the later stages of the experiment, S1 treatment produced an evident contraction in the growth of Vivara, Murano and Edwina, which resulted in a decrease in plant Area (Fig. 3). Conversely, only a slight decrease in Area was induced by intermediate salt stress in Cantus and no significant effect was observed for Ania (Fig. 3). Likewise, the early growth of strawberry plants undergoing severe salt stress (S2) was negligibly affected in comparison to the control (Fig. 3). However, prolonged severe salt stress induced a marked decrease in the plant Area in all the varieties. Reduction of the plant area growth rate is reported as a common response in plants when exposed to salt stress already at the early stages of plant development (Murill-Amador 2015, Johansen et al. 2019, Corrado et al. 2021, Tian et al. 2021). Therefore, it was interesting that the analyzed strawberry varieties were not affected by plant area reduction at the early stage, but specifically after ca. 20 days of exposure (Fig. 3). Though in a cultivar-specific manner, the extent of growth inhibition occurring at the late stage of the experiment was larger for S2 than S1 treatment, indicating the dose effect of salinity on the plant development.

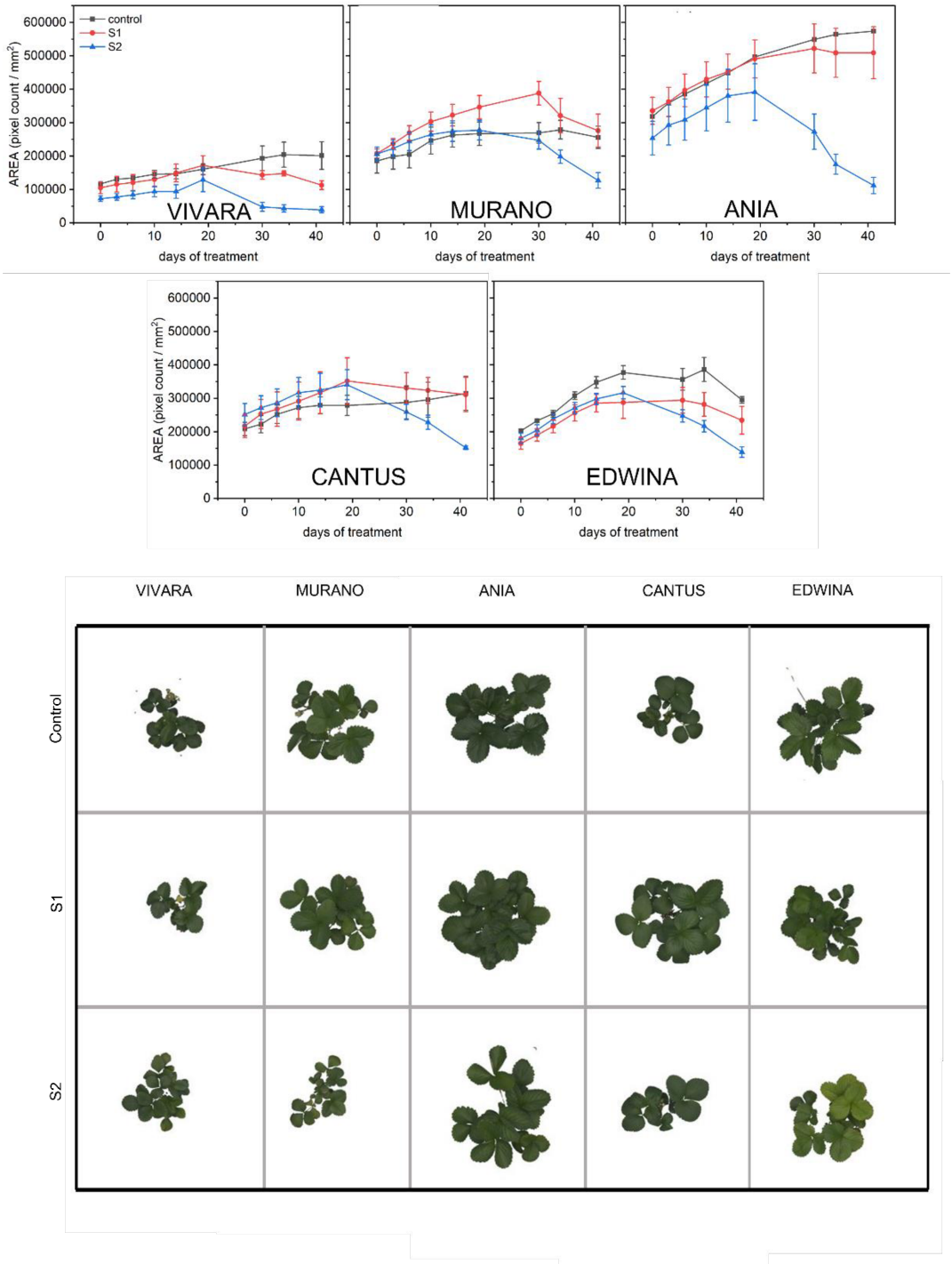

Figure 3. Plant area trends during the experiment with five strawberry cultivars (Vivara, Murano, Ania, Cantus and Edwina). Black dots connected with black lines represent the average values of the control group (plants irrigated with only water), red dots connected with red lines represent the average values of the S1 group (moderate salt stress, plants treated with water with NaCl addition until reaching the conductivity value of 2 mS cm^{-1}), blue dots connected with blue lines represent the average values of the S2 group (severe salt stress, plants treated with water supplemented with NaCl until reaching the conductivity value of 4 mS cm^{-1}). Error bars represent SE for n=7-8. In the lower part of the figure representative RGB images of individual plants of each variety in control, S1 and S2 irrigation conditions are presented at the day 19 of treatment.

Other morphometric features were analyzed through RGB imaging leading to synthetic parameters descriptive of the shoot morphology. Among them, the most sensitive to the presence of salt stress were plant compactness, plant isotropy and leaf slenderness (other morphometric parameters are provided as Supplementary materials). Plant Compactness is obtained by dividing the plant area by the convex hull area, i.e., the smallest area enclosed by the outer contour of the plant. Therefore, this parameter provides an objective quantification of the "density" of a plant (e.g., Kim et al. 2020). Loss of plant compactness in response to salt stress was previously reported (Sorrentino et al. 2022), and a strong reduction in such parameter was indeed apparent in all the S2 treated varieties (Fig. 4). However, at the early stages of the experiment, such response was not uniform in the different varieties. In Murano, the S2 samples had lower compactness already from the first experimental week (Fig. 4); conversely, in Ania and Edwina plants no differences were induced by the saline irrigation conditions, while in Vivara and Cantus the plant compactness tended to increase in response to salinity stress (Fig. 4). The progressive loss of compactness appeared in both S1 and S2 plants only at the later stages of the experiment, in which the dose-dependent response became apparent (Fig. 4).

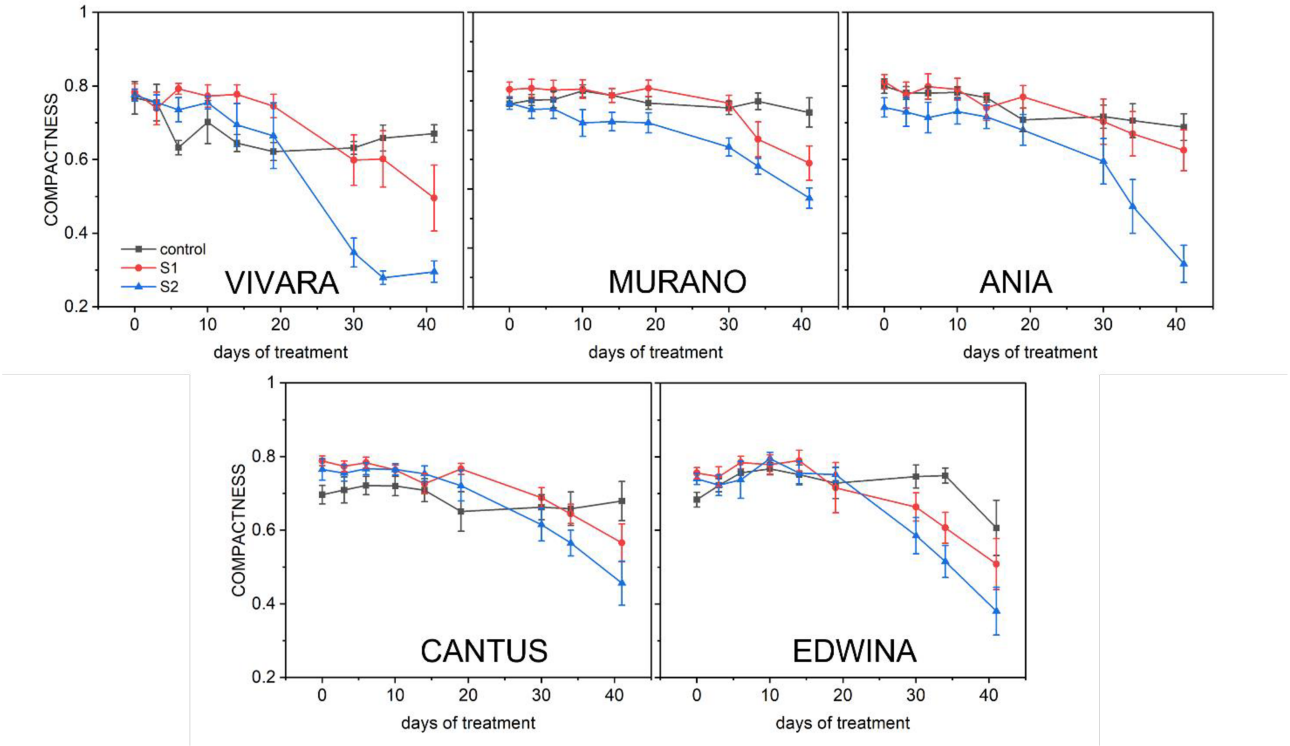

Figure 4. Plant compactness trends during the experiment with five strawberry cultivars (Vivara, Murano, Ania, Cantus and Edwina). Symbols and abbreviations as in Figure 3.

Plant isotropy quantifies the degree of uniformity of a plant in all orientations and is a helpful parameter describing the geometry of rosette plants (Gao et al. 2020). Isotropy tended to slowly decrease over time in all

the irrigation conditions, highlighting the mode of radially irregular shoot development specific to *Fragaria* × *ananassa*, e.g., linked to the lateral emergence of stolons. However, the decline was generally more marked in presence of increasing salt concentrations in water (Fig. 5). A clear effect of salinity to reduce the plant isotropy was seen only at the late stages of the experiment, sometimes featuring an abrupt decrease (e.g., S1 treatment of Murano). In general, the isotropy reduction was a later response compared to the decrease in plant compactness (Fig. 4-5). Similarly, the slenderness of leaves (SOL) was stable until the 19th experimental day in all cultivars, whereas in the second part of the experiment there was a strong raise of SOL dependent on the salt concentration applied (Fig. 6). The extent of SOL increase was also evidently cultivar-specific, with a striking increment in Edwina, followed by Ania, Cantus and Murano, down to the only small increase in Vivara. Increase in SOL is considered an adaptive response to salinity stress (Awila et al. 2016, Sorrentino et al. 2022) and the small variation occurring in Vivara suggested a less effective acclimation potential of such cultivar to salt stress, which was further analyzed based on chlorophyll fluorescence parameters.

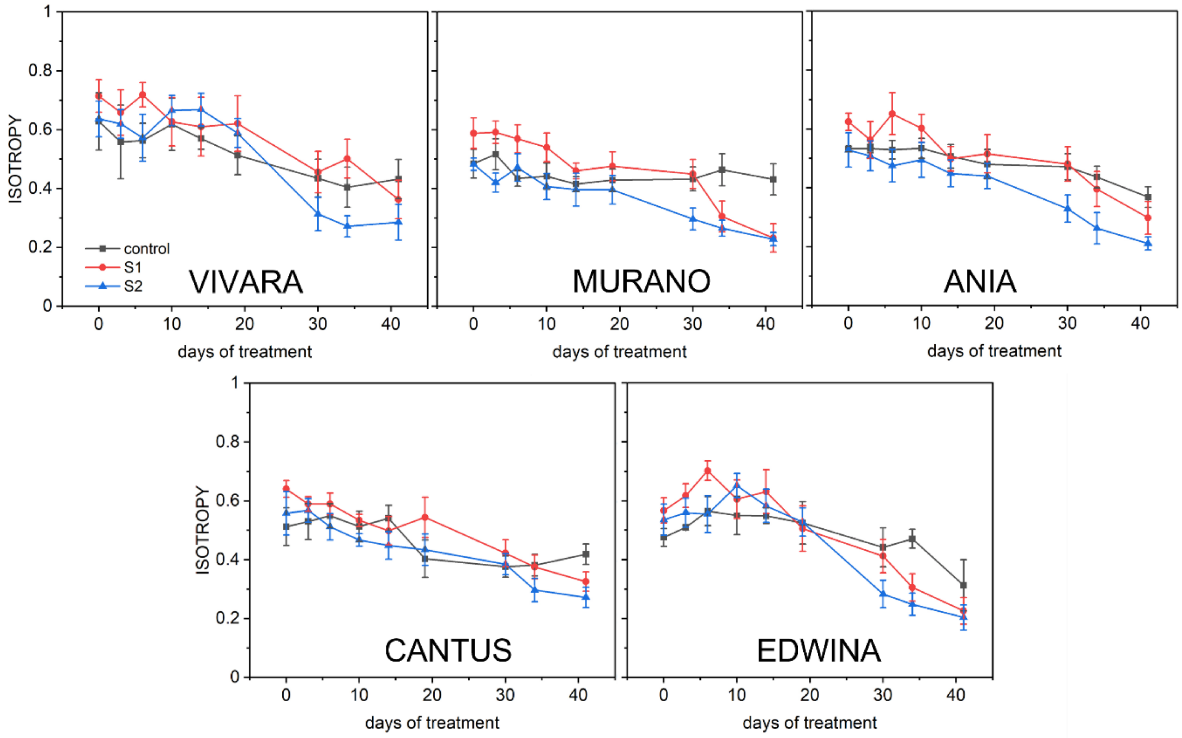

Figure 5. Plant isotropy trends during the experiment with five strawberry cultivars (Vivara, Murano, Ania, Cantus and Edwina). Symbols and abbreviations as in Figure 3.

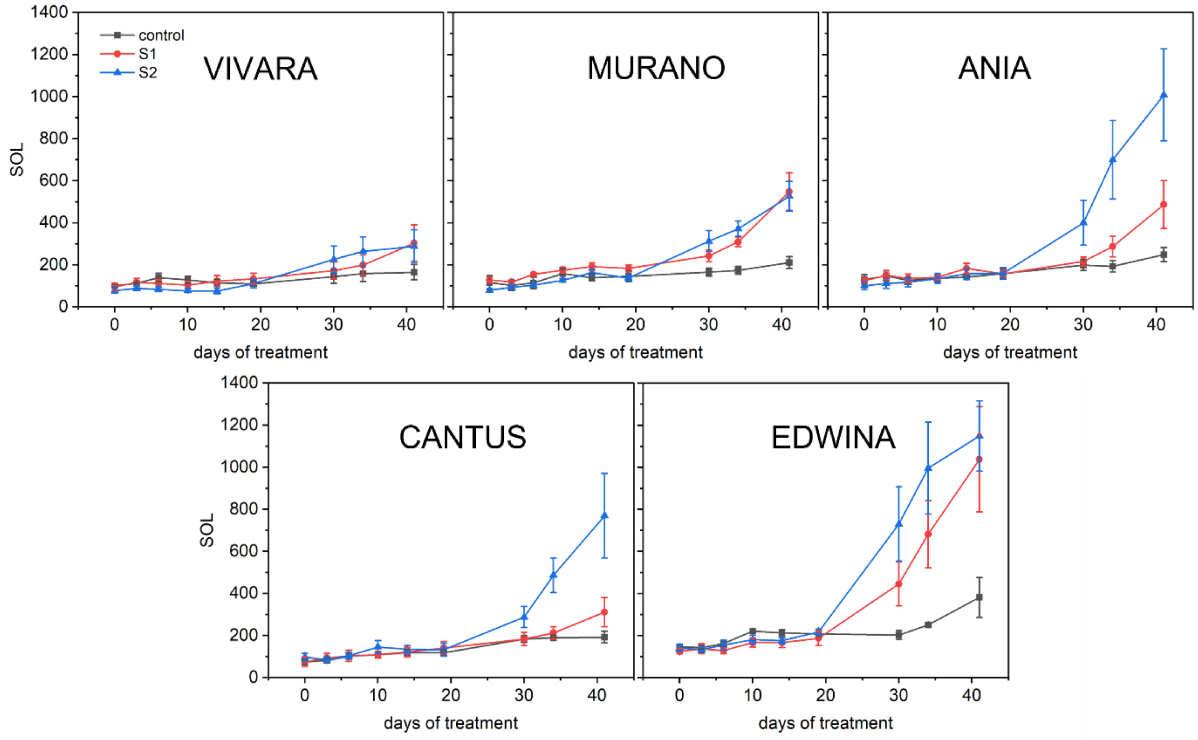

Figure 6. Slenderness of leaves (SOL) trends during the experiment with five strawberry cultivars (Vivara, Murano, Ania, Cantus and Edwina). Symbols and abbreviations as in Figure 3.

Effect of salt treatment on photosynthetic efficiency and light energy management

PSII photochemical efficiency (F_V/F_M), quantum yield of non-regulatory energy dissipation in PSII [Y(NO)], quantum yield of regulatory thermal dissipation [Y(NPQ)], and thermal dissipation parameter (NPQ) trends over the time of treatment were recorded for each cultivar.

As an estimate of PSII maximum quantum yield, F_V/F_M is known to be sensitive to biotic and abiotic stresses, reflecting the occurrence of PSII photoinhibition or photodamage (Na et al. 2014, Stirbet et al. 2018, Faseela et al. 2019). The time-course of F_V/F_M is reported in Fig. 7. In control plants, such parameter was almost constant throughout the experiment, with only a small and very gradual declined in Edwina. Already from the first few days, the detrimental effects of the salinity treatment were extremely apparent in Vivara plants exposed to severe salt stress S2. A decline in F_V/F_M also occurred in the other varieties but with a considerable delay compared to Vivara, i.e., after 30 days of treatment. Conversely, intermediate salinity stress S1 produced a significant decline in F_V/F_M on the last days of treatment only in Vivara and Murano.

Y(NO) is commonly used as an indicator of the reduction state of the electron transport chain (ETC): high values of such parameter indicate that the ETC is highly reduced, symptom of a deregulated electron transport (Ferroni et al. 2020). Y(NO) quantum yield was measured at the end of 180 s light induction and is termed

Y(NOss), that is Y(NO) at the steady state. The adaptation of a common induction protocol to the scope of fast plant phenotyping, though reducing to only 3 min the exposure to actinic light, requires the experimenter to accept the approximation that the steady state is reached, i.e., cyclic electron transport and photosynthetic control mediated by Cytochrome b_6f have been activated (Huang et al. 2010, Tikkanen et al. 2015, Huang et al. 2018, Yamamoto and Shikanai 2019, Tan et al. 2020, Zhang et al. 2021). The results are reported in Fig. 8. Again, in control plants, Y(NOss) only showed minor fluctuations during the experiment, while major increases were observed in salt-treated plants. S2 irrigation of Vivara plants induced a strong increase in Y(NOss) already after five days of treatment, and such increase continued for the rest of the experiment, suggesting a reduced ability in controlling the reduction state of the ETC. Severe salt stress increased Y(NOss) also in the other varieties, although later and to a lesser extent in comparison to Vivara. In the last experimental week, Y(NOss) also raised in the presence of intermediate salinity stress S1, except in Ania and Cantus, while in Murano, the effects of intermediate and severe salt stress were almost superimposable.

The extent of thermal dissipation of excess absorbed energy was quantified in terms of Y(NPQ) quantum yield or using the Stern-Volmer NPQ parameter (Bilger and Björkman 1990, Hendrickson et al. 2004, Ferroni et al. 2014, Lazar 2015). The values calculated at the end of the 3-min-long exposure to actinic light are denoted as (quasi)-steady state Y(NPQss) and NPQss, reported in Fig. 9 and 10, respectively. In control plants, Y(NPQss) remained stable throughout the experiment, with NPQss displaying wider variations due to the broader range of values intrinsic to such parameter. Specular to the behavior of Y(NOss), Vivara plants were inefficient in inducing thermal dissipation when exposed to severe salt stress already in the first experimental week. In the other S2-treated varieties, the decline in thermal dissipation capacity appeared after 19 days, with a progressive decay of Y(NPQss) and NPQss to extremely low values, close to those observed in Vivara. Particularly, the last cultivar showing a decline in Y(NPQss) was Edwina, after 30 days. The response of thermal dissipation parameters to the intermediate salinity S1 was obviously less intense in all cultivars; a late decrease in Y(NPQss) and NPQss occurred in Murano and Edwina.

Overall, from the point of view of PSII-related parameters, the intermediate salt stress was well tolerated by Ania and Cantus, while it interfered with the normal photosynthetic functions in Vivara, Murano and Edwina at a late stage of exposure. Severe salt stress induced more marked alterations of the excitation energy management in all examined varieties, but particularly intense in Vivara.

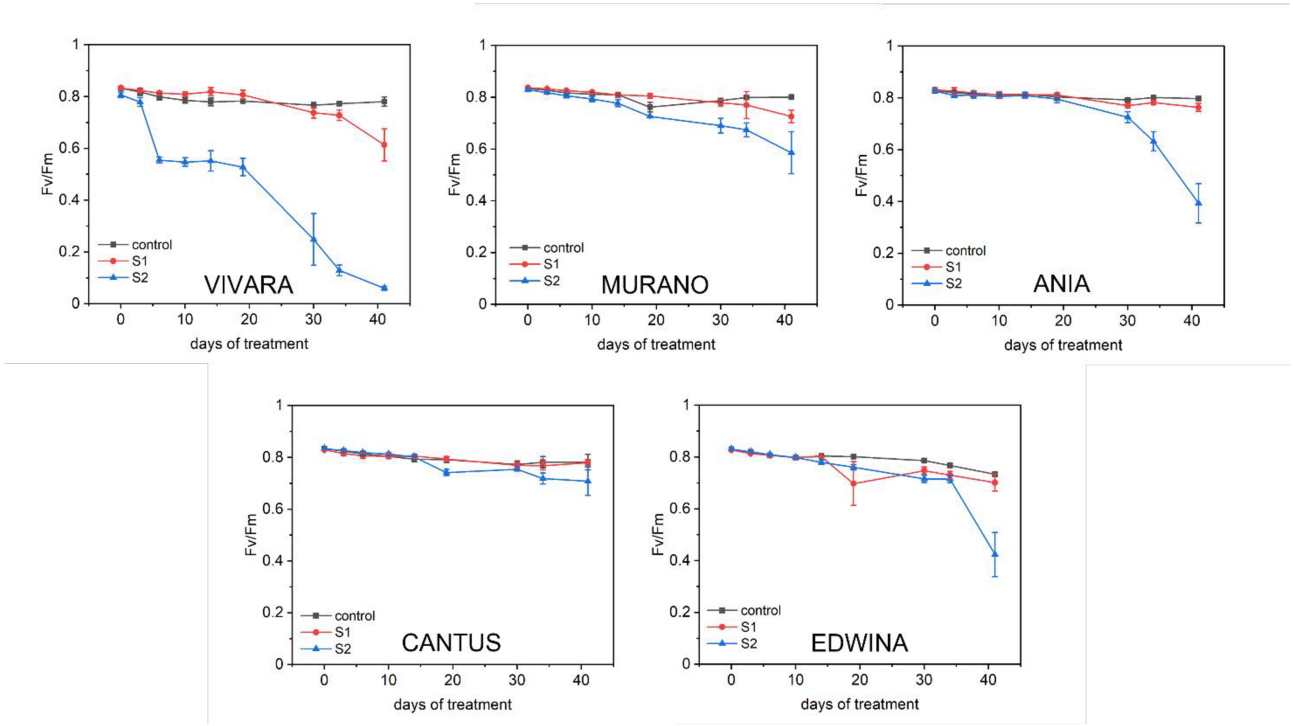

Figure 7. PSII photochemical efficiency (Fv/Fm) trends during the experiment with five strawberry cultivars (Vivara, Murano, Ania, Cantus and Edwina). Symbols and abbreviations as in Figure 3.

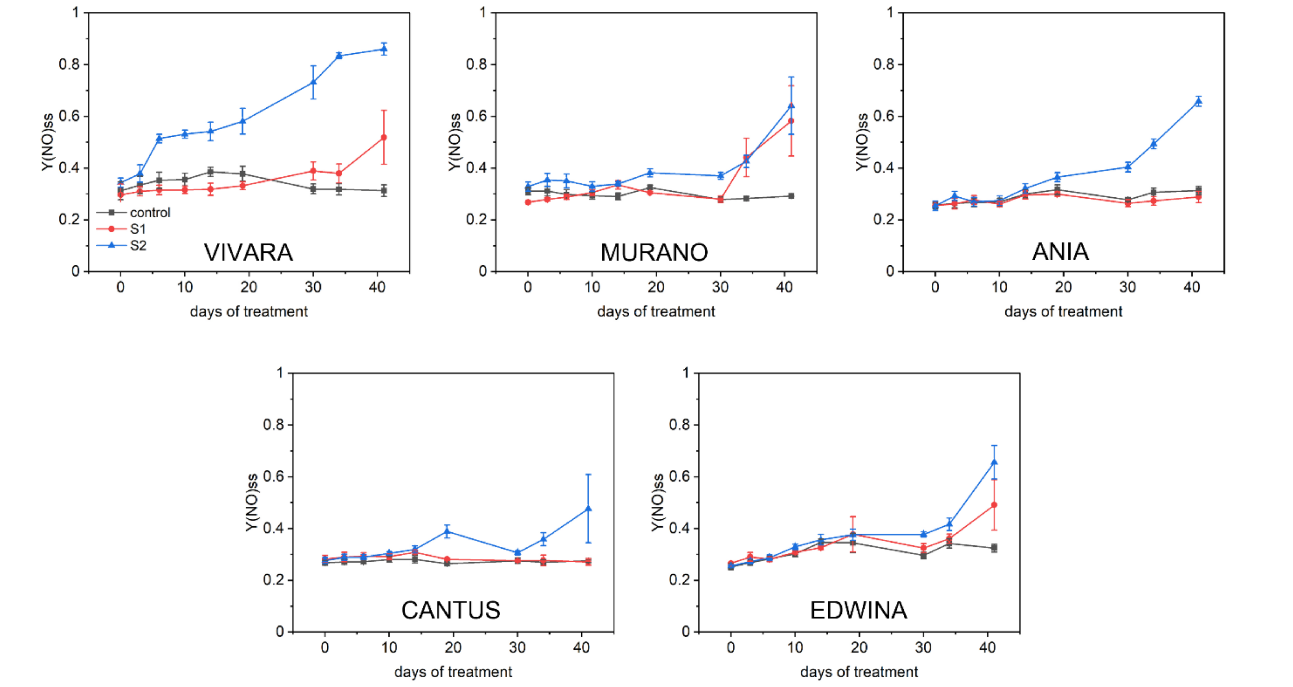

Figure 8. Quantum yield of non-regulatory energy loss [Y(NOss)] trends during the experiment with five strawberry cultivars (Vivara, Murano, Ania, Cantus and Edwina). Y(NOss) was calculated according to Hendrickson et al. (2004). Symbols and abbreviations as in Figure 3.

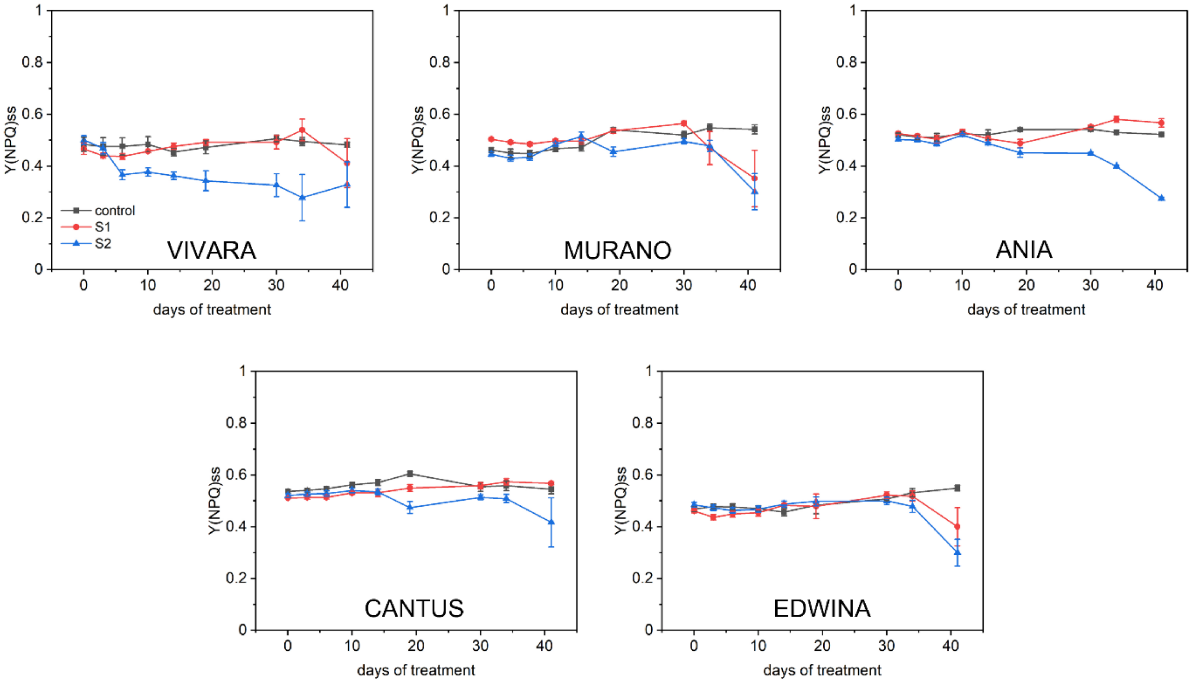

Figure 9. Quantum yield of PSII regulatory thermal dissipation [Y(NPQss)] trends during the experiment with five strawberry accessions (Vivara, Murano, Ania, Cantus and Edwina). Y(NPQss) was calculated according to Hendrickson et al. (2004). Symbols and abbreviations as in Figure 3.

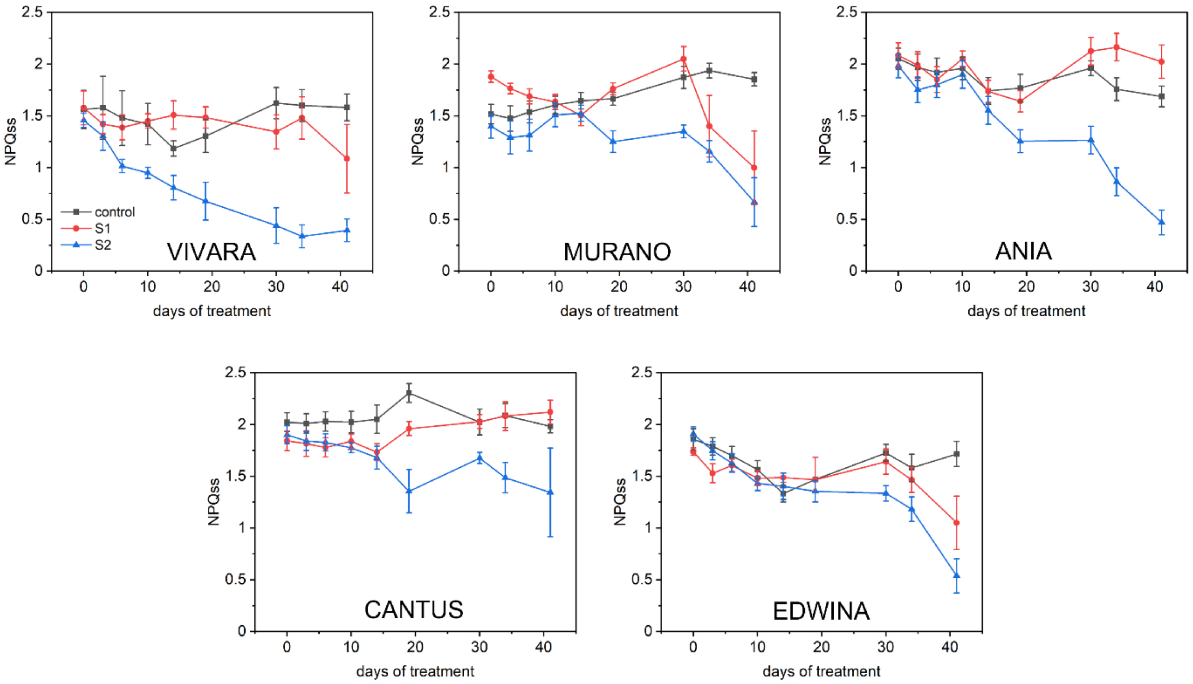

Figure 10. Thermal dissipation capacity (NPQss) trends during the experiment with five strawberry cultivars (Vivara, Murano, Ania, Cantus and Edwina). Symbols and abbreviations as in Figure 3.

Effect of salt treatment on R_{Fd} - the vitality index

R_{Fd} quantifies the photosynthetic activity of the whole leaf and, since its introduction by Hartmut K. Lichtenthaler, it is referred to as the "vitality index" of the plant (Lichtenthaler et al. 1983, 1986). In samples probed with saturating light, R_{Fd} is directly correlated with the net CO_2 assimilation rate of the whole leaf, therefore it is a useful tool to assess the net photosynthetic activity of a plant (Lichtenthaler et al. 2005). In the automated phenotyping approach, the robustness of R_{Fd} as an estimator of the whole plant photosynthetic capacity is increased by the whole plant fluorescence imaging approach. The time-course of R_{Fd} is reported in Fig. 11. R_{Fd} values in control plants were decreasing during the first 17 days of experiment, except for Cantus. However, in the second part of the experiment, R_{Fd} became nearly stationary or even steadily increasing in the case of Murano. The divergence between S2 and control plants was apparent from the very first days of sampling in a cultivar-specific fashion: the strongest effect on R_{Fd} was observed for Vivara plants from the very beginning of the treatment, while the slightest characterized Edwina, in which the divergence of S2-treated plants from the controls occurred after 19 days, with a final drop at 41 days. The other cultivars showed a response collectively spanning between these two extremes, particularly R_{Fd} tended to stabilize in Murano and Cantus, whereas it was monotonically decreasing in Ania. Conversely, the effects of intermediate salt stress S1 were less apparent, with strong reductions of R_{Fd} in Vivara and Murano plants only in the last experimental week. Curiously, Murano seemed to benefit from a moderate saline stress during the first two weeks of treatment, only subsequently followed by a decrease in R_{Fd}.

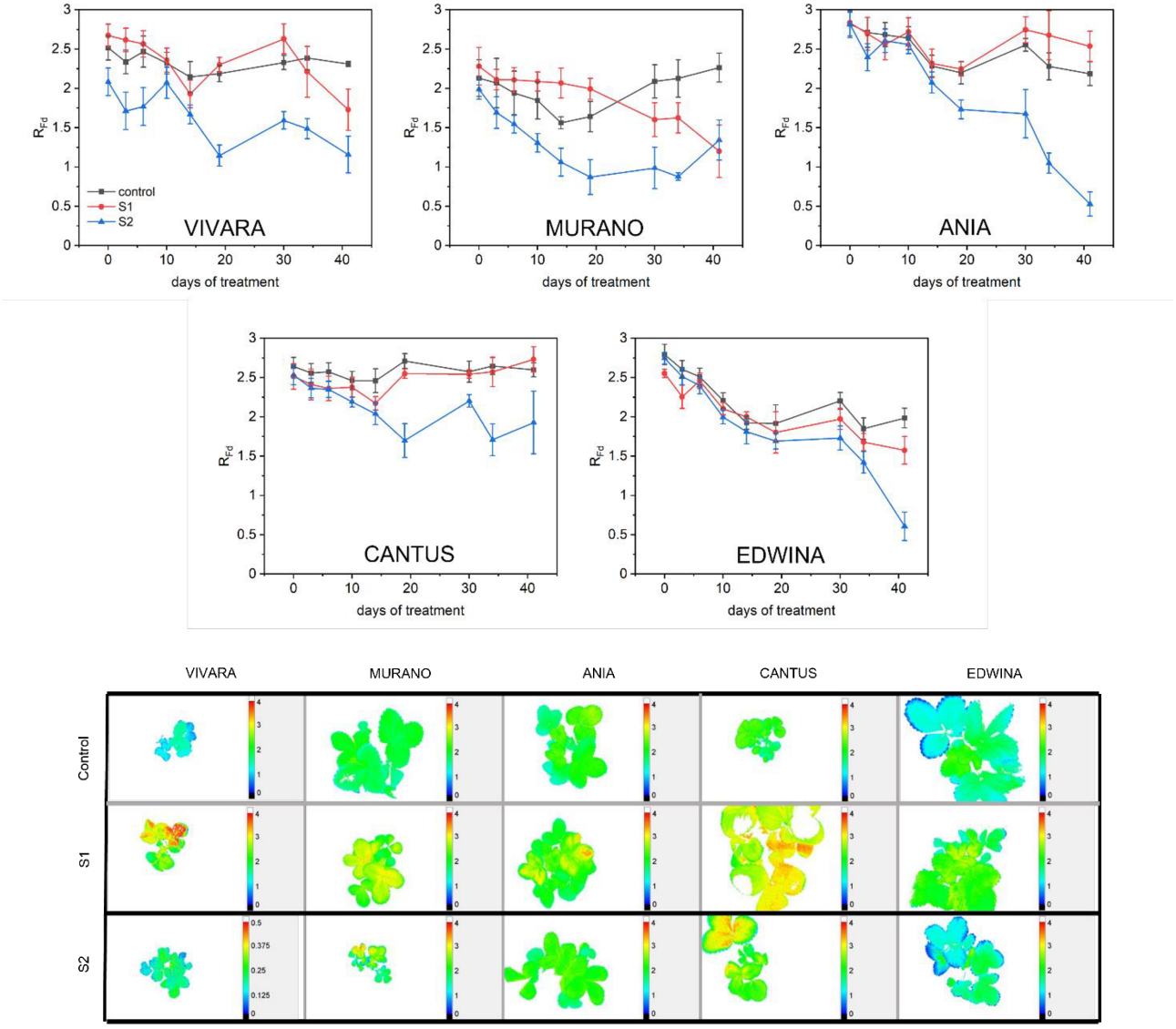

Figure 11. Lichtenthaler's "vitality index" (R_{Fd}) trends during the experiment with five strawberry cultivars (Vivara, Murano, Ania, Cantus and Edwina), as calculated according to Lichtenthaler et al. (2005). Symbols and abbreviations as in Figure 3. In the lower part of the figure is reported the R_{Fd} index imaging corresponding to the day 19 of treatment.

Comparative sensitivity of morphometric and fluorometric parameters

Salt effects were more clearly emerging after 19 days of treatment, and the alterations seemed to be better evidenced by fluorometric than morphometric parameters (Fig. 3-11). To help disentangle the extent of salt-treatment-induced alterations and thus order the cultivars in a salt-sensitivity series, spider graphs were built for each salt treatment (S1 or S2) and type of parameter (morphometric and fluorometric) at the 19th day of experiment. Although a similar comparative approach would have emphasized differences between cultivars if applied to data at day 41, the choice of the 19th day was drive by the rationale of the early detection of stress

effects. The results reported in Fig. 12 represent the relative average variation of the treated sample with respect to the corresponding average values of the controls, to which the value 1 was assigned.

Interestingly, the morphometric parameters seemed more affected by the intermediate than the severe salt stress. In S1 plants, Area was increasing in Murano and Cantus, unaltered in Vivara and Ania, and lower in Edwina compared to the respective control. The Area increase was confirmed in Murano and Cantus also under S2 conditions, while in the other cultivars it was ca. 20% less. The morphometric parameters related to the plant shape allowed a good differentiation of the cultivars only under the moderate salt stress S1, while they were less robust under the more severe S2. In plants exposed to S1 there was a clear tendency to maintain or even increase the overall shoot isotropy and compactness, while the SOL was higher in treated Vivara, Murano and Cantus, and equal or lower in Ania and Edwina respectively (Fig. 12). However, under S2 the three parameters varied in a relatively narrow range around the respective controls (Fig.12). In particular, an early increase in plant compactness and isotropy marked the onset of the response to an intermediate salt stress in all examined strawberry varieties, except Edwina, whereas, in the presence of S2, both tended not to change or at most to slightly decrease. Collectively, the behavior of the compactness parameter in strawberry was in contradiction with previous reports, in which the loss in compactness was instead identified as an early symptom of salt stress in lettuce (Sorrentino et al. 2022). A shown in Fig. 4-5, the strong decrease in isotropy and compactness in both S1 and S2 conditions occurred in the final part of the experiment as a late event in the response of strawberry to salt stress. Interestingly, the early occurrence of increased compactness and isotropy only under S1 suggested the somewhat counterintuitive hypothesis that these two parameters could reflect the level of increasing sensitivity to salt stress in a series represented by Vivara-Cantus (more sensitive), Murano-Ania (intermediate sensitivity), Edwina (less sensitive) (Fig. 4). In general, the severity series cannot be reconstructed with a sufficient degree of confidence under S2 based on morphometrics.

Contrasting to the morphometric parameters, the fluorometric parameters examined on the 19th day of treatment tended to worsen in response to the increasing salt concentration (Fig. 12). However, the conclusions about the sensitivity series resulting from the two salinity levels were different.

In the presence of S1, the PSII photochemical efficiency was the same as in the controls, only except Edwina, in which F_V/F_M was 20% less. With regard to the other parameters, Murano, Ania and Cantus had a similar behavior to the control, while in Vivara Y(NOss) was lower and Y(NPQss), NPQss and R_{Fd} increased. In contrast, in Edwina plants Y(NOss) was higher, while Y(NPQss), NPQss and R_{Fd} were lower than in the control. According to these observations, Vivara seemed the most tolerant to the intermediate salt stress. In fact, maintaining a low Y(NOss) usually means an efficient control of the reduction state of the ETC, and therefore an efficient photosynthetic regulation operated by the Cytochrome b_6f and the cyclic electron transport (Huang et al. 2010, Tikkanen et al. 2015, Huang et al. 2018, Yamamoto and Shikanai 2019, Tan et al. 2020, Zhang et al. 2021). At the same time, the increased ability in inducing the thermal dissipation, which

likewise is largely linked to an active cyclic electron flow (Munekage et al. 2002, Suorsa et al. 2013, Ferroni et al. 2020), could in principle ensure a more efficient light energy management. However, in lettuce and tomato, higher levels of thermal dissipation were reported as early symptoms of the onset of salt stress in previous reports (Sorrentino et al. 2022). Therefore, the NPQss increase characterizing Vivara, associated to enhanced photosynthetic metabolism as expressed by higher R_{Fd}, could be interpreted as a first symptom of the salt-induced alterations occurring in the photosynthetic membrane. Accordingly, the trending increase in NPQss occurring later in other cultivars, particularly Ania, would suggest a higher tolerance to salt stress than in Vivara (Fig. 10).

The scenario was more dramatic in plants treated with S2, in which several parameters diverged from the respective control values, allowing us to define a salt-sensitivity series with a high degree of confidence (Fig. 12). F_V/F_M was strongly affected in Vivara, in which the decrease was around 35%. A remarkable decrease was also present in the thermal dissipation parameters: in Vivara and Cantus, Y(NPQss) and NPQss were almost halved, in Murano and Ania the decrease was smaller, although still marked. Differently, in Edwina little to no difference were found compared to the controls and, accordingly, it was the most efficient in maintaining the control of the ETC redox state by keeping Y(NOss) values close to those of the controls. A moderate increase in Y(NOss) was observed in Ania and Murano, while the ETC reduction state was strongly deregulated in Vivara and Cantus (+50% in both, Fig. 12). A very clear decreasing series was visible with R_{Fd}: compared to the corresponding controls, the R_{Fd} reduction was minimal in Edwina (-10%), moderate in Ania, followed by Cantus and finally by Murano and Vivara, with only 50% R_{Fd} (Fig. 12). Increments in Y(NOss) and, conversely, decrements in thermal dissipation capacity and R_{Fd} are alarming red flags for the plant fitness. The inability in maintaining an oxidized ETC could produce major damages to one of the most vulnerable sites of the photosynthetic membrane, *i.e.*, Photosystem I (PSI) (Sonoike et al. 1995, Sonoike 2011, Tikkanen et al. 2014). PSI becomes photodamaged when the electron flow from PSII exceeds the capacity of PSI end acceptors to receive electrons, thus leading to the generation of reactive oxygen species that inactivate the photosystem (Tikkanen et al. 2014, Huang et al. 2016, Shimaka and Miyake 2018, 2019). The consequences of an extended PSI photodamage are extremely penalizing to the plant fitness, because the PSI repair system takes several days, dramatically undermining the photosynthetic capacity of the plant (Shimaka and Miyake 2018, Lima-Melo et al. 2019). The photosynthetic apparatus exploits several strategies – the so-called "P700 oxidation system" (Shimaka and Miyake 2018) – to avoid this scenario, including the induction of the cyclic electron transport and the consequent increase in trans-thylakoid ΔpH (Yamamoto and Shikanai 2019). Primarily, the ΔpH acts at the Cytochrome b_6f level, downregulating the electron transfer from the plastoquinone pool to the plastocyanin, thus alleviating the electronic pressure on PSI acceptor side (Huang et al. 2010, Tikkanen et al. 2015, Huang et al. 2018, Yamamoto and Shikanai, 2019, Tan et al. 2020, Zhang et al. 2021). Secondly, the ΔpH induces the NPQ, which down-regulates the activity of PSII and very likely also PSI (Grieco et al. 2012, Ruban 2018); whether NPQ may participate in limiting the electron transport from PSII to PSI, to facilitate the PSI oxidized state, is a conceivable but questioned issue (Tikkanen et al. 2015). Only Edwina plants were able

to maintain levels of ETC redox state regulation, thermal dissipation, and photosynthetic activity close to the controls, testifying to the high level of salt tolerance in this cultivar. Conversely, Cantus and even more Vivara displayed significant alterations of the normal functions of the photosynthetic apparatus (Fig. 12). Both cultivars are subjected to similarly high levels of membrane over-reduction, but Cantus seems overall more capable to keep the photosynthetic function under control, with a preserved PSII maximum quantum yield. Differently, in Vivara the deregulation of the electron flow was associated to a loss of PSII photochemistry. Photoinhibition of PSII function can be the negative result of the excessive plastoquinone reduction. Interestingly, among all cultivars, only Vivara experienced a marked loss of PSII function upon the 3 min-long exposure to actinic light, showing an usually strong susceptibility of PSII to photoinhibition (see Supplementary materials) not only under S2, but also S1 treatment. This response could suggest a regulatory role of PSII photoinhibition in the salt-sensitive cultivar Vivara. In fact, a sustained depression in PSII activity can also have an acclimative meaning to limit the electron inflow into the chain and preserve PSI integrity, while ensuring a sufficient synthesis of ATP for the cell metabolism (Huang et al. 2018, Sun et al. 2020).

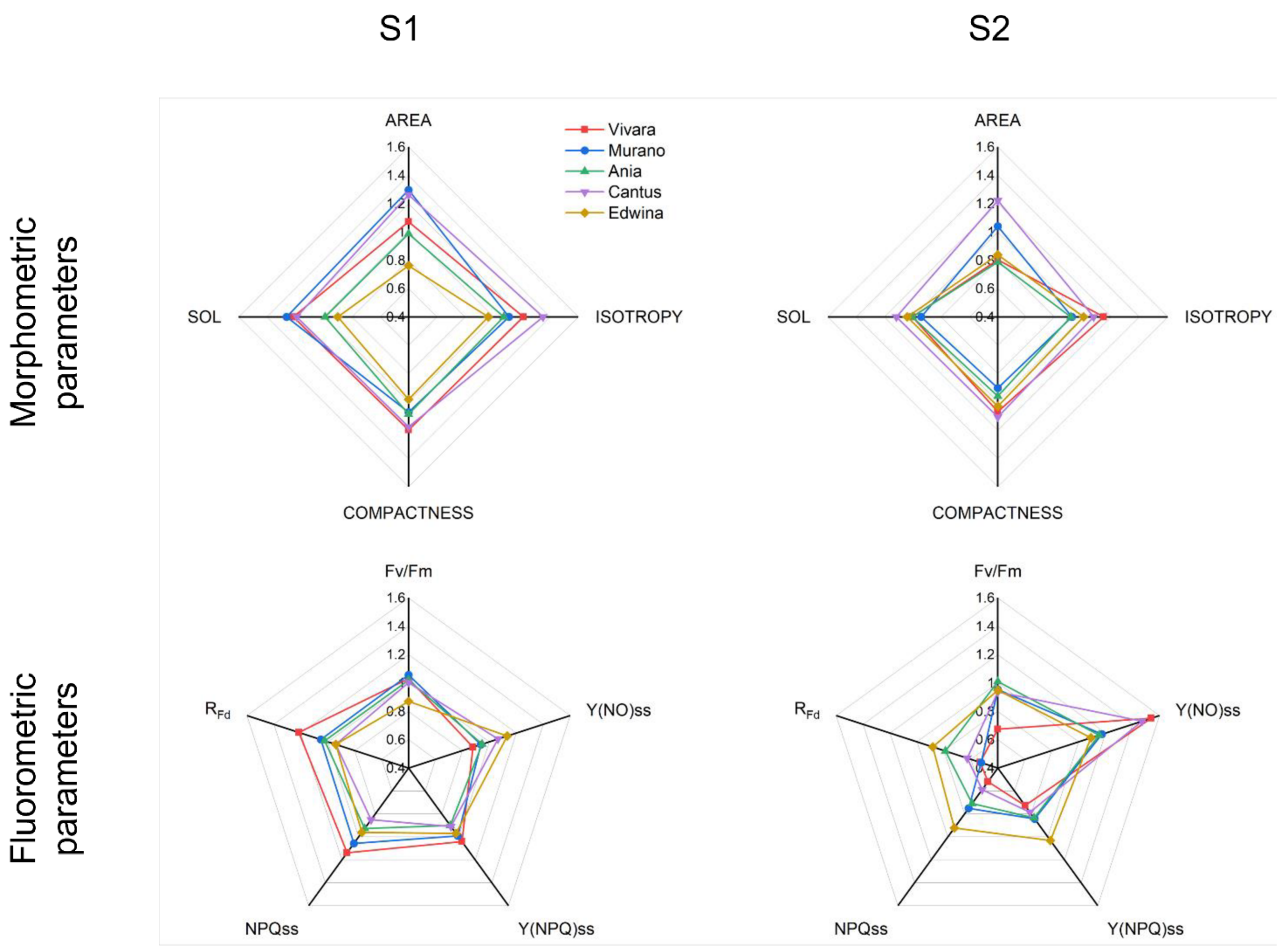

Figure 12. Spider graphs showing the variation of morphometric and fluorometric parameters in S1 and S2 strawberry plants normalized to the respective control for each cultivar. Each point represents the average normalized value of a given parameter for the respective salinity treatment. Parameters are defined in Tables 2 and 3.

Conclusions

The strict control of the environmental conditions in the automated phenotyping facility, including the growth chamber and the measuring cabins connected to it through a plant-to-sensor system, allows to isolate the specific effects of the salt treatment from any other possible environmental disturbance, which is instead typical of the field conditions. Nevertheless, it is assumed that the controlled growth coupled with the automated phenotyping can provide basic information to drive subsequent research in the field, where predictions can be put to test. Although the plant phenome can be ideally described by a tremendous multiplicity of parameters, only some specific subsets of them can be useful to support a screening program. In this comparative study, developed on a 40 days-timeline, the morphometric parameters were slowly responsive to the imposition of different degrees of salt stress, hence being not suitable for future phenotyping applications to reveal the onset of salt stress in strawberry varieties. Parameters reflecting indirectly the photosynthetic performance are instead confirmed to be among the most powerful when a response to stress is phenotyped in crops (van Bezouw et al. 2019).

Fluorometric parameters were fast-responsive to the imposition of salt stress, with visible effects in correspondence of the 19th day of treatment, and therefore well before the onset of more dramatic effects on the shoot morphology. Therefore, such parameters have potential for plant phenotyping programs of strawberry cultivars. Moreover, their relation to the overall crop productivity invites to be explored more in depth to unveil the mechanisms underlying the tolerance to stress. Some hints about the wide physiological diversity of strawberry cultivars with respect to salt stress emerged in this study. The most responsive fluorometric parameters, such as Y(NOss), Y(NPQss), NPQ ss and R_{Fd} can be measured in a short time (after 3 minutes of high light induction in this experiment; Fig. 2) and therefore could be the perfect deal for the collection of a conspicuous amount of data in a very short time from many samples, as is required in plant phenotyping studies. Such parameters were also descriptive of major alterations occurring in the photosynthetic membrane and pointed out the progressive inability of salt-treated plants to control the linear electron flow from PSII to PSI. The decrease in Y(NPQss) and NPQss observed in the least tolerant varieties, Vivara and Cantus, was symptomatic of a reduced ability to induce sufficient levels of thermal dissipation, and consequently their inefficiency in building the necessary proton gradient across the thylakoid membrane needed to ensure the optimal light excitation management. Therefore, the regulation of the ETC reduction state was compromised in the sensitive varieties, being apparent already at the 19th day and progressively deteriorating throughout the experiment. Such alterations can be extremely harmful, primarily leading to the overreduction of the PSI end acceptors, and therefore increasing the probability for PSI photodamage. Since the damage of PSI is very slowly reversible and its repair is extremely expensive for the plant, it can be a possible cause for the reduction of the photosynthetic capacity as assessed by the vitality index R_{fd}.

In the severity series, Edwina exhibited a good tolerance even to the severe salt stress, since the divergences between treated and control plants were comprised in a small variability range. While at the 19th day Vivara and Cantus showed clear signs of electron flow deregulation, Edwina plants were still very efficient in regulating the control of electron transfer from PSII to PSI. However, it should be noticed that, different to the other cultivars and independent of the salt treatment, Edwina was possibly less stable under the controlled growth chamber conditions and showed a tendency to die. This observation could affect the significance of the results, particularly their reproducibility to the field.

The transferability of phenotyping results obtained in a controlled environment to real field conditions is always a critical step in the selection process. In the field, even in the most controlled context, the environment is characterized by unpredictable fluctuations, first of all of the light. Interestingly, the superimposed light variations not necessarily have a negative effect on the plant performance. For example, Esmaeilizadeh et al. (2020) analyzed the effect of specific light wavelength supplementation on the response of strawberry cv. Camarosa to salt and alkaline stress and found an improvement of photosynthetic parameters under red and blue light enrichment. Some of the strawberry cultivars used in our research are the outcome of the most recent breeding efforts by C.I.V. to obtain plants coupling good organoleptic and technological features with plant rusticity, to possibly extend the cultivations to less favorable land, including territories exposed to salt stress. A preliminary field trial was carried out at the C.I.V. from May to September 2021 imposing three separate salinity levels (1.5, 3.0 and 4.5 mS cm^{-1}) to the same varieties analyzed in the present study. The experimental setup was different from that described in this work, since the cultivation was in the open field, exposed to wide oscillations of the environmental conditions, and the cultivation was performed using an organic soil substrate instead of inert sand. Nonetheless, valuable insights could be drawn from it and compared with the experiment in controlled environment. Of particular interest is the check for consistency between predictive salt-sensitivity of cultivars indoors and their cumulative productivity under field conditions. The measurements very clearly revealed that the moderate salt treatments enhanced the productivity of Edwina plants, while decreasing it in the other varieties (Fig. 13). The maximum increment was recorded in plants irrigated with 3 mS cm^{-1}, but an increasing trend was still visible at 4.5 mS cm^{-1}. A good tolerance to intermediate salt stress (1.5 and 3 mS cm^{-1}) was also found in Murano and Ania plants, which were however negatively affected by the highest salinity level (Fig. 13). Conversely, Cantus and, more markedly, Vivara productivities were strongly undermined by all salt treatments (Fig. 13). It is evident that four fluorometric parameters, namely Y(NOss), Y(NPQss), NPQss and R_{Fd}, evaluated in the controlled phenotyping experiment, closely match the gradient in plant productivity gain/loss outdoors determined by the salt treatments. Therefore, the fluorescence parameters in the indoor experiment are potential indicators of salinity stress tolerance in strawberry cultivated outdoors. Interestingly, their variation emerging in controlled conditions after less than 20 days of exposure to salt stress have a very high predictive value with respect to the field outcome, particularly the cumulative productivity, whose analysis requires instead an entire vegetative season of monitoring. To the specific scope of the breeder, Edwina, though less productive than other cultivars, has a great potential for the cultivation

under conditions usually deemed harsh for strawberry. Moreover, the chance to obtain information on salt tolerance from the early phases of treatment may suggest that long-term growth problems in an artificial environment, such as the premature senescence of Edwina, can be neglected.

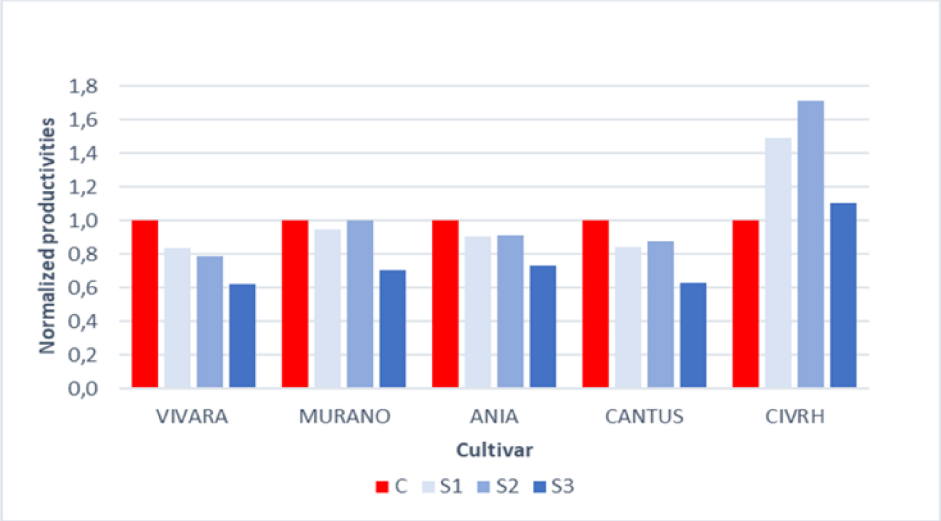

Figure 13. Normalized cumulative fruit productivity during the spring-summer 2021 of the five varieties (Vivara, Murano, Ania, Cantus and CIVRH/Edwina) cultivated in the open field and exposed to salt stress. Red bars represent the reference values for each variety (set to 1), blue-shaded bars the productivity of salt treated plants. The electric conductivity of 1.5 mS cm^{-1} in S1, 3 mS cm^{-1} in S2 and 4.5 mS cm^{-1} in S3 were reached by adding NaCl to the irrigation water.

Acknowledgement

This project was financed by the Slovak Academy Information Agency (SAIA) mobility program scholarship and was made possible thanks to the supervision of Prof. Ing. Marian Brestič and the technical and theoretical support by Prof. Ing. Marek Živčák and Ing. Marek Kovar (Slovak University of Agriculture, Nitra). Marzio Zaccarini and Alessandro Forlani (Consorzio Italiano Vivaisti) are kindly thanked for providing the plant material and for their constant support in the field work.

References

Al-Shorafa, W., Mahadeen, A., & Al-Absi, K. (2014). Evaluation for salt stress tolerance in two strawberry cultivars. *American Journal of Agricultural and Biological Sciences*, *9*(3), 334-341.

Arif, Y., Singh, P., Siddiqui, H., Bajguz, A., & Hayat, S. (2020). Salinity induced physiological and biochemical changes in plants: An omic approach towards salt stress tolerance. *Plant Physiology and Biochemistry*, *156*, 64-77.

Awlia, M., Nigro, A., Fajkus, J., Schmoeckel, S. M., Negrão, S., Santelia, D, Trtílek, M., Tester, M., Julkowska, M. M., & Panzarová, K. (2016). High-throughput non-destructive phenotyping of traits that contribute to salinity tolerance in *Arabidopsis thaliana*. *Frontiers in Plant Science*, *7*, 1414.

Baker, N. R., & Rosenqvist, E. (2004). Applications of chlorophyll fluorescence can improve crop production strategies: an examination of future possibilities. *Journal of Experimental Botany*, *55*(403), 1607-1621.

Bani, A., Daghari, I., Hatira, A., Chaabane, A., & Daghari, H. (2021). Sustainable management of a cropping system under salt stress conditions (Korba, Cap-Bon, Tunisia). *Environmental Science and Pollution Research*, *28*(34), 46469-46476.

Bilger, W., & Björkman, O. (1990). Role of the xanthophyll cycle in photoprotection elucidated by measurements of light-induced absorbance changes, fluorescence and photosynthesis in leaves of *Hedera canariensis*. *Photosynthesis Research*, *25*(3), 173-185.

Borawska-Jarmułowicz, B., Mastalerczuk, G., Pietkiewicz, S., & Kalaji, M. H. (2014). Low temperature and hardening effects on photosynthetic apparatus efficiency and survival of forage grass varieties. *Plant, Soil and Environment*, *60*(4), 177-183.

Cardeñosa, V., Medrano, E., Lorenzo, P., Sánchez-Guerrero, M. C., Cuevas, F., Pradas, I., & Moreno-Rojas, J. M. (2015). Effects of salinity and nitrogen supply on the quality and health-related compounds of strawberry fruits (*Fragaria× ananassa* cv. Primoris). *Journal of the Science of Food and Agriculture*, *95*(14), 2924-2930.

Chen, T. W., Kahlen, K., & Stützel, H. (2015). Disentangling the contributions of osmotic and ionic effects of salinity on stomatal, mesophyll, biochemical and light limitations to photosynthesis. *Plant, Cell & Environment*, *38*(8), 1528-1542.

Corrado, G., Vitaglione, P., Chiaiese, P., & Rouphael, Y. (2021). Unraveling the modulation of controlled salinity stress on morphometric traits, mineral profile, and bioactive metabolome equilibrium in hydroponic basil. *Horticulturae*, *7*(9), 273.

Cuevas, J., Daliakopoulos, I. N., del Moral, F., Hueso, J. J., & Tsanis, I. K. (2019). A review of soil-improving cropping systems for soil salinization. *Agronomy*, *9*(6), 295.

Dąbrowski, P., Baczewska, A. H., Pawluśkiewicz, B., Paunov, M., Alexantrov, V., Goltsev, V., & Kalaji, M. H. (2016). Prompt chlorophyll a fluorescence as a rapid tool for diagnostic changes in PSII structure inhibited by salt stress in perennial ryegrass. *Journal of Photochemistry and Photobiology B: Biology*, *157*, 22-31.

Esmaeilizadeh, M., Malekzadeh Shamsabad, M. R., Roosta, H. R., Dąbrowski, P., Rapacz, M., Zieliński, A., Wróbel, J., & Kalaji, H. M. (2021). Manipulation of light spectrum can improve the performance of photosynthetic apparatus of strawberry plants growing under salt and alkalinity stress. *PLoS One*, *16*(12), e0261585.

Faseela, P., Sinisha, A. K., Brestič, M., & Puthur, J. T. (2019). Chlorophyll *a* fluorescence parameters as indicators of a particular abiotic stress in rice. *Photosynthetica*, *57*(SI), 108-115.

Ferreira, J. F., Liu, X., & Suarez, D. L. (2019). Fruit yield and survival of five commercial strawberry cultivars under field cultivation and salinity stress. *Scientia Horticulturae*, *243*, 401-410.

Ferroni, L., Angeleri, M., Pantaleoni, L., Pagliano, C., Longoni, P., Marsano, F., Aro, E. M., Suorsa, M., Baldisserotto, C., Giovanardi, M., Cella, R., & Pancaldi, S. (2014). Light-dependent reversible phosphorylation of the minor photosystem II antenna Lhcb6 (CP 24) occurs in lycophytes. *The Plant Journal*, *77*(6), 893-905.

Ferroni, L., Živčak, M., Sytar, O., Kovár, M., Watanabe, N., Pancaldi, S., Baldisserotto, C., & Brestič, M. (2020). Chlorophyll-depleted wheat mutants are disturbed in photosynthetic electron flow regulation but can retain an acclimation ability to a fluctuating light regime. *Environmental and Experimental Botany*, *178*, 104156.

Flowers, T. J., & Colmer, T. D. (2008). Salinity tolerance in halophytes. *New Phytologist*, 945-963.

Gilroy, S., Suzuki, N., Miller, G., Choi, W. G., Toyota, M., Devireddy, A. R., & Mittler, R. (2014). A tidal wave of signals: calcium and ROS at the forefront of rapid systemic signaling. *Trends in plant science*, *19*(10), 623-630.

Grieco, M., Tikkanen, M., Paakkarinen, V., Kangasjärvi, S., & Aro, E. M. (2012). Steady-state phosphorylation of light-harvesting complex II proteins preserves photosystem I under fluctuating white light. *Plant Physiology*, *160*(4), 1896-1910.

Grieve, C. M., Grattan, S. R., & Maas, E. V. (2012). Plant salt tolerance. *ASCE Manual and Reports on Engineering Practice*, *71*, 405-459.

Hendrickson, L., Furbank, R. T., & Chow, W. S. (2004). A simple alternative approach to assessing the fate of absorbed light energy using chlorophyll fluorescence. *Photosynthesis research*, *82*(1), 73-81.

Hernández, J. A. (2019). Salinity tolerance in plants: trends and perspectives. *International Journal of Molecular Sciences*, *20*(10), 2408.

Hernandez, J. A., Campillo, A., Jimenez, A., Alarcon, J. J., & Sevilla, F. (1999). Response of antioxidant systems and leaf water relations to NaCl stress in pea plants. *The New Phytologist*, *141*(2), 241-251.

Huang, W., Yang, Y. J., Hu, H., & Zhang, S. B. (2016). Moderate photoinhibition of photosystem II protects photosystem I from photodamage at chilling stress in tobacco leaves. *Frontiers in Plant Science*, *7*, 182.

Huang, W., Yang, Y. J., Zhang, S. B., & Liu, T. (2018). Cyclic electron flow around photosystem I promotes ATP synthesis possibly helping the rapid repair of photodamaged photosystem II at low light. *Frontiers in Plant Science*, *9*, 239.

Huang, W., Zhang, S. B., & Cao, K. F. (2010). Stimulation of cyclic electron flow during recovery after chilling-induced photoinhibition of PSII. *Plant and Cell Physiology*, *51*(11), 1922-1928.

Humplík, J. F., Lazár, D., Husičková, A., & Spíchal, L. (2015). Automated phenotyping of plant shoots using imaging methods for analysis of plant stress responses–a review. *Plant Methods*, *11*(1), 1-10.

Jajoo, A. (2013). Changes in photosystem II in response to salt stress. In *Ecophysiology and responses of plants under salt stress* (pp. 149-168). Springer, New York, NY.

James, R. A., Rivelli, A. R., Munns, R., & von Caemmerer, S. (2002). Factors affecting CO_2 assimilation, leaf injury and growth in salt-stressed durum wheat. *Functional Plant Biology*, *29*(12), 1393-1403.

Johansen, K., Morton, M. J., Malbeteau, Y. M., Aragon, B., Al-Mashharawi, S. K., Ziliani, M. G., Angel, Y., Fiene, G., Negrão, S. C. S., Mousa, M. A. A., Tester M. A., & McCabe, M. F. (2019). Unmanned aerial vehicle-based phenotyping using morphometric and spectral analysis can quantify responses of wild tomato plants to salinity stress. *Frontiers in Plant Science*, *10*, 370.

Kim, S. L., Kim, N., Lee, H., Lee, E., Cheon, K. S., Kim, M., Baek, J., Choi, I., Ji, H., Yoon, I. S., Kwon, T. R. & Kim, K. H. (2020). High-throughput phenotyping platform for analyzing drought tolerance in rice. *Planta*, *252*(3), 38.

Klughammer, C., & Schreiber, U. (2008). Complementary PS II quantum yields calculated from simple fluorescence parameters measured by PAM fluorometry and the Saturation Pulse method. *PAM application notes*, *1*(2), 201-247.

Lazár, D. (2006). The polyphasic chlorophyll *a* fluorescence rise measured under high intensity of exciting light. *Functional Plant Biology*, *33*(1), 9-30.

Lazár, D. (2015). Parameters of photosynthetic energy partitioning. *Journal of Plant Physiology*, *175*, 131-147.

Lichtenthaler, H. K., Burgstahler, R., Buschmann, C., Meier, D., Prenzel, U., & Schönthal, A. (1983). Effect of high light and high light stress on composition, function and structure of the photosynthetic apparatus. In *Effects of Stress on Photosynthesis* (pp. 353-370). Springer, Dordrecht.

Lichtenthaler, H. K., Buschmann, C., & Knapp, M. (2005). How to correctly determine the different chlorophyll fluorescence parameters and the chlorophyll fluorescence decrease ratio R_{Fd} of leaves with the PAM fluorometer. *Photosynthetica*, *43*(3), 379-393.

Lichtenthaler, H. K., Buschmann, C., Rinderle, U., & Schmuck, G. (1986). Application of chlorophyll fluorescence in ecophysiology. *Radiation and Environmental Biophysics*, *25*(4), 297-308.

Lima-Melo, Y., Gollan, P. J., Tikkanen, M., Silveira, J. A., & Aro, E. M. (2019). Consequences of photosystem-I damage and repair on photosynthesis and carbon use in *Arabidopsis thaliana*. *The Plant Journal*, *97*(6), 1061-1072.

Linn, A. I., Zeller, A. K., Pfündel, E. E., & Gerhards, R. (2021). Features and applications of a field imaging chlorophyll fluorometer to measure stress in agricultural plants. *Precision Agriculture*, *22*(3), 947-963.

Mahajan, S., & Tuteja, N. (2005). Cold, salinity and drought stresses: an overview. *Archives of Biochemistry and Biophysics*, *444*(2), 139-158.

Martinez Barroso, M., & Alvarez, C. E. (1997). Toxicity symptoms and tolerance of strawberry to salinity in the irrigation water. *Scientia Horticulturae*, *71*(3-4), 177-188.

Mehta, P., Allakhverdiev, S. I., & Jajoo, A. (2010). Characterization of photosystem II heterogeneity in response to high salt stress in wheat leaves (*Triticum aestivum*). *Photosynthesis Research*, *105*(3), 249-255.

Mehta, P., Jajoo, A., Mathur, S., & Bharti, S. (2010). Chlorophyll *a* fluorescence study revealing effects of high salt stress on Photosystem II in wheat leaves. *Plant Physiology and Biochemistry*, *48*(1), 16-20.

Mitsuya, S., Takeoka, Y., & Miyake, H. (2000). Effects of sodium chloride on foliar ultrastructure of sweet potato (*Ipomoea batatas* Lam.) plantlets grown under light and dark conditions in vitro. *Journal of Plant Physiology*, *157*(6), 661-667.

Munekage, Y., Hojo, M., Meurer, J., Endo, T., Tasaka, M., & Shikanai, T. (2002). PGR5 is involved in cyclic electron flow around photosystem I and is essential for photoprotection in *Arabidopsis*. *Cell*, *110*(3), 361-371.

Munns, R., & Termaat, A. (1986). Whole-plant responses to salinity. *Functional Plant Biology*, *13*(1), 143-160.

Munns, R., & Tester, M. (2008). Mechanisms of salinity tolerance. *Annual Review of Plant Biology*, *59*, 651.

Murillo-Amador, B., Nieto-Garibay, A., Troyo-Diéguez, E., García-Hernández, J. L., Hernández-Montiel, L., & Valdez-Cepeda, R. D. (2015). Moderate salt stress on the physiological and morphometric traits of *Aloe vera* L. *Botanical Sciences*, *93*(3), 639-648.

Na, Y. W., Jeong, H. J., Lee, S. Y., Choi, H. G., Kim, S. H., & Rho, I. R. (2014). Chlorophyll fluorescence as a diagnostic tool for abiotic stress tolerance in wild and cultivated strawberry species. *Horticulture, Environment, and Biotechnology*, *55*(4), 280-286.

Negrão, S., Schmöckel, S. M., & Tester, M. (2017). Evaluating physiological responses of plants to salinity stress. *Annals of Botany*, *119*(1), 1-11.

Ondrašek, G., Romić, D., Romić, M., Duralija, B., & Mustač, I. (2006). Strawberry growth and fruit yield in a saline environment. *Agriculturae Conspectus Scientificus*, *71*(4), 155-158.

Pan, T., Liu, M., Kreslavski, V. D., Zharmukhamedov, S. K., Nie, C., Yu, M., Kuznetsov, V. V., Allakhverdiev S.I., Shabala, S. (2021). Non-stomatal limitation of photosynthesis by soil salinity. *Critical Reviews in Environmental Science and Technology*, *51*(8), 791-825.

Patel, M. K., Kumar, M., Li, W., Luo, Y., Burritt, D. J., Alkan, N., & Tran, L. S. P. (2020). Enhancing salt tolerance of plants: From metabolic reprogramming to exogenous chemical treatments and molecular approaches. *Cells*, *9*(11), 2492.

Pérez-Bueno, M. L., Pineda, M., & Barón, M. (2019). Phenotyping plant responses to biotic stress by chlorophyll fluorescence imaging. *Frontiers in Plant Science*, *10*, 1135.

Qadir, M., Quillérou, E., Nangia, V., Murtaza, G., Singh, M., Thomas, R. J., Drechsel, P., Noble, A. D. (2014). Economics of salt-induced land degradation and restoration. In *Natural Resources Forum* (Vol. 38, No. 4, pp. 282-295).

Rahman, M. M., Mostofa, M. G., Keya, S. S., Siddiqui, M. N., Ansary, M. M. U., Das, A. K., Rahman, M. A., Tran, L. S. P. (2021). Adaptive mechanisms of halophytes and their potential in improving salinity tolerance in plants. *International Journal of Molecular Sciences*, *22*(19), 10733.

Rajabi Dehnavi, A., Zahedi, M., Ludwiczak, A., Cardenas Perez, S., & Piernik, A. (2020). Effect of salinity on seed germination and seedling development of sorghum (*Sorghum bicolor* (L.) Moench) genotypes. *Agronomy*,*10*(6), 859.

Ritzema, H. P. (2016). Drain for Gain: Managing salinity in irrigated lands—A review. *Agricultural Water Management*, *176*, 18-28.

Roy, S. J., Negrão, S., & Tester, M. (2014). Salt resistant crop plants. *Current Opinion in Biotechnology*, *26*, 115-124.

Ruban, A. V. (2018). Light harvesting control in plants. *FEBS Letters*, *592*(18), 3030-3039.

Schreiber, U. (2004). Pulse-amplitude-modulation (PAM) fluorometry and saturation pulse method: an overview. In *Chlorophyll a fluorescence: a signature of photosynthesis*, 279-319.

Shimakawa, G., & Miyake, C. (2018). Oxidation of P700 ensures robust photosynthesis. *Frontiers in Plant Science*, *9*, 1617.

Shimakawa, G., & Miyake, C. (2019). What quantity of photosystem I is optimum for safe photosynthesis?. *Plant Physiology*, *179*(4), 1479-1485.

Song, P., Wang, J., Guo, X., Yang, W., & Zhao, C. (2021). High-throughput phenotyping: Breaking through the bottleneck in future crop breeding. *The Crop Journal*, *9*(3), 633-645.

Sonoike, K. (2011). Photoinhibition of photosystem I. *Physiologia plantarum*, *142*(1), 56-64.

Sonoike, K., Terashima, I., Iwaki, M., & Itoh, S. (1995). Destruction of photosystem I iron-sulfur centers in leaves of *Cucumis sativus* L. by weak illumination at chilling temperatures. *FEBS letters*, *362*(2), 235-238.

Sorrentino, M., Panzarová, K., Spyroglou, I., Spíchal, L., Buffagni, V., Ganugi, P., ... & De Diego, N. (2021). Integration of phenomics and metabolomics datasets reveals different mode of action of biostimulants based on protein hydrolysates in *Lactuca sativa* L. and *Solanum lycopersicum* L. Under Salinity. *Frontiers in Plant Science*, *12*.

Stirbet, A., Lazár, D., & Kromdijk, J. (2018). Chlorophyll *a* fluorescence induction: can just a one-second measurement be used to quantify abiotic stress responses?. *Photosynthetica*, *56*(1), 86-104.

Sun, H., Zhang, S. B., Liu, T., & Huang, W. (2020). Decreased photosystem II activity facilitates acclimation to fluctuating light in the understory plant Paris polyphylla. *Biochimica et Biophysica Acta (BBA)-Bioenergetics*, *1861*(2), 148135.

Suorsa, M., Järvi, S., Grieco, M., Nurmi, M., Pietrzykowska, M., Rantala, M., Kangasjärvi, S., Paakkarinen, V., Tikkanen, M., Jansson, S., & Aro, E. M. (2012). PROTON GRADIENT REGULATION5 is essential for proper acclimation of *Arabidopsis* photosystem I to naturally and artificially fluctuating light conditions. *The Plant Cell*, *24*(7), 2934-2948.

Tan, S. L., Liu, T., Zhang, S. B., & Huang, W. (2020). Balancing light use efficiency and photoprotection in tobacco leaves grown at different light regimes. *Environmental and Experimental Botany*, *175*, 104046.

Tian, Y., Xie, L., Wu, M., Yang, B., Ishimwe, C., Ye, D., & Weng, H. (2021). Multicolor fluorescence imaging for the early detection of salt stress in *Arabidopsis*. *Agronomy*, *11*(12), 2577.

Tikkanen, M., Mekala, N. R., & Aro, E. M. (2014). Photosystem II photoinhibition-repair cycle protects Photosystem I from irreversible damage. *Biochimica et Biophysica Acta (BBA)-Bioenergetics*, *1837*(1), 210-215.

Tikkanen, M., Rantala, S., & Aro, E. M. (2015). Electron flow from PSII to PSI under high light is controlled by PGR5 but not by PSBS. *Frontiers in plant science*, *6*, 521.

van Bezouw, R. F., Keurentjes, J. J., Harbinson, J., & Aarts, M. G. (2019). Converging phenomics and genomics to study natural variation in plant photosynthetic efficiency. *The Plant Journal*, *97*(1), 112-133.

Wallender, W. W., & Tanji, K. K. (2011). Agricultural salinity assessment and management. Reston, VA: American Society of Civil Engineers.

Yaghubi, K., Ghaderi, N., Vafaee, Y., & Javadi, T. (2016). Potassium silicate alleviates deleterious effects of salinity on two strawberry cultivars grown under soilless pot culture. *Scientia Horticulturae*, *213*, 87-95.

Yamamoto, H., & Shikanai, T. (2019). PGR5-dependent cyclic electron flow protects photosystem I under fluctuating light at donor and acceptor sides. *Plant physiology*, *179*(2), 588-600.

Yang, W., Feng, H., Zhang, X., Zhang, J., Doonan, J. H., Batchelor, W. D., Xiong, L., Yan, J. (2020). Crop phenomics and high-throughput phenotyping: past decades, current challenges, and future perspectives. *Molecular Plant*, *13*(2), 187-214.

Zhang, S. B., Wang, J. H., & Huang, W. (2021). Pre-illumination at high light significantly alleviates the over-reduction of photosystem I under fluctuating light. *Plant Science*, *312*, 111053.

Zörb, C., Geilfus, C. M., & Dietz, K. J. (2019). Salinity and crop yield. *Plant Biology*, *21*, 31-38.

Supplementary materials

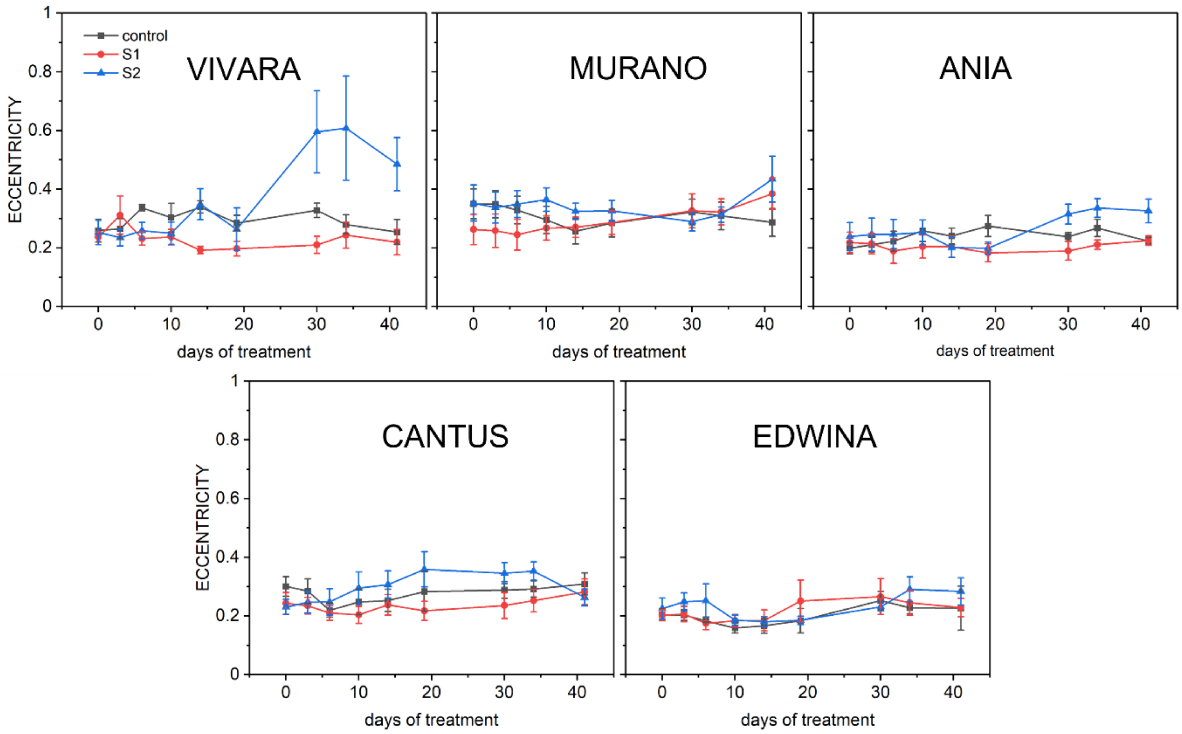

Supplementary Figure1. Plant eccentricity trends during the experiment with five strawberry cultivars (Vivara, Murano, Ania, Cantus and Edwina). Symbols and abbreviations as in Figure 3 of the main text.

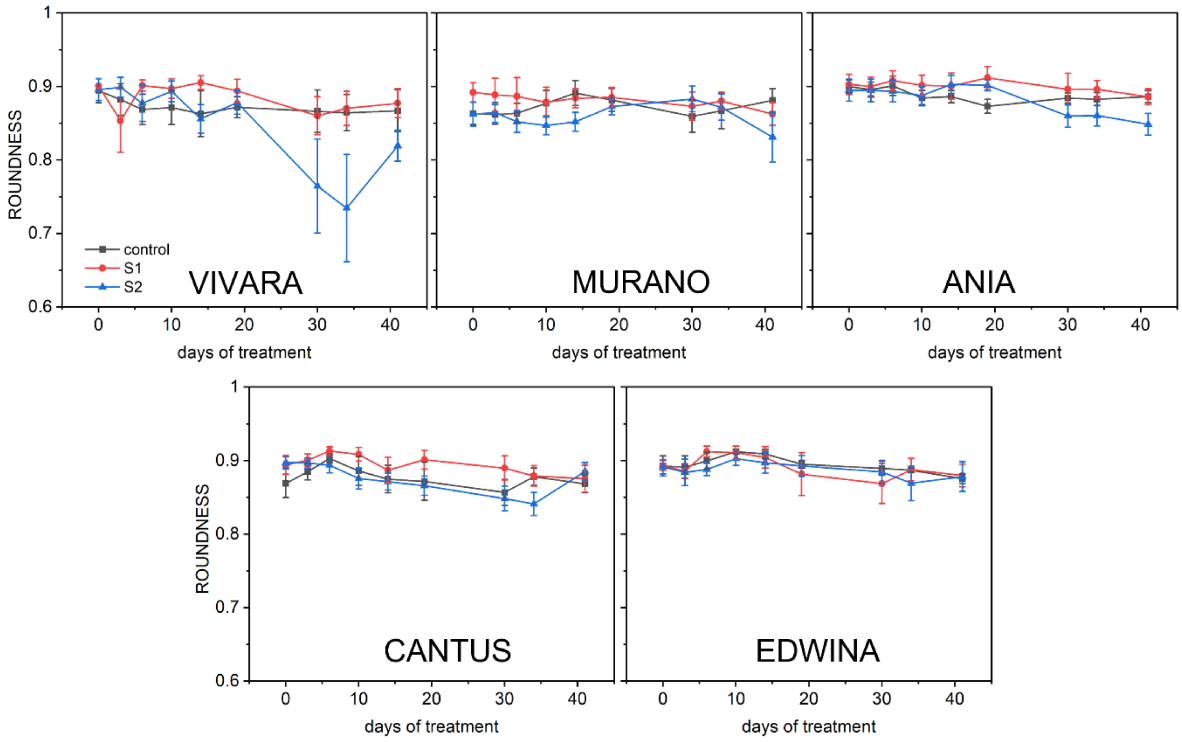

Supplementary Figure 2. Plant roundness trends during the experiment with five strawberry cultivars (Vivara, Murano, Ania, Cantus and Edwina). Symbols and abbreviations as in Figure 3 of the main text.

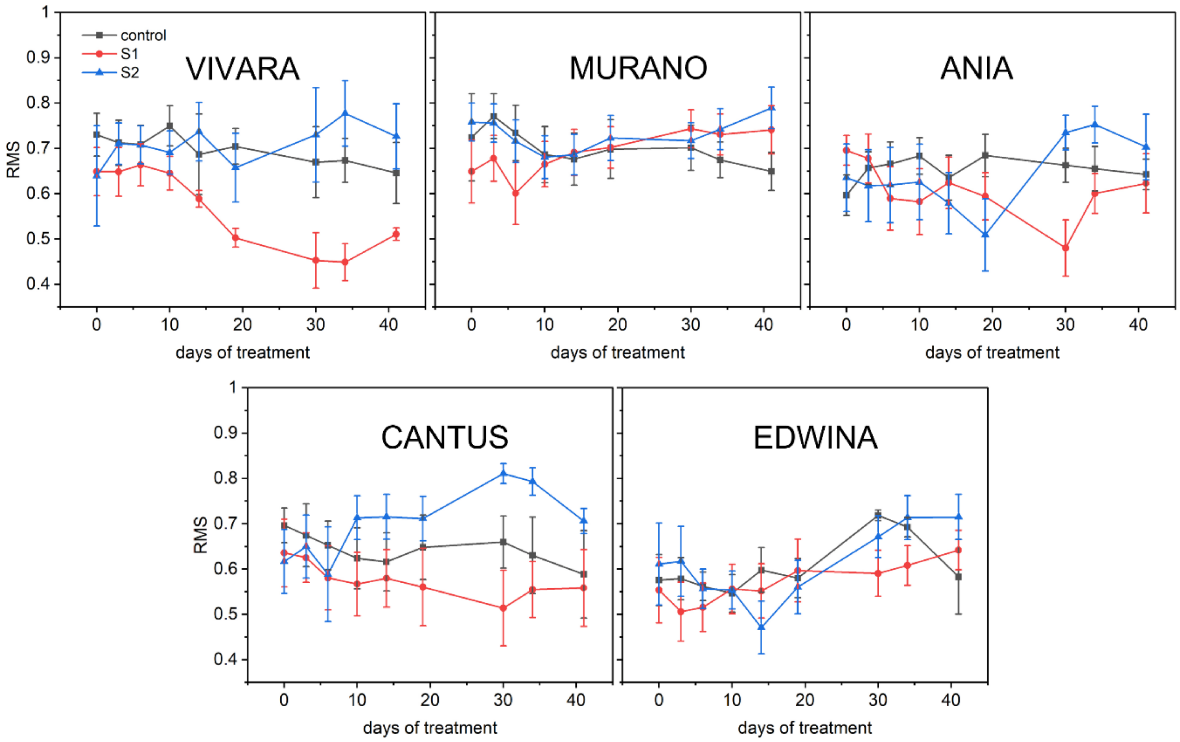

Supplementary Figure 3. Plant rotational mass symmetry (RMS) trends during the experiment with five strawberry cultivars (Vivara, Murano, Ania, Cantus and Edwina). Symbols and abbreviations as in Figure 3 of the main text.

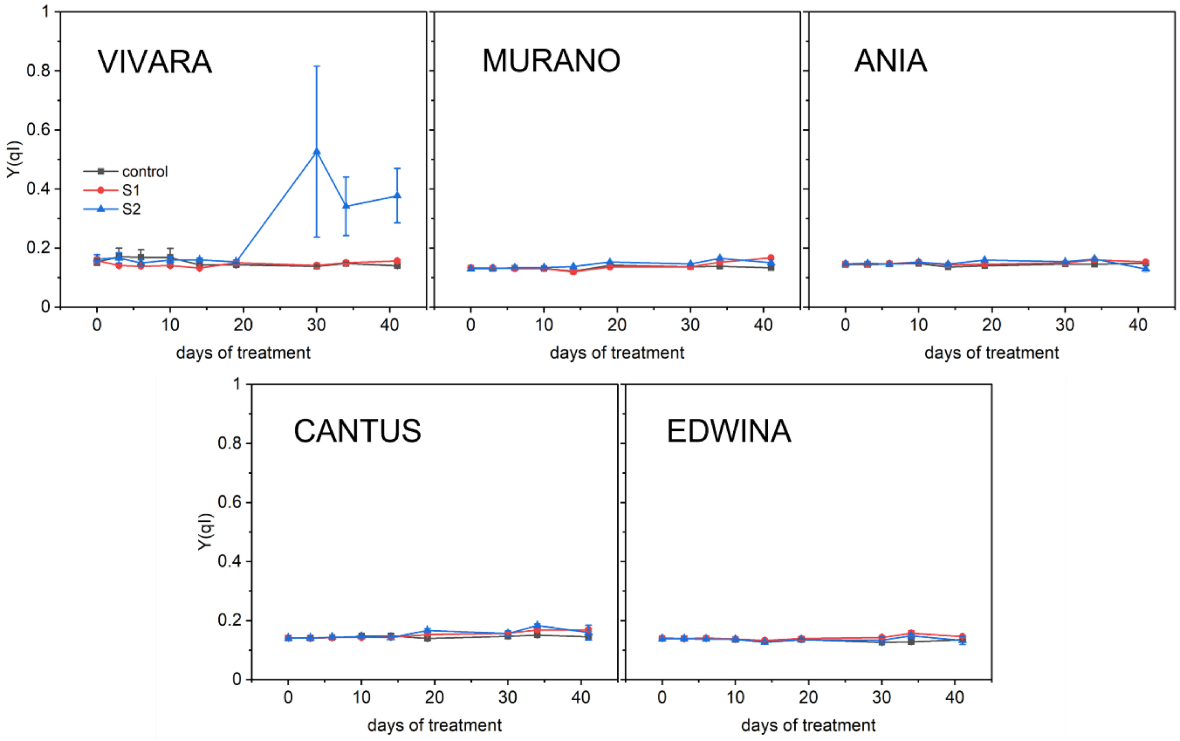

Supplementary Figure 4. Quantum yield of PSII photoinhibition trends during the experiment with five strawberry cultivars (Vivara, Murano, Ania, Cantus and Edwina). Symbols and abbreviations as in Figure 3 of the main text.

Concluding remarks and future perspectives

Two main research lines have been developed during these three years of PhD course. The first line was focused on the characterization of the thylakoid membrane structure and dynamics in *Selaginella martensii*. The novel information obtained by means of chlorophyll fluorescence analysis, associated with other methods, deepens our understanding of the specificity of the thylakoid organization in a representative of the diminutive group of vascular plants known as lycophytes, which has undergone an evolution of the photosynthetic apparatus parallel to that of the other, dominating clade of euphyllophytes. Examples of such evolutionary outcomes in *Selaginella* species encompass the unique chloroplast structure (Sheue et al. 2007), the PSII antenna complement and its functional flexibility (Ferroni et al. 2014, 2016), the unusually high thermal dissipation capacity (Ferroni et al. 2018, 2020), the long-term regulation of the leaf diffusional limitations of photosynthesis (Ferroni et al. 2021).

The first aim was to characterize the dynamics of PSII photoinhibition and photoprotection in *S. martensii* to understand whether a constant NPQ capacity in plants grown in strongly contrasting light regimes (Ferroni et al. 2016) likewise corresponded to a constant capacity of PSII photoprotection (Chapter 1). The work elucidated the importance of photoprotective NPQ (pNPQ), as determined by the fluorometric protocol proposed by Ware et al. (2015), in determining the degree of sensitivity to PSII photoinhibition in *S. martensii* plants acclimated to different light conditions: similar total NPQ amplitudes actually hid different levels of pNPQ and, in plants acclimated to high light intensity, higher levels of the latter corresponded to a lower sensitivity to PSII photoinhibition. Moreover, the work highlighted the relevance of PSII antenna uncoupling in inducing high levels of pNPQ: plants grown under a high light regime were the most prone to LHCII antenna uncoupling from PSII and benefitted from higher PSII photoprotection. The results were finalized in a publication in the international peer-reviewed journal *Physiologia Plantarum*. The work also gained a special focus in the Journal, which dedicated a comment “IN THE SPOTLIGHT” written by Robert H. Calderon (Department of Plant Physiology, Umeå University, Umeå, Sweden) (Fig. 1). The comment, including an artistic translation of the main message, underlined the significance of the findings and suggested their implications in the context of the characterization of the thylakoid membrane dynamics in lycophytes and early divergent plants (Fig. 2).

DOI: 10.1111/ppl.13671

IN THE SPOTLIGHT

Physiologia Plantarum

A lycophyte's plight when the light is too bright

Robert H. Calderon

Department of Plant Physiology, Umeå University, Umeå, Sweden

Correspondence
Robert H. Calderon, Department of Plant Physiology, Umeå University, Umeå, Sweden.
Email: robert.calderon@umu.se

Linked article: This spotlight refers to Colpo et al. (2021). To view this article, please visit https://doi.org/10.1111/ppl.13604

Figure 1. Extract from Calderon (2022) proposing a comment on Colpo et al. (2022).

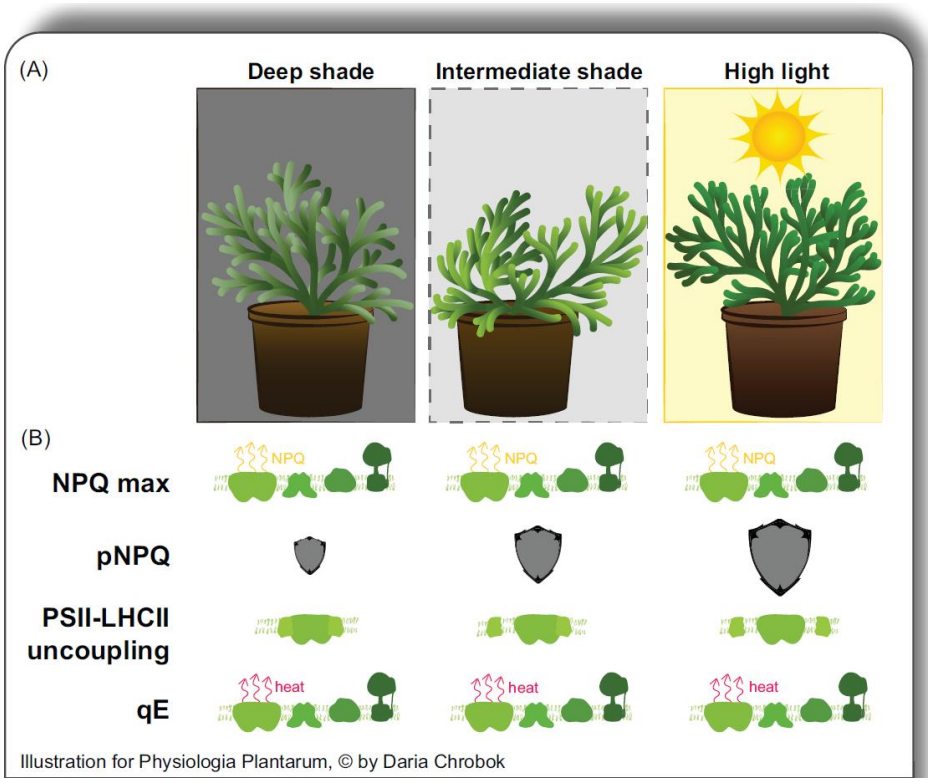

Figure 2. Artistic representation of the results described in Colpo et al. (2022), as interpreted by the professional illustrator Daria Chrobok (https://www.dariasciart.com) for the comment by Calderon (2022).

Progresses have been made also in the characterization of the ultrastructure and organization of *S. martensii* thylakoid membrane in the plant grown under natural shade conditions (Chapter 2). The uniqueness of the giant chloroplast makes it not obvious whether the shade-adaptation traits characterized in detail in angiosperms are confirmed in a lycophyte. In this study, the chlorophyll fluorescence analysis was used to

independently support the inferences derived from combined ultrastructural, biochemical and EPR analyses. While it was confirmed that *S. martensii* has a typical pigment composition and PSI/PSII ratio of a shade-adapted plant, the electron microscopy morphometrics revealed that the lycophyte grana are laterally extended rather than developed vertically, as instead was expected from the well-established response to shade in angiosperms. Furthermore, the average length of the granum – nearly 700 nm – was significantly beyond the optimal functional length limit of 500 nm hypothesized for the correct diffusion of the soluble electron carriers in angiosperms (Höhner et al. 2020). These findings are extremely important, since they demonstrate that the correct functionality of the photosynthetic apparatus was achieved differently in angiosperms and lycophytes. For example, the slow diffusion of electron carriers in a lycophyte may explain the need for the fast and intense induction of NPQ, as well as, in the general context of photosynthetic regulation in *S. martensii*, it suggests that the organization of LHCII in this species may have other characteristics of uniqueness. Further steps forward in the knowledge of the photosynthetic organization in *S. martensii* were made analyzing the LHCII dynamics in response to acclimation to different light conditions. The preliminary results, obtained with steady-state chlorophyll spectrofluorometry, indicate that in *S. martensii* LHCII antenna might function as harvesting complex for PSI also in conditions of dark acclimation, which should instead promote a nearly complete association of LHCII to only PSII (Appendix 1). The data available to date suggest a permanent and stable association between LHCII and PSI. More insights into the dynamics of LHCII will be provided from the results of the time-resolved chlorophyll fluorescence measurements performed in collaboration with Prof. Roberta Croce at the LaserLab center in the Vrije University of Amsterdam (NL). While such results will hopefully clarify the extent to which LHCII is used by *S. martensii* as an antenna for PSI, other questions remain about the modulation of LHCII association with PSII, particularly in the grana cores. The long-term changes in LHCII:PSII stoichiometry, complicated by the use of a large fraction of LHCII as an antenna for PSI, make it uncertain whether the antenna size of PSII is variable or not. Investigation on this aspect has been undertaken analyzing OJIP transients, and the preliminary result suggest interesting modulations of the PSII connectivity, a quite controversial issue in photosynthesis studies (Appendix 2).

The second research line of the PhD program was the application of fluorometric techniques in the context of the photosynthetic plant phenotyping, again taking advantage of the information derived from chlorophyll fluorescence analysis.

A first research project was performed on a minipanel of chlorophyll-depleted mutants of durum and bread wheat, in continuity with the previous works in collaboration with Prof. Ing. Marian Brestič at the University of Agriculture (SUA) in Nitra (SK) (Ferroni et al. 2020, 2022). After the experiences in the phenotyping facility, a validation of the previous findings was necessary under natural conditions, particularly to ascertain the impact of the deregulated electron flow control characterizing the mutants to different levels of severity. The wheat lines were sewed and cultivated outdoors in semi-field conditions at the Botanical Garden of Ferrara, to understand the impact of the outdoor cultivation on mutant lines and to find correlations between fluorometric and productivity parameters (Chapter 3). The research exploited combined quenching and OJIP

analyses, and particularly it shows the usefulness of the pNPQ method previously developed in *S. martensii* (Chapter 1) and here adapted to the scope of wheat phenotyping. The correlation analysis revealed that specific early measured fluorometric parameters can be robust predictors of the overall productivity of the wheat plants. This project lays the groundwork for further characterization of the mutants, which is currently underway involving the characterization of elemental content and stable C and N isotopic composition of leaves and grains.

Photosynthetic plant phenotyping techniques were also employed in a research project in collaboration with C.I.V. (Consorzio Italiano Vivaisti), a varietal selection center based in Comacchio (Ferrara, Italy). The project focused on two types of applications of fluorometric phenotyping methods: one carried out on commercial apple varieties to search for water stress resistant rootstocks, the other aimed at screening five commercial strawberry varieties for salt stress resistance. This project was very uplifting in that it allowed us to establish a valuable partnership to test whether knowledge gained in the laboratory could be applied in the open field and support specific needs of breeders. The most suited method for plant phenotyping was OJIP transient analysis: hundreds of transients were recorded over an entire vegetative season and still require extensive elaboration, so they are not presented *in extenso* in this Thesis, but shortly presented in Appendix 3 regarding the main results of the experiment with apple rootstocks. The challenging complexity of the real agricultural context with respect to the research of salt-tolerant strawberry varieties suggested that a parallel research could be profitably performed in a phenotyping facility. Therefore, an experiment was set up at the Slovak PlantScreen™ Phenotyping Unit (SPPU) of the SUA with the collaboration and supervision of Prof. Ing. Marian Brestič. The experiment was performed in controlled environmental conditions, hence allowing a better understanding of the onset of the stress response in the plants, as evidenced by chlorophyll fluorescence imaging associated with whole plant morphometrics (Chapter 4). Nonetheless, the results presented in this Thesis represent only a part of the data collected in SPPU but already very informative about the comparative salt-tolerance of the five strawberry varieties. The variety Edwina, the most recently marketed by C.I.V., resulted the most tolerant. The treatment and interpretation of the not yet analyzed data, including simultaneous measurements of PSI and PSII activity (DUAL-PAM), as well as the redox state of the intersystem electron carriers (DUAL-KLAS-NIR), will potentially enrich this work with functional details.

The works presented in this Thesis have the potential to lead to new research projects aiming at expanding the knowledge on basic photosynthetic functioning and applications of chlorophyll fluorometric techniques in the frame of plant phenotyping. In addition, the projects pursued during the three-year-long PhD course have allowed past scientific collaborations to be strengthened and new and potentially fruitful ones to be created, thus creating a fertile ground for new and innovative research in the field of photosynthesis from structure to function.

Acknowledgements

I would like to thank my academic tutor Prof. Lorenzo Ferroni for his help and support. The success of this PhD. Project would have never been possible without his wise advice and his honest and precious friendship. A big thanks to Prof. Simonetta Pancaldi for well-managing the research group and make the laboratory a pleasant place to do research and being productive. I want to thank also all the other members of the laboratory which accompanied me throughout these three years: Prof. Costanza Baldisserotto, Dr. Sara Demaria, Dr. Michele Maglie, Dr. Luna Ardondi, Dr. Elisa Benà, Dr. Essi Ruohisto and Dr. Pierluigi Giacò, they have been excellent collaborators and friends.

I want to mention also the external people I collaborated with: Prof. Roberta Croce and her collaborators, who supervised and helped me during my research stay at the Vrije University of Amsterdam; Prof. Ing. Marian Brestič who hosted and supervised me at the Slovak University of Agriculture in Nitra and all his research group, in particular Prof. Ing Marek Živčak and Dr. Ing. Marek Kovar; Prof. Alessandra Molinari who allowed the EPR experiments; Marzio Zaccarini and Alessandro Forlani who gave me the technical and theoretical support during the research project at the Consorzio Italiano Vivaisti in Comacchio; Fausto Molinari and Roberta Marchesini for taking care of the plants in the Botanical Garden of the University of Ferrara; Paola Boldrini for the excellent technical assistance at the Electron Microscopy Center of the University of Ferrara.

A big hug to my family and my friends, who were always by my side and helped me to overcome the most difficult moments.

References

Anderson, J. M. (1986). Photoregulation of the composition, function, and structure of thylakoid membranes. *Annual Review of Plant Physiology*, *37*(1), 93-136.

Anderson, J. M., & Aro, E. M. (1994). Grana stacking and protection of photosystem II in thylakoid membranes of higher plant leaves under sustained high irradiance: an hypothesis. *Photosynthesis Research*, *41*, 315-326.

Anderson, J. M., Chow, W. S., & Goodchild, D. J. (1988). Thylakoid membrane organisation in sun/shade acclimation. *Functional Plant Biology*, *15*(2), 11-26.

Andersson, B., & Anderson, J. M. (1980). Lateral heterogeneity in the distribution of chlorophyll-protein complexes of the thylakoid membranes of spinach chloroplasts. *Biochimica et Biophysica Acta (BBA)-Bioenergetics*, *593*(2), 427-440.

Armbruster, U., Labs, M., Pribil, M., Viola, S., Xu, W., Scharfenberg, M., Hertle, A.P., Rojahn, U., Jensen, P.E., Rappaport, F., Joliot, P., Dörmann, P., Wanner, G., & Leister, D. *Arabidopsis* CURVATURE THYLAKOID1 proteins modify thylakoid architecture by inducing membrane curvature. *Plant Cell, 25*, 2661–2678 (2013).

Aro, E. M., Virgin, I., & Andersson, B. (1993). Photoinhibition of photosystem II. Inactivation, protein damage and turnover. *Biochimica et Biophysica Acta (BBA)-Bioenergetics*, *1143*(2), 113-134.

Baker, N. R. (2008). Chlorophyll fluorescence: a probe of photosynthesis in vivo. *Annuual Review of Plant Biology*, *59*, 89-113.

Benson, S. L., Maheswaran, P., Ware, M. A., Hunter, C. N., Horton, P., Jansson, S., Ruban, A. V., & Johnson, M. P. (2015). An intact light harvesting complex I antenna system is required for complete state transitions in Arabidopsis. *Nature Plants*, *1*(12), 1-9.

Betterle, N., Ballottari, M., Zorzan, S., de Bianchi, S., Cazzaniga, S., Dall'Osto, L., Morosinotto, T., & Bassi, R. (2009). Light-induced dissociation of an antenna hetero-oligomer is needed for non-photochemical quenching induction. *Journal of Biological Chemistry*, *284*(22), 15255-15266.

Bielczynski, L. W., Xu, P., & Croce, R. (2022). PSII supercomplex disassembly is not needed for the induction of energy quenching (qE). *Photosynthesis Research*, *152*(3), 275-281.

Björkman, O., & Demmig-Adams, B. (1995). Regulation of photosynthetic light energy capture, conversion, and dissipation in leaves of higher plants. *Ecophysiology of Photosynthesis*, 17-47.

Boekema, E. J., Jensen, P. E., Schlodder, E., van Breemen, J. F., van Roon, H., Scheller, H. V., & Dekker, J. P. (2001). Green plant photosystem I binds light-harvesting complex I on one side of the complex. *Biochemistry*, *40*(4), 1029-1036.

Bradbury, M., & Baker, N. R. (1981). Analysis of the slow phases of the in vivo chlorophyll fluorescence induction curve. Changes in the redox state of photosystem II electron acceptors and fluorescence emission from photosystems I and II. *Biochimica et Biophysica Acta (BBA)-Bioenergetics*, *635*(3), 542-551.

Brestic, M., Zivcak, M., Kalaji, H. M., Carpentier, R., & Allakhverdiev, S. I. (2012). Photosystem II thermostability in situ: environmentally induced acclimation and genotype-specific reactions in *Triticum aestivum* L. *Plant Physiology and Biochemistry*, *57*, 93-105.

Bro, E., Meyer, S., & Genty, B. (1996). Heterogeneity of leaf CO2 assimilation during photosynthetic induction. *Plant, Cell & Environment*, *19*(12), 1349-1358.

Bukhov, N. G., & Carpentier, R. (2003). Measurement of photochemical quenching of absorbed quanta in photosystem I of intact leaves using simultaneous measurements of absorbance changes at 830 nm and thermal dissipation. *Planta*, *216*, 630-638.

Caffarri, S., Tibiletti, T., C Jennings, R., & Santabarbara, S. (2014). A comparison between plant photosystem I and photosystem II architecture and functioning. *Current Protein and Peptide Science*, *15*(4), 296-331.

Calderon, R. H. (2022). A lycophyte's plight when the light is too bright. *Physiologia Plantarum*, *174*(2).

Cazzaniga, S., Dall'Osto, L., Kong, S. G., Wada, M., & Bassi, R. (2013). Interaction between avoidance of photon absorption, excess energy dissipation and zeaxanthin synthesis against photooxidative stress in A *rabidopsis*. *The Plant Journal*, *76*(4), 568-579.

Ceppi, M. G., Oukarroum, A., Çiçek, N., Strasser, R. J., & Schansker, G. (2012). The IP amplitude of the fluorescence rise OJIP is sensitive to changes in the photosystem I content of leaves: a study on plants exposed to magnesium and sulfate deficiencies, drought stress and salt stress. *Physiologia Plantarum*, *144*(3), 277-288.

Chaux, F., Peltier, G., & Johnson, X. (2015). A security network in PSI photoprotection: regulation of photosynthetic control, NPQ and O2 photoreduction by cyclic electron flow. *Frontiers in Plant Science*, *6*, 875.

Colpo, A., Baldisserotto, C., Pancaldi, S., Sabia, A., & Ferroni, L. (2022). Photosystem II photoinhibition and photoprotection in a lycophyte, *Selaginella martensii*. *Physiologia Plantarum*, *174*(1), e13604.

Dai, Y., Shen, Z., Liu, Y., Wang, L., Hannaway, D., & Lu, H. (2009). Effects of shade treatments on the photosynthetic capacity, chlorophyll fluorescence, and chlorophyll content of *Tetrastigma hemsleyanum* Diels et Gilg. *Environmental and Experimental Botany*, *65*(2-3), 177-182.

Daley, P. F., Raschke, K., Ball, J. T., & Berry, J. A. (1989). Topography of photosynthetic activity of leaves obtained from video images of chlorophyll fluorescence. *Plant Physiology*, *90*(4), 1233-1238.

Danielsson, R., Albertsson, P.A., Mamedov, F., & Styring, S. (2004). Quantification of photosystem I and II in different parts of the thylakoid membrane from spinach. *Biochimica et Biophysica Acta (BBA)–Bioenergetics, 1608*(1), 53-61.

de Sousa, C. A. F., de Paiva, D. S., Casari, R. A. D. C. N., de Oliveira, N. G., Molinari, H. B. C., Kobayashi, A. K., Magalhaes, P. C., Gomide, R. L., & Souza, M. T. (2017). A procedure for maize genotypes discrimination to drought by chlorophyll fluorescence imaging rapid light curves. *Plant Methods*, *13*, 1-17.

Demmig, B., Cleland, R. E., & Björkman, O. (1987). Photoinhibition, 77K chlorophyll fluorescence quenching and phosphorylation of the light-harvesting chlorophyll-protein complex of photosystem II in soybean leaves. *Planta*, *172*, 378-385.

Demmig-Adams, B., Muller, O., Stewart, J. J., Cohu, C. M., & Adams III, W. W. (2015). Chloroplast thylakoid structure in evergreen leaves employing strong thermal energy dissipation. *Journal of Photochemistry and Photobiology B: Biology*, *152*, 357-366.

Duysens, L., & Sweers, H. (1963). Mechanisms of Two Photochemical Reactions as Studied by Means of Fluorescence, 353–372. *Studies on Microalgae and Photosynthetic Bacteria, Special Issue of Plant and Cell Physiol. Tokyo: University of Tokyo Press*.

Galka, P., Santabarbara, S., Khuong, T. T. H., Degand, H., Morsomme, P., Jennings, R. C., Boekema, E. J., & Caffarri, S. (2012). Functional analyses of the plant photosystem I–light-harvesting complex II supercomplex reveal that light-harvesting complex II loosely bound to photosystem II is a very efficient antenna for photosystem I in state II. *The Plant Cell*, *24*(7), 2963-2978

Farquhar, G. D., von Caemmerer, S. V., & Berry, J. A. (1980). A biochemical model of photosynthetic CO_2 assimilation in leaves of C 3 species. P*lanta*, *149*, 78-90.

Fernyhough, P., Foyer, C. H., & Horton, P. (1984). Increase in the level of thylakoid protein phosphorylation in maize mesophyll chloroplasts by decrease in the transthylakoid pH gradient. *FEBS letters*, *176*(1), 133-138.

Ferroni, L., Angeleri, M., Pantaleoni, L., Pagliano, C., Longoni, P., Marsano, F., Aro, E. M., Suorsa, M., Baldisserotto, C., Giovanardi, M., Cella, R., & Pancaldi, S. (2014). Light-dependent reversible phosphorylation of the minor photosystem II antenna Lhcb6 (CP 24) occurs in lycophytes. *The Plant Journal*, *77*(6), 893-905.

Ferroni, L., Colpo, A., Baldisserotto, C., & Pancaldi, S. (2021). In an ancient vascular plant the intermediate relaxing component of NPQ depends on a reduced stroma: Evidence from dithiothreitol treatment. *Journal of Photochemistry and Photobiology B: Biology*, *215*, 112114.

Ferroni, L., Cucuzza, S., Angeleri, M., Aro, E. M., Pagliano, C., Giovanardi, M., Baldisserotto, C., & Pancaldi, S. (2018). In the lycophyte *Selaginella martensii* is the “extra-qT” related to energy spillover? Insights into photoprotection in ancestral vascular plants. *Environmental and Experimental Botany*, *154*, 110-122.

Ferroni, L., Suorsa, M., Aro, E. M., Baldisserotto, C., & Pancaldi, S. (2016). Light acclimation in the lycophyte *Selaginella martensii* depends on changes in the amount of photosystems and on the flexibility of the light-harvesting complex II antenna association with both photosystems. *New Phytologist*, *211*(2), 554-568.

Ferroni, L., Živčak, M., Kovar, M., Colpo, A., Pancaldi, S., Allakhverdiev, S. I., & Brestič, M. (2022). Fast chlorophyll a fluorescence induction (OJIP) phenotyping of chlorophyll-deficient wheat suggests that an enlarged acceptor pool size of Photosystem I helps compensate for a deregulated photosynthetic electron flow. *Journal of Photochemistry and Photobiology B: Biology*, *234*, 112549.

Ferroni, L., Živčak, M., Sytar, O., Kovár, M., Watanabe, N., Pancaldi, S., Baldisserotto, C., & Brestič, M. (2020). Chlorophyll-depleted wheat mutants are disturbed in photosynthetic electron flow regulation but can retain an acclimation ability to a fluctuating light regime. *Environmental and Experimental Botany*, *178*, 104156.

Fracheboud Y., & Leipner J. (2003). The application of chlorophyll fluorescence to study light, temperature, and drought stress. *Practical Applications of Chlorophyll Fluorescence in Plant Biology*.. 125-150, Kluwer Acad. Publ. Dordrecht 2003.

Gao, G., Tester, M. A., & Julkowska, M. M. (2020). The use of high-throughput phenotyping for assessment of heat stress-induced changes in Arabidopsis. *Plant Phenomics*, *2020*.

Genty, B., Briantais, J. M., & Baker, N. R. (1989). The relationship between the quantum yield of photosynthetic electron transport and quenching of chlorophyll fluorescence. *Biochimica et Biophysica Acta (BBA)-General Subjects*, *990*(1), 87-92.

Gilmore, A. M., Shinkarev, V. P., Hazlett, T. L., & Govindjee. (1998). Quantitative analysis of the effects of intrathylakoid pH and xanthophyll cycle pigments on chlorophyll a fluorescence lifetime distributions and intensity in thylakoids. *Biochemistry*, *37*(39), 13582-13593.

Goldschmidt-Clermont, M., & Bassi, R. (2015). Sharing light between two photosystems: mechanism of state transitions. *Current Opinion in Plant Biology*, *25*, 71-78.

Grieco, M., Suorsa, M., Jajoo, A., Tikkanen, M., & Aro, E. M. (2015). Light-harvesting II antenna trimers connect energetically the entire photosynthetic machinery—including both photosystems II and I. *Biochimica et Biophysica Acta (BBA)-Bioenergetics*, *1847*(6-7), 607-619.

Gu, L., Grodzinski, B., Han, J., Marie, T., Zhang, Y. J., Song, Y. C., & Sun, Y. (2022). Granal thylakoid structure and function: explaining an enduring mystery of higher plants. *New Phytologist*, *236*(2), 319-329.

Guo, Y., Lu, Y., Goltsev, V., Strasser, R. J., Kalaji, H. M., Wang, H., ... & Qiang, S. (2020). Comparative effect of tenuazonic acid, diuron, bentazone, dibromothymoquinone and methyl viologen on the kinetics of Chl a fluorescence rise OJIP and the MR820 signal. *Plant Physiology and Biochemistry*, *156*, 39-48.

Hendrickson, L., Furbank, R. T., & Chow, W. S. (2004). A simple alternative approach to assessing the fate of absorbed light energy using chlorophyll fluorescence. *Photosynthesis Research*, *82*, 73-81.

Höhner, R., Pribil, M., Herbstová, M., Lopez, L. S., Kunz, H. H., Li, M., Wood, M., Svoboda, V., Puthiyaveetil, S., Leister D., & Kirchhoff, H. (2020). Plastocyanin is the long-range electron carrier between photosystem II and photosystem I in plants. *Proceedings of the National Academy of Sciences*, *117*(26), 15354-15362.

Holzwarth, A. R., Miloslavina, Y., Nilkens, M., & Jahns, P. (2009). Identification of two quenching sites active in the regulation of photosynthetic light-harvesting studied by time-resolved fluorescence. *Chemical Physics Letters*, *483*(4-6), 262-267.

Horton, P. (2012). Optimization of light harvesting and photoprotection: molecular mechanisms and physiological consequences. *Philosophical Transactions of the Royal Society B: Biological Sciences*, *367*(1608), 3455-3465.

Horton, P., & Black, M. T. (1980). Activation of adenosine 5′-triphosphate induced quenching of chlorophyll fluorescence by reduced plastoquinone, the basis of state I–state II transitions in chloroplasts, *FEBS Letters*, *119,* 141–144.

Horton, P., Ruban, A. V., & Walters, R. G. (1996). Regulation of light harvesting in green plants. *Annual Review of Plant Biology*, *47*(1), 655-684.

Huang, W., Yang, Y. J., Zhang, S. B., & Liu, T. (2018). Cyclic electron flow around photosystem I promotes ATP synthesis possibly helping the rapid repair of photodamaged photosystem II at low light. *Frontiers in Plant Science*, *9*, 239.

Huang, W., Yang, Y. J., Hu, H., & Zhang, S. B. (2016). Moderate photoinhibition of photosystem II protects photosystem I from photodamage at chilling stress in tobacco leaves. *Frontiers in Plant Science*, *7*, 182.

Ilík, P., Schansker, G., Kotabová, E., Váczi, P., Strasser, R. J., & Barták, M. (2006). A dip in the chlorophyll fluorescence induction at 0.2–2 s in Trebouxia-possessing lichens reflects a fast reoxidation of photosystem I. A comparison with higher plants. *Biochimica et Biophysica Acta (BBA)-Bioenergetics*, *1757*(1), 12-20.

Jahns, P., Latowski, D., & Strzalka, K. (2009). Mechanism and regulation of the violaxanthin cycle: the role of antenna proteins and membrane lipids. *Biochimica et Biophysica Acta (BBA)-Bioenergetics*, *1787*(1), 3-14.

Järvi, S., Suorsa, M., & Aro, E. M. (2015). Photosystem II repair in plant chloroplasts—Regulation, assisting proteins and shared components with photosystem II biogenesis. *Biochimica et Biophysica Acta (BBA)-Bioenergetics*, *1847*(9), 900-909.

Johnson, M. P. (2018). Metabolic regulation of photosynthetic membrane structure tunes electron transfer function. *Biochemical Journal*, *475*(7), 1225-1233.

Johnson, M.P., (2020). Photosynthesis, *Essays in Biochemistry*, *60* 255–273.

Johnson, M. P., Vasilev, C., Olsen, J. D., & Hunter, C. N. (2014). Nanodomains of cytochrome b 6 f and photosystem II complexes in spinach grana thylakoid membranes. *The Plant Cell*, *26*(7), 3051-3061.

Johnson, M. P., & Wientjes, E. (2020). The relevance of dynamic thylakoid organisation to photosynthetic regulation. *Biochimica et Biophysica Acta (BBA)-Bioenergetics*, *1861*(4), 148039.

Joliot, P., & Johnson, G. N. (2011). Regulation of cyclic and linear electron flow in higher plants. *Proceedings of the National Academy of Sciences*, *108*(32), 13317-13322.

Joliot, P., & Joliot, A. (2002). Cyclic electron transfer in plant leaf. *Proceedings of the National Academy of Sciences*, *99*(15), 10209-10214.

Joly, D., Jemâa, E., & Carpentier, R. (2010). Redox state of the photosynthetic electron transport chain in wild-type and mutant leaves of *Arabidopsis thaliana*: impact on photosystem II fluorescence. *Journal of Photochemistry and Photobiology B: Biology*, *98*(3), 180-187.

Kalachanis, D., & Manetas, Y. (2010). Analysis of fast chlorophyll fluorescence rise (O-K-J-I-P) curves in green fruits indicates electron flow limitations at the donor side of PSII and the acceptor sides of both photosystems. *Physiologia Plantarum*, *139*(3), 313-323.

Kalaji, H. M., Rastogi, A., Živčák, M., Brestic, M., Daszkowska-Golec, A., Sitko, K., Alsharafa, K. Y., Lofri, R., Stypinski, P., Samborska, I. A., & Cetner, M. D. (2018). Prompt chlorophyll fluorescence as a tool for crop phenotyping: an example of barley landraces exposed to various abiotic stress factors. *Photosynthetica*, *56*(3), 953-961.

Kalaji, H. M., Schansker, G., Brestic, M., Bussotti, F., Calatayud, A., Ferroni, L., Goltsev, V., Guidi, L., Jajoo, A., Li, P., Losciale, P., Mishra, V. K., Misra, A. N., Nebauer, S. G., Pancaldi, S., Panella, C., Pollastrini, M., Suresh, K., Tambussi, E., Yanniccari, M., Živčak, M., Cetner, M. D., Samborska, I. A., Stirbet, A., Olsovska, K., Kunderlikova, K., Shelonzek, H., Rusinowski, S., & Bąba, W. (2017). Frequently asked questions about chlorophyll fluorescence, the sequel. *Photosynthesis Research*, *132*, 13-66.

Kalaji, H. M., Schansker, G., Ladle, R. J., Goltsev, V., Bosa, K., Allakhverdiev, S. I., Brestic, M., Bussotti, F., Calatayud, A., Dabrowski, P., Elsheery, N. I., Ferroni, L., Guidi, L., Hogewoning, S. W., Jajoo, A., Misra, A. N., Nebauer, S. G.,

Pancaldi, S., Penella, C., Poli, D. B., Pollastrini, M., Romanowska-Duda, Z. B., Rutkowska, B., Serodio, J., Suresh, K., Szulc, W., Tambussi, E., Yanniccari, M., & Živčak, M. (2014). Frequently asked questions about in vivo chlorophyll fluorescence: practical issues. *Photosynthesis Research*, *122*, 121-158.

Kirchhoff, H. (2019). Chloroplast ultrastructure in plants. *New Phytologist*, *223*(2), 565-574.

Klughammer, C., & Schreiber, U. (2008). Complementary PS II quantum yields calculated from simple fluorescence parameters measured by PAM fluorometry and the Saturation Pulse method. *PAM application notes*, *1*(2), 201-247.

Kouřil, R., Wientjes, E., Bultema, J. B., Croce, R., & Boekema, E. J. (2013). High-light vs. low-light: effect of light acclimation on photosystem II composition and organization in *Arabidopsis thaliana*. *Biochimica et Biophysica Acta (BBA)-Bioenergetics*, *1827*(3), 411-419.

Kramer, D. M., Avenson, T. J., & Edwards, G. E. (2004). Dynamic flexibility in the light reactions of photosynthesis governed by both electron and proton transfer reactions. *Trends in Plant Science*, *9*(7), 349-357.

Kramer, D. M., Johnson, G., Kiirats, O., & Edwards, G. E. (2004b). New fluorescence parameters for the determination of QA redox state and excitation energy fluxes. *Photosynthesis Research*, *79*, 209-218.

Küpper, H., Benedikty, Z., Morina, F., Andresen, E., Mishra, A., & Trtílek, M. (2019). Analysis of OJIP chlorophyll fluorescence kinetics and QA reoxidation kinetics by direct fast imaging. *Plant physiology*, *179*(2), 369-381.

Laisk, A., & Oja, V. (2013). Thermal phase and excitonic connectivity in fluorescence induction. *Photosynthesis Research*, *117*, 431-448.

Laisk, A., & Oja, V. (2018). Kinetics of photosystem II electron transport: a mathematical analysis based on chlorophyll fluorescence induction. *Photosynthesis Research*, *136*, 63-82.

Lazár, D. (2015). Parameters of photosynthetic energy partitioning. *Journal of Plant Physiology*, *175*, 131-147.

Lazarević, B., Šatović, Z., Nimac, A., Vidak, M., Gunjača, J., Politeo, O., & Carović-Stanko, K. (2021). Application of phenotyping methods in detection of drought and salinity stress in basil (Ocimum basilicum L.). *Frontiers in Plant Science*, *12*, 629441.

Li, H., Wang, P., Weber, J. F., & Gerhards, R. (2017). Early identification of herbicide stress in soybean (*Glycine max* (L.) Merr.) using chlorophyll fluorescence imaging technology. *Sensors*, *18*(1), 21.

Li, X. P., Gilmore, A. M., Caffarri, S., Bassi, R., Golan, T., Kramer, D., & Niyogi, K. K. (2004). Regulation of photosynthetic light harvesting involves intrathylakoid lumen pH sensing by the PsbS protein. *Journal of Biological Chemistry*, *279*(22), 22866-22874.

Li, Z., Wakao, S., Fischer, B. B., & Niyogi, K. K. (2009). Sensing and responding to excess light. *Annual Review of Plant Biology*, *60*, 239-260.

Lichtenthaler, H. K., Buschmann, C., & Knapp, M. (2005). How to correctly determine the different chlorophyll fluorescence parameters and the chlorophyll fluorescence decrease ratio R Fd of leaves with the PAM fluorometer. *Photosynthetica*, *43*, 379-393.

Lichtenthaler, H. K., & Babani, F. (2004). Light adaptation and senescence of the photosynthetic apparatus. Changes in pigment composition, chlorophyll fluorescence parameters and photosynthetic activity. *Chlorophyll a fluorescence: a signature of photosynthesis*, *19*, 713-736.

Lima-Melo, Y., Gollan, P. J., Tikkanen, M., Silveira, J. A., & Aro, E. M. (2019). Consequences of photosystem-I damage and repair on photosynthesis and carbon use in Arabidopsis thaliana. *The Plant Journal*, *97*(6), 1061-1072.

Magyar, M., Sipka, G., Kovács, L., Ughy, B., Zhu, Q., Han, G., ... & Garab, G. (2018). Rate-limiting steps in the dark-to-light transition of Photosystem II-revealed by chlorophyll-a fluorescence induction. *Scientific Reports*, *8*(1), 2755.

Malnoë, A., Schultink, A., Shahrasbi, S., Rumeau, D., Havaux, M., & Niyogi, K. K. (2018). The plastid lipocalin LCNP is required for sustained photoprotective energy dissipation in Arabidopsis. *The Plant Cell*, *30*(1), 196-208.

Mathur, S., Jain, L., & Jajoo, A. (2018). Photosynthetic efficiency in sun and shade plants. *Photosynthetica*, *56*, 354-365.

Mathur, S., Jajoo, A., Mehta, P., & Bharti, S. (2011). Analysis of elevated temperature-induced inhibition of photosystem II using chlorophyll a fluorescence induction kinetics in wheat leaves (*Triticum aestivum*). *Plant Biology*, *13*(1), 1-6.

Mathur, S., Kalaji, H. M., & Jajoo, A. (2016). Investigation of deleterious effects of chromium phytotoxicity and photosynthesis in wheat plant. *Photosynthetica*, *54*(2), 185-192.

Matsubara, S., & Chow, W. S. (2004). Populations of photoinactivated photosystem II reaction centers characterized by chlorophyll a fluorescence lifetime in vivo. *Proceedings of the National Academy of Sciences*, *101*(52), 18234-18239.

Mekala, N. R., Suorsa, M., Rantala, M., Aro, E. M., & Tikkanen, M. (2015). Plants actively avoid state transitions upon changes in light intensity: role of light-harvesting complex II protein dephosphorylation in high light. *Plant Physiology*, *168*(2), 721-734.

Mehta, P., Jajoo, A., Mathur, S., & Bharti, S. (2010). Chlorophyll a fluorescence study revealing effects of high salt stress on Photosystem II in wheat leaves. *Plant Physiology and Biochemistry*, *48*(1), 16-20.

Nawrocki, W. J., Liu, X., Raber, B., Hu, C., De Vitry, C., Bennett, D. I., & Croce, R. (2021). Molecular origins of induction and loss of photoinhibition-related energy dissipation qI. *Science Advances*, *7*(52), eabj0055.

Nicol, L., Nawrocki, W. J., & Croce, R. (2019). Disentangling the sites of non-photochemical quenching in vascular plants. *Nature Plants*, *5*(11), 1177-1183.

Nilkens, M., Kress, E., Lambrev, P., Miloslavina, Y., Müller, M., Holzwarth, A. R., & Jahns, P. (2010). Identification of a slowly inducible zeaxanthin-dependent component of non-photochemical quenching of chlorophyll fluorescence generated under steady-state conditions in Arabidopsis. *Biochimica et Biophysica Acta (BBA)-Bioenergetics*, *1797*(4), 466-475.

Noble, E., Kumar, S., Görlitz, F. G., Stain, C., Dunsby, C., & French, P. M. (2017). In vivo label-free mapping of the effect of a photosystem II inhibiting herbicide in plants using chlorophyll fluorescence lifetime. *Plant Methods*, *13*, 1-16.

Osmond, C. B., Berry, J. A., Balachandran, S., Büchen-Osmond, C., Daley, P. F., & Hodgson, R. A. J. (1990). Potential consequences of virus infection for shade-sun acclimation in leaves. *Botanica Acta*, *103*(3), 226-229.

Oukarroum, A., Schansker, G., & Strasser, R. J. (2009). Drought stress effects on photosystem I content and photosystem II thermotolerance analyzed using Chl a fluorescence kinetics in barley varieties differing in their drought tolerance. *Physiologia Plantarum*, *137*(2), 188-199.

Pan, X., Ma, J., Su, X., Cao, P., Chang, W., Liu, Z., Zhang, X., & Li, M. (2018). Structure of the maize photosystem I supercomplex with light-harvesting complexes I and II. *Science*, *360*(6393), 1109-1113.

Pesaresi, P., Hertle, A., Pribil, M., Kleine, T., Wagner, R., Strissel, H., Ilhnatowicz, A., Bonardi, V., Scharfenberg, M., Schneider, A., Pfannschmidt, T., & Leister, D. (2009). Arabidopsis STN7 kinase provides a link between short-and long-term photosynthetic acclimation. *The Plant Cell*, *21*(8), 2402-2423.

Pfündel, E. (1998). Estimating the contribution of photosystem I to total leaf chlorophyll fluorescence. *Photosynthesis Research*, 56, 185-195.

Plöchinger, M., Torabi, S., Rantala, M., Tikkanen, M., Suorsa, M., Jensen, P. E., Aro, E. M., & Meurer, J. (2016). The low molecular weight protein PsaI stabilizes the light-harvesting complex II docking site of photosystem I. *Plant Physiology*, *172*(1), 450-463.

Porcar-Castell, A., Tyystjärvi, E., Atherton, J., Van der Tol, C., Flexas, J., Pfündel, E. E., ... & Berry, J. A. (2014). Linking chlorophyll a fluorescence to photosynthesis for remote sensing applications: mechanisms and challenges. *Journal of Experimental Botany*, *65*(15), 4065-4095.

Pribil, M., Pesaresi, P., Hertle, A., Barbato, R., & Leister, D. (2010). role of plastid protein phosphatase TAP38 in LHCII dephosphorylation and thylakoid electron flow, *PLoS Biology*, e100288.

Quick, W. P., & Stitt, M. (1989). An examination of factors contributing to non-photochemical quenching of chlorophyll fluorescence in barley leaves. *Biochimica et Biophysica Acta (BBA)-Bioenergetics*, *977*(3), 287-296.

Rantala, M., Rantala, S., & Aro, E. M. (2020). Composition, phosphorylation and dynamic organization of photosynthetic protein complexes in plant thylakoid membrane. *Photochemical & Photobiological Sciences*, *19*(5), 604-619.

Rantala, M., Tikkanen, M., & Aro, E. M. (2017). Proteomic characterization of hierarchical megacomplex formation in Arabidopsis thylakoid membrane. *The Plant Journal*, *92*(5), 951-962.

Rintamäki, E., Martinsuo, P., Pursiheimo, S., & Aro, E. M. (2000). Cooperative regulation of light-harvesting complex II phosphorylation via the plastoquinol and ferredoxin-thioredoxin system in chloroplasts. *Proceedings of the National Academy of Sciences*, *97*(21), 11644-11649.

Rodriguez-Heredia, M., Saccon, F., Wilson, S., Finazzi, G., Ruban, A. V., & Hanke, G. T. (2022). Protection of photosystem I during sudden light stress depends on ferredoxin: NADP (H) reductase abundance and interactions. *Plant Physiology*, *188*(2), 1028-1042.

Ruban, A. V. (2016). Nonphotochemical chlorophyll fluorescence quenching: mechanism and effectiveness in protecting plants from photodamage. *Plant physiology*, *170*(4), 1903-1916.

Ruban, A. V. (2018). Light harvesting control in plants. *FEBS Letters*, *592*(18), 3030-3039.

Schansker, G. (2022). Determining photosynthetic control, a probe for the balance between electron transport and Calvin–Benson cycle activity, with the DUAL-KLAS-NIR. *Photosynthesis Research*, *153*(3), 191-204.

Schansker, G., Tóth, S. Z., Holzwarth, A. R., & Garab, G. (2014). Chlorophyll a fluorescence: beyond the limits of the QA model. *Photosynthesis Research*, *120*, 43-58.

Schansker, G., Tóth, S. Z., & Strasser, R. J. (2006). Dark recovery of the Chl a fluorescence transient (OJIP) after light adaptation: The qT-component of non-photochemical quenching is related to an activated photosystem I acceptor side. *Biochimica et Biophysica Acta (BBA)-Bioenergetics*, *1757*(7), 787-797.

Schöttler, M. A., & Tóth, S. Z. (2014). Photosynthetic complex stoichiometry dynamics in higher plants: environmental acclimation and photosynthetic flux control. *Frontiers in Plant Science*, *5*, 188.

Schreiber, U., Neubauer, C., & Klughammer, C. (1989). Devices and methods for room-temperature fluorescence analysis. *Philosophical Transactions of the Royal Society of London. B, Biological Sciences*, *323*(1216), 241-251.

Schuller, J. M., Birrell, J. A., Tanaka, H., Konuma, T., Wulfhorst, H., Cox, N., Schuller, S. K., Thiemann, J., Lubitz, W., Sétif, P., Ikegami, T., Genji Kurisu, B. D. E., & Nowaczyk, M. M. (2019). Structural adaptations of photosynthetic complex I enable ferredoxin-dependent electron transfer. *Science*, *363*(6424), 257-260.

Schumann, T., Paul, S., Melzer, M., Dörmann, P., & Jahns, P. (2017). Plant growth under natural light conditions provides highly flexible short-term acclimation properties toward high light stress. *Frontiers in Plant Science*, *8*, 681.

Sheng, X., Liu, Z., Kim, E., & Minagawa, J. (2021). Plant and algal PSII–LHCII supercomplexes: structure, evolution and energy transfer. *Plant and Cell Physiology*, *62*(7), 1108-1120.

Sheue, C. R., Sarafis, V., Kiew, R., Liu, H. Y., Salino, A., Kuo-Huang, L. L., Yang, Y. P., Tsai, C. C., Lin, C. H., Yong, J. W. H., & Ku, M. S. (2007). Bizonoplast, a unique chloroplast in the epidermal cells of microphylls in the shade plant *Selaginella erythropus* (Selaginellaceae). *American Journal of Botany*, *94*(12), 1922-1929.

Shi, Q., Sun, H., Timm, S., Zhang, S., & Huang, W. (2022). Photorespiration alleviates photoinhibition of photosystem I under fluctuating light in tomato. *Plants*, *11*(2), 195.

Shimakawa, G., & Miyake, C. (2018). Oxidation of P700 ensures robust photosynthesis. *Frontiers in Plant Science*, *9*, 1617.

Shimakawa, G., & Miyake, C. (2019). What quantity of photosystem I is optimum for safe photosynthesis?. *Plant Physiology*, *179*(4), 1479-1485.

Siebke, K., & Weis, E. (1995). Assimilation images of leaves of Glechoma hederacea: analysis of non-synchronous stomata related oscillations. *Planta*, *196*, 155-165.

Sipka, G., Magyar, M., Mezzetti, A., Akhtar, P., Zhu, Q., Xiao, Y., ... & Garab, G. (2021). Light-adapted charge-separated state of photosystem II: structural and functional dynamics of the closed reaction center. *The Plant Cell*, *33*(4), 1286-1302.

Sonoike, K. (2011). Photoinhibition of photosystem I. *Physiologia Plantarum*, *142*(1), 56-64.

Staehelin, L. A., & Paolillo, D. J. (2020). A brief history of how microscopic studies led to the elucidation of the 3D architecture and macromolecular organization of higher plant thylakoids. *Photosynthesis Research*, *145*(3), 237-258.

Stirbet, A. (2013). Excitonic connectivity between photosystem II units: what is it, and how to measure it?. *Photosynthesis Research*, *116*, 189-214.

Stirbet, A., & Govindjee (2011). On the relation between the Kautsky effect (chlorophyll a fluorescence induction) and photosystem II: basics and applications of the OJIP fluorescence transient. *Journal of Photochemistry and Photobiology B: Biology*, *104*(1-2), 236-257.

Stirbet, A., & Govindjee (2012). Chlorophyll a fluorescence induction: a personal perspective of the thermal phase, the J–I–P rise. *Photosynthesis research*, *113*(1-3), 15-61.

Strasser, R. J., & Srivastava, A. (1995). Polyphasic chlorophyll a fluorescence transient in plants and cyanobacteria. *Photochemistry and Photobiology*, *61*(1), 32-42.

R.J. Strasser, M. Tsimilli-Michael, A. Srivastava, Analysis of the chlorophyll a fluorescence transient, in: G. Papageorgiou, Govindjee (Eds.), Chlorophyll *a* Fluorescence: A Signature of Photosynthesis, Advances in Photosynthesis and Respiration, Springer, Dordrecht, 2004, pp. 321–362.

Sun, D., Zhu, Y., Xu, H., He, Y., & Cen, H. (2019). Time-series chlorophyll fluorescence imaging reveals dynamic photosynthetic fingerprints of sos mutants to drought stress. *Sensors*, *19*(12), 2649.

Suorsa, M., Rantala, M., Mamedov, F., Lespinasse, M., Trotta, A., Grieco, M., Vuotio, E., Tikkanen, M., Järvi, S., & Aro, E. M. (2015). Light acclimation involves dynamic re-organization of the pigment–protein megacomplexes in non-appressed thylakoid domains. *The Plant Journal*, *84*(2), 360-373.

Takagi, D., Ishizaki, K., Hanawa, H., Mabuchi, T., Shimakawa, G., Yamamoto, H., & Miyake, C. (2017). Diversity of strategies for escaping reactive oxygen species production within photosystem I among land plants: P700 oxidation system is prerequisite for alleviating photoinhibition in photosystem I. *Physiologia Plantarum*, *161*(1), 56-74.

Tan, S. L., Liu, T., Zhang, S. B., & Huang, W. (2020). Balancing light use efficiency and photoprotection in tobacco leaves grown at different light regimes. *Environmental and Experimental Botany*, *175*, 104046.

Tietz, S., Hall, C. C., Cruz, J. A., & Kramer, D. M. (2017). NPQ (T): a chlorophyll fluorescence parameter for rapid estimation and imaging of non-photochemical quenching of excitons in photosystem-II-associated antenna complexes. *Plant, Cell & Environment, 4(*8), 1243-1255.

Tiwari, A., Mamedov, F., Grieco, M., Suorsa, M., Jajoo, A., Styring, S., Tikkanen, M., & Aro, E. M. (2016). Photodamage of iron–sulphur clusters in photosystem I induces non-photochemical energy dissipation. *Nature Plants*, *2*(4), 1-9.

Tomar, R. S., & Jajoo, A. (2014). Fluoranthene, a polycyclic aromatic hydrocarbon, inhibits light as well as dark reactions of photosynthesis in wheat (*Triticum aestivum*). *Ecotoxicology and Environmental Safety*, *109*, 110-115.

Tóth, S. Z., Schansker, G., Garab, G., & Strasser, R. J. (2007). Photosynthetic electron transport activity in heat-treated barley leaves: the role of internal alternative electron donors to photosystem II. *Biochimica et Biophysica Acta (BBA)-Bioenergetics*, *1767*(4), 295-305.

Tsai, Y. C., Chen, K. C., Cheng, T. S., Lee, C., Lin, S. H., & Tung, C. W. (2019). Chlorophyll fluorescence analysis in diverse rice varieties reveals the positive correlation between the seedlings salt tolerance and photosynthetic efficiency. *BMC plant biology*, *19*, 1-17.

Tsimilli-Michael, M. (2020). Revisiting JIP-test: An educative review on concepts, assumptions, approximations, definitions and terminology. *Photosynthetica*, *58*, 275-292.

Tsimilli-Michael, M., & Strasser, R. J. (2008). In vivo assessment of stress impact on plant's vitality: applications in detecting and evaluating the beneficial role of mycorrhization on host plants. *Mycorrhiza: state of the art, genetics and molecular biology, eco-function, biotechnology, eco-physiology, structure and systematics*, 679-703.

Valcke, R. (2021). Can chlorophyll fluorescence imaging make the invisible visible?. *Photosynthetica*, *59*(SPECIAL ISSUE), 381-398.

Vredenberg, W. (2011). Kinetic analyses and mathematical modeling of primary photochemical and photoelectrochemical processes in plant photosystems. *Biosystems*, *103*(2), 138-151.

Wang, M., Dai, W., Du, J., Ming, R., Dahro, B., & Liu, J. H. (2019). ERF 109 of trifoliate orange (Poncirus trifoliata (L.) Raf.) contributes to cold tolerance by directly regulating expression of Prx1 involved in antioxidative process. *Plant Biotechnology Journal*, *17*(7), 1316-1332.

Ware, M. A., Belgio, E., & Ruban, A. V. (2015). Photoprotective capacity of non-photochemical quenching in plants acclimated to different light intensities. *Photosynthesis Research*, *126*, 261-274.

Wientjes, E., van Amerongen, H., & Croce, R. (2013). LHCII is an antenna of both photosystems after long-term acclimation. *Biochimica et Biophysica Acta (BBA)-Bioenergetics*, *1827*(3), 420-426.

Wientjes, E., van Amerongen, H., & Croce, R. (2013b). Quantum yield of charge separation in photosystem II: functional effect of changes in the antenna size upon light acclimation. *The Journal of Physical Chemistry B*, *117*(38), 11200-11208.

Wood, W. H., MacGregor-Chatwin, C., Barnett, S. F., Mayneord, G. E., Huang, X., Hobbs, J. K., Hunter, C. N., & Johnson, M. P. (2018). Dynamic thylakoid stacking regulates the balance between linear and cyclic photosynthetic electron transfer. *Nature Plants*, *4*(2), 116-127.

Yamamoto, H., & Shikanai, T. (2019). PGR5-dependent cyclic electron flow protects photosystem I under fluctuating light at donor and acceptor sides. *Plant physiology*, *179*(2), 588-600.

Yang, W., Feng, H., Zhang, X., Zhang, J., Doonan, J. H., Batchelor, W. D., ... & Yan, J. (2020). Crop phenomics and high-throughput phenotyping: past decades, current challenges, and future perspectives. *Molecular Plant*, *13*(2), 187-214.

Yokono, M., Takabayashi, A., Akimoto, S., & Tanaka, A. (2015). A megacomplex composed of both photosystem reaction centres in higher plants. *Nature Communications*, *6*(1), 6675.

Yokono, M., Takabayashi, A., Kishimoto, J., Fujita, T., Iwai, M., Murakami, A., Akimot, s., & Tanaka, A. (2019). The PSI–PSII megacomplex in green plants. *Plant and Cell Physiology*, *60*(5), 1098-1108.

Zhang, S. B., Wang, J. H., & Huang, W. (2021). Pre-illumination at high light significantly alleviates the over-reduction of photosystem I under fluctuating light. *Plant Science*, *312*, 111053.

Živčak, M., Brestic, M., & Kalaji, H. M. (2014). Photosynthetic responses of sun-and shade-grown barley leaves to high light: is the lower PSII connectivity in shade leaves associated with protection against excess of light?. *Photosynthesis Research*, *119*, 339-354.

Živčak, M., Brestic, M., Balatova, Z., Drevenakova, P., Olsovska, K., Kalaji, H. M., Yang, X., & Allakhverdiev, S. I. (2013). Photosynthetic electron transport and specific photoprotective responses in wheat leaves under drought stress. *Photosynthesis Research*, *117*, 529-546.

Zivcak, M., Brestic, M., Kunderlikova, K., Olsovska, K., & Allakhverdiev, S. I. (2015). Effect of photosystem I inactivation on chlorophyll a fluorescence induction in wheat leaves: does activity of photosystem I play any role in OJIP rise?. *Journal of Photochemistry and Photobiology B: Biology*, *152*, 318-324.

Appendix 1

Functional characterization of the light harvesting complex II (LHCII) in *Selaginella martensii*

Selaginella martensii Spring (Lycopodiophyta) is an ancient vascular plant characterized by a peculiar thylakoid membrane structure and dynamics. Differently from the most studied land plants, *S. martensii* contains an overabundance of Light Harvesting Complex II (LHCII) in comparison to the photosystem availability (Ferroni et al. 2016). Most LHCII is in the form of free trimers, and only a small fraction of it is bound to PSII or organized in megacomplexes with PSI and PSII (Ferroni et al. 2016). In angiosperms, the LHCII found in excess of that stably associated with PSII is generally deemed to be involved in excess energy dissipation (Holzwarth et al. 2009, Nicol et al. 2019, Shukla et al. 2020) and excitation balancing between the two photosystems (Wientjes et al. 2013, Grieco et al. 2016, Wood and Johnson, 2020). In *S. martensii* the excess LHCII could be mostly coupled with PSI or uncoupled from photosystems.

This project aimed at measuring the degree of association of LHCII with each photosystem in different light conditions. The hypothesis was tested whether LHCII works as an antenna for PSI even in the dark, and whether the PSII functional antenna size undergoes short-term changes. Other related aims were the quantification of the LHCII amount uncoupled from the photosystems and the detection of energy spillover from PSII to PSI, in continuity with previous works on *S. martensii* (Colpo et al. 2022, Ferroni et al. 2021). The experiment involved biochemical analyses on the composition of the thylakoid membrane, steady state absorption and fluorescence measurements on intact thylakoids and isolated complexes on thylakoids previously short-term acclimated to the different conditions, such as darkness (relaxed thylakoid membrane), low-intensity light (maximization of PSI-LHCII association) and far-red light (maximization of PSII-LHCII association).

Illumination treatments and thylakoids isolation were performed in the Laboratory of Plant Cytophysiology at the University of Ferrara. *S. martensii* plants were acclimated to dark for 30 minutes or treated with 60 minutes of low light (100 µmol photons m^{-2} s^{-1}) or exposed to far-red light (15 minutes exposure). Thylakoids were extracted according to Giovanardi et al. (2018). Thylakoids were shipped in dry ice to the LaserLab laboratories at the Vrije University of Amsterdam (NL) and stored in fridges at -80 °C until use.

The biochemical characterization of the membrane complexes separation profiles was performed by ultracentrifugation on sucrose gradient as described in Tian et al. (2015).

Fluorescence emission spectra of bands separated from sucrose density gradient and intact thylakoids were analysed at room temperature and at 77 K on a Fluorolog 3.22 spectrofluorometer (HORIBA Jobin Yvon,

Longjumeau, France). Together with *S. martensii* thylakoids, *Arabidopsis thaliana* thylakoids were analysed as a reference.

The result of the band separation on a sucrose gradient is shown in Fig. 1, in which the assignment of each band to a specific thylakoid complex is reported. The main differences between *S. martensii* and *A. thaliana* separation profiles were the absence of the band 4 (LHCII-M trimer + minor antennae) in dark-acclimated *S. martensii* and the detection of an additional band in all *S. martensii* samples (band 6'). The reduced abundance of Lhcb monomers (B2), PSII core dimers (B5), PSI-LHCI (B6) and PSII supercomplexes (B7) in *S. martensii* samples was evident compared to *A. thaliana*. At the same time, *S. martensii* samples were enriched in LHCII trimer band (B3). These comparative results were consistent with the previous knowledge about *S. martensii* thylakoid membrane structure and organization, with a lower (PSI+PSII)/LHCII ratio compared to *A. thaliana*. The presence of band 6', assigned to a complex containing PSI and PSII, is also in line with the idea of an extensive contact of the two photosystems in *S. martensii* membranes (Ferroni et al. 2016), most probably allowed by the complex tridimensional structure of the thylakoid system, in which a part of the stroma thylakoids is enclosed inside the network formed by the grana stacks (Chapter 2).

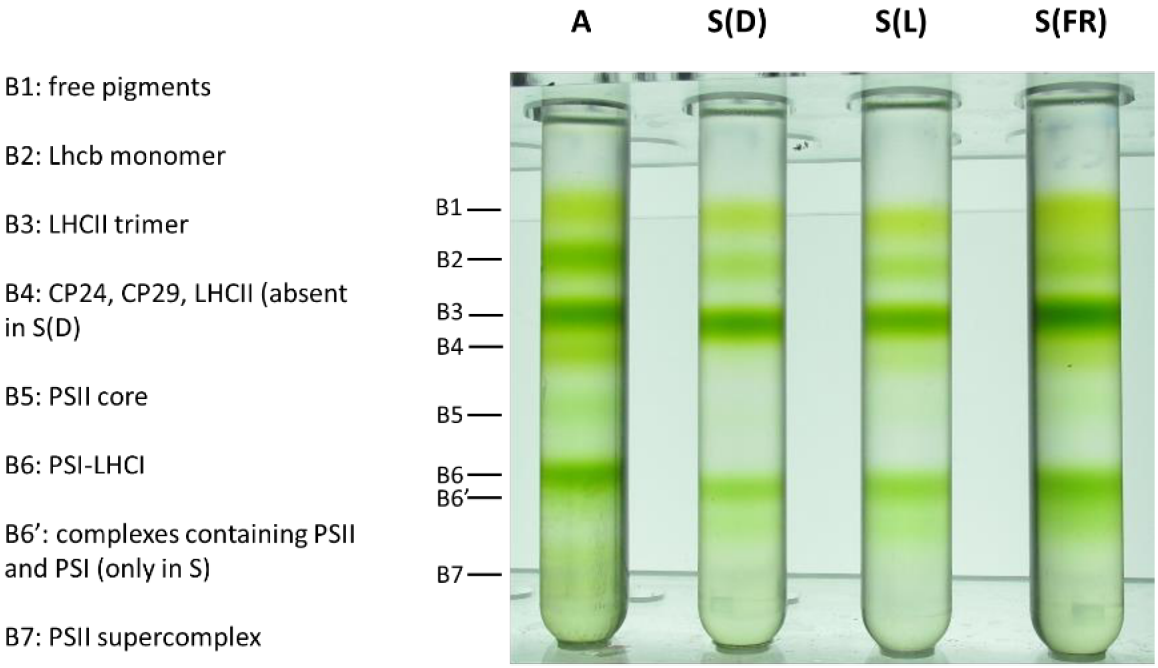

Figure 1. Separation profile of *Arabidopsis thaliana* and *Selaginella martensii* after ultracentrifugation on sucrose density gradient.

In Fig. 2 the spectra acquired from the whole thylakoids at the spectrofluorometer are reported (77K measurements by exciting the sample at the wavelength of 465 nm). On the left, normalization was done on the emission peak of PSI (about 730 nm), while on the right on the peak of PSII (about 680 nm). Taking sample D as a reference, short-term acclimation to low light (sample L, in green) resulted in a reduction of the functional association of LHCII with PSII to the benefit of association with PSI, as the state transition of LHCII antennae from PSII to PSI is stimulated, so that excitation is distributed in a balanced manner between the two photosystems (exposure to growth light, in fact, stimulates this process). In contrast, exposure to FR light resulted in an increased association of LHCII with PSII compared with PSI (far-red light in fact has the effect of selectively exciting PSI). The comparative analysis between the three conditions (D, L, FR) confirmed the hypothesis that the LHCII antenna is functionally associated with PSI under dark conditions and could be (partly) uncoupled from it by FR. This result was a first indication in *S. martensii* of the surprising functional flexibility of the LHCII antenna to associate with PSII or PSI in response to different light conditions.

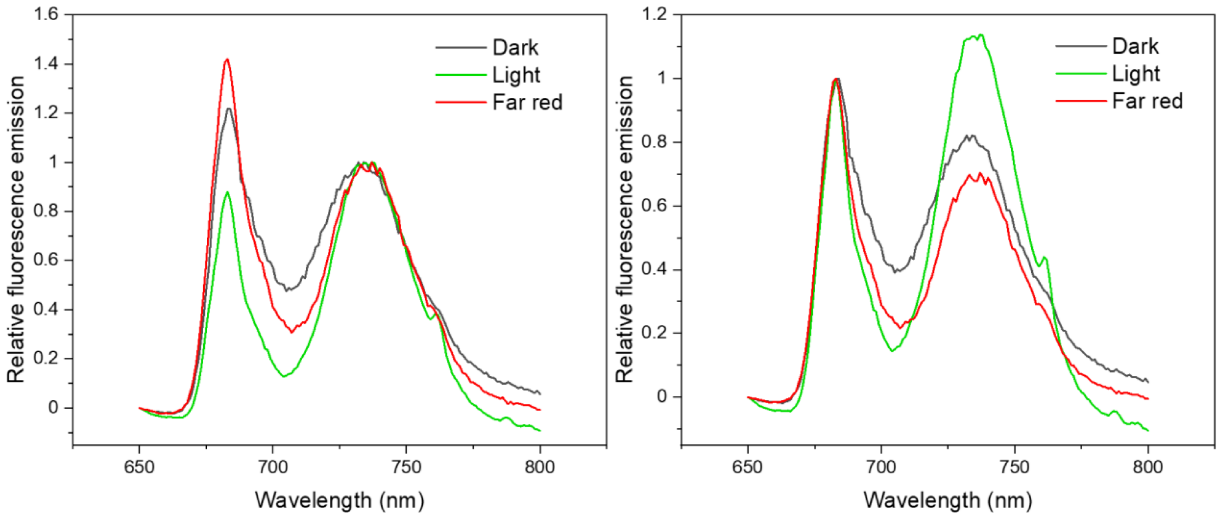

Figure 2. 77 K fluorescence emission profiles of whole thylakoids of *Selaginella martensii* plants acclimated to dark (black line), low light (green line) and far-red light (red line).

Acknowledgements

The project was financed by the LaserLab Europe infrastructure and was made possible thanks to the supervision of Prof. Roberta Croce and the technical and theoretical support by Dr. Chen Hu for the biochemical analyses and Dr. Ahmad Bhatti for the biophysical analyses.

References

Colpo, A., Baldisserotto, C., Pancaldi, S., Sabia, A., & Ferroni, L. (2022). Photosystem II photoinhibition and photoprotection in a lycophyte, Selaginella martensii. *Physiologia Plantarum*, *174*(1), e13604.

Ferroni, L., Suorsa, M., Aro, E. M., Baldisserotto, C., & Pancaldi, S. (2016). Light acclimation in the lycophyte *Selaginella martensii* depends on changes in the amount of photosystems and on the flexibility of the light-harvesting complex II antenna association with both photosystems. *New Phytologist*, *211*(2), 554-568.

Giovanardi, M., Pantaleoni, L., Ferroni, L., Pagliano, C., Albanese, P., Baldisserotto, C., & Pancaldi, S. (2018). In pea stipules a functional photosynthetic electron flow occurs despite a reduced dynamicity of LHCII association with photosystems. *Biochimica et Biophysica Acta (BBA)-Bioenergetics*, *1859*(10), 1025-1038.

Grieco, M., Suorsa, M., Jajoo, A., Tikkanen, M., & Aro, E. M. (2015). Light-harvesting II antenna trimers connect energetically the entire photosynthetic machinery—including both photosystems II and I. *Biochimica et Biophysica Acta (BBA)-Bioenergetics*, *1847*(6-7), 607-619.

Holzwarth, A. R., Miloslavina, Y., Nilkens, M., & Jahns, P. (2009). Identification of two quenching sites active in the regulation of photosynthetic light-harvesting studied by time-resolved fluorescence. *Chemical Physics Letters*, *483*(4-6), 262-267.

Nicol, L., Nawrocki, W. J., & Croce, R. (2019). Disentangling the sites of non-photochemical quenching in vascular plants. *Nature Plants*, *5*(11), 1177-1183.

Shukla, M. K., Watanabe, A., Wilson, S., Giovagnetti, V., Moustafa, E. I., Minagawa, J., & Ruban, A. V. (2020). A novel method produces native light-harvesting complex II aggregates from the photosynthetic membrane revealing their role in nonphotochemical quenching. *Journal of Biological Chemistry*, *295*(51), 17816-17826.

Tian, L., Dinc, E., & Croce, R. (2015). LHCII populations in different quenching states are present in the thylakoid membranes in a ratio that depends on the light conditions. *The Journal of Physical Chemistry Letters*, *6*(12), 2339-2344.

Wientjes, E., van Amerongen, H., & Croce, R. (2013). LHCII is an antenna of both photosystems after long-term acclimation. *Biochimica et Biophysica Acta (BBA)-Bioenergetics*, *1827*(3), 420-426.

Wood, W. H., & Johnson, M. P. (2020). Modeling the role of LHCII-LHCII, PSII-LHCII, and PSI-LHCII interactions in state transitions. *Biophysical Journal*, *119*(2), 287-299.

Appendix 2

Photosystem II functional antenna size and excitonic connectivity in *Selaginella martensii*

Selaginella martensii displays a surprising ability to survive and acclimate to different light regimes, such as deep shade and full sunlight (Ferroni et al. 2016, 2021). The long-term photosynthetic acclimation process varies the Photosystem II / Photosystem I (PSII/PSI) ratio, while the relative content of PSII Light Harvesting Complex (LHCII) remains invariable. The latter is a peculiarity of the lycophyte because the majority of the vascular plants cope with the increasing light availability decreasing the amount of LHCII. The degree of association between LHCII and the two photosystems is subjected to major long-term rearrangements in *S. martensii*: LHCII association to PSII is more relevant in shade plants, while sun plants are characterized by more extensive LHCII-PSI associations (Ferroni et al. 2016). Such rearrangements strongly influence several functional properties of the photosynthetic membrane (Chapter 1), but most of the features that allow the efficient light acclimation of *S. martensii* to different light regimes remains still unclear.

This work aims to investigate how the long-term light acclimation affects two main aspects of the light harvesting process, i.e., the functional antenna size of PSII and the excitonic connectivity between PSII units. *S. martensii* plants were acclimated long-term to deep shade (L), intermediate shade (M) and full sunlight (H). The OJIP transients were measured using a Handy-PEA fluorometer (Hansatech, UK) after exposure to two different conditions: 20 minutes of dark acclimation or 20 minutes of far-red light (FR) exposure. Dark acclimation generally allows the discharge of electrons in the membrane and permits the recovery of all the excitation energy quenching components to evaluate the two parameters in a relaxed condition (Stirbet and Govindjee 2011). However, the discharge may be incomplete because of residual electron recycling from the stroma to plastoquinone. Moreover, the antenna size of PSII may be not the maximum possible because of the LHCII serving PSI in darkness (Appendix 1). The preferential excitation of PSI by FR allows the full plastoquinone oxidation and promotes the migration of LHCII to the PSII region, potentially reestablishing the maximum PSII antenna size. The functional antenna of PSII was measured as the ABS/RC parameter according to the Theory of Energy Fluxes (Strasser et al. 2004, Stirbet and Govindjee 2011); the PSII excitonic connectivity was analyzed based on the curvature of the O-K trait (0.02-0.3 ms) according to the model by Strasser and Stirbet (2001).

Fig. 1 shows that ABS/RC is poorly dependent on the light acclimation regime and only partly responding to the short-term FR treatment. More interestingly, the PSII excitonic connectivity is strongly dependent on the light acclimation regime and well responsive to FR. In fact, FR significantly reduced the connectivity between PSII units, and this effect was more relevant in H plants. Collectively, the results obtained suggest that each PSII unit is served by a nearly constant LHCII antenna complement independent of the growth light regime.

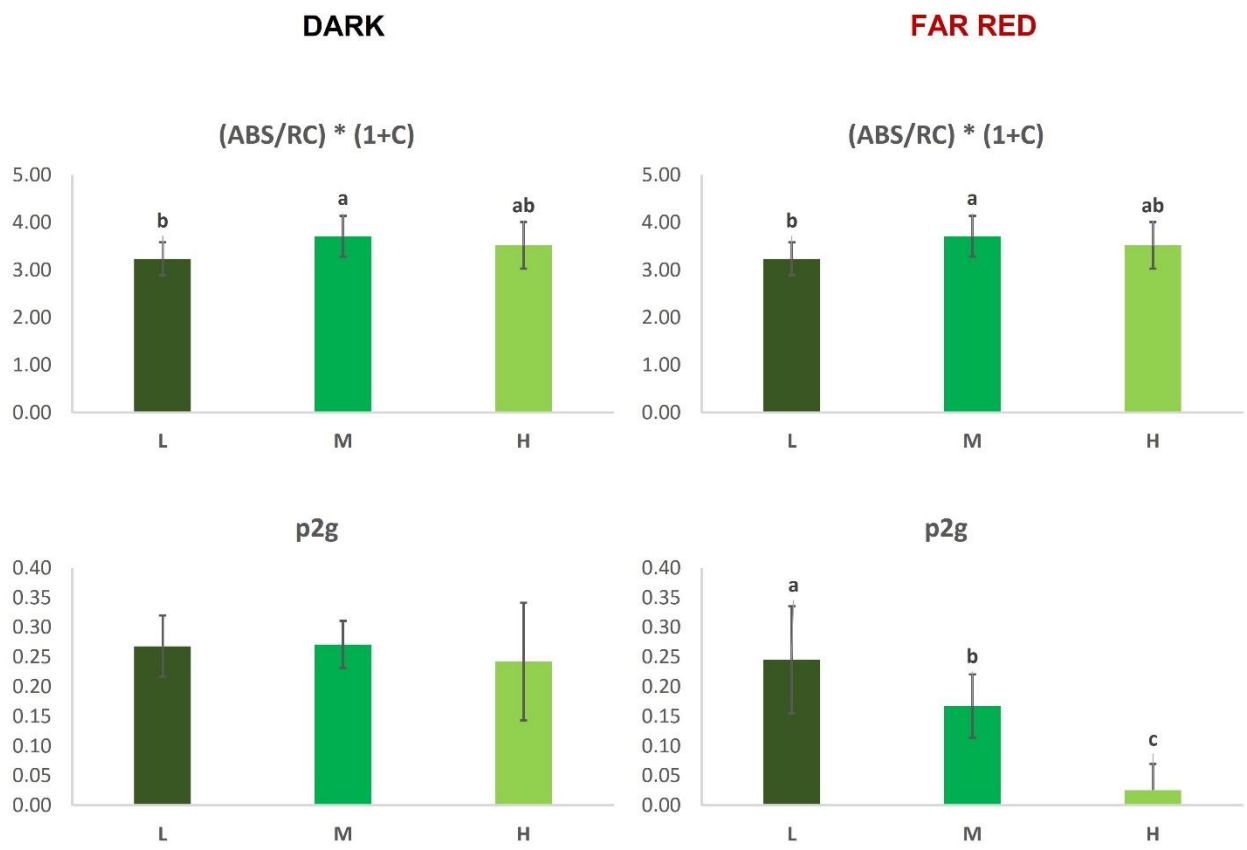

Figure 1. PSII antenna size accounting for the PSII connectivity (ABS/RC)*(1+C) (where C is the curvature parameter) and corresponding values of overall grouping probability between PSII units (p2g) measured in *Selaginella martensii* plants acclimated to contrasting light regimes (L=deep shade, M= intermediate shade and H=full sunlight). On the left, the values measured in dark acclimated plants (20 minutes), on the right the values for far-red light acclimated plants (20 minutes). Histogram represents average values ±standard error for n = 7-10; different letters indicate a significant difference at $P < 0.05$, as determined using one-factor ANOVA followed by Tukey's test

The abundant LHCII trimers characterizing *S. martensii* thylakoids presumably form a lake that embeds both PSI (Ferroni et al. 2016, Appendix 1) and PSII; however, in the grana appressions the extreme abundance of LHCII very likely does not allow a permissive distance for the connectivity of the PSII units. The result is that the PSII units exhibit an intriguing “puddle” organization, which becomes a prefect “zero-connectivity” in H plants, possibly participating in PSII photoprotection (Živčak et al. 2014). This organization is compatible with the extreme thylakoid appression which in *S. martensii* emphasizes the lateral extension of the grana partitions (Chapter 2).

References

Ferroni, L., Brestič, M., Živčak, M., Cantelli, R., & Pancaldi, S. (2021). Increased photosynthesis from a deep-shade to high-light regime occurs by enhanced CO2 diffusion into the leaf of *Selaginella martensii*. *Plant Physiology and Biochemistry*, 160, 143-154.

Ferroni, L., Suorsa, M., Aro, E. M., Baldisserotto, C., & Pancaldi, S. (2016). Light acclimation in the lycophyte *Selaginella martensii* depends on changes in the amount of photosystems and on the flexibility of the light-harvesting complex II antenna association with both photosystems. *New Phytologist*, *211*(2), 554-568.

Stirbet, A., Govindjee (2011). On the relation between the Kautsky effect (chlorophyll a fluorescence induction) and photosystem II: basics and applications of the OJIP fluorescence transient. *Journal of Photochemistry and Photobiology B: Biology*, 104(1-2), 236-257.

Strasser, R. J., & Stirbet, A. D. (2001). Estimation of the energetic connectivity of PS II centres in plants using the fluorescence rise O–J–I–P: Fitting of experimental data to three different PS II models. *Mathematics and Computers in Simulation*, 56(4-5), 451-462.

Strasser, R.J., Tsimilli-Michael, M., Srivastava, A., Analysis of the chlorophyll *a* fluorescence transient, in: G. Papageorgiou, Govindjee (Eds.), Chlorophyll a Fluorescence: A Signature of Photosynthesis, Advances in Photosynthesis and Respiration, Springer, Dordrecht, 2004, pp. 321–362.

Zivcak, M., Brestic, M., Kalaji, H. M., & Govindjee (2014). Photosynthetic responses of sun-and shade-grown barley leaves to high light: is the lower PSII connectivity in shade leaves associated with protection against excess of light?. *Photosynthesis Research*, 119, 339-354.

Appendix 3

In-field chlorophyll *a* fluorescence-based phenotyping of drought stress effect on three apple tree (*Malus domestica* Borkh) rootstocks

The plant lifetime is characterized by a continuous fight-to-survive against environmental stresses, both biotic and abiotic. Within the latter, drought stress has become a hot topic because of its impact on the natural ecosystem fitness as well as on the crop productivity. The prevention of irreversible damages due to such unfavorable environmental conditions depends on the responsiveness of environmental operators, farmers, and scientists, which are constantly in the search for fast and non-invasive screening techniques. Some of these techniques rely on the monitoring of the plant photosynthetic efficiency using field tools, such as portable fluorometers.

In this work, the progress of drought stress in apple trees (*Malus domestica* Borkh) during the productive season (May-September) was monitored using a pocket plant phenotyping approach based on chlorophyll *a* direct fluorescence measurement (HandyPEA fluorometer, Hansatech, Norfolk, UK). Drought resistance in apple is strongly dependent on the rootstock used (Tworkowski et al. 2016). The comparative study was performed on *M. domestica* cv. Superchief® trees grafted on three different rootstocks: CIVP21^{pbr}, M106, M26. CIVP21^{pbr} is a new rootstock patented by Consorzio Italiano Vivaisti and was selected for its wide root system, potentially supporting a superior resistance to drought stress. The plants were cultivated in water shortage conditions and compared to their control counterpart, which were normally irrigated throughout the season. Soil moisture and temperature were monitored using Watermark (Irrometer, Riverside, USA) sensors. Measurements were performed at intervals of 7-10 days during the whole experiment.

Fig. 1 illustrates the variation in soil moisture and temperature during the experiment. After ca. 20 days from the interruption of the irrigation, the soil water tension reached a value of 13 kPa, with three subsequent rain events reestablishing temporarily a higher soil water content (though not evident from the average water content monitoring at 10 cm). In sandy soils, the need for crop irrigation to avoid cavitation and turgor loss in plants already occurs at soil moisture tensions as low as 10 kPa, when the soil starts to lose water (Souza et al. 2021). Therefore, the drought stress experienced by the plants was moderate and chronic.

The fluorescence parameters monitored during the experiment were calculated from the OJIP transient according to the JIP-test theory (Strasser et al. 2004, Stirbet and Govindjee 2011). To help disentangle the comparative effect of drought stress in the presence of other variations induced by environmental factors, for each rootstock type the parameters were normalized on the corresponding well-watered controls. The results indicated that drought stress had an influence on several fluorometric parameters, with variable intensity depending on the rootstock. Fig. 2 shows two selected parameters which have a potential as indexes to assess the effect of a moderate chronic drought stress. Fv/Fo relates to the photochemical capacity of PSII; $PI_{abs\ tot}$ is

the performance index on absorption basis, derived from the Energy Flux Theory. The latter is a parameter depending on the apparent PSII antenna size, the PSII photochemical activity, the probability of electron transport from PSII to the plastoquinone pool and the probability of electron transport from the plastoquinone to the PSI end acceptors. As a very comprehensive parameter and despite its large variability, it shows the decline in the potential photosynthetic performance during the experiment in all rootstocks, without a clear differential response between the rootstocks.

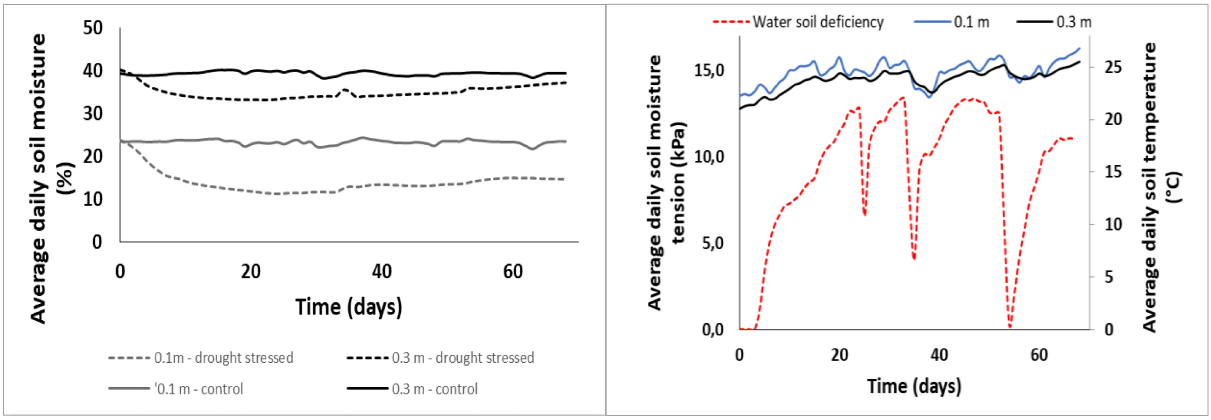

Figure 1. On the left, average daily soil moisture at a depth of 10 cm and 30 cm in the irrigated or non-irrigated parcels; on the right, the average soil moisture is expressed as water potential in the non-irrigated parcel, being 0 kPa in the irrigated parcel. The corresponding variations in soil temperature are also shown.

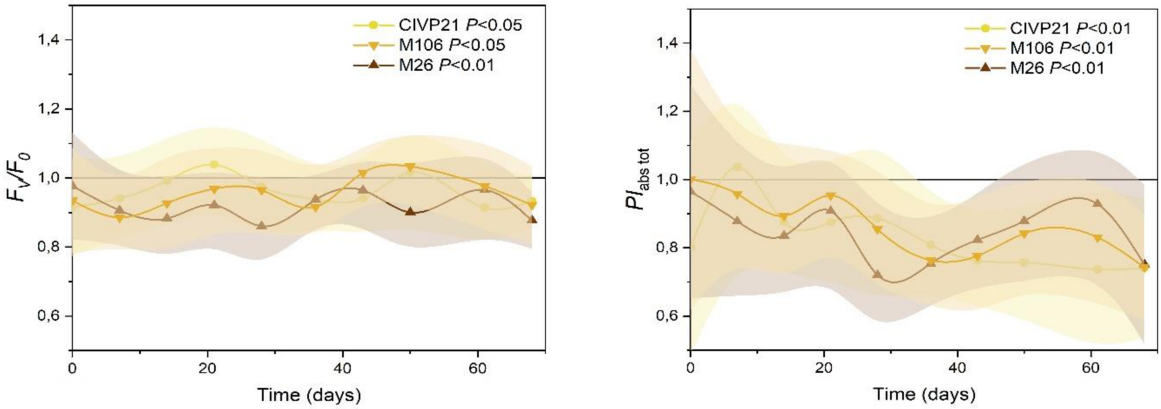

Figure 2. Examples of JIP-test-derived parameters evaluated in apple trees with three different rootstocks under drought stress. On the left, the time-course variation of the photochemical capacity of PSII, Fv/Fo; on the right the performance index on absorption basis $PI_{abs\ tot}$. The parameters values of the irrigated controls are assigned a value of 1; the colored bands represent standard deviations (*N*=15-25 determinations).

At the end of the season, the plant productivity was evaluated and is reported in Fig. 3. The low soil moisture negatively affected the seasonal productivity of all water-stressed rootstocks compared to control plants. Although the normalized average harvest underwent a 30% decline in all cases, the rootstocks showed a

specificity with respect to the fruit number and shape. M26 maintained a higher fruits production than M106 and CIVP21[pbr], but its fruits had a lower average weight.

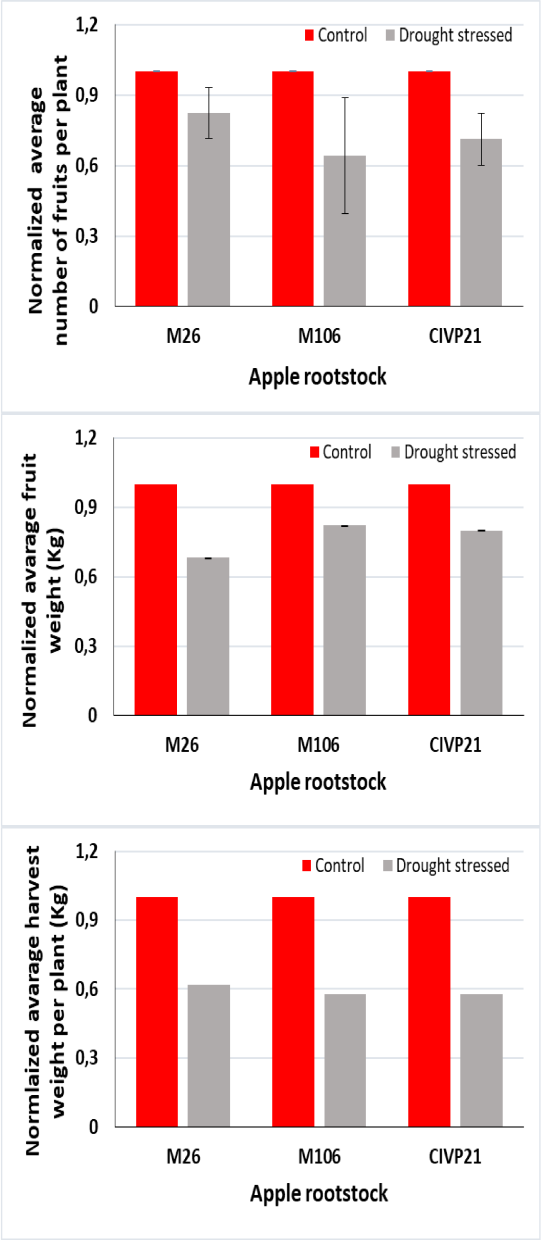

Figure 3. Production yields evaluated in apple trees with three different rootstocks under drought stress, normalized to the corresponding well-watered plants. Results are averages with standard deviations (N=3-5 plants per type).

The comparison of fluorometric and productive results indicate the complexity of response to drought depending on the rootstock. At a first glance, the similar overall decline in $PI_{abs\ tot}$ was in line with the same loss in productivity experienced by all rootstocks. However, drought stress influenced differentially the plants if interest is in the two basic properties if fruits, i.e., their number and weight. Although the JIP-test is being used for the analysis of apple cultivars and rootstocks to drought (e.g., Mihaljević et al. 2021, Shi et al. 2020), there is a still unexplored potential of the JIP parameters in a predictive way. The subsequent phases of the research will screen the whole set of JIP-test parameters for significant correlations with the productive yields. Moreover, as an alternative approach, the large datasets of OJIP transients make them suitable to the analysis with artificial intelligence and deep learning methods.

Acknowledgments

This research was developed within the project "*Metodi fluorimetrici innovativi a supporto della selezione varietale di fragola e di portinnesti di melo contro lo stress idrico*" granted to Lorenzo Ferroni by the University of Ferrara with the contribution of the Camera di Commercio Industria, Artigianato e Agricoltura di Ferrara (Bando 2019). Marzio Zaccarini and Alessandro Forlani (Consorzio Italiano Vivaisti) are kindly thanked for their excellent constant support in the field work.

References

Mihaljević, I., Viljevac Vuletić, M., Šimić, D., Tomaš, V., Horvat, D., Josipović, M., et al. (2021). Comparative study of drought stress effects on traditional and modern apple cultivars. *Plants*, 10(3), 561.

Shi, C. Y., Liu, L., Li, Q. L., Wei, Z. F., & Gao, D. T. (2022). Comparison of drought resistance of rootstocks' M9-T337'and'M26'grafted with'Huashuo'apple. *Horticulture, Environment, and Biotechnology*, 63(3), 299-310.

Souza, J. V., Ming, L. C., Santos, M. A., Simon, J. E., Juliani, H. R., & Saad, J. C. (2021). Effect of water regime and harvest stage on essential oil accumulation in basil plant growing in sandy soil. *Irrigation Science*, 39, 493-503.

Stirbet, A., Govindjee (2011). On the relation between the Kautsky effect (chlorophyll a fluorescence induction) and photosystem II: basics and applications of the OJIP fluorescence transient. Journal of Photochemistry and Photobiology B: Biology, 104(1-2), 236-257.

Strasser, R.J., Tsimilli-Michael, M., Srivastava, A., Analysis of the chlorophyll a fluorescence transient, in: G. Papageorgiou, Govindjee (Eds.), Chlorophyll a Fluorescence: A Signature of Photosynthesis, Advances in Photosynthesis and Respiration, Springer, Dordrecht, 2004, pp. 321–362.

Tworkoski, T., Fazio, G., & Glenn, D. M. (2016). Apple rootstock resistance to drought. *Scientia Horticulturae*, 204, 70-78.

Publications and other activities

Publications presented in this thesis

Colpo, A., Baldisserotto, C., Pancaldi, S., Sabia, A., & Ferroni, L. (2022). Photosystem II photoinhibition and photoprotection in a lycophyte, *Selaginella martensii*. *Physiologia Plantarum*, *174*(1), e13604.

Colpo, A., Demaria, S., Baldisserotto, C., Pancaldi, S., Brestič, M., Živčak, M., & Ferroni, L. Long-term alleviation of the functional phenotype in chlorophyll-deficient wheat and impact on productivity: a semi-field phenotyping experiment. (2023) *Plants*, accepted with revisions.

Additional publications

Ferroni, L., Colpo, A., Baldisserotto, C., & Pancaldi, S. (2021). In an ancient vascular plant the intermediate relaxing component of NPQ depends on a reduced stroma: Evidence from dithiothreitol treatment. *Journal of Photochemistry and Photobiology B: Biology*, *215*, 112114.

Ferroni, L., Živčak, M., Kovar, M., Colpo, A., Pancaldi, S., Allakhverdiev, S. I., & Brestič, M. (2022). Fast chlorophyll a fluorescence induction (OJIP) phenotyping of chlorophyll-deficient wheat suggests that an enlarged acceptor pool size of Photosystem I helps compensate for a deregulated photosynthetic electron flow. *Journal of Photochemistry and Photobiology B: Biology*, *234*, 112549.

Pardi-Comensoli, L., Tonolla, M., Colpo, A., Palczewska, Z., Revikrishnan, S., Heeb, M., Brunner, I., & Barbezat, M. (2022). Microbial Depolymerization of Epoxy Resins: A Novel Approach to a Complex Challenge. *Applied Sciences*, *12*(1), 466.

Congresses, seminars and schools

1. **Oral presentation: ANDREA COLPO**, SIMONETTA PANCALDI, LORENZO FERRONI, Photoprotection in *Selaginella martensii* Spring (Lycopodiophyta) acclimated to different light regimes, Conference of Young Botanists (CYBO), Genova, 6.02.2020.

2.**Poster: ANDREA COLPO**, SIMONETTA PANCALDI, LORENZO FERRONI, Quantification of Photosystem II photoprotection in *Selaginella martensii* Spring (Lycopodiophyta) acclimated to different light regimes, Virtual Botany Conference (Botany2020, Botanical Society of America), 29.07.2020.

3. **Poster: ANDREA COLPO**, SIMONETTA PANCALDI, LORENZO FERRONI, Fluorometric evaluation of PSII antenna size in *Selaginella martensii* acclimated to contrasting light regimes, SPPS PhD Students Conference, from basics to bioeconomy (Scandinavian Plant Physiology Society), online conference, 3.09.2020.

4.**Oral presentation: ANDREA COLPO**, SIMONETTA PANCALDI, LORENZO FERRONI, Photosystem II photoprotection and antenna uncoupling in *Selaginella martensii* Spring acclimated to different light regimes, phenotyping of mature chlorophyll-deficient wheat mutant lines cultivated under fluctuating natural light, 115° Congresso della Società Botanica Italiana (VI International Plant Science Conference), online, 9-11.09.2020.

5.**Oral Presentation: ANDREA COLPO,** LORENZO FERRONI: Investigation on Photosystem II functional antenna size and excitonic connectivity in *Selaginella martensii*, Riunione annuale dei gruppi di lavoro *SBI*, Biologia Cellulare e Molecolare Biotecnologie e Differenziamento, online, 16-18.06.2021.

6.**Poster: ANDREA COLPO,** COSTANZA BALDISSEROTTO, SIMONETTA PANCALDI, LORENZO FERRONI: Effects of long-term light acclimation on Photosystem II functional antenna size and excitonic connectivity in *Selaginella martensii*, Virtual Botany Conference (Botany2021, Botanical Society of America), online, 18-23.07.2021.

7.**Oral Presentation: ANDREA COLPO,** MARIAN BRESTIC, ALESSANDRA SABIA, SIMONETTA PANCALDI, LORENZO FERRONI: Photosynthetic phenotyping of mature chlorophyll-deficient wheat mutant lines cultivated under fluctuating natural light, 116° Congresso della Società Botanica Italiana (VII International Plant Science Conference), online, 8-10.09.2021.

8.**Oral Presentation**: LORENZO FERRONI, **ANDREA COLPO**, ALESSANDRA MOLINARI, SIMONETTA PANCALDI Quantitative assessment of the thylakoid membrane appression in the chloroplast of *Selaginella martensii* Spring (Lycopodiophyta), 116° Congresso della Società Botanica Italiana (VII International Plant Science Conference), online, 8-10.09.2021.

9.**Poster**: **ANDREA COLPO**, SARA DEMARIA, MARZIO ZACCARINI, ALESSANDRO FORLANI, ELENA MARROCCHINO, LORENZO FERRONI: In field assessment of drought stress effect on the

photosynthetic apparatus functionality in three different apple tree (*Malus domestica* Borkh) rootstocks. VIII International Plant Sciences Conference, Bologna, 9.09.2022.

10.**Poster**: LORENZO FERRONI, SARA DEMARIA, **ANDREA COLPO**, SIMONETTA PANCALDI: Afternoon changes in the structure and function of the gigantic chloroplast of *Selaginella martensii* Spring. 117° Congresso della Società Botanica Italiana (VIII International Plant Sciences Conference), Bologna, 9.09.2022.

Projects and scholarships participation

Partecipation in the project "*Fenomica vegetale con lo strumento open source MultispeQ e la piattaforma PhotosynQ: fattibilità, efficacia e potenzialità*" granted by "Fondo per l'Incentivazione alla Ricerca (FIR) 2020" of the University of Ferrara (principal investigator Lorenzo Ferroni).

Partecipation in the project "*Metodi fluorimetrici innovativi a supporto della selezione varietale di fragola e di portinnesti di melo contro lo stress idrico*" by the University of Ferrara with the contribution by the Camera di Commercio Industria, Artigianato e Agricoltura di Ferrara (Call 2019; principal investigator Lorenzo Ferroni).

Granted with a scholarship for the research project "*Functional characterization of Light-harvesting complex II in* Selaginella martensii" at the Vrije University of Amsterdam financed by the LaserLab Europe infrastructure.

Granted with a scholarship for the research project "*Phenotyping of photosynthetic traits to support the selection of strawberry accessions resistant to drought stress*" at the University of Agriculture in Nitra financed by the Slovak Academy Information Agency (SAIA, SK).

Other relevant activities

Correlator for bachelor's and master's thesis at the University of Ferrara.

Appointment as "Cultore della materia" for the teaching course of Plant Biology in the bachelor's degree in Biological Sciences - University of Ferrara, 4.06.2020.

Integrative teaching activities: "*Metodi di riconoscimento di materiali vegetali al microscopio ottico*", integrated course in Plant Biology and Physiology at the University of Ferrara, 03-05.2021.

Member of the Botanical Society of America (15.12.2021)

Teaching tutor for the integrated course in Plant Biology and Physiology at the University of Ferrara, 05.2022.

Lecturer for the seminar "Screening of three apple trees (*Malus domestica*) rootstock varieties for drought resistance" in the framework of the course "GEOCHEMICAL AND ISOTOPIC FINGERPRINT AS TOOLS FOR FOOD TRACEABILITY AND FOOD SAFETY" of the master's degree course in Food Safety and Food Risk Management of the University of Bologna, 20.05.2022.

Successful completion of the 14-week program course "*Plant Breeding 2 Fight Hunger*" at the Michigan State University (MSU, US), 16.05.2022-18.08.2022.